INTERNATIONAL DOCTORAL
SCHOOL OF THE USC

Ana
Justo Vega

PhD Thesis

Towards comprehensive nanoparticle assessment in biological media: Application of Single-Particle, Single-Cell, and Laser Ablation ICP-MS

Santiago de Compostela, 2025

Doctoral Programme in Chemical Science and Technology

ESCOLA DE DOUTORAMENTO
INTERNACIONAL DA USC

DOCTORAL THESIS

TOWARDS COMPREHENSIVE NANOPARTICLE ASSESSMENT IN BIOLOGICAL MEDIA: APPLICATION OF SINGLE-PARTICLE, SINGLE-CELL, AND LASER ABLATION ICP-MS

Ana Justo Vega

Supervisor/s: Antonio Moreda Piñeiro

María Raquel Domínguez González

Tutor: Antonio Moreda Piñeiro

PHD PROGRAMME IN CHEMICAL SCIENCE AND TECHNOLOGY

SANTIAGO DE COMPOSTELA

2025

DECLARATION OF CONFLICT OF INTEREST

USC
UNIVERSIDADE
DE SANTIAGO
DE COMPOSTELA

DECLARATION OF CONFLICT OF INTEREST

I, Ana Justo Vega, hereby declare that there are no conflicts of interest regarding the research presented in this doctoral thesis entitled "Towards comprehensive nanoparticle assessment in biological media: Application of Single-Particle, Single-Cell, and Laser Ablation ICP-MS".

All financial support received during this doctoral thesis has been detailed. I confirm that I have no financial, personal, or professional relationships that could have influenced the results, interpretation, or presentation of this work.

Santiago de Compostela, 14th October 2025.

USC
UNIVERSIDADE DE SANTIAGO DE COMPOSTELA

FUNDING

USC
UNIVERSIDADE
DE SANTIAGO
DE COMPOSTELA

FUNDING

The following institutions financially supported the present doctoral thesis:

- Consellería de Cultura, Educación, Formación Profesional e Universidades da Xunta de Galicia (predoctoral grant ED481A/2022)
- Xunta de Galicia (Grupo de Referencia cometitiva, ED431C 2022/029)
- Ministerio de Ciencia, Innovación y Universdidades – Agencia Española de Investigación (FOODNANRISK, reference PID2021-125276NB-100)
- European Union (Erasmus+ 2022/2023)

LIST OF PUBLICATIONS AND CONTRIBUTION

USC
UNIVERSIDADE
DE SANTIAGO
DE COMPOSTELA

LIST OF PUBLICATIONS AND CONTRIBUTION

– Chapter 1

Ana Justo-Vega, Raquel Domínguez-González, Pilar Bermejo-Barrera, Antonio Moreda-Piñeiro, Prospects of surfactant assisted dispersive liquid–liquid microextraction for the selective extraction of silver and titanium dioxide nanoparticles from tap water and determination by spICP-MS, Journal of Analytical Atomic Spectrometry 39, 573-581 (2024). https://doi.org/10.1039/D3JA00227F

Impact factor (2024): 3.1
Rank by Journal Impact Factor (2024) Spectroscopy, 9/44 (Q1)
Citations: 7
CrediT authorship contribution statement (Ana Justo-Vega): Writing – original draft, Software, Methodology, Investigation, Formal analysis, Data curation.

– Chapter 2

Ana Justo-Vega, Claudia Torrente-Seco, Lidia Janza-Candal, Manuel Aboal-Somoza, Raquel Domínguez-González, Pilar Bermejo-Barrera, Antonio Moreda-Piñeiro, Surfactant-assisted dispersive liquid–liquid microextraction and centrifugal ultrafiltration as potential extraction procedures for silver and titanium dioxide nanoparticles from human urine, Microchemical Journal 211, 113072 (2025). https://doi.org/10.1016/j.microc.2025.113072

Impact factor (2024): 5.1
Rank by Journal Impact Factor (2024) Analytical Chemistry, 23/111 (Q1)
Citations: 1
CrediT authorship contribution statement (Ana Justo-Vega): Writing – original draft, Investigation, Formal analysis, Data curation.

– Chapter 3

Ana Justo-Vega, Sara Vázquez-Pérez, Raquel Domínguez-González, Pilar Bermejo-Barrera, Antonio Moreda-Piñeiro, Enzymatic hydrolysis for pre-treating human serum before titanium dioxide nanoparticles assessment by spICP-MS, Talanta 291, 127766 (2025). https://doi.org/10.1016/j.talanta.2025.127766

Impact factor (2024): 6.1
Rank by Journal Impact Factor (2024) Analytical Chemistry, 14/111 (Q1)
Citations: 0
CrediT authorship contribution statement (Ana Justo-Vega): Writing – original draft, Validation, Software, Formal analysis, Data curation.

– Chapter 4

Ana Justo-Vega, Raquel Domínguez-González, Pilar Bermejo-Barrera, Antonio Moreda-Piñeiro, Javier Jiménez-Lamana, Silver nanoparticles behaviour in exposed human red blood cells by single cell–inductively coupled plasma–mass spectrometry, Talanta 298, Part B, 128972 (2026). https://doi.org/10.1016/j.talanta.2025.128972

Impact factor (2024): 6.1
Rank by Journal Impact Factor (2024) Analytical Chemistry, 14/111 (Q1)
Citations: 0
CrediT authorship contribution statement (Ana Justo-Vega): Writing – original draft, Software, Methodology, Investigation, Formal analysis, Data curation.

USC UNIVERSIDADE DE SANTIAGO DE COMPOSTELA

ACKNOWLEDGEMENTS

USC
UNIVERSIDADE
DE SANTIAGO
DE COMPOSTELA

ACKNOWLEDGEMENTS

Ós pilares da miña vida, ós que dan sentido a todo isto.

Ós meus pais,

Por acompañarme dende o inicio, que non é o mesmo que o inicio desta tese. A vós que vos debo todo: cada etapa, cada título académico, cada logro que hoxe se consagra neste doutoramento, é froito tamén do voso suor e o voso traballo. Non podo devolver todo o que me destes, pero que o orgullo de que este título tamén leve o voso nome sirva como agradecemento. Un título que conseguimos en conxunto, coas oportunidades que desafortunadamente vós non tivestes pero que loitastes para asegurarvos de que si as tivera eu. Aquí se xuntan o esforzo económico de mandar a vosa filla estudar á universidade, as bágoas ao despedirse dela cando estaba lonxe e tamén o agarimo á volta. Papá, mamá, conseguímolo.

Á miña irmá,

A miña metade e o tesouro máis grande que teño. A persoa á que acudo para recargar as pilas, a que sempre ten todo e máis para ofrecerme e a que me acompañaría ao fin do mundo. A miña cómplice e a miña defensora. Sei que nunca deixarás de burlarte de min e de narrar a túa anécdota favorita na que chego chorando a casa por suspender un exame pero, hoxe reescribimos a historia: igual "isto de estudar" si que é o meu. E tamén ao meu cuñi *Pabliño*, por xuntos regalarme o máis bonito do mundo.

Por seguir recorrendo o camiño a vosa *Veriña*.

Á Adrián,

Pola túa fe en min. Por ser o motor cando me faltan forzas e as ás cando toca voar lonxe da casa. Pola tenrura de comprender e apoiarme nesta etapa, por mirarme como se fose capaz de todo, que me contaxia de seguridade e motivación para seguir. Pola forza de ser equipo e axudarme a alcanzar a meta. Porque agora, xuntos, formamos parte dese 0.7 %.

Ó meu círculo,

Ós que escoitan falar de química, sen entender nin unha soa palabra do que digo. Ós que preguntan que tal vai a tese, sen chegar a entender moi ben en que consiste. Ós que arriman o ombro cando a vida se pon difícil e celebran os meus éxitos como propios. Ó meu *hometeam*, que fai do fogar un lugar ao que querer volver sempre. A *Pit* e *Anto*, por facer da vida un campamento constante. A *Jav*, por camiñar sempre un pasiño por diante de min e tenderme a man. A *Soni*, por ser a mellor relación a distancia que existe e facerme sentir o seu abrazo a centos de quilómetros. À *Jimmy*, qui a fait de la France une deuxième maison pour moi et qui m'a ouvert les portes de sa vie sans même me connaître. Je te porte dans mon cœur.

Gracias también,

A mis tutores. A *Antonio*, por la confianza y la libertad con las que siempre me has permitido trabajar. Tu dedicación, generosidad y pasión por lo que haces, han sido siempre un ejemplo a seguir. Siento un orgullo sincero de haber podido trabajar mano a mano contigo. A *Raquel*, por animarme a formar parte y acercarme el lado más divulgativo de la ciencia. Sé que las puertas de tu despacho estarán siempre abiertas para mí.

A *Pilar*, por la cercanía, la confianza, y por animarnos siempre a dar lo mejor de nosotros mismos. Por ser inspiración para que nuevas generaciones de jóvenes investigadoras vean, a través de ti, la certeza de un futuro.

A *Mari Carmen*, por aportarnos el aspecto más humano. Por la preocupación más allá de la investigación, las clases y la ciencia. Por ser el *¿qué tal estáis?* del día a día tan necesario.

A *Elena*, por la paciencia y la calma con la que resuelve las preguntas y su dedicación como profesora.

A *Manolo*, por permitirte acudir a él con cualquier tipo de duda y por su determinación hasta ser capaz de resolverla.

A *Paloma*, por todo. Con la gratitud y la convicción humilde de que el laboratorio funciona día a día gracias a ella.

A *Marta Lores*, por compartir laboratorio. Por hacer que todo parezca fácil e impulsarnos a confiar en que somos capaces de conseguirlo todo, alejándonos de ser LME.

A *Javier*, por dejar las formalidades a un lado y salirse del rol típico de profesor. Por la cercanía con la que educas, la amabilidad de recibir y tratar a estudiantes extranjeros y, como no, el sentido del humor.

To *Prof. Frank Vanhaecke*, for the kindness of welcoming me into his research group for three months and for the valuable lessons I learnt during my time there.

A *Thillini, Kolita, Vane* y *Cristian*, por haber compartido días de laboratorio, cafés, dudas y consejos sobre cómo hacer mejor las cosas.

A *Ala*, por la dinámica tan respetuosa y cariñosa que tenemos de discutir y llevarnos siempre la contraria. Por ser siempre el primero en querer ayudar. España siempre te recibirá con los brazos abiertos porque esta ya es tu casa.

A *Vanesiña*, por endulzarnos los días con chocolatinas, notitas de ánimo y millones de abrazos.

A *Iria*, por haber compartido un año especialmente intenso, entre mascarillas, becas rechazadas, dudas vitales existenciales y la certeza de que los problemas son menos problemas cuando los verbalizas.

A *Juanjo*, por absolutamente todo. Por pasar de compañero a amigo, aunque nunca olvidaré que tenía que arrancarte las palabras al principio. Me llena de orgullo ver cómo hemos crecido

USC UNIVERSIDADE DE SANTIAGO

y lo cuantísimo que hemos aprendido todos estos años. Admiro tu bondad, tu generosidad infinita y la dedicación que le pones a todo lo que haces. Gracias por la motivación cuando flaquea, los cientos de memes y por estar dispuesto a ayudar en cualquier momento.

A *Iván*, por ser fiel compañero de congresos y excursiones. Prepárate: eres el siguiente (guiño guiño).

A *Sheilis*, por tus abrazos cada mañana, los descansos para recargar fuerzas con café y los coti coti. Porque siempre tienes una forma muy dulce de ponerle corazón a todo lo que haces. Aunque ahora cueste verlo, todo irá a mejor.

A *Iria Valdoviño*, por sembrar el caos nada más entrar, pero qué caos más bonito. Recuerda siempre que no tienes que pedir permiso para comerte el mundo.

Gracias tamén aos que me coidan dende o ceo,

Ana

USC
UNIVERSIDADE DE SANTIAGO DE COMPOSTELA

Dedicada á mina irmá

USC
UNIVERSIDADE
DE SANTIAGO
DE COMPOSTELA

TABLE OF CONTENTS

USC
UNIVERSIDADE
DE SANTIAGO
DE COMPOSTELA

TABLE OF CONTENTS

ABSTRACT **1**

RESUMO **8**

I. INTRODUCTION **15**

1 INTRODUCTION TO NANOTECHNOLOGY **16**

1.1 History, scientific story and today's global landscape 16
1.2 Nanomaterials: definition, classification and properties 19
1.3 Titanium dioxide nanoparticles 23
1.4 Silver nanoparticles 26

2 NANOTOXICITY AND POTENTIAL HAZARDS **28**

2.1 Nanotoxicity mechanisms 28
2.2 Silver and titanium dioxide NPs toxicity studies 30
2.3 Regulatory framework 33

3 PRESENCE OF NANOPARTICLES IN THE ENVIRONMENT **35**

3.1 Environmental dynamics of NMs as contaminants 35
3.2 Alleviation of environmental stress by NMs 39

4 HUMAN BIOMONITORING **41**

4.1 Routes of exposure 41
4.2 ADME process 45
4.3 Biofluids under study 47
4.3.1 Blood *47*
4.3.2 Urine *48*

5 ASSESSMENT OF INORGANIC NANOPARTICLES: ADVANCED ANALYTICAL TECHNIQUES **50**

5.1 Methods for sample preparation 50
5.1.1 Surfactant-assisted dispersive liquid-liquid microextraction (SA-DLLME) *50*
5.1.2 Enzymatic hydrolysis *54*
5.1.3 Centrifugal ultrafiltration (UF) *55*
5.2 Quantification and characterization of NPs: ICP-MS-based techniques 56
5.2.1 spICP-MS *59*
5.2.2 SC-ICP-MS *61*
5.2.3 LA-ICP-MS *62*

II. OBJECTIVES **65**

III. METHODOLOGY **67**

IV. RESULTS **70**

IV. PART A: PUBLISHED RESULTS **71**

USC UNIVERSIDADE DE SANTIAGO DE COMPOSTELA

CHAPTER 1. PROSPECTS OF SURFACTANT ASSISTED DISPERSIVE LIQUID-LIQUID MICROEXTRACTION FOR THE SELECTIVE EXTRACTION OF SILVER AND TITANIUM DIOXIDE NANOPARTICLES FROM TAP WATER AND DETERMINATION BY SPICP-MS 72

GRAPHICAL ABSTRACT 73
ABSTRACT 74
1.1 INTRODUCTION 74
1.2 METHODOLOGY 76
1.2.1 Chemicals and standards 76
1.2.2 Instrumentation 76
1.2.3 SA-DLLME extraction procedure 77
1.2.4 Operating conditions for spICP-MS measurements 77
1.3 RESULTS AND DISCUSSION 78
1.3.1 Optimization of the SA-DLLME experimental parameters 78
1.3.2 Effect of the volume of the 49:1 Triton X-114/1,2-dichloroethane mixture 78
1.3.3 Effect of vortex (extraction) time and speed 79
1.3.4 Effect of centrifugation speed and time 81
1.4 ANALYTICAL PERFORMANCE 83
1.4.1 Calibration and matrix effect 83
1.4.2 Limits of detection and limits of quantification 83
1.4.3 Selectivity of the SA-DLLME procedure for nanoparticle forms of Ti and Ag 84
1.4.4 Analytical recovery assays 84
1.5 CONCLUSIONS 86
1.6 ACKNOWLEDGEMENTS 87
1.7 REFERENCES 87

CHAPTER 2. SURFACTANT-ASSISTED DISPERSIVE LIQUID-LIQUID MICROEXTRACTION AND CENTRIFUGAL ULTRAFILTRATION AS POTENTIAL EXTRACTION PROCEDURES FOR SILVER AND TITANIUM DIOXIDE NANOPARTICLES FROM HUMAN URINE 92

GRAPHICAL ABSTRACT 93
ABSTRACT 93
2.1 INTRODUCTION 94
2.2 EXPERIMENTAL 95
2.2.1 Instrumentation 95
2.2.2 Materials and reagents 96
2.2.3 Urine sample collection 96
2.2.4 Surfactant assisted – DLLME extraction procedure 96
2.2.5 Centrifugal UF conditions 97
2.2.6 spICP-MS analysis 97
2.3 RESULTS AND DISCUSSION 98
2.3.1 Optimization extraction/preconcentration procedures 98
2.3.2 Analytical performance 102
2.4 CONCLUSIONS 106
2.5 FUNDING SOURCES 108
2.6 REFERENCES 108
SUPPLEMENTARY INFORMATION 113

CHAPTER 3. ENZYMATIC HYDROLYSIS FOR PRE-TREATING HUMAN SERUM BEFORE TITANIUM DIOXIDE NANOPARTICLES ASSESSMENT BY SPICP-MS 118

GRAPHICAL ABSTRACT 119
ABSTRACT 119

USC UNIVERSIDADE DE SANTIAGO DE COMPOSTELA

3.1 Introduction 120
3.2 Materials and methods 121
3.2.1 Instrumentation 121
3.2.2 Reagents 122
3.2.3 Human serum samples 122
3.2.4 Enzyme mixture preparation 122
3.2.5 Enzymatic hydrolysis process 123
3.2.6 Centrifugal ultrafiltration process 123
3.2.7 Operating conditions for spICP-MS determination of TiO_2NPs 123
3.2.8 High resolution transmission electronic microscopy and EDX analysis 124
3.3 Results and discussion 125
3.3.1 Optimization of the enzymatic hydrolysis process 125
3.3.2 Analytical performance 128
3.3.3 Applications 129
3.4 Conclusions 129
3.5 Funding sources 131
3.6 Acknowledgements 131
3.7 References 132

CHAPTER 4. SILVER NANOPARTICLES BEHAVIOUR IN EXPOSED HUMAN RED BLOOD CELLS BY SINGLE CELL – INDUCTIVELY COUPLED PLASMA – MASS SPECTROMETRY 136

Graphical Abstract 137
Abstract 137
4.1 Introduction 138
4.2 Experimental 139
4.2.1 Instrumentation 139
4.2.2 Reagents and consumables 140
4.2.3 Red Blood Cells Sample Collection and Isolation Protocol 140
4.2.4 Red Blood Cells Exposure Protocol 141
4.2.5 Single-cell ICP-Ms analysis 141
4.2.6 Preparation of RBCs sections for TEM analysis 143
4.3 Results and discussion 143
4.3.1 Feasibility studies 143
4.3.2 Effect of dose concentration and incubation time 145
4.3.3 Influence of nanoparticle size on AgNPs-RBCs association 149
4.4 Conclusions 150
4.5 Acknowledgements 151
4.6 References 151
Supplementary Information 157

IV. PART B: UNPUBLISHED RESULTS 160

CHAPTER 5. ADVANCEMENTS IN LA-ICP-MS: PRELIMINARY INSIGHTS INTO THE OPTIMIZATION OF A NEW CALIBRATION APPROACH AND A MICROWELL ARRAY DESIGN FOR SINGLE-CELL TRAPPING 161

Abstract 162
5.1 Introduction 162
5.2 Experimental 163
5.2.1 Instrumentation 163
5.2.2 Materials and Reagents 164
5.2.3 Protocol to prepare gelatine microdroplets 165
5.2.4 Design and manufacturing of a microwell array master mold by photolithography 166

USC UNIVERSIDADE DE SANTIAGO DE COMPOSTELA

5.2.5 Negative-PDMS mold from the master mold *166*
5.2.6 Cell culture and exposure *166*
5.3 RESULTS AND DISCUSSION 167
Part A: Feasibility studies of a gelatine-based microdroplet calibration approach *167*
Part B: Feasibility studies of a microwell array design for single-cell trapping–Optimization *175*
5.4 CONCLUSIONS 179
5.5 REFERENCES 180
SUPPLEMENTARY INFORMATION 182

V. INTEGRATIVE DISCUSSION 183

VI. CONCLUSIONS 194

VII. REFERENCES 197

ANNEX I. PERMISSIONS 227

USC UNIVERSIDADE DE SANTIAGO DE COMPOSTELA

ABBREVIATIONS

USC
UNIVERSIDADE
DE SANTIAGO
DE COMPOSTELA

ABBREVIATIONS

A

AA – Air-assisted

ACC – American Chemistry Council

AF4 – Asymmetric-Flow Field-Flow Fractionation

Ag – Silver

AgNPs – Silver nanoparticles

AuNPs – Gold nanoparticles

C

C/Fe3C NPs – Carbon-coated iron carbide nanoparticles

CAGR – Compound annual growth rate

CE – Capillary electrophoresis

CECs – Contaminants of emerging concerns

CEN – European Standardization Committee

CMC – Critical micelle concentration

CNT – Carbon nanotube

CRMs – Certified reference materials

CTAB – Cetyltrimethylammonium bromide

D

DCP – Direct current plasma

DES – Deep eutectic solvent

DIHEN – Direct injection high-efficiency

DLLME – Dispersive liquid-liquid microextraction

DLS – Dynamic light scattering

DMEM – Dulbecco's Modified Eagle Medium

USC UNIVERSIDADE DE SANTIAGO DE COMPOSTELA

DRC – Dynamic reaction cell

E

EA – Effervescence-assisted

EAA – Essential amino acids

EC – European Commission

EDL – Electric double layer

EDTA – Ethylenediaminetetraacetic acid

EDX – Energy dispersive X-rays spectrometry

EF – Enrichment factor

EFSA – European Food Safety Authority

EM – Electron microscopy

ENMs – Engineered nanomaterials

ETV-ICP-MS – Electrothermal vaporization inductively coupled plasma-mass spectrometry

EU – European Union

F

FBS – Fetal bovine serum

FEM – Field emission

FFF – Field flow fractionation

FFFF – Flow field flow fractionation

FIM – Field ion microscope

G

GI – Gastro – intestinal

GO – graphene oxide

H

HBL – Hydrophile-lipophile balance number

HDC – Hydrodynamic chromatography

HF-LPME – Hollow fiber liquid-phase microextraction

HOMO – Highest occupied molecular orbital

HRTEM – High resolution transmission electronic microscopy

USC DE COMPOSTELA

I

IARC – International Agency for Research on Cancer

ICP-AES – Inductively coupled plasma atomic emission spectrometry

ICP-MS – Inductively coupled plasma mass spectrometry

ICP-OES – Inductively coupled plasma optical emission spectrometry

IEC – Ion exchange chromatography

IL – Ionic liquid

ISO – International Organization for Standardization

L

LA-ICP-MS – Laser ablation inductively coupled plasma mass spectrometry

LCA – Life cycle assessment

LLE – Liquid-liquid extraction

LOD – Limit of detection

LOD_{NP} – Number concentration limit of detection

LODsize – Size limit of detection

LPME – Liquid-phase microextraction

LSD – Least Significant Difference

LUMO – Lowest unoccupied molecular orbital

M

MALS – Multiple angle light scattering

MDs – Microdroplets

MECs – Measured environmental concentrations

MIL – Magnetic ionic liquid

MIP – Microwave-induced plasma

MWCNTs – Multiwalled carbon nanotubes

MWCO – Molecular weight cut-off

N

NMs – Nanomaterials

NNI – National Nanotechnology Initiative

USC DE COMPOSTELA

NPD – Nanotechnology Products Database

NPs – Nanoparticles

O

OECD – Organization for Economic Co-operation and Development

P

PBS – Phosphate buffered saline

PDMS – Polydimethylsiloxane

PNs – Pneumatic nebulizers

PTFE – Poly(tetrafluoroethylene)

PtNPs – Platinum nanoparticles

Q

QDs – Quantum dots

R

RBCs – Red blood cells

REACH – Registration, Evaluation, Authorization and Restriction of Chemicals

RF – Radio frequency

rGO – reduced graphene oxide

ROS – Reactive oxygen species

RSD – Relative standard deviation

S

SA-DLLME – Surfactant-assisted dispersive liquid-liquid microextraction

SB – Stratum basale

SC – Stratum corneum

SCCP – Scientific Committee on Consumer Products

SCCS – Scientific Committee on Consumer Safety

SCENIHR – Scientific Committee on Emerging and Newly Identified Health Risks

SC-ICP-MS – Single Cell inductively coupled plasma mass spectrometry

SDME – Single-drop microextraction

SDS – Sodium dodecyl sulphate

USC DE COMPOSTELA

SeNPs – Selenium nanoparticles

SG – Stratum granulosum

spICP-MS – Single-particle inductively coupled plasma mass spectrometry

SPIONs – Superparamagnetic iron oxide nanoparticles

SPR – Surface plasmon resonance

SRM – Standard Reference Material

SS – Stratum spinosum

STM – Scanning tunneling microscope

T

TE – Transport efficiency

TEM – Transmission electron microscopy

TiO_2 – Titanium dioxide

TiO_2NPs – Titanium dioxide nanoparticles

TMAH – Tetramethylammonium hydroxide

U

UA – Ultrasound-assisted

UF – Ultrafiltration

USNs – Ultrasonic nebulizers

UV – Ultra-violet

V

VA – Vortex-assisted

W

WBCs – White blood cells

WHO – World Health Organization

WPMN – Working Party on Manufactured Nanomaterials

WWTP – Wastewater treatment plants

Z

ZnONPs – Zinc oxide nanoparticles

USC UNIVERSIDADE DE SANTIAGO DE COMPOSTELA

LIST OF FIGURES

USC
UNIVERSIDADE
DE SANTIAGO
DE COMPOSTELA

LIST OF FIGURES

Figure 1. Timeline of major breakthroughs and milestones in nanotechnology from ancient times to nowadays. 17

Figure 2. Number of publications in Web of Science database from 1961 to 2024 using "nanoscience" or "nanotechnology" as keyword in (A) the world and (B) Spain. 18

Figure 3. Applications of TiO_2NPs by subdivision. 25

Figure 4. Applications of AgNPs by subdivision. 27

Figure 5. NMs can be released into the environment from different sources, during their production, usage, and disposal. 40

Figure 6. NMs exposure routes and secondary target organs different from portal of entry… 44

Figure 7. Chemical structure and formula of Triton X-114. 53

Figure 8. Diagram of the SA-DLLME extraction process. 54

Figure 9. Schematic diagram of UF workflow. 55

Figure 10. Photograph of a plasma torch mounted in an instrument. 58

Figure 11. Temporal evolution of spICP-MS (solid dark bars) and SC-ICP-MS (dashed lines) in number of publications since 2000 to 2024, using ‘spICP-MS’ or ‘single particle ICP-MS’ and ‘SC-ICP-MS’ or ‘single cell ICP-MS’ as keywords. Source Web of Science, September 2025. 61

Figure 12. Photograph of an Asperon^{TM} spray chamber for single-cell analysis mounted in an instrument. 62

Figure 13. Laser Ablation NWR-213 unit (New Wave Research, Inc., CA, USA) coupled to NexION 2000 ICP-MS (Perkin Elmer, Waltham, MA, USA). 63

Figure 14. Effect of the volume of 49:1 Triton X-114/1,2-dichloroethane (a), vortexing time (b) and vortexing (c) on the analytical recovery of AgNPs and TiO_2NPs. 80

Figure 15. TEM image and EDS spectra of the 100 nm TiO_2NPs standard. 81

Figure 16. Effect of the centrifugation speed (a) and centrifugation time (b) on the analytical recovery of AgNPs and TiO_2NPs. 82

Figure 17. Representative histograms for extracts from a tap water sample spiked with 50 µg L^{-1} of 100 nm TiO_2NPs (a) and 12 $\times 10^4$ mL^{-1} of 40 nm AgNPs (b). 86

Figure 18. Effect of the volume of the 49:1 surfactant (TX-114)/extractant ($C_2H_4Cl_2$) mixture. Conditions: AgNPs, 64 ng L^{-1}(A), TiO_2NPs 25 µg L^{-1} (B); centrifugation time, 5 min;

centrifugation speed, 2500 rpm; centrifugation temperature, 4 °C; vortex time, 30 s; vortex speed, 1500 rpm; error bars correspond to the SD of 3 experimental replicates (n=9 spICP-MS measurements). 100

Figure 19. Optimization of the number of washing cycles. Conditions: AgNPs (40nm, $1.23x10^5$ NPs mL^{-1}), TiO_2NPs (100 nm, 26.7 µg L^{-1}); error bars correspond to the SD of 2 experimental replicates (n=6 spICP-MS measurements). 101

Figure 20. Selection of the appropriate washing solvent. Conditions: AgNPs (60 nm, $2.75x10^4$ NPs mL^{-1}), TiO_2NPs (100 nm, 1.6 µg L^{-1}); error bars correspond to the SD of 2 experimental replicates (n=6 spICP-MS measurements) 101

Figure 21. Values of mean and most frequent sizes for 40nm-AgNPs (A) and 60nm-AgNPs (B) at low spiking level* (L) and high spiking level* (H); error bars correspond to the SD of 3 experimental replicates (n=9 spICP-MS measurements).*See table 10 for concentrations... 106

Figure 22. Values of mean and most frequent sizes for 50nm-TiO_2NPs (A) and 100nm-TiO_2NPs (B) at low spiking level* (L) and high spiking level* (H). error bars correspond to the SD of 3 experimental replicates (n=9 spICP-MS measurements). *See table 11 for concentrations.. 107

Figure 23. HRTEM image and EDX spectrum of 60 nm AgNPs standard. 113

Figure 24. HRTEM image and EDX spectrum of 40 nm AgNPs standard. 113

Figure 25. HRTEM image and EDX spectrum of 100 nm TiO_2NPs standard. 114

Figure 26. Effect of the centrifugation speed on the extraction efficiency. Conditions: AgNPs, 64 ng L^{-1}(A), TiO_2NPs 1 µg L^{-1} (B); volume of the 49:1 surfactant (TX-114)/extractant ($C_2H_4Cl_2$) mixture, 1 mL; centrifugation time, 5 min; centrifugation temperature, 4 ºC, vortex time, 30 s; vortex speed, 1500 rpm; error bars correspond to the SD of 3 experimental replicates (n=9 spICP-MS measurements). 114

Figure 27. Effect of the centrifugation time on the extraction efficiency. Conditions: AgNPs, 64 ng L^{-1}(A), TiO_2NPs 1 µg L^{-1} (B); volume of the 49:1 surfactant (TX-114)/extractant ($C_2H_4Cl_2$) mixture, 1 mL; centrifugation speed, 3500 rpm; centrifugation temperature, 4 °C; vortex time, 30 s; vortex speed, 1500 rpm; error bars correspond to the SD of 3 experimental replicates (n = 9 spICP-MS measurements). 115

Figure 28. Effect of the vortex time on the extraction efficiency. Conditions: AgNPs, 64 ng L^{-1}(A), TiO_2NPs 1 µg L^{-1} (B); volume of the 49:1 surfactant (TX-114)/extractant ($C_2H_4Cl_2$) mixture, 1 mL; centrifugation speed, 3500 rpm; centrifugation time, 10 min; centrifugation temperature, 4 °C; vortex speed, 1500 rpm; error bars correspond to the SD of 3 experimental replicates (n = 9 spICP-MS measurements). 116

Figure 29. Effect of the vortex speed on the extraction efficiency. Conditions: AgNPs, 64 ng L^{-1}(A), TiO_2NPs 1 µg L^{-1} (B); volume of the 49:1 surfactant (TX-114)/extractant ($C_2H_4Cl_2$) mixture, 1 mL; centrifugation speed, 3500 rpm; centrifugation time, 10 min; centrifugation temperature, 4 °C; vortex time, 30 s; error bars correspond to the SD of 3 experimental replicates (n = 9 spICP-MS measurements). 117

Figure 30. Schematic diagram of the experimental workflow followed. 123

USC UNIVERSIDADE DE SANTIAGO DE COMPOSTELA

Figure 31. HRTEM image (a) and EDX spectrum showing Ti characteristics peaks at 4.5 keV (TiK_a) and 5.0 keV (TiK_b) (b) of a slurry containing 100 nm TiO_2NPs standard at 10 mg L^{-1} TiO_2NPs. 126

Figure 32. Effect of the enzyme (pancreatin plus lipase) concentration (a), hydrolysis time (b), orbital-horizontal shaking rate (c), and number of UF rinsings (d) on the TiO_2NPs mass concentration and mean size for serum samples spiked with 63.5 µg L^{-1} TiO_2NPs (n=9). ... 127

Figure 33. Histograms for TiO_2NPs size distribution in a spiked serum sample at 63.5 µg L^{-1} (TiO_2NPs mass concentration) without enzymatic hydrolysis and with UF (a) and after enzymatic hydrolysis and UF (b). 130

Figure 34. HRTEM image for spiked serum samples at 63.5 TiO_2NPs µg L^{-1} without enzymatic hydrolysis and with UF (a) and after enzymatic hydrolysis and UF (c) and EDX spectrum showing Ti characteristics peaks at 4.5 keV (TiK_a) and 5.0 keV (TiK_b) for spiked serum samples at 63.5 TiO_2NPs µg L^{-1} without enzymatic hydrolysis and with UF (b) and after enzymatic hydrolysis and UF (d). 131

Figure 35. Effect of exposure time (8, 12, and 24 hours) on 40 nm-AgNPs uptake by RBCs. Conditions: concentration ratio 1:50 cell/NP, 39 ºC, 94.5 % relative humidity, 5.0 % CO_2; error bars correspond to the standard deviation of 3 experimental replicates (n=6 ICP-MS measurements). 145

Figure 36. Ag mass distribution histogram after exposure times of 8 h (A), 12 h (B), and 24 h (C) in detected RBCs. Coloured dash lines correspond to the median mass values of the distribution, the grey line represents the 8 h–corresponding to the mass of 3 AgNPs, the light-blue line the 12 h–5 AgNPs, and the dark-blue line the 24 h–8 AgNPs. (Conditions: 40 nm-AgNPs, concentration ratio 1:50 cell/NP, histograms correspond to one biological sample replicate)..... 147

Figure 37. TEM images of a section of a RBCs sample exposed to 40 nm-AgNPs for 24 hours, from lower (A) to higher (D) magnification range. Panels C and D display the same region at different magnifications, while panels A and B depict separate regions. 148

Figure 38. Comparison between 20 nm-AgNPs (black lines) and 40 nm-AgNPs (red lines). Solid lines represent the calculated RBCs number concentration (L^{-1}) for 8, 12, and 24 h of exposure; whereas dash lines stand for the percentage (%) of silver-containing RBCs..... 150

Figure 39. Supernatant silver concentration (µg L^{-1}) after 8, 12, and 24 hours of exposure. Concentration expressed as the sum of the first (3 replicates) and second (3 replicates) supernatants (n=12 ICP-MS measurements). 157

Figure 40. Time resolved ICP-MS profiles obtained with SPCal software for a RBCs sample exposed to 20 nm-AgNPs, ratio 1:50 cell/NP, for 24 hours (A), the corresponding control sample (B), the first supernatant collected (C), and the second supernatant collected after the first wash with 1.0 % PBS (D) (Conditions: (A) and (B) 2000-fold diluted, (C) and (D) no dilution). 158

Figure 41. TEM images of a RBCs control sample (not exposed to AgNPs). Panels A and B display the same magnification but different regions of the sample..... 159

USC
UNIVERSIDADE DE SANTIAGO DE COMPOSTELA

Figure 42. Exported images from Chromium 3 operating software (Teledyne Photon Machines) of some of the MDs prepared. 165

Figure 43. Silicon master mold consisting of eight square sections (0.3 x 0.3 cm, ~2,000 pillars) and three rectangular sections (0.6 x 2.5 cm, ~15,000 pillars) (A). Pillar characterization included measurements of height (B), diameter (C), and inter-well distance (D)..... 167

Figure 44. Graphical representation of the particle count per laser fluence value in microdroplet 1 (dashed black line) and microdroplet 2 (solid black line). 169

Figure 45. Signal contribution from the glass slide in B, compared to the background signal in A. 170

Figure 46. Effect of the laser fluence upon ablation..... 170

Figure 47. Comparison between the time scan and the corresponding intensity histogram of a high (2.0 J cm^{-2}) and low (0.4 J cm^{-2}) laser fluence. 171

Figure 48. Image obtained from the Chromium software with the middle and edge positions ablated (A), and the particle count of In in those positions under different laser fluences applied (B). 172

Figure 49. Images showing ^{115}In (used as IS) and ^{107}Ag map intensities within a MD. 173

Figure 50. Images showing ^{115}In (used as IS) and ^{197}Au map intensities within a MD. 174

Figure 51. Map intensity of a less concentrated 100 nm-AuNPs gelatine standard (In used as IS). 175

Figure 52. Influence of the settling time on the percentage of microwell occupancy based on single-cell or multiple-cell occupancy. Conditions: CO_2 atmosphere, 100,000 cells mL^{-1} cell concentration, DMEM resuspension medium. 177

Figure 53. Influence of cell concentration on the percentage of microwell occupancy based on single-cell or multiple-cell occupancy. Conditions: CO_2 atmosphere, 30 min settling time, DMEM resuspension medium. 178

Figure 54. Different behaviour of control (unexposed) Caco-2 cells versus exposed cells to 30 nm AuNPs and 60 nm AuNPs. (Conditions: 24 h exposure, cell:NP ratio 1:50). 179

Figure 55. Microscope images under natural lighting (A), using a DAPI filter (B), and the overlay result (C). (Conditions: unexposed Caco-2 cells, 30 min settling time, 100,000 cell mL^{-1}, DMEM resuspension medium, CO_2 atmosphere). 182

Figure 56. Overview of the connection between chapters. 184

USC UNIVERSIDADE DE SANTIAGO DE COMPOSTELA

LIST OF TABLES

USC
UNIVERSIDADE
DE SANTIAGO
DE COMPOSTELA

LIST OF TABLES

Table 1. Literature examples of NM toxicity in different organisms. 29

Table 2. Literature examples of in vitro and in vivo Ag and TiO_2NPs toxicity studies on several cell lines and living organisms. 31

Table 3. Instrumental spICP-MS conditions. 77

Table 4. Mean sizes of AgNPs and TiO_2NPs under several operational conditions. 79

Table 5. Number concentration and size limit of detection of the method. 84

Table 6. Analytical recovery of the spICP-MS measurements and of the over-all procedure (SA-DLLME and spICP-MS). 85

Table 7. Default instrumental and data acquisition parameters. 97

Table 8. Number concentration and size detection limits (5-sigma criterion) (n=11). 103

Table 9. Analytical performances of the proposed method and reported methodologies for AgNPs and TiO_2NPs in urine. 103

Table 10. AgNPs analytical recoveries and relative standard deviation (%) for both extraction techniques. 104

Table 11. TiO_2NPs analytical recoveries and relative standard deviation (%) for both extraction techniques. 105

Table 12. Operating conditions for spICP-MS analysis. 124

Table 13. TiO_2NPs mass concentration and mean size, and analytical recovery for a serum sample subjected to UF and to enzymatic hydrolysis (4.0 h) and UF. 129

Table 14. Instrumental conditions and data acquisition parameters for SC-ICP-MS analysis. 141

Table 15. Detected events, mean signal, median mass and number concentration of RBCs containing AgNPs (number concentration referred to the ICP-MS). Values expressed as mean ± standard deviation (n=6). 144

Table 16. Number concentration of RBCs containing 40 nm-AgNPs, silver mass concentration, and the calculated AgNPs per cell. (Conditions: dose concentration ratio 1:50 cell/NP, results expressed as mean ± standard deviation, n=6). 146

Table 17. Number concentration of RBCs containing 20 nm-AgNPs, percentage of RBCs containing 20 nm-AgNPs, and calculated AgNPs per cell. (Conditions: dose concentration ratio 1:50 cell/NP, results expressed as mean ± standard deviation, n=6). 149

USC DE COMPOSTELA

Table 18. Silver concentration in detected RBCs, expressed as mean ± standard deviation (n=6). 157

Table 19. Spiked concentrations for the gelatine solutions. 165

Table 20. Instrumental ICP-MS parameters. 167

Table 21. Gelatine quantification by ICP-MS. 168

Table 22. Number of shots per laser fluence value. 169

Table 23. TE (%) calculation for 100 nm and 30 nm AuNPs (n=3). 173

Table 24. Total number of microwells considered, number of occupied microwells, and percentage of microwell occupancy for different time intervals. 176

Table 25. Total number of microwells considered, number of occupied microwells, and percentage of microwell occupancy for different cell concentrations. 177

Table 26. Percentage of microwell occupancy for control (unexposed) and exposed Caco-2 cells (n=2). 178

USC UNIVERSIDADE DE SANTIAGO DE COMPOSTELA

ABSTRACT

USC
UNIVERSIDADE
DE SANTIAGO
DE COMPOSTELA

ABSTRACT

Nanotechnology and nanoscience currently represent one of the most dynamic and transformative fields of scientific and technological knowledge. Their evolution over recent decades, together with the development of increasingly precise characterization and imaging techniques, has enabled the design, manipulation, and application of materials at the nanometric scale, which exhibit unique properties compared to their macroscopic counterparts. These materials, known as nanomaterials (NMs), have dimensions ranging between 1 and 100 nm and possess distinctive physicochemical characteristics, such as a high surface-to-volume ratio, quantum confinement effects, exceptional optical or magnetic properties, and markedly enhanced catalytic reactivity.

The significance of nanoscience lies in its capacity to integrate diverse disciplines–including physics, chemistry, engineering, biology, medicine, and toxicology–while offering innovative solutions across multiple industrial sectors. At present, nanotechnology plays an active role in electronics, renewable energy, construction, automotive engineering, agriculture, the textile and food industries, military defence, cosmetics, and, most prominently, the healthcare sector. The global market for NMs, valued at more than 10 billion USD in 2020, exhibits an annual growth rate exceeding 17 %, anticipating an economic and social impact of major proportions.

Among the wide variety of nanomaterials under study, two categories stand out due to their extensive use and the controversy surrounding their safety: silver nanoparticles (AgNPs) and titanium dioxide nanoparticles (TiO_2NPs).

AgNPs are widely recognized for their antimicrobial, antiviral, and antifungal properties. These characteristics have led to their incorporation into thousands of consumer products, including textiles, household appliances, food packaging, personal hygiene products, and medical devices. Moreover, their applications in regenerative medicine, dentistry, and drug delivery position them as promising tools for the advancement of nanomedicine. However, both *in vitro* and *in vivo* studies have demonstrated that AgNPs can induce oxidative stress, DNA damage, alterations in cell viability and proliferation, apoptosis, and necrosis, as well as adverse effects in aquatic and terrestrial organisms. Their ability to generate reactive oxygen species (ROS) and the potential release of silver ions endow these nanoparticles with a toxic potential that cannot be overlooked.

On the other hand, TiO_2NPs, have traditionally been used as white pigments due to their opacity and brightness, as well as in industrial applications that exploit their photocatalytic properties and their capacity to scatter ultraviolet radiation. They are present in paints, coatings, plastics, cosmetics, pharmaceuticals, and, until recently, in food products as additive E171. Their ability to reflect and absorb UVA and UVB radiation made them an essential component of sunscreens. Nevertheless, recent evaluations have questioned their safety: studies have

shown that they can induce pulmonary inflammation, metabolic disturbances, genetic damage, and adverse effects on aquatic organisms and soil microorganisms. The controversy intensified following the decision of the European Union to ban the use of E171 as a food additive, due to uncertainty regarding its potential genotoxicity.

The widespread presence of these nanoparticles in the global market inevitably translates into their release into the environment. NMs, already considered emerging pollutants, reach water, soil, sediments, and the atmosphere through industrial production, the use of consumer products, and waste disposal. Once in the environment, they undergo physical, chemical, and biological transformations–such as aggregation, dissolution, photoreactions, or interactions with organic matter–that alter their behaviour, bioavailability, and toxicity. Consequently, they may accumulate in aquatic and terrestrial ecosystems, enter food chains, and disrupt biodiversity.

In the context of human health, exposure pathways are multiple: inhalation, ingestion, dermal penetration, intravenous injection, and even ocular contact. Experimental studies indicate that nanoparticles can cross biological barriers, distribute to secondary organs such as the liver, spleen, kidneys, or brain, and trigger inflammatory and immune responses. The uncertainty surrounding their long-term bioaccumulation and their potential carcinogenic or genotoxic effects positions nanotoxicology as a pressing research priority.

In this regard, the discipline of nanotoxicology has emerged as a response to the need to understand the risks associated with NM exposure. Unlike conventional toxicology, risk assessment at the nanoscale requires consideration of additional parameters, such as particle size, distribution, shape, aggregation state, surface charge, and chemical coatings. The complexity of these interactions makes the detection and characterization of nanoparticles in environmental and biological matrices a first-order analytical challenge.

Moreover, regulatory progress remains slow due to the absence of standardized definitions and the lack of reliable data on nanoparticle production, release, and actual environmental concentrations. While certain sectors—such as cosmetics, medical devices, and food—have begun to be regulated, environmental protection against NP contamination still presents significant legislative gaps. For these reasons, it is essential to justify the study and development of new analytical tools capable of detecting, quantifying, and characterizing nanoparticles with high precision and sensitivity across different matrices.

Within this context, inductively coupled plasma mass spectrometry (ICP-MS) has established itself as the most promising analytical platform for nanometrology. Its advanced modes–such as single-particle ICP-MS (spICP-MS), single-cell ICP-MS (scICP-MS), and its combination with laser ablation (LA-ICP-MS)–provide detailed information on concentrations (both in mass and particle number) and size distributions with unprecedented sensitivity. Nevertheless, their practical application to real matrices requires addressing critical challenges in calibration, extraction, and sample pretreatment; without these, the reliability and reproducibility of results remain compromised.

The thesis outlined here addresses precisely these challenges, presenting five studies that together constitute complementary chapters of a unified narrative. Its ultimate goal is to construct an integrated perspective that captures the complete trajectory of nanoparticles, from

USC DE COMPOSTELA

their presence in the environment to their interactions within human cells. To this end, each chapter develops methodological innovations tailored to a specific compartment: tap water as an environmental source of exposure (Chapter 1); urine and serum as biomonitoring matrices (Chapters 2 and 3); red blood cells as a model for cellular interactions (Chapter 4); and, finally, Chapter 5, which presents potential innovations focused on biological analysis through LA-ICP-MS.

Chapter 1: Prospects of surfactant assisted dispersive liquid-liquid microextraction for the selective extraction of silver and titanium dioxide nanoparticles from tap water and determination by spICP-MS.

The widespread use of inorganic nanoparticles (NPs), especially silver (Ag) and titanium dioxide (TiO_2) NPs, has led to growing concern about their impact on human health and the environment. Inorganic nanoparticles are present in a large variety of products including cosmetics, foodstuffs, and medical goods, and NPs releasing from consumers' products into the environment can be therefore expected. Because of the low concentration levels of NPs in water, special care must be taken when developing new reliable analytical methods. In the current research, the possibilities of surfactant-assisted dispersive liquid–liquid microextraction (SA-DLLME) in combination with single-particle inductively coupled plasma mass spectrometry (spICP-MS) have been explored/discussed. Optimum conditions for the preconcentration of TiO_2NPs and AgNPs were 10 mL of water sample, 1.0 mL of the Triton X114/1,2-dichloroethane (49:1) mixture, vortexing at 1500 rpm for 30 s, and centrifugation at 3500 rpm for 5 min. The collected organic phase was finally diluted to 1–2 mL with 1% (w/v) glycerol, leading to an enrichment factor within the 5–10 range. The developed procedure (sample pre-treatment and spICPMS) led to a size detection limit (5σ criteria) of 65.8 and 16.7 nm for TiO_2NPs and AgNPs, respectively. The limit of detection in number concentration was 6.06×10^6 L^{-1} for AgNPs and 2.85×10^6 L^{-1} for TiO_2NPs, whereas the limit of detection for dissolved Ag and Ti mass concentrations was found to be 0.435 and 9.82 ng L^{-1}, respectively. The operational simplicity, low cost and less consumption of organic solvents make SA-DLLME a greener and faster choice compared to classical liquid–liquid extraction techniques.

Chapter 2: Surfactant-assisted dispersive liquid-liquid microextraction and centrifugal ultrafiltration as potential extraction procedures for silver and titanium dioxide nanoparticles from human urine.

Inorganic nanoparticles (NPs) hold great promise in nanomedicine, cosmetics, the food industry and other human-related sectors, raising concerns about their safety and effects on biological systems. Urine shows great potential as a biological compartment for biomonitoring, but the presence of NPs in urine (basal levels) is expected to be very low and requires advanced instrumentation as well as sample pretreatment. This study reports on the use of single particle inductively coupled plasma mass spectrometry (spICP-MS) as a tool for the assessment of silver nanoparticles (AgNPs) and titanium dioxide nanoparticles (TiO_2NPs) in urine, previously extracted/preconcentrated by two different approaches: surfactant-assisted dispersive liquid–liquid microextraction (SA-DLLME) and centrifugal ultrafiltration (UF). Optimal experimental conditions for SA-DLLME were: 10 mL urine, 1.0 mL surfactant/extractant mixture, vortexing at 2000 rpm for 30 s and a final centrifugation step at 3500 rpm for 10 min. Centrifugal ultrafiltration (molecular weight cut-off (MWCO) of 30 kDa, 5000 × g, 25 min, 1 rinsing cycle with 1.0 % (v/v) glycerol) showed improved results for NP preconcentration using up to 30 mL

of urine. An improved limit of detection (number concentration) was achieved with UF (3.1 × 102 and 2.9 × 10^2 particle mL^{-1} for TiO_2NPs and AgNPs, respectively), while the analytical recovery of both methods was similar for TiO_2NPs (in the range of 77–97 % for SA-DLLME and between 74 and 99 % for UF) and from 81 to 88 %, and from 90 to 115 % for AgNPs when using SA-DLLME and UF, respectively.

Chapter 3: Enzymatic hydrolysis for pre-treating human serum before titanium dioxide nanoparticles assessment by spICP-MS.

The current use of inorganic nanoparticles (NPs) in many industrial sectors, particularly in the food industry, has led to growing concerns about the toxicity of these emerging materials to humans. Therefore, NPs assessment in foodstuff, environmental materials and biological fluids is becoming an important topic, and the development of reliable quantification/characterization analytical methods is needed. The presence of NPs in blood and urine can be expected because of the bioavailability/assimilation of these entities by the organism. However, the determination of NPs in biofluids is a challenge mainly due to the complexity of the sample and the low levels of NPs (basal levels). The research on new methodologies for sample treatment is therefore needed.

The possibilities of enzymatic hydrolysis followed by centrifugal ultrafiltration for isolating titanium dioxide nanoparticles (TiO_2NPs) from serum samples have been explored in the current research. Hydrolysis of serum′s matrix components was performed with a pancreatin-lipase mixture (0.1 % (w/v) each one) operating at pH 7.4 and 37 ºC for 4.0 h under orbital - horizontal shaking at 150 rpm. In addition, centrifugal ultrafiltration (30 kDa molecular weight cutoff (MWCO) membrane) was optimised for removing enzymes residues and other matrix′s components. The developed method showed a limit of detection of 6.89 × 10^3 NPs mL^{-1}, and a limit of detection in size of 36 nm, whereas analytical recovery for spiking assays with 100 nm TiO_2NPs were within the 103−114 % range.

Chapter 4: Silver nanoparticles behaviour in exposed human red blood cells by single cell – inductively coupled plasma – mass spectrometry.

Research concerning nanoparticles, NPs, at the single cell level is at the forefront of recent investigations. With the widespread use of silver nanoparticles (AgNPs) in fields like nanomedicine and nanobiotechnology, human exposure has increased. Investigating cellular response to NP exposure in terms of NPs distribution within a cell population is essential. In this sense, single cell (SC)-ICP-MS is a powerful and promising technique that provides quantitative information on a cell-to-cell basis. The present work, in a proof-of-principle experiment, investigates the feasibility of SC-ICP-MS for the determination of surface-adsorbed and intracellular AgNPs in exposed human red blood cells (RBCs). Firstly, RBCs were isolated from whole blood and subsequently incubated with AgNPs suspensions. The exposure was conducted at two dosing concentrations in a low cell:NP ratio of 1:1, and a higher cell:NP ratio of 1:50, for 8, 12, and 24 hours. Results showed that the low AgNPs dose concentration had a negligible effect on the uptake by cells, whereas higher doses exhibited a time-dependent uptake. Under specific conditions, the quantification yielded an estimate of 3 AgNPs $cell^{-1}$ after 8 hours of exposure, 5 AgNPs $cell^{-1}$ after 12 hours of exposure, and 8 AgNPs $cell^{-1}$ after 24 hours of exposure. SC-ICP-MS methodology proved to be an excellent tool to track and confirm the presence of AgNPs-containing cells.

USC UNIVERSIDADE DE SANTIAGO DE COMPOSTELA

Chapter 5: Advancements in LA-ICP-MS: Preliminary insights into the optimization of a new calibration approach and a microwell array design for single-cell trapping.

In this study, we report advancements for the application in LA-ICP-MS: (i) an innovative calibration approach based on gelatine microdroplets, and (ii) the design of a polydimethylsiloxane (PDMS)-based microwell array for controlled single-cell trapping. Gelatine microdroplets were prepared as spiked standards with both ionic and NP solutions, enabling complete ablation ad mitigating issues of representativeness and heterogeneity typical of conventional droplet-based approaches. Parallel, efforts focused on the fabrication and optimization of microwell arrays tailored for Caco-2 cells, ensuring efficient single-cell trapping under controlled CO_2 atmosphere. Key parameters influencing trapping efficiency– including settling time, cell concentration, cell resuspension medium, and NP exposure– were systematically evaluated. Collectively, these findings provide preliminary insights into practical calibration solutions and cell-handling strategies that advance the reliability of LA-ICP-MS, with broad implications for nanotoxicology, bioimaging, and nanomedicine.

When considered together, the five studies form a coherent narrative that traces the life cycle of nanoparticles in the body, from the point of entry to their behaviour at the cellular level. Environmental analyses reveal actual sources of exposure. Studies on serum and urine show methodologies for determining particles in circulation and in excretion products. At the cellular level, it is demonstrated that NPs can be incorporated by red blood cells, with notable variability between cells. Advances in calibration and cellular manipulation at the individual level ensure quantitative and reproducible support for LA-ICP-MS analyses. In this way, the thesis constructs a continuous exposure-effect at the organism level, from the environment to the cellular level.

This thesis is structured as a compendium of five studies: three of them published, one accepted for publication, and a final chapter that compiles initial results on laser ablation with biological applications. Each chapter is organised like a scientific article, with an abstract, introduction, materials and methods, results and discussion, conclusions, and bibliographical references, which guarantees the autonomy of each study but also its inclusion in a common research project. In addition, the thesis includes a general introduction that establishes the theoretical framework and the conceptual and methodological foundations necessary for an in-depth understanding of the studies carried out during the doctoral stage and places the work developed in the broader context of nanometrology research. The thesis's integrative discussion delves into greater detail on its development. It shows the integrative context in which the different studies are integrated and highlights the coherence between them as well as their biological relevance, both in the detection of NPs in environmental and biological matrices and in the evaluation of their behaviour and possible toxicological implications. Likewise, common limitations encountered, such as the complexity of biological samples or analytical challenges arising from low NP concentrations, are examined, and the similarities and complementarities between the different chapters are presented, establishing a bridge between them that facilitates understanding and integration into an overall vision. Finally, the general conclusions summarise the individual contributions of each study and integrate them into an overall interpretation that highlights the methodological and conceptual advances achieved, offering a set of useful analytical tools for the scientific community and representing a significant, albeit modest, contribution to the progress of the discipline.

USC UNIVERSIDADE DE SANTIAGO DE COMPOSTELA

It is also necessary to recognise the current limitations. The lack of certified reference standards for NPs prevents robust calibration and makes it difficult to compare results between different laboratories. The available methods still have problems distinguishing between particulate and dissolved analytes. The techniques presented were validated in AgNPs and TiO_2NPs, but their application needs to be extended to other nanomaterials, given that there is a wide range of possibilities. In addition, detection-focused analyses must be complemented by toxicological tests that allow the presence of nanoparticles to be correlated with specific cellular effects, such as DNA damage, inflammatory responses, or metabolic alterations.

In short, the thesis summarised here should not be understood as a sum of isolated technical innovations, but rather as the construction of an integrated whole that improves our ability to detect and quantify nanoparticles in different contexts, linking environmental matrices as sources of exposure and reaching down to the cellular level to reveal direct interactions. Its contribution is twofold: on the one hand, it provides a powerful and transferable methodological arsenal; on the other, it offers a conceptual framework that integrates the environment and the organism into a common narrative of exposure and effect. Thus, it places nanometrology in a strategic position to address the challenges of current nanotoxicology, consolidating the bridge between analytical innovation, biological relevance and social utility.

USC
UNIVERSIDADE DE SANTIAGO DE COMPOSTELA

RESUMO

USC
UNIVERSIDADE
DE SANTIAGO
DE COMPOSTELA

RESUMO

A nanotecnoloxía e a nanociencia representan na actualidade un dos campos máis dinámicos e transformadores do coñecemento científico e tecnolóxico. A súa evolución nas últimas décadas, unida ao desenvolvemento de técnicas de caracterización e imaxe cada vez máis precisas, permitiu o deseño, manipulación e aplicación de materiais a escala nanométrica con propiedades únicas fronte aos seus homólogos macroscópicos. Estes materiais, denominados nanomateriais (NMs), teñen dimensións comprendidas entre 1 e 100 nm e posúen características físico-químicas particulares, como unha elevada relación superficie/volume, efectos de confinamento cuántico, propiedades ópticas ou magnéticas excepcionais, así como unha reactividade catalítica moi superior.

A importancia da nanociencia radica na súa capacidade para integrar disciplinas diversas–como a física, a química, a enxeñaría, a bioloxía, a medicina ou a toxicloxía–ofrecendo solucións innovadoras en múltiples sectores industriais. Actualmente, a nanotecnoloxía atópase presente en electrónica, enerxías renovables, construción, automoción, agricultura, industria téxtil e alimentaria, defensa, cosmética e, de maneira destacada, no ámbito sanitario. O mercado global dos NMs, valorado en máis de 10.000 millóns de dólares no ano 2020, presenta unha taxa de crecemento anual superior ao 17 %, o que anticipa un impacto económico e social de primeira magnitude.

Entre a gran diversidade de nanomateriais estudados, dúas categorías destacan polo seu uso estendido e pola controversia xerada en relación coa súa seguridade: as nanopartículas de prata (AgNPs) e as nanopartículas de dióxido de titanio (TiO_2NPs).

As AgNPs son amplamente recoñecidas polas súas propiedades antimicrobianas, antivirais e antifúnxicas. Estas características fixeron posible a súa incorporación a milleiros de produtos de consumo, incluíndo téxtiles, electrodomésticos, envases de alimentos, produtos de hixiene persoal e dispositivos médicos. Ademais, as súas aplicacións na medicina rexenerativa, na odontoloxía e na administración de fármacos sitúanas como unha ferramenta prometedora no desenvolvemento da nanomedicina. Porén, estudos *in vitro* e *in vivo* demostraron que as AgNPs poden inducir estrés oxidativo, danos no ADN, alteracións na viabilidade e proliferación celular, apoptose e necrose, así como efectos adversos en organismos acuáticos e terrestres. A súa capacidade para xerar especies reactivas de osíxeno (ROS) e a posible liberación de ións de prata confiren a estas nanopartículas un potencial tóxico que non pode ser ignorado.

Pola súa parte, as TiO_2NPs empregáronse tradicionalmente como pigmentos brancos pola súa opacidade e brillo, así como en aplicacións industriais que aproveitan as súas propiedades fotocatalíticas e de dispersión da radiación ultravioleta. Están presentes en pinturas, recubrimentos, plásticos, cosméticos, produtos farmacéuticos e, ata hai pouco, tamén en alimentos como aditivo E171. A súa capacidade para reflectir e absorber radiacións UVA e UVB converteunas en compoñente esencial de cremas solares. Non obstante, recentes

USC DE COMPOSTELA

avaliacións puxeron en cuestión a súa inocuidade: estudos demostraron que poden inducir inflamación pulmonar, alteracións metabólicas, danos no material xenético e efectos adversos sobre organismos acuáticos e microorganismos do solo. A controversia intensificouse tras a decisión da Unión Europea de prohibir o uso do aditivo E171 en alimentación debido á incerteza sobre a súa potencial xenotoxicidade.

A presenza masiva destas nanopartículas no mercado global tradúcese inevitabelmente na súa liberación ao medio ambiente. Os NMs, considerados xa contaminantes emerxentes, chegan ás augas, solos, sedimentos e atmosfera a través da produción industrial, do uso de produtos de consumo e da eliminación de residuos. Unha vez no medio, sofren procesos de transformación física, química e biolóxica–como agregación, disolución, fotorreaccións ou interacción con materia orgánica–que modifican o seu comportamento, biodispoñibilidade e toxicidade. Así, poden acumularse en ecosistemas acuáticos e terrestres, entrar nas cadeas tróficas e provocar alteracións na biodiversidade.

No eido da saúde humana, as vías de exposición son múltiples: inhalación, inxestión, penetración dérmica, inxección intravenosa e mesmo contacto ocular. Estudos experimentais sinalan que as nanopartículas poden atravesar barreiras biolóxicas, distribuírse a órganos secundarios como fígado, bazo, riles ou cerebro, e desencadear respostas inflamatorias e inmunitarias. A incerteza sobre a súa bioacumulación a longo prazo e os seus posibles efectos carcinoxénicos ou xenotóxicos sitúa a nanotoxicidade como unha prioridade de investigación.

Neste contexto, a disciplina da nanotoxicología emerxe como resposta á necesidade de comprender os riscos asociados á exposición a NMs. A diferenza da toxicología convencional, a avaliación de riscos a nivel nano require considerar parámetros adicionais como tamaño, distribución, forma, estado de agregación, carga superficial e recubrimentos químicos. A complexidade destas interaccións fai que a determinación e caracterización das nanopartículas en matrices ambientais e biolóxicas constitúa un desafío analítico de primeira orde.

Ademais, a regulación segue avanzando con dificultade debido á ausencia de definicións normalizadas e á falta de datos fiables sobre produción, liberación e concentración ambiental real de nanopartículas. Mentres que algúns sectores–como os cosméticos, dispositivos médicos e alimentos–comezan a estar regulados, a protección ambiental fronte á contaminación por NPs aínda presenta importantes lagoas lexislativas. Por todo isto, resulta fundamental xustificar o estudo e desenvolvemento de novas ferramentas analíticas que permitan detectar, cuantificar e caracterizar as nanopartículas con precisión e sensibilidade en diferentes matrices.

Neste contexto, a espectrometría de masas con plasma acoplado indutivamente (ICP-MS) impúxose como a plataforma analítica máis prometedora para a nanometroloxía. Os seus modos avanzados, como o single-particle ICP-MS (spICP-MS), o single-cell ICP-MS (SC-ICP-MS) ou a combinación con ablación láser (LA-ICP-MS), permiten obter información sobre concentracións (en masa e en número de partículas) e distribucións de tamaños cunha sensibilidade sen precedentes. Non obstante, a súa aplicación práctica en matrices reais require resolver problemas de calibración, extracción e pretratamento de mostra que, de non abordarse, comprometen a fiabilidade e a reproducibilidade dos resultados.

A tese da que se ofrece aquí unha visión panorámica, aborda precisamente estes retos, amosando cinco estudos que funcionan como capítulos complementarios dun relato común. O seu obxectivo último é construír unha narrativa integrada que permita comprender o percorrido

USC DE COMPOSTELA

completo das nanopartículas dende o medio ambiente até o interior de células humanas. Para iso, cada capítulo desenvolve innovacións metodolóxicas adaptadas a un compartimento distinto: auga da billa como fonte ambiental de exposición (capítulo 1), ouriños e soro como matrices de biomonitorización (capítulos 2 e 3), glóbulos vermellos (capítulo 4) como modelo de interacción celular, e un último capítulo (capítulo 5) onde se presentan posibles innovacións enfocadas á análise biolóxica mediante LA-ICP-MS.

Capítulo 1: Perspectivas da microextracción líquido-liquido dispersiva asistida por tensioactivos (SA-DLLME) para a extracción selectiva de nanopartículas de prata e dióxido de titanio en auga da billa e determinación mediante spICP-MS.

O uso xeneralizado de nanopartículas inorgánicas (NPs), especialmente de prata (Ag) e de dióxido de titanio (TiO_2), xerou unha crecente preocupación acerca do seu impacto na saúde humana e no medio ambiente. As nanopartículas inorgánicas están presentes nunha gran variedade de produtos, incluídos cosméticos, alimentos e artigos médicos, polo que se pode esperar a liberación de NPs desde os produtos de consumo cara ao medio ambiente. Debido ás baixas concentracións de NPs na auga, é necesario ter especial coidado ao desenvolver novos métodos analíticos confiables. Na presente investigación exploráronse as posibilidades da microextracción líquido–líquido dispersiva asistida por tensioactivos (SA-DLLME, polas súas siglas en inglés) en combinación coa espectrometría de masas con plasma axustado inductivamente de partícula única (spICP-MS). As condicións óptimas para a preconcentración de TiO_2NPs e AgNPs foron: 10 mL de mostra de auga, 1,0 mL da mestura Triton X114/1,2-dicloroetano (49:1), axitación con vórtex a 1500 rpm durante 30 s e centrifugación a 3500 rpm durante 5 min. A fase orgánica colleitada diluíuse finalmente a 1–2 mL con glicerol ao 1 % (p/v), o que conduciu a un factor de enriquecemento no rango de 5–10. O procedemento desenvolvido (pretratamento da mostra e spICP-MS) permitiu obter un límite de detección en tamaño (criterio 5σ) de 65,8 e 16,7 nm para TiO_2NPs e AgNPs, respectivamente. O límite de detección en concentración numérica foi de $6{,}06 \times 10^6$ L^{-1} para AgNPs e $2{,}85 \times 10^6$ L^{-1} para TiO_2NPs, mentres que o límite de detección para as concentracións másicas disoltas de Ag e Ti foi de 0,435 e 9,82 ng L^{-1}, respectivamente. A simplicidade operativa, o baixo custo e o menor consumo de disolventes orgánicos fan que SA-DLLME sexa unha opción máis ecolóxica e rápida en comparación coas técnicas clásicas de extracción líquido–líquido.

Capítulo 2: Microextracción líquido-líquido dispersiva asistida por tensioactivos e ultrafiltración como posibles procedementos de extracción de nanopartículas de prata e dióxido de titanio de mostras de ouriños.

As nanopartículas inorgánicas (NPs) teñen un gran potencial na nanomedicina, a cosmética, a industria alimentaria e outros sectores relacionados co ser humano, o que xera preocupación acerca da súa seguridade e os seus efectos sobre os sistemas biolóxicos. Os ouriños amosan un gran potencial como compartimento biolóxico para a biomonitorización, pero espérase que a presenza de NPs en ouriños (niveis basais) sexa moi baixa e requira instrumentación avanzada, así como un pretratamento da mostra. Este estudo pretende reflexar o uso da espectrometría de masas con plasma acoplado inductivamente de partícula única (spICP-MS) como ferramenta para a avaliación de nanopartículas de prata (AgNPs) e de dióxido de titanio (TiO_2NPs) en ouriños, previamente extraídas/preconcentradas mediante dous enfoques diferentes: a microextracción líquido–líquido dispersiva asistida por tensioactivos

(SA-DLLME) e a ultrafiltración (UF). As condicións experimentais óptimas para SA-DLLME foron: 10 mL de ouriños, 1,0 mL da mestura tensioactivo/extractante, axitación en vórtex a 2000 rpm durante 30 s e un paso final de centrifugación a 3500 rpm durante 10 min. A ultrafiltración (cun corte de peso molecular–MWCO–de 30 kDa, 5000 × g, 25 min, 1 ciclo de enxaugue con glicerol ao 1,0 % (v/v)) mostrou mellores resultados para a preconcentración de NPs utilizando ata 30 mL de ouriños. Alcanzouse un mellor límite de detección (en concentración numérica) con UF ($3{,}1 \times 10^2$ e $2{,}9 \times 10^2$ partículas mL^{-1} para TiO_2NPs e AgNPs, respectivamente), mentres que a recuperación analítica de ámbolos métodos foi similar para TiO_2NPs (no rango de 77–97 % para SA-DLLME e entre 74 e 99 % para UF) e do 81 ao 88 %, e do 90 ao 115 % para AgNPs ao usar SA-DLLME e UF, respectivamente.

Capítulo 3: Hidrólise enzimática para o pretratamento de soro humano antes da avaliación de nanopartículas de dióxido de titanio mediante spICP-MS.

O uso actual de nanopartículas inorgánicas (NPs) en moitos sectores industriais, particularmente na industria alimentaria, xerou unha crecente preocupación sobre a toxicidade destes materiais emerxentes nos seres humanos. Por iso, a avaliación de NPs en alimentos, materiais ambientais e fluídos biolóxicos está a converterse nun tema importante, e necesítase o desenvolvemento de métodos analíticos fiables de cuantificación/caracterización. A presenza de NPs en sangue e ouriños pode esperarse debido á biodispoñibilidade e á asimilación destas entidades polo organismo. Con todo, a determinación de NPs en biofluídos constitúe un desafío principalmente pola complexidade da mostra e os baixos niveis de NPs (niveis basais). Por tanto, requírese investigación en novas metodoloxías para o tratamento de mostras. Na presente investigación exploráronse as posibilidades da hidrólise enzimática seguida de ultrafiltración para o illamento de nanopartículas de dióxido de titanio (TiO_2NPs) a partir de mostras de soro. A hidrólise dos compoñentes da matriz do soro levouse a cabo cunha mestura pancreatina-lipasa (0,1 % (p/v) cada unha) operando a pH 7,4 e 37 ºC durante 4,0 h, con axitación orbital-horizontal a 150 rpm. Ademais, optimizouse a ultrafiltración (membrana con límite de corte de peso molecular (MWCO) de 30 kDa) para eliminar residuos enzimáticos e outros compoñentes da matriz. O método desenvolvido mostrou un límite de detección de $6{,}89 \times 10^3$ NPs mL^{-1} e un límite de detección en tamaño de 36 nm, mentres que a recuperación analítica en ensaios de adición con TiO_2NPs de 100 nm estivo no rango do 103–114 %.

Capítulo 4: Estudo do comportamento das nanopartículas de prata en glóbulos vermellos humanos expostos mediante espectrometría de masas con plasma de acoplamento inductivo a nivel de célula individual (SC-ICP-MS).

A investigación sobre nanopartículas (NPs) a nivel celular individual atópase á vangarda dos estudos recentes. Co uso xeneralizado de nanopartículas de prata (AgNPs) en campos como a nanomedicina e a nanobiotecnoloxía, a exposición humana aumentou. Investigar a resposta celular á exposición a NPs en termos da súa distribución dentro dunha poboación celular resulta esencial. Neste sentido, a espectrometría de masas con plasma acoplado inductivamente a nivel de célula individual (SC-ICP-MS) é unha técnica poderosa e prometedora que proporciona información cuantitativa célula por célula. O presente traballo, nun experimento de proba de concepto, investiga a viabilidade de SC-ICP-MS para a determinación de AgNPs adsorbidas na superficie e de AgNPs intracelulares en glóbulos vermellos humanos (RBCs, das súas siglas en inglés) expostos. En primeiro lugar, illáronse RBCs a partir de sangue total e posteriormente incubaronse con suspensións de AgNPs. A exposición levouse a cabo con dúas concentracións:

nunha relación baixa célula:NP de 1:1 e nunha relación alta célula:NP de 1:50, durante 8, 12 e 24 horas. Os resultados amosaron que a dose baixa de AgNPs tivo un efecto insignificante na captación celular, mentres que as doses máis altas mostraron unha captación dependente do tempo. Baixo condicións específicas, a cuantificación estimouse aproximadamente en 3 AgNPs por célula tras 8 horas de exposición, 5 AgNPs por célula tras 12 horas de exposición e 8 AgNPs por célula tras 24 horas de exposición. A metodoloxía SC-ICP-MS demostrou ser unha excelente ferramenta para rastrexar e confirmar a presenza de células que conteñen AgNPs.

Capítulo 5: Avances en LA-ICP-MS: resultados preliminares sobre a optimización dun novo enfoque de calibración e o deseño dun material baseado en micropozos para o illamento individual de células.

Neste estudo preséntanse avances para a aplicación en LA-ICP-MS: (i) un enfoque novo de calibración baseado en microgotas de xelatina, e (ii) o deseño dunha matriz de micropozos de polidimetilsiloxano (PDMS) para a captura controlada de células individuais. As microgotas de xelatina preparáronse como estándares enriquecidos tanto con solucións iónicas como con solucións de NPs, o que permitiu unha ablación completa e mitigou os problemas de representatividade e heteroxeneidade típicos dos enfoques convencionais baseados en pingas de maior tamaño. De forma paralela, realizáronse esforzos na fabricación e optimización de matrices de micropozos adaptadas a células Caco-2, garantindo unha captura eficiente de células individuais baixo atmosfera controlada de CO_2. Avaliáronse sistematicamente os parámetros crave que inflúen na eficiencia de captura, incluíndo o tempo de sedimentación, a concentración celular, o medio de resuspensión celular e a exposición a NPs. En conxunto, estes achados proporcionan información preliminar sobre solucións prácticas de calibración e estratexias de manipulación celular que melloran a fiabilidade de LA-ICP-MS, con amplas implicacións en nanotoxicoloxía, bioimaxen e nanomedicina.

Se se consideran conxuntamente, os cinco estudos conforman unha narrativa coherente que percorre o ciclo de vida das nanopartículas no organismo, dende o punto de entrada até o comportamento a nivel celular. As análises ambientais evidencian fontes reais de exposición. Os estudos en soro e ouriños amosan metodoloxías para poder determinar partículas en circulación e en produtos de excreción. A nivel celular, demóstrase que as NPs poden ser incorporadas por glóbulos vermellos, con variabilidade notable entre células. Os avances en calibración e manipulación celular a nivel individual aseguran un respaldo cuantitativo e reproducible para as análises por LA-ICP-MS. Deste modo, a tese constrúe un continuo exposición-efecto a nivel organismo, dende o medio ambiente ata o nivel celular.

A presente tese estrutúrase como compendio de cinco estudos: tres deles publicados, un aceptado para publicación e un último capítulo que recolle resultados iniciais sobre ablación láser con aplicacións biolóxicas. Cada capítulo presenta unha organización propia de artigo científico, con resumo, introdución, materias e métodos, resultados e discusión, conclusións e referencias bibliográficas o que garante a autonomía de casa estudo pero tamén a súa inserción nun proxecto investigador común. Complementariamente, a tese inclúe unha introdución xeral que establece o marco teórico e os fundamentos conceptuais e metodolóxicos precisos para comprender en profundidade os estudos realizados ao longo da etapa de doutoramento e sitúa os traballos desenvoltos nun contexto máis amplo da investigación en nanometroloxía. Na discusión integradora da tese afóndase con maior detalle no desenvolvemento da mesma. Amósase o contexto integrador no que se integran os distintos estudos e destácase a coherencia

USC DE COMPOSTELA

entre eles así como a súa relevancia biolóxica, tanto na detección de NPs en matrices ambientais e biolóxicas como na avaliación do seu comportamento e posibles implicacións toxicolóxicas. Así mesmo, examínanse as limitacións comúns atopadas, tales como a complexidade das mostras biolóxicas ou os retos analíticos derivados das baixas concentracións de NPs, e preséntanse as similitudes e complementariedades entre os distintos capítulos, establecendo unha ponte entre eles que facilite a comprensión e a integración nunha visión en conxunto. Finalmente, nas conclusións xerais sintetízanse as contribucións individuais de cada estudo e intégranse nunha interpretación global que pon en valor o avance metodolóxico e conceptual acadado, ofrecendo un conxunto de ferramentas analíticas útiles para a comunidade científica e representando unha contribución significativa, aínda que modesta, ao progreso da disciplina.

Cómpre recoñecer tamén as limitacións actuais. A falta de estándares certificados de referencia para NPs impide unha calibración robusta e dificulta a comparativa entre distintos laboratorios. Os métodos dispoñibles seguen tendo problemas para distinguir entre analíticos particulado e disoltos. As técnicas presentadas foron validadas en AgNPs e TiO_2NPs, pero cómpre estender a súa aplicación a outros nanomateriais, dado que existe un amplo abanico de posibilidades. Ademais, as análises centradas na detección deben complementarse con ensaios toxicolóxicos que permitan correlacionar a presenza de nanopartículas con efectos celulares concretos, como danos no ADN, respostas inflamatorias ou alteracións metabólicas.

En definitiva, a tese que aquí se sintetiza non debe entenderse como unha suma de innovacións técnicas illadas, senón como a construción dun todo integrado que mellora a nosa capacidade de detectar e cuantificar nanopartículas en diferentes contextos, que vincula fontes ambientais como fontes de exposición e que chega até a escala celular para revelar interaccións directas. A súa contribución é dobre: por unha banda, achega un arsenal metodolóxico robusto e transferible; pola outra, ofrece un marco conceptual que integra medio ambiente e organismo nun relato común de exposición e efecto. Así, sitúa a nanometroloxía nun lugar estratéxico para afrontar os retos da nanotoxicoloxía actual, consolidando a ponte entre innovación analítica, relevancia biolóxica e utilidade social.

USC
UNIVERSIDADE DE SANTIAGO DE COMPOSTELA

I. INTRODUCTION

USC
UNIVERSIDADE
DE SANTIAGO
DE COMPOSTELA

1 INTRODUCTION TO NANOTECHNOLOGY

The dawn of nanomaterials (NMs) is thought to be the Big Bang where nanostructured materials originated during the formation of the universe from the early meteorites [1]. Thereafter, volcanic ash, ocean spray, rocks weathering, radioactive decay, and forest fire products became the principal natural sources of NMs. Since the early 2000s, scientific interest on nanotechnology has grown exponentially. Advancements in imaging techniques have significantly propelled nanoscience and nanotechnology research, opening the door to industrial applications. NMs exhibit unique physicochemical properties that markedly differentiate them from their bulk counterparts. Currently, nanotechnology integrates multiple disciplines, including chemistry, biology, physics, engineering, medicine, and toxicology, with NMs being presented as innovative solutions to improve the quality of life.

1.1 HISTORY, SCIENTIFIC STORY AND TODAY'S GLOBAL LANDSCAPE

Although NMs have only been a hot topic for the past 25 years, they have been employed by ancient civilizations since prehistoric times. Analysis of prehistoric cave paintings in the Sulawesi caves of Indonesia and the Chauvet-Pont-d'Arc cave in France revealed the presence of carbon NMs derived from the soot and waxes used for painting, dating back to approximately 40,000 and 34,000 BCE, respectively [2,3]. Other examples of the use of NMs by ancient civilizations are the blue pigments, Egyptian blue ($CaCuSi_4O_{10}$) and Han blue ($BaCuSi_4O_{10}$) [4–6]. Historical and archaeological evidence indicates that Egyptian blue was being synthesized in Egypt during the third millennium BCE. Similarly, Han blue was found on Chinese artefacts from the Han dynasty epoch (208 BCE-220 CE). Several examples exist for the use of nanoparticles (NPs) by glass-artisans [7–10]. Red glasses found in Italy (1200-200 BCE) were coloured due to the presence of copper (Cu) NPs in the matrix. Likewise, Celtic red enamels dated from 400 and 100 BCE contained CuNPs and cuprite (Cu_2O). The use of metallic NPs spread during the Roman period [11,12]. This is the case of the famous 4th-century CE Roman glass Lycurgus Cup, now part of the collection of the British Museum [13]. It is renowned for its dichroic glass effect; this is, changing colour based on light direction. It looks opaque greenish-yellow when lit from the outside but shows a translucent red when lit from inside. Analysis of the glass revealed that the dichroism is caused by the presence of a silver-gold (Ag-Au) NPs alloy [14]. Afterwards, glass manufacturing spread considerably, and 9th century saw the emergence of lustreware, a special type of pottery decoration that generates an iridescent effect [15–17]. This lustre contains mainly Ag and CuNPs, among other NPs, dispersed in the ceramic glaze. During the mid-19th century, the famous Satsuma glasses that had CuNPs incorporated, were produced in Japan following a similar technique [18]. Likewise, during 6th-15th centuries, glass windows of European cathedrals owed their vibrant colours to the presence of Au, Ag and other metal oxides NPs [19].

USC UNIVERSIDADE DE SANTIAGO DE COMPOSTELA

However, the scientific story of nanotechnology began much later. For ease of reference, Figure 1 presents the major breakthroughs and milestones that have defined nanotechnology over the years.

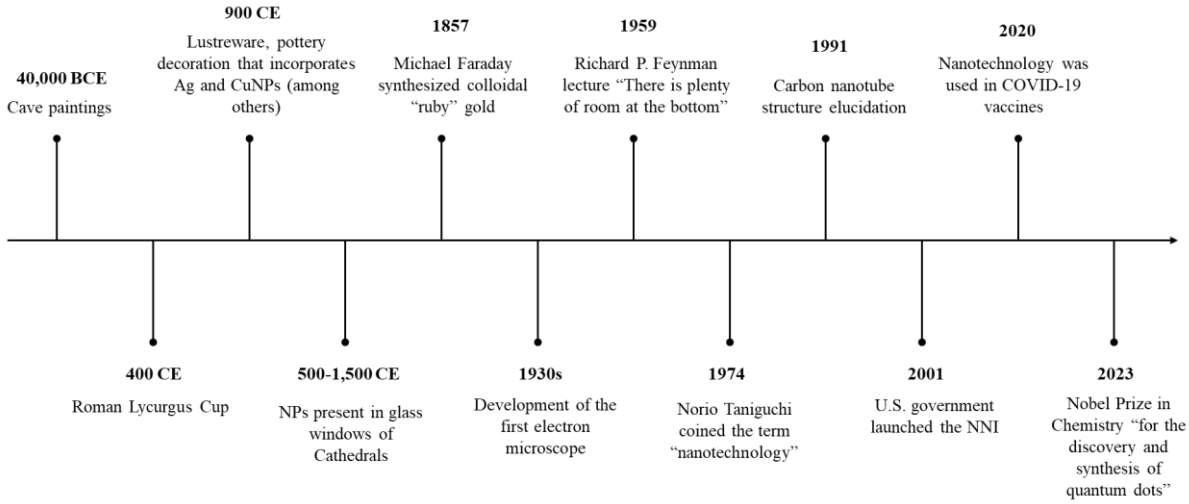

Figure 1. Timeline of major breakthroughs and milestones in nanotechnology from ancient times to nowadays.

The origin reports us back to 1857, when Michael Faraday documented the synthesis of colloidal "ruby" gold, and demonstrated that AuNPs produces different coloured solutions under specific lighting conditions [20]. A major milestone was the development of electron microscopy (EM) and the later application of field emission (FEM) allowing near-atomic-resolution images in the 1930s [21]. Years later, in 1951, Erwin Müller pioneered the field ion microscope (FIM) to image individual tungsten atoms. The famous lecture "There is plenty of room at the bottom" by Richard P. Feynman in 1959 marked a turning point. Today, it is considered the first lecture on technology and engineering at the atomic scale, and the origin of the nanotechnological paradigm [22]. However, it was not until 1974 that Japanese scientist Norio Taniguchi (Tokyo Science University) formulated the term "nanotechnology" to describe processing of materials with atomic-scale accuracy [23]. In 1986, Eric Drexler published *Engines of Creation: The Coming Era of Nanotechnology*, significantly contributing to the dissemination of the idea within both scientific and public spheres [24]. The same year, Gerd Binning and Heinrich Rohrer (IBM Zurich) won the Nobel Prize in Physics for their design of the scanning tunneling microscope (STM) in 1981 [25]. Three years later, in 1989, scientists at IBM's Almaden Research Centre, succeeded at manipulating individual Xenon atoms to spell out the IBM logo [26]. This fact demonstrated what Feynman predicted back in the day when he foresaw the future of nanotechnology, "*the principles of physics, as far as I can see, do not speak against the possibility of manoeuvring things atom by atom*". During the 1990s, enormous progress was made to advance in the field [24,26]. In 1991, Sumio Iijima discovered the carbon nanotube (CNT); in 1992, C.T. Kresge discovered the nanostructured catalytic materials MCM-41 and MCM-48; in 1993, Moungi Bawendi invented a method for controlled synthesis of nanocrystals (quantum dots); in 1999, Chad Mirkin invented dip-pen nanolithography. The growing scientific interest and significant progress made thus far laid the groundwork for the boom of the nanotechnology era. To promote nanoscale science and technology, the U.S.

USC DE SANTIAGO DE COMPOSTELA

government launched the National Nanotechnology Initiative (NNI) in 2001, becoming the first country to run a state-funded program on nanotechnology. Since then, the first consumer products based on nanotechnology appeared on the market, and new developments continue to emerge as we speak. Several examples can be cited: in 2003, N. Halas, J. West, R. Drezek, and R. Pasqualini developed size-tuned gold nanoshells; in 2006, J. Tour *et al.* built a nanoscale car made of oligo (phenylene ethynylene); in 2016, researchers at Berkeley Lab created a transistor with a working 1-nanometer gate; in 2019, M. Stevens and S. Bhatia engineered an innovative diagnostic device using nanosensors linked to gold nanoclusters, which changes colour when cancer biomarkers are detected; in 2020, lipid NPs were employed as drug carriers in the COVID-19 mRNA vaccines developed by Pfizer-BioNTech and Moderna; and in 2023, the Nobel Prize in Chemistry was awarded to Moungi G. Bawendi, Louis E. Brus and Aleksey Yekimov "for the discovery and synthesis of quantum dots" [25]. All this enthusiasm was reflected in the growing number of publications on the subject over these years, as shown in Figure 2.

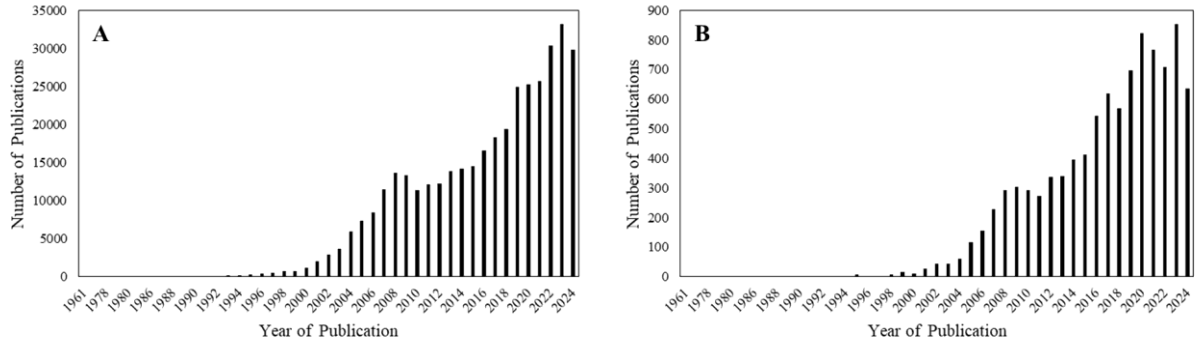

Figure 2. Number of publications in Web of Science database from 1961 to 2024 using "nanoscience" or "nanotechnology" as keyword in (A) the world and (B) Spain.

Nanotechnology has transformed and benefited nearly all industrial domains to date, and its further growth is projected to lead to emerging uses and applications. The global NMs market was estimated at USD 10.3 billion in 2020 and is expected to grow to USD 38.1 billion by 2029 at a compound annual growth rate (CAGR) of 17.8 %. In volume, the global NMs market size accounted for 11 million tonnes [27]. According to Nanotechnology Products Database (NPD), there are currently available more than 11,100 nanotechnology-based consumer products, being electronics the leading sector [28]. Nonetheless, nanotechnology plays an important role in aerospace and defence industries, healthcare and cosmetics, agriculture, sports and fitness, renewable energies, construction and automotive, home appliances, textiles, food/beverages, and environment [9,28–31]. A few examples can be listed for each industrial application. In electronics, the major application of NMs is in lighting technologies (LEDs and OLEDs), in integrated circuits, lasers, sensors, and processors. The healthcare and cosmetic sector uses NMs for tissue engineering, pharmaceuticals, medical supplies (respiratory masks, detection kits, wound dressing, disinfectant solution, etc.), skin care, personal care and make-up products (sunscreen, lotions, nail polish, toothpaste, etc.). The agriculture industrial sector includes NMs in fertilizers, in animal husbandry products such as supplements or antibiotics, and in plant breeding (plant growth regulator, seed speed, fruit enhancer). Nanotechnology flourished in various areas of sports and fitness as water- and stain-

USC DE COMPOSTELA

repellent, wrinkle-free and anti-bacterial clothing, shoes soccer, football, and baseball reinforce with CNTs, and to improve flexibility, resistance and durability in tennis, badminton and squash rackets. Renewable energies sector benefits from nanotechnology including it in batteries, solar and fuel cells, and in power transmission connectors. Construction industry is also one of the biggest sectors that incorporates nanotechnology, mainly in masonry materials, decoration and structural materials. Maintenance and auto parts and additives are the target products in the automative sector, mainly to improve scratch and corrosion resistance, UV protection, car polish, and friction resistance. The military uses nanotechnology to develop more sensitive sensor systems to biological agents and drugs. In the home appliance industry, nanostructured materials are exploited as housecleaning products and in cookware design to improve heat insulation, stain resistance and lightweight properties. In the field of textile, nanotechnology is used to produce fibres, yarns, and fabrics taking advantage of anti-bacterial and anti-microbial activity, odour resistant, quick-drying and anti-static properties. The largest manufacturing sector in the world among all industrial divisions is the food industry. In this regard, nanotechnology is poised to improve food growth and packaging. Nanotechnology is also penetrating in the environment industry to assist with air and soil remediation, as well as water and wastewater purification.

1.2 NANOMATERIALS: DEFINITION, CLASSIFICATION AND PROPERTIES

Nanoscience and nanotechnology are two research disciplines dedicated to the study and manipulation of matter at the nanometre scale. To date, several international organizations and regulatory committees have proposed scientific definitions for the term 'nanomaterial' (NM), although consensus has not been reached. According to International Organization for Standardization (ISO) ISO/TS 80004-1 [32] nanomaterial is a "material with any external dimension in the nanoscale (length range approximately from 1 nm to 100 nm) or having internal structure or surface structure in the nanoscale" . This definition is also supported by the European Standardisation Committee (CEN). In 2006, the Organisation for Economic Co-operation and Development (OECD) established the Working Party on Manufactured Nanomaterials (WPMN) and agreed upon the definition of nanomaterial as "material which is either a nano-object or is nanostructured" [33]. On the other hand, the EU Scientific Committee on Emerging and Newly Identified Health Risks (SCENIHR) provided the following suggestion for NM definition: "any form of a material that is composed of discrete functional parts, many of which have one or more dimensions of the order of 100 nm or less" [34]. The EU Scientific Committee on Consumer Products (SCCP) issued in 2007 a glossary of terms, where nanomaterial means "material with one or more external dimensions, or and internal structure, on the nanoscale, which could exhibit novel characteristics compared to the same material without nanoscale features" [35]. The American Chemistry Council (ACC) states that "an engineered nanomaterial is any intentionally produced material that has a size in 1, 2, or 3-dimensions of typically between 1-100 nanometers. It is noted that neither 1 nm nor 100 nm is a 'bright line' and data available for materials outside of this range may be valuable" [33]. The ACC also specifies that the following are included in the definition:

(a) "Buckyballs are also included even though they have a size < 1 nm
(b) Aggregates and agglomerates with size > 100 nm are included if breakdown may occur creating particles in the 1-100 nm range during the lifecycle"

USC UNIVERSIDADE DE SANTIAGO DE COMPOSTELA

And that the following are specifically excluded from being 'engineered nanomaterials':

(a) "Materials that do not have properties that are novel/unique/new compared to the non nanoscale form of a material of the same composition
(b) Materials that are soluble in water or in biologically relevant solvents
(c) For those particles that have a particle distribution such that exceeds the 1-100 nm range (e.g. 50-500 nm) if less than 10 % of the distribution falls between 1-100 nm it may be considered as non an engineered nanomaterial. The 10 % level may be on a mass or surface are basis, whichever is more inclusive
(d) Micelles and single polymer molecules"

In 2011, the European Commission (EC) adopted the first definition of nanomaterial in the 2011/696/EU Recommendation. Nonetheless, this recommendation has recently been updated by 2022/C 229/01 [36], where nanomaterial means "a natural, incidental or manufactured material consisting of solid particles that are present, either on their own or as identifiable constituent particles in aggregates or agglomerates, and where 50 % or more of these particles in the number-based size distribution fulfil at least one of the following conditions:

(a) One or more external dimensions of the particle are in the size range 1 nm to 100 nm;
(b) The particle has an elongated shape, such as a rod, fibre or tube, where two external dimensions are smaller than 1 nm and the other dimension is larger than 100 nm;
(c) The particle has a plate-like shape, where on external dimension is smaller than 1 nm and the other dimensions are larger than 100 nm".

So far, the EC NM definition has received the most support from the scientific community and international committees. In turn, the ISO also provides a definition for the term 'nanoparticle' as "nano-object with all external dimensions in the nanoscale", being nano-object a "discrete piece of material with one, two or three external dimensions in the nanoscale" [32].

NMs are frequently classified into four main categories according to their composition: carbon-based, inorganic, organic nanomaterials, and hybrid nanocomposites. Some authors divide inorganic NMs into metals and metal oxides, and non-metal inorganics due to the relevance of the metallic group [37]. Metals and metal oxides are by far the most prevalent NMs in consumer products, with silver (Ag), gold (Au) and titanium dioxide (TiO_2) NPs topping the list. Inorganic (non-metal-containing) NMs include semiconductor nanocrystals such as CdS quantum dots (QDs) and aluminosilicates like zeolites and clays. Nanocarbon materials encompass a range of structures, including nanodiamonds, fullerenes, nanotubes, and two-dimensional nanoplates such as graphene and graphene oxide. Organic NMs include polymers, dendrimers, micelles, liposomes, and ferritin. Nonetheless, alternative classifications are also made and widely reported in the literature [1,38].

Based on dimensionality, we can find zero-dimensional (0D), one-dimensional (1D), two-dimensional (2D), and three-dimensional (3D) materials. 0D NMs have all three

USC DE SANTIAGO DE COMPOSTELA

dimensions within the nanoscale (< 100 nm), as seen in NPs and QDs. 1D NMs, such as nanotubes, nanowires, and nanofilaments, have one dimension exceeding 100 nm, while the other two remain in the nanoscale. 2D materials have two dimensions outside the nanometre scale, with graphene being the best example. 3D materials present all three dimensions above 100 nm, and are often box-shaped structures, such as 3D WO_3 nanowire network.

According to their origin, NMs can be categorized as natural, incidental or engineered. Natural NMs occur as a result of (bio)geochemical or mechanical natural processes. Some examples are wax crystals that coat lotus leaves, nacre, corals, the gecko foot spatulas, volcanic ash, and ocean spray. Incidental NMs are unintentional by-products of human activity, such as vehicle exhaust gases, welding gases, solid fuel heating, and combustion during cooking. Engineered NMs (ENMs) are human-produced materials for specific applications. Within this category, bioinspired NMs represent a specific type of ENMs whose properties mimic those of natural NMs or biological systems.

The physicochemical properties of NMs are directly related to the reduction in size to the nanometre scale. As the size approaches the nanoscale, the surface-to-volume ratio increases, and the percentage of surface atoms becomes more significant. The high surface area over volume ratio is the responsible behind the unique properties of NMs. Physical properties such as melting point, optical adsorption, catalytic activity, and electrical and thermal conductivity vary greatly with size change. But also, chemical interactions with biomolecules and cells are different at the nanoscale level, emphasizing the potential of NMs as delivery transporters for drugs, proteins, and enzymes into cells. In the context of NMs properties, it is essential to highlight three fundamental concepts: (i) surface effects, (ii) quantum confinement effects, and (iii) surface charge and stability [39,40].

(i) Surface effects

NMs present a large fraction of surface atoms compared to interior atoms. This in turn leads to an increase in the number of reactive surface sites, meaning that NMs interact with the environment more effectively compared to bulk materials. Interior atoms exhibit greater coordination and stability than surface atoms. Thus, the smaller the particle, the greater the proportion of surface atoms, and the lower the average binding energy per atom. A further consequence when the surface-to-volume ratio increases as size decreases, is that other properties -such as phase transition temperature and solubility- also follow this inverse scaling relationship.

(ii) Quantum confinement effects

The appearance of quantum effects at the nanoscale is also responsible for the distinct properties of NMs. Quantum confinement effects explain electron behaviour in terms of energy levels, potential wells, valence and conduction bands, and band gaps. The confinement refers to restricting the motion of freely moving electrons to discrete energy levels when particle size is comparable to electron's wavelength. This confinement alters the material's band structure, increasing the bandgap and leading to size-dependent properties like fluorescence colour.

(iii) Surface charge and stability

USC UNIVERSIDADE DE SANTIAGO DE COMPOSTELA

Surface charge dictates properties and behaviour of NMs as it influences stability, aggregation, environmental interactions and functional group affinity. In aqueous solution, particles become charged through protonation/deprotonation, forming an electric double layer (EDL) that balances the surface charge. This leads to the formation of an electrostatic potential known as zeta potential, which is a standard measure of surface charge. Zeta potential reflects the degree of electrostatic repulsion between particles; the higher the magnitude (positive or negative) the greater the colloidal stability and the less the particle tendency to aggregate [41].

NMs features are influenced not only by size but also by shape and by chemical structure and composition. Atoms can arrange themselves in different ways and thus, one particular NM can exhibit different crystal structures, each with different physicochemical properties. For example, titanium dioxide (TiO_2) NPs can exist as rutile with a tetragonal structure, as anatase also with tetragonal structure, and as brookite with an orthorhombic structure. Although rutile and anatase present tetragonal structure both, interatomic distances and connectivity of the chains differ. These differences in crystalline forms result in different mass densities and electronic band structures. Anatase phase shows improved antibacterial and photocatalytic activity compared to the other two crystalline forms [42].

– Catalytic reactivity

The high reactivity of NMs, resulting from the elevated number of surface atoms along with unique electronic structures, makes them highly advantageous for applications in catalysis. Due to their high surface-to-volume ratio, which translates into increased reaction region, and the possibility to manipulate the morphology, NMs are promising heterogeneous catalysts [43]. Moreover, crystallographic defects, such as vacancies, introduce irregular bonding environments that amplify reactivity. These distinctive features at the nanoscale enable chemical transformations to occur under milder conditions compared to bulk materials.

– Optical properties

The optical behaviour of NMs, such as reflection, transmission, absorption, and light emission, is entirely governed by their electronic structure [44,45]. This structure depends on the morphology and, ultimately, on the dominant role of surface atoms. Two key factors explain the unique optical properties of NMs: quantum effects and surface plasmon resonance (SPR) [46,47]. Optical properties such as emission and absorption occur when electron transition between the valence band (highest occupied molecular orbital -HOMO-) and the conduction band (lowest unoccupied molecular orbital -LUMO-) happens. At the nanoscale, the bandgap between HOMO and LUMO increases with particle size decrease, especially for semiconductor NMs. Adjusting the size, shape, or composition of NMs allows precise tuning of their emission wavelengths, from ultraviolet to visible and near-infrared regions of the spectrum. SPR becomes the primary mechanism governing the optical properties of NMs when the particle size is smaller than the wavelength of the incident radiation. SPR occurs when free electrons in the conduction band are coherently excited and oscillate in-phase with applied light energy. This contrasts with bulk materials, which

are unable to produce SPR. Metals like gold and silver can sustain surface plasmon modes, where free electrons resonate at a frequency determined by particle size and shape. For example, 100 nm Ag nanoprisms produce red colour, while 40 nm Ag spheres generate blue colour [39].

– Magnetic properties

NMs exhibit unique magnetic behaviours compared to analogous bulk materials, primarily due to surface and interface effects such as symmetry breaking, charge transfer, and modified magnetic interactions. Their high surface-to-volume ratio leads to different magnetic coupling between atoms. In ferromagnetic materials, magnetism depends on particle size: particles smaller than a critical size behave as single magnetic domains with uniform magnetism, while larger ones form multiple domains with nonuniform magnetism. The magnetic response is typically described my remanence and coercivity, the latter being strongly sensitive to particle size. A clear example of the distinct magnetic properties of NMs compared to their bulk counterparts is Fe_3O_4 NPs, which show superparamagnetic-like behaviour, while bulk iron oxide (Fe_3O_4) is ferromagnetic [39].

– Electrical properties

Electrical properties, such as conductivity or resistivity, also vary when examined at the nanoscale level. Due to the quantization of electron energy, the electrical conductivity of NMs is generally lower compared to bulk materials, as the HOMO-LUMO bandgap increases with particle size decrease, especially for semiconductor NMs. However, as the electronic structure strongly depends on particle size, these properties are subjected to modification [39].

– Mechanical properties

NMs provide a large surface area and may be easily modified, leading to improved mechanical features like hardness, adhesion, stress, strain, and elastic modulus [48]. Like other physicochemical properties, mechanical properties are also size-dependent. For example, decreasing the size of SiO_2 nanoparticle assemblies from 300 nm to 10 nm, the particles became drastically harder, stiffer, and tougher, according to An *et al* [49].

– Thermal properties

NMs exhibit enhanced thermal characteristics, compared to their fluid counterparts, due to their extensive surface area that facilitates direct heat transfer at the surface of the material. Ultimately, thermal conductivity is affected by temperature, size, shape, and NP concentration [48].

These unique and tuneable properties present NMs with exceptional potential for a wide range of applications in diverse areas of research and industry.

1.3 TITANIUM DIOXIDE NANOPARTICLES

USC DE COMPOSTELA

Titanium (Ti) is the ninth most abundant element in the Earth's crust. Due to its strong affinity for oxygen and other elements, Ti does not naturally occur in its pure metallic state.

The +4 oxidation state is the most stable and frequent, but it additionally shows di (+2) and trivalent (+3) valence states [50]. Titanium dioxide, TiO_2 (CAS-No. 13463-67-7), is also known as titania or Ti white. It is the naturally occurring oxide of Ti, white, odourless, and non-flammable powder with a molecular weight of 79.9 g mol^{-1}, boiling point of 2,972 ºC, melting point of 1,843 ºC, and relative density of 4.26 g cm^{-3} at 25 ºC [51]. It has been extensively used as white pigment due to its high refractive index and brightness, and as semiconductor material because its stable pH range, chemical inertness, and band edge deposition [52]. It possesses three crystalline structures: anatase, rutile, and brookite. Among them, anatase is found to be the more reactive and cause more toxic effects [51,53]. TiO_2 has long been considered an ideal NM due to its non-toxic nature. However, this 'non-toxic' perception is undergoing significant scrutiny recently. Initially, the International Agency for Research on Cancer (IARC) classified TiO_2 as a Group 2B carcinogen (possibly carcinogenic to humans) via inhalation [54]. However, a 2022 ruling by the European Court of Justice annulled this classification, citing errors in the study's reliability and acceptability, as well as the failure to demonstrate the intrinsic carcinogenic properties required by criteria [55]. Besides, the withdrawal of TiO_2 as a food additive (E171) in Europe [56] helped exacerbate the controversy on TiO_2NPs safety. TiO_2 is massively employed, with an estimate worldwide production of 3,000 tons $year^{-1}$ in 2011 [57], and a global market size of about 17 billion USD in 2020 [58]. Additionally, TiO_2 represents 70 % of the total global pigment production volume [50], is present as excipient in an estimate of 91,000 approved drugs [59], and ranks among the top five NPs used in consumer products [50].

Linking physicochemical properties to industrial applications

The high whiteness, strong opacifying power, thermal stability, and photocatalytic properties explain the wide range of applications and increasing global production of TiO_2NPs [60]. The photocatalytic property is one of the most exploited in industrial applications. Some researchers attribute this enhanced catalytic activity to their high surface area, while others suggest it is due to the predominance of the anatase phase over rutile. TiO_2NPs are employed in various catalytic applications, notably as semiconductor photocatalyst for the remediation of contaminated water, and as photoactive component in solar cells [50]. The photocatalytic effect has also been used for self-cleaning and anti-fogging purposes, including TiO_2NPs in self-cleaning tiles and windows, and antifogging car mirrors [61]. Additionally, TiO_2NPs are capable of reflecting and scattering both UVA (320-400 nm) and UVB (290-320 nm) radiation. Thus, they are approved as UV blockers in sunscreens formulations [62,63].

Because of its white colour, TiO_2NPs are employed for pigment whitening in a myriad of consumer products, including paints, inks, and varnishes; plastics, papers, ceramics, surface coatings; cosmetics; and pharmaceuticals [64]. Up to 2022, TiO_2NPs were employed as part of the food additive E171 as brightener and flavour enhancer and included in candies, sweets, chewing gums, skim milk, sauces, dried vegetables, nuts, seeds, and soups [58]. However, the scenario changed in 2021 when the European Food Safety Authority (EFSA) conducted a safety assessment of E171–that contains TiO_2 in nanoform– and concluded that it 'can no longer be considered as safe when used as a food additive' due to potential genotoxicity could not be ruled out. Following these considerations, the European Commission banned the use of E171 in Regulation (EU) 2022/63 [65].

In the field of medicine, TiO_2 has long been used in articulating prosthetic implants, particularly those for the hip and knee [66]. Currently, in nanomedicine, TiO_2NPs are being explored as potential treatments for some skin conditions, such as acne vulgaris, atopic dermatitis, and hyperpigmented skin lesions [67]. Figure 3 provides an overview of the most prominent areas of application of TiO_2NPs by subdivision.

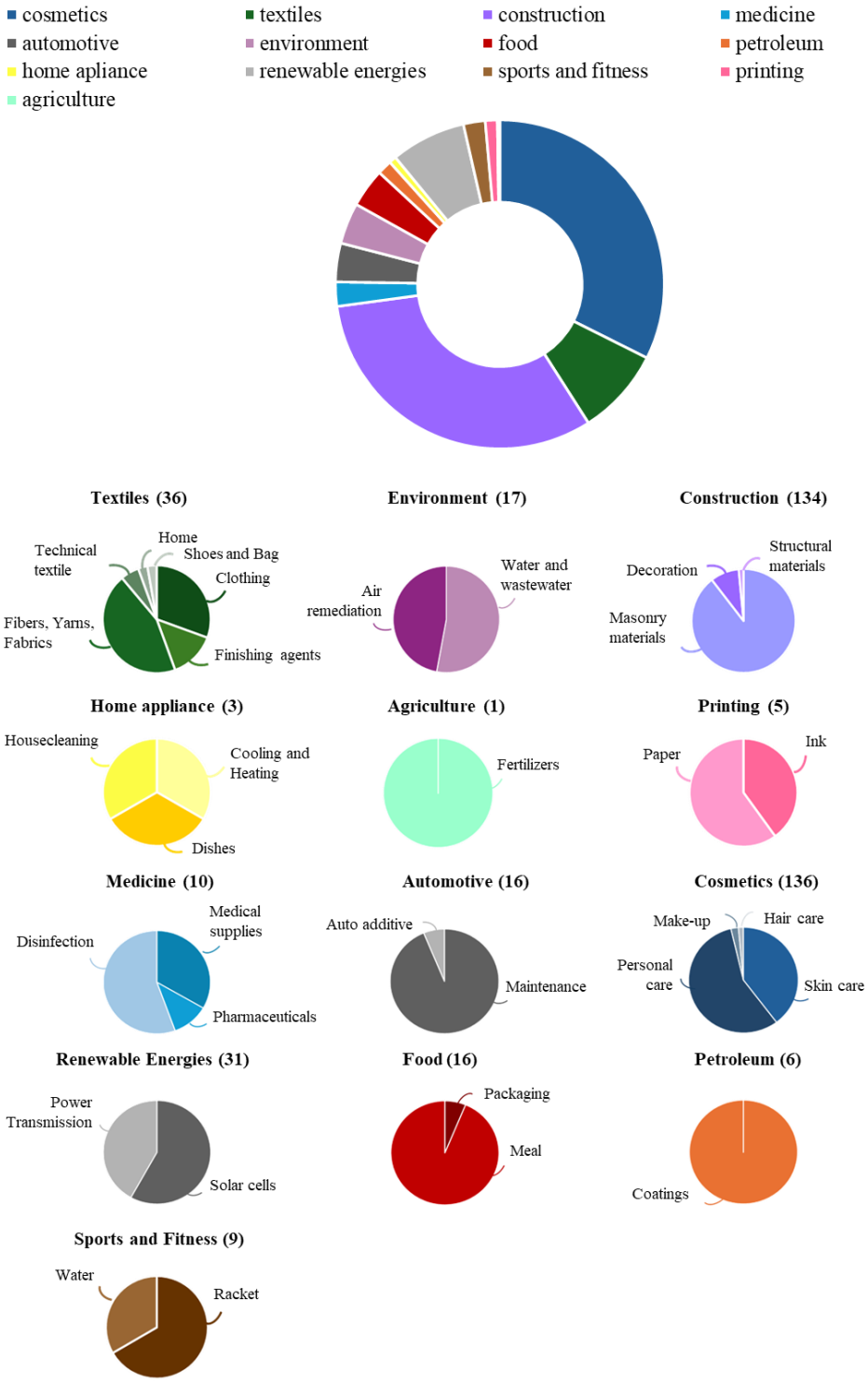

Figure 3. Applications of TiO_2NPs by subdivision.

1.4 SILVER NANOPARTICLES

Silver (Ag) is a naturally occurring element with an atomic weight of 107.8 g mol^{-1}, boiling point of 2,162ºC, melting point of 961.8 ºC and density of 10.49 g cm^{-3} at 25 ºC. Pure silver has a brilliant white metallic lustre, is very ductile and malleable and has the highest electrical and thermal conductivity of all metals [68].

It has been known since ancient times and has been historically employed for currency, jewellery, and silverware; and for maintaining the purity of liquids such as water, wine, vinegar, and milk [69,70]. AgNPs are among the most widely used NMs. It has been reported that AgNPs are employed by 44 % of 34 companies engaged in the production and/or supply of NMs, followed by gold (Au) NPs (41 %), and TiO_2NPs with a 29 % [71]. The worldwide production of AgNPs has been estimated to be 55 ton $year^{-1}$ in 2011 by Piccino *et al*. [57]. Nonetheless, subsequent assessments have proposed significantly higher figures, with a total annual production of around 320-450 tons [72,73]. Despite the discrepancies, it is clear that a large volume of AgNPs is required to satisfy the market demand. A number of databases cataloguing consumer products that contain ENMs are currently available. Hansen *et al*. [74] established "The Nanodatabase" in Denmark (http://nanodb.dk/), an inventory of commercially available products in the European consumer market. The inventory is updated periodically, and currently (June 2025) lists a total of 5,367 products of which 763 are registered as silver-containing products. On the other hand, according to the Nanotechnology Products Database (http://product.statnano.com) [28], there is a total of 11,149 products, among which 1,093 are reported to contain nanosilver.

The extensive and increasing use of AgNPs can be associated to the antibacterial, antiviral, and antifungal properties exhibited [75]. The antimicrobial characteristics of silver, bulk and colloidal, have been recognised for centuries, and it has been an important asset in Chinese and Indian Ayurveda medicine [76]. Nowadays, AgNPs are exploited in several fields including cosmetics, electronics, household appliances, textiles, food industry, and medicine. Figure 4 shares the use of nano-Ag in each industry by subdivision.

Antimicrobial activity

Sondi and Salopek-Sondi [77] were among the first to scientifically evaluate and describe AgNPs activity against *Escherichia coli*, and to present potential mechanisms of action. To date, the exact mode of action is not completely understood, but several mechanisms have been proposed [78]: (i) direct interaction of AgNPs with bacterial cell membranes, causing membrane structural changes and damages leading to increase cell permeability and complexation with internal components [77,79]; (ii) production of reactive oxygen species (ROS) and free radicals, which induce cell damage [80]; (iii) release of silver ions, which strongly interact with thiol (-SH) groups and with phosphorous-containing basses of the DNA preventing cell division and DNA replications, leading to cell death [79,81].

Since the late 1800s, bacteria have been identified as a primary cause of multiple human diseases, prompting substantial attempts to address them: vaccination, improvement of hygiene conditions, and the development of antibiotics [82]. However, the extensive use of broad-spectrum antibiotics has resulted in microbial resistance to antimicrobial agents used against

USC DE COMPOSTELA

different infections. AgNPs emerge as promising antimicrobial agents in the need to explore new alternatives for the treatment and management of infectious diseases [75]. AgNPs have been investigated for the treatment of wounds [83], in the development of nano-containing materials for bone implants [84], in dentistry [85] (endodontics, orthodontics, restorative, and implant dentistry), in drug delivery [82], in eye care [82], as disinfectants [76], and as antibacterials, antivirals, anti-protozoals, anti-arthropods, and anticancerous agents [86].

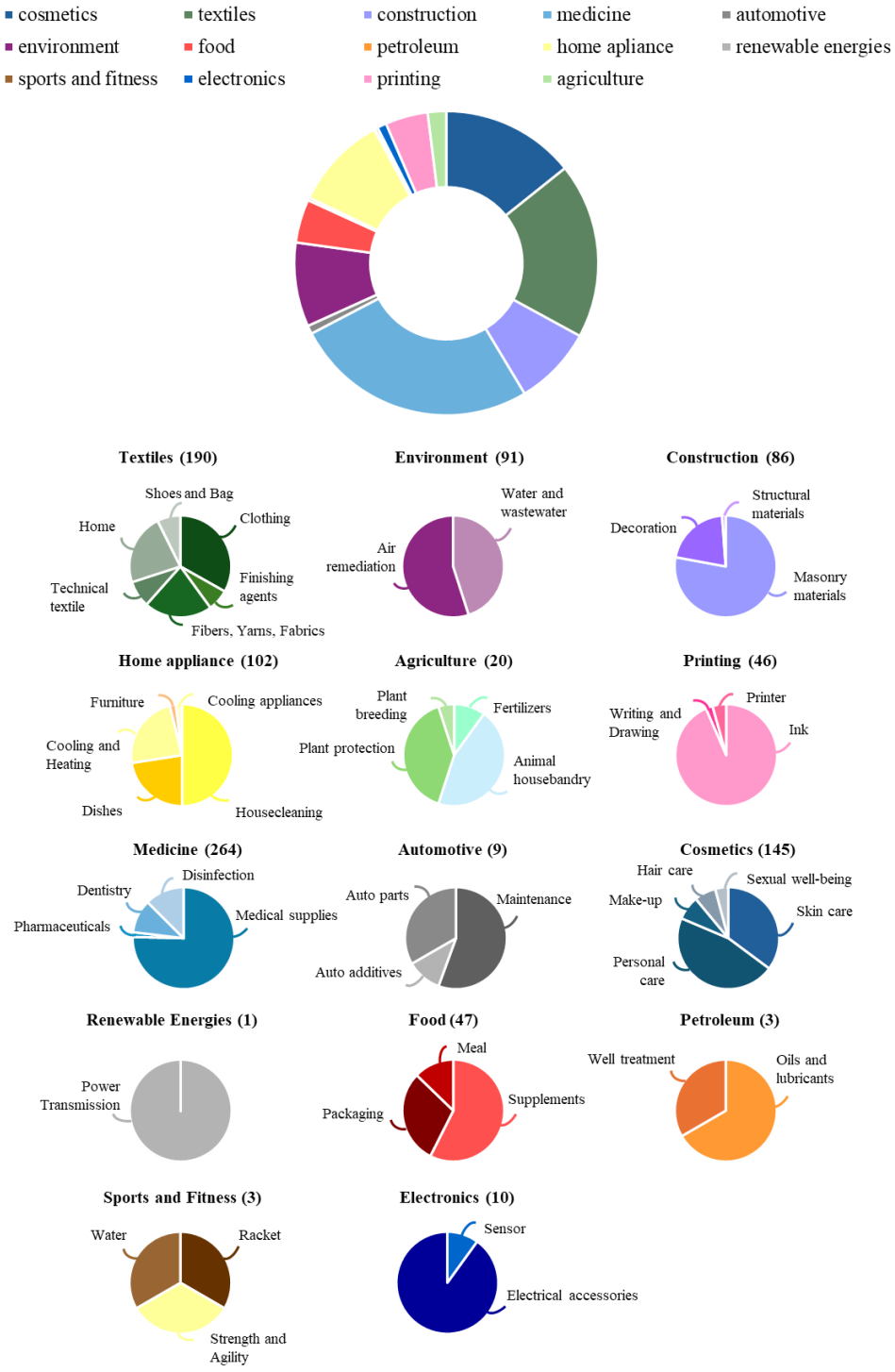

Figure 4. Applications of AgNPs by subdivision.

2 NANOTOXICITY AND POTENTIAL HAZARDS

Toxicology is historically closely associated with Paracelsus, who introduced the fundamental concepts of dose and dose-response and is famously credited with the phrase "the dose makes the poison" [87]. However, the key parameters for conventional toxicology may not be applicable or not be sufficient for nanotoxicology. The study of the adverse effects and toxicity of NMs is commonly referred to as nanotoxicology [88]. It is a relatively recent field, developed years after the initial boom of nanotechnology. The widespread and ever-growing use of NMs has raised concerns around potential nanotoxicity on human health and the environment. Hence, in order to prevent possible harmful effects and provide safer and more reliable nanotechnology, the entire research community and regulatory agencies have been urged to address knowledge gaps.

2.1 NANOTOXICITY MECHANISMS

It has been discussed how physicochemical properties of NMs offer great potential in the development of new technological applications, and how they differ from the characteristics of their bulk counterparts. However, these very attributes also raise concerns about possible adverse effects on human health and the environment. Traditionally, toxicity may occur as a function of exposure route, dose, concentration, time, and/or frequency. However, in the evaluation of nanotoxicology, additional factors need to be considered, including chemical composition, size, surface chemistry, and shape [88]. When addressing optical properties of NMs, it was shown that little modifications in NP size and shape influence the colour of the solution. In this case, slight variations in surface chemistry may modify toxicity, biodistribution, clearance and elimination profiles. Therefore, drawing general conclusions about NP toxicity is challenging, as nanotoxicity depends on complex interactions between physicochemical qualities and biological environments. Even so, there is experimental evidence available that points towards significant toxicity for a range of NPs both *in vitro* and *in vivo*. It has been observed that NPs may trigger processes of oxidative stress, inflammation, and indirect DNA damage in living organisms [89]. A major nanotoxicity mechanism is the generation of reactive oxygen species (ROS), e.g., super oxides ($O_2^{\cdot -}$) and hydroxyl radicals ($^{\cdot}OH$) [90]. This production of ROS generates an imbalance in the cell's natural state causing oxidative stress. For example, transition metal ions can participate in Fenton chemistry by reacting with hydrogen peroxide, leading to the formation of highly reactive hydroxyl radicals, as follows:

$$M^{n+} + H_2O_2 \rightarrow M^{(n+1)} + {}^{\cdot}OH + OH^-$$

Where M represents a transition metal. The increase in the intracellular ROS levels can trigger additional ROS release from mitochondria through a mechanism known as ROS-induced ROS release, which consequently amplifies oxidative imbalance. At this point,

elevated ROS levels can induce damage to cellular organelles, DNA, cell membranes, and ion channels. Oxidative damage to the cellular genetic machinery within a single cell is defined as primary indirect genotoxicity. On the other hand, primary direct genotoxicity occurs when a NM directly interferes with the structure and function of DNA. Nonetheless, this type of mechanism is less observed for NP toxicity. Aside from primary genotoxicity, secondary genotoxicity can take place. The damage produced in cells may compromise organ performance, potentially leading to organ damage or inflammation. Additionally, cell death mechanisms like apoptosis, necrosis, and pyroptosis can release intracellular content triggering local inflammatory reactions or systemic immune responses. This chronic pro-inflammatory response triggered by immune cells induces the so-called secondary genotoxicity [88,90,91].

To illustrate the broad range of possible adverse effects and toxicities associated with NPs -such as neurotoxicity, pulmonary toxicity, genotoxicity, and vascular dysfunction-, a compilation of studies has been summarized in Table 1.

Table 1. Literature examples of NM toxicity in different organisms.

No.	Adverse effect	Nanomaterials	Exposure route and dose	Test subject	Reference
1	Neurotoxicity	Fe_3O_4NPs (<20 nm)	NA NA	Human	[88]
2	Pulmonary toxicity	Chemically complex mixtures (10-80 nm)	Inhalation 30,000 NPs cm^{-3}	Human	[92]
3	Vascular dysfunction	Diesel exhaust NPs (<100 nm)	Inhalation 1,2000,000 NPs cm^{-3}	Human	[93]
4	Angiogenesis and Inflammation	NiTiNPs (60 nm)	Cell incubation 0.1 mg NiTi mL^{-1}	THP-1 monocytes and EA.hy926 human endothelial cells	[94]
5	Dermal lesions	ZnONPs (50 nm)	Dermal 2.5 µg mL^{-1}	Mice	[95]
6	Reduced algal cell viability and growth	Cellulose nanofibers (CNF) and multi-walled carbon nanotubes (MWCNT)	NA NA	*Chlorella vulgaris*	[96]
7	Negative impact on AMF association	ZnONPs	Soil application 500 mg kg^{-1}	Arbuscular Mycorrhizal Fungi (AMF)	[97]
8	Negative effect on module formation	TiO_2 (<50 nm), ZnO (<50 nm), Fe_2O_3NPs (80-94 nm)	*Soil application* *3-6 g L^{-1}*	*Rhizobium leguminosarum*	[96]
9	Suppressed nitrification kinetics	CuNPs (35 nm)	Soil application 1-100 mg kg^{-1}	Soil nitrifying bacteria	[98]
10	Growth inhibition, nuclear condensation, metabolic changes leading to apoptosis	MoO_3NPs (>100 nm)	Cell incubation 10-200 mg L^{-1}	*Aspergillus flavus and A. niger*	[99]

USC UNIVERSIDADE DE SANTIAGO DE COMPOSTELA

11	Destruction of fungal mycelia, loss of cytoplasm, cell wall damage, oxidative stress	Nanodiamonds (< 5nm)	Cell incubation 0-1.0 mg mL^{-1}	*Phanerochaete chrysosporium*	[100]
12	Reduced cell viability and proliferative capability	Co (28 nm), Fe (25 nm), Ni (20 nm) NPs	Cell incubation 0.5-6 μg mL^{-1}	Adipose tissue derived Mesenchymal Stem Cells (eAdMSCs)	[101]
13	Feeding inhibition and intestine obstruction	AuNPs (20 nm)	Ingestion 600 μg L^{-1}	*Daphnia magna*	[102]
14	Biochemical, metabolic, and genetic effects	AuNPs (~4 nm)	Ingestion 1-50 μg L^{-1}	*Daphnia magna*	[102]
15	Phototoxicity, lipid peroxidation, DNA damage	ZnS QDs (< 50 nm)	Ingestion 10-1000 μg L^{-1}	*Danio rerio* (zebrafish) embryos	[103]
16	Vision impairment	CdO (70 nm)	Ingestion 0.03 mg CdONPs mL^{-1}	*Drosophila melanogaster* (fruit fly)	[104]

2.2 SILVER AND TITANIUM DIOXIDE NPS TOXICITY STUDIES

Nanotoxicity assessment can be conducted following different approaches: *in vitro*, *in vivo*, *ex vivo*, and *in silico*. *In vitro* involves the use of cell models, *in vivo* refers to animal testing, *ex vivo* uses perfused organs, an *in silico* relies on molecular docking simulations. *In vitro* assays to evaluate NP cytotoxicity are usually categorized into five groups: cell viability and proliferation, ROS generation, cellular stress, cell morphology phenotyping, and cell-NP uptake [105]. Within a biological medium NPs are forced to interact with the environment, which may alter their physicochemical properties. To gain stability, NPs often associate with surrounding biomolecules forming what is known as a biomolecular corona, or a protein corona when formed solely of proteins [106,107]. This change in physicochemical properties affects the interactions with cells, consequently affecting the cellular uptake and nanotoxicity. As it has been previously discussed in various sections, the surface characteristics are more important than the bulk characteristics in this context. Therefore, NP size, shape, and surface charge will have a tremendous impact on toxicity. In general terms, smaller and charged NPs have been reported to have higher cellular uptake and higher cytotoxicity.

AgNPs have shown to influence different cells causing apoptosis, lipid peroxidation, and DNA damage [105]. TiO_2NPs have been proved to exert significant toxic effects, including cell metabolic change, chronic pulmonary inflammation, and pro-inflammatory effects in cells [105]. Table 2 compiles a summary of Ag and TiO_2NPs-induced perturbations on several cell lines and living organisms.

USC UNIVERSIDADE DE SANTIAGO DE COMPOSTELA

Table 2. Literature examples of in vitro and in vivo Ag and TiO_2NPs toxicity studies on several cell lines and living organisms.

NP type	Test species	Toxicity	Type of study	Reference
Ag				
1	Rats, mice	Liver injuries (hepatic fibrosis, carcinogenesis, tumorigenesis)	*In vivo* and *in vitro*	[108]
2	Human epithelial cell lines A549, HK-2, HepG2	Cytotoxicity, DNA damage	*In vitro*	[109]
3	Human T-lymphocyte Jurkat cells	Cytotoxicity	*In vitro*	[110]
4	Rat primary astrocytes and rat glioma C6	Decreased cell viability and proliferation, induced cell necrosis and apoptosis	*In vitro*	[111]
5	Mice	Embryonic developmental retardation	*In vivo*	[112]
6	Human Chang liver cells	ROS generation and reduced glutathione (GSH)	*In vitro*	[113]
7	A549 alveolar epithelial cells and lymphoblastoid TK6 cells	Affected cell survival and induced high levels of DNA damage	*In vitro*	[114]
8	Human BEAS-2B lung cells	Cytotoxicity	*In vitro*	[115]
9	RAW264.7 mouse peritoneal macrophage cells	Cytotoxicity	*In vitro*	[116]
10	BEAS-2B, RAW264.7, and MH-S (murine alveolar macrophage) cell lines	Cytotoxicity, genotoxicity	*In vitro*	[117]
11	Porcine kidney (Pk15) cells	Decreased cell viability	*In vitro*	[118]
12	*C. vulgaris, Dunaliella tertiolecta*	ROS production that induces lipid peroxidation and a decrease of cell viability	*In vivo*	[119,120]
13	Nitrifying bacteria culture	Cell death mediated by intracellular ROS	*In vivo*	[119,121]
14	Natural aquatic bacterial assemblages	Oxidative stress mediated by ROS	*In vivo*	[119,122]
15	*Escherichia coli, Staphylococcus aureus*	Growth inhibition, membrane damage, ROS generation	*In vivo*	[80,119]
16	*Daphnia magna*	Feeding inhibition and intestine obstruction	*In vivo*	[123,124]
17	*Daphnia magna*	Biochemical, metabolic, and genetic effects	*In vivo*	[125,126]
18	*Daphnia magna*	Reproductive impairments	*In vivo*	[127–129]
19	*Daphnia magna*	Behavioural alterations	*In vivo*	[130]

USC UNIVERSIDADE DE SANTIAGO DE COMPOSTELA

20	Zebrafish embryos	Mitochondrial dysfunction	*In vivo*	[131–133]
21	*Azotobacter vinelandii*	Reduced cell number, induced apoptosis and structural damage	*In vivo*	[96]
22	*Glomus aggregatum*	Reduced mycorrhizal colonization, glomalin content, and mycorrhizal responsiveness	*In vivo*	[96]
TiO_2				
1	Rats	Multi-organ injury	*In vivo*	[134]
2	Arbuscular Mycorrhizal Fungi (AMF)	Inhibition of AMF symbiosis in rice roots	*In vivo*	[135]
3	*Rhizobium leguminosarum*	Negative effect on nodule formation	*In vivo*	[96]
4	*Daphnia magna*	Body burial and formation of gas bubbles inside the body	*In vivo*	[136–138]
5	*Daphnia magna*	Feeding inhibition and intestine obstruction	*In vivo*	[139]
6	*Daphnia magna*	Behavioural alterations	*In vivo*	[140,141]
7	Zebrafish embryos	Neurotoxicity, behavioural disruptions	*In vivo*	[142]
8	Rats, mice	Liver injuries (hepatic fibrosis, carcinogenesis, tumorigenesis)	*In vivo* and *in vitro*	[108]
9	Rats, mice	Acute pulmonary inflammation and fibrosis	*In vivo*	[90]
10	A549 alveolar epithelial cells and lymphoblastoid TK6 cells	DNA damage and slight cytotoxicity	*In vitro*	[114]
11	Mice	Lung inflammation	*In vivo*	[143]
12	BEAS-2B (human bronchial epithelial) cells	Cytotoxicity	*In vitro*	[144]
13	Chlamydomonas reinhardtii	Generation of ROS	*In vitro*	[145]
14	*Chlorella sp.*	Generation of ROS	*In vivo*	[146]
15	*Bacillus subtilis, E. coli*	Growth inhibition	*In vivo*	[147]
16	*Anabaena variabilis*	ROS formation, oxidative stress	*In vitro*	[148]
17	*E. coli*	ROS formation	*In vitro*	[149]
18	*Pseudomonas aeruginosa*	Membrane integrity, intracellular ROS	*In vitro*	[150]

USC UNIVERSIDADE DE SANTIAGO DE COMPOSTELA

2.3 REGULATORY FRAMEWORK

It is well recognised now that regulation of NMs is an urgent concern. The risks associated with exposure to NMs are still unanswered and the impact on both the environment and human health needs to be elucidated. However, establishing effective regulatory framework needs prior risk assessment studies. The existing methods for risk assessment require adaption for NMs, as a large number of parameters, compared to conventional chemicals, needs to be assessed. While conventional analytes can typically be characterized by concentration and chemical composition alone, NMs demand a more comprehensive assessment. In addition to concentration (expressed in terms of mass and particle number) and chemical composition, parameters such as size and size distribution, shape, agglomeration/aggregation state, surface composition, and crystalline structure must also be considered. As a result, there has been a strong effort to develop analytical methods for the detection, characterization, and quantification of NMs. These efforts also focus on establishing validated standardized protocols and reference materials.

One of the first challenges when addressing regulation and legislation is the lack of a standardized definition of NM. As discussed in section *1.2 Nanomaterials: definition, classification, and properties*, multiple definitions for the term have been proposed by different regulatory bodies. Despite interpretations, regulatory organizations recognize the importance of size and size distribution, and number-based concentration in the characterization of NMs.

In the context of the European Union (EU), legislation is gradually being updated to include specific requirements for NMs, and new regulations are emerging that address the use of NMs in consumer products and medical devices. The EU legislation is accessible online at https://eur-lex.europa.eu/ , and the main pieces of EU legislation that explicitly includes NMs are the following:

- Commission Regulation (EC) **450/2009** of 29 May 2009 on active and intelligent materials and articles intended to come into contact with food [151].
- Regulation (EC) **1223/2009** of the European Parliament and of the Council of 30 November 2009 on cosmetics products [152].
- Regulation (EU) **1169/2011** of the European Parliament and of the Council of 25 October 2011 on the provision of food information to consumers [153].
- Regulation (EU) **528/2012** of the European Parliament and of the Council of 22 May 2012 concerning the making available on the market and use of biocidal products [154].
- Regulation (EU) **2015/2283** of the European Parliament and of the Council of 25 November 2015 on novel foods [155].
- Regulation (EU) **2017/745** of the European Parliament and of the Council of 5 April 2017 on medical devices [156].
- Commission Regulation (EU) **2022/63** of 14 January 2022 amending Annexes II and III to Regulation (EC) No 1333/2008 of the European Parliament and of the Council as regards the food additive titanium dioxide (E171).

USC UNIVERSIDADE DE SANTIAGO DE COMPOSTELA

As of 1 January 2020, the Registration, Evaluation, Authorization, and Restriction of Chemicals (REACH) Regulation EC 1907/2006, apply legal requirements for companies that manufacture or import nanoforms. These obligations address specific information requirements included in revised annexes I, III, and VI-XII [157].

Besides Regulations, which are the main legal instrument in the EU along with Directives, key Scientific Opinions from European committees have been published. These opinions mainly involve guidance on the safe use of NMs. The European Food Safety Authority (EFSA) published a scientific opinion on the safety assessment of selenium nanoparticles (SeNPs) for use in active food contact materials. The conclusion is that SeNPs pose no safety risk to consumers when used in multilayer films with a polyolefin layer separating them from the food, regardless of the food type or contact conditions [158].

Additionally, the Scientific Committee on Consumer Safety (SCCS) was requested to publish an opinion on the safety of colloidal silver when used in cosmetics (including toothpastes and skin-care products) with a maximum concentration limit of 1 %. Finally, the SCCS/1596/18 (October 2018) was unable to determine the safety of colloidal silver in nano form for use in oral and dermal cosmetics due to a number of major data gaps [159]. Years later, the SCCS publishes an Opinion SCCS/1165/24 considering "*micron-sized particulate Silver not safe at concentrations up to 0.2 % in rinse-off and 0.3 % in leave-on cosmetic products when used alone or in combination*" but safe when "*used in eye shadow and oral exposure products (lip balm, toothpaste and mouthwash) either used alone or in combination*" [160]. On 24-25 June 2021, SCCS adopted two Opinions on: (i) Platinum (nano), colloidal Platinum (nano) and Acetyl tetrapeptide-17 colloidal Platinum (nano) [161], and (ii) Gold (nano), colloidal Gold (nano), Gold Thioethylamino Hyaluronic Acid (nano) and Acetyl heptapepetide-9 colloidal Gold (nano) [162]. In either case, SCCS concludes that "*it is not possible to carry out a safety assessment of the NMs due to limited or missing essential information*". However, the SCCS also states that there is a basis for concern on the use of these NMs in cosmetic products, and points out some pieces of scientific literature suggesting possible accumulation of AuNPs in certain organs–notably the liver and spleen– and potential mutagenic/genotoxic effects.

USC UNIVERSIDADE DE SANTIAGO DE COMPOSTELA

3 PRESENCE OF NANOPARTICLES IN THE ENVIRONMENT

The exponential global increase in the production, usage, and disposal of NMs is resulting in their inevitable release into the environment. To such an extent that NMs are now considered contaminants of emerging concerns (CECs) [163]. TiO_2NPs, zinc oxide (ZnO) NPs, and AgNPs are considered the major priority materials for the Organization for Economic Co-operation and Development (OECD) [164]. From diverse sources, NMs are entering air, waters, and soils and sediments compartments. The current environmental implications of NMs are not fully understood, and uncertainties remain regarding their potential hazards and underlying mechanisms.

3.1 ENVIRONMENTAL DYNAMICS OF NMS AS CONTAMINANTS

NMs are not static entities and once entered the environment they undergo diverse transformation processes. NM ecotoxicology involves understanding fate and transport, bioavailability, and NM uptake by ecological receptors [165]. NMs can enter environmental media via the following emission scenarios: (i) release during nano-based materials production, (ii) release while in use, and (iii) release via the direct or indirect disposal of NM-containing waste-products [163].

The environmental fate of NMs encompasses both the chemical and physical transformations they undergo within natural ecosystems, as well as their mobility and distribution within specific environments. These transformation processes are influenced by the physicochemical properties (mainly surface properties) of NMs and by environmental conditions such as pH, ionic strength, temperature, organic matter content, oxygen concentration, and the occurrence of other chemicals [165]. Multiple transformations processes may occur simultaneously and can interact or interferer with one another. Three major transformation processes can explain the environmental fate of NMs [164]:

(i) Physical: homo- and hetero-aggregation, agglomeration, sedimentation, and deposition
(ii) Chemical: dissolution, redox reactions, photochemical reactions, and corona formation
(iii) Biological: biodegradation and biomodification

Once transformed, their fate and transport change and NMs can accumulate in various compartments, including water, sediments, soil, wastewater sludge, and air. Figure 5 provides a graphical overview of the different emission scenarios considered and the distribution between compartments.

USC UNIVERSIDADE DE SANTIAGO

In addition, aquatic and terrestrial ecosystems are often exposed to various chemical stressors, raising concerns that NMs can act as vectors for traditional pollutants [166]. This

highlights the importance of considering the potential interactions and combined effects of NMs with other environmental stressors.

Environmental risk is defined as the possibility and consequences of ecosystem or human health damage caused by environmental pollution [167]. The World Economic Forum's Global Risks Report 2024 identifies environmental risk as one of the most critical global threats [168]. As NMs are increasingly recognized as emerging pollutants, it becomes essential to understand their fate and potential ecological impacts to effectively assess and manage the challenges linked to their widespread use and release. It has been published scientific evidence demonstrating the presence and transport of NMs in environmental systems. Based on this evidence, the first studies modelling and predicting NPs environmental concentrations have appeared, although the real numbers remain uncertain due to the absence of reliable data on NP production –typically estimated through surveys to producers and extrapolated from regional to global scales [169]. As can be seen in Section 2.3 *Regulatory framework*, existing NMs regulation mostly affects cosmetic products, medical devices, and the food industry, with minimal emphasis on environmental protection. This regulatory gap could result in unfavourable environmental changes and adverse effects on ecosystems, posing a risk of NMs being transferred to trophic levels via the food chain.

NMs in water

NMs can enter aquatic systems via (i) wastewater treatment plant effluents, (ii) direct usage (e.g., application of NMs-based paintings on boats, release from human's sunscreens during swimming, or swimwear textiles), and (iii) indirect deposition from air compartments or rainwater runoff [169].

When released into water, dissolution is one of the main transformation processes NMs undergo, mainly metallic NPs. This dissolution can be explained by (i) the formation of partially soluble metal-oxides [170], (ii) the oxidation of the particle constituents [171,172], and (iii) the complexation of the particle constituents [173]. Nonetheless, sulfidation processes may also occur, which retard oxidation and, ultimately, dissolution [174]. Due to their inherently photoactive nature, TiO_2NPs are prone to photoreactions, which can affect their coating, oxidation state, generation of ROS, and environmental persistence [175]. In aquatic media, NPs may remain suspended in water (in between cold and warm currents), settle into sediments, or associate with organic matter (OM) [166]. Aggregation is a common process for NMs in water, which increases particle size, but more importantly reduces the available surface area, thereby decreasing their reactivity. As OM concentrations are typically higher compared to NPs, hetero-aggregations are favoured.

The NP size is a key parameter because it influences their bioavailability to organisms. When aggregates grow too large to pass through the cell wall or membrane, uptake may be hindered. In contrast, dissolution (or partial dissolution), resulting in smaller particle sizes, can enhance cellular transport. Also, transport through aquatic environment is size-dependent. Large aggregates are quickly deposited, and their transport and bioavailability greatly restricted. Conversely, small aggregates are widely transported and have more tendency to interact with organisms [176].

USC UNIVERSIDADE DE SANTIAGO DE COMPOSTELA

Avant *et al.* [177] investigated the environmental fate of multiwalled carbon nanotubes (MWCNTs), graphene oxide (GO), and reduced graphene oxide (rGO) across different aquatic environments. The research used the Water Quality Analysis Simulation Program 8 (WASP8) to model the release of these NMs into the environment to understand their fate in the water column and sediments. The findings of the study suggest a significant accumulation of MWCNTs and GO in sediments over prolonged periods, and a higher GO and rGO concentration in the water column compared to MWCNTs.

Life cycle assessment (LCA) is a powerful tool to quantify the overall burden of contaminants to the environment [178]. Pourzahedi *et al.* carried out a LCA on AgNPs from fifteen different consumer products. Results showed that the environmental impact from the release of AgNPs in products with the highest leaching rates was significantly lower than the impact associated with the production of those products. *Mitrano et al.* also employed a LCA approach to study AgNPs release from textiles, finding that greater releases occurred during the use phase –particularly through laundry–compared to the disposal phase in landfills. According to Corsi *et al.* [163] among all categories of products, the textile-one is recognised as the main contributor of AgNPs release into water bodies.

Li *et al.* investigated the extent to which wastewater treatment plants (WWTP) effluents impact the occurrence of AgNPs in surface waters. The authors found that WWTPs removed more than 96.4 % of AgNPs present in wastewater influent. Although these effluents were the source of significant AgNPs increase in rivers. *Mahdi et al.* studied the transport of AgNPs through runoff and erosion. It was observed that AgNPs can be carried by both overland flow and eroded sediment. AgNPs concentration increased with repeated rainfall events, and increasing the slope of the flume led to greater overall transport via runoff sediments. *Markus et al.* modelled the transport of ZnO, TiO_2, and AgNPs along the Rhine River, revealing that NPs can travel long distances, similar to suspended particulate matter [178].

Gottschalk *et al.* predicted AgNPs concentration to be 0.764 and 0.116 ng L^{-1} in European and North American surface waters, respectively [179]. Likewise, modelled concentrations for TiO_2NPs in surface waters were 0.015 and 0.002 μg L^{-1} for Europe and North America, respectively [179]. Neal *et al.* modelled TiO_2NPs average concentration in UK surface water to be 2.1 μg L^{-1} in the range of 0.55-6.48 μg L^{-1} [180].

NMs in soil and sediment

As previously mentioned, NPs can migrate across aquatic environments or suffer from deposition ending up in the sediment layer. Fine-grained suspended sediments–clays, OM, iron oxides, and other minerals– are considered the primary carriers of pollutants in surface waters. Once settled to the sediment bed, cohesive sediments gradually consolidate decreasing resuspendability over time [181]. Similar to colloids, the sedimentation and diffusion of NPs are driven by gravity and Brownian motion, respectively [182]. In porous media, NP movement is governed by Brownian motion. However, as NPs aggregate, their gravitational settling increases, promoting interactions with soil surfaces. The strength of these interactions is influenced by the surface charges of both NPs and soil. Similar charges lead to repulsion and higher NP mobility, while opposite charges result in attraction and sorption, reducing NP transport.

Soil and sediment are considered final accumulating sinks of NMs and a possible source of groundwater contamination. Experimental data indicate that up to 99 % of TiO_2NPs entering the WWTPs are retained in the sludge, and that the major input of NPs into soils is believed to be the application of sewage sludge to agricultural land [182].

A dynamic material-flow analysis model identifies nanoscale TiO_2 reaching input mass of about 44,000 tons in marine sediments and AgNPs reaching about 30 tons [163]. Environmental AgNPs concentration are estimated at 30.1 mg kg^{-1} in sediments and 2.3 mg kg^{-1} in sludge and treated soils [183], within the range 0.19-470.65 μg kg^{-1} for sediments [184], and around 1 μg g^{-1} for biosolids according to Gottschalk *et al.* [179]. Metcalfe *et al.* [185] monitored AgNPs in water, suspended sediments, and bottom sediments in Lake Ontario, Canada, near a WWTP. Findings indicated that over 75 % of the determined Ag was bound to bottom and suspended sediment fractions, and that less than 2 % of the total silver concentration (97-509 μg kg^{-1}) was identified as Ag nanoparticulate form. Cong *et al.* reported that the concentration of AgNPs in sediments from an estuary in Denmark was in the range of 0.27 ± 0.01 μg kg^{-1} [186].

Similarly, TiO_2NPs concentration in sediments are estimated to be within the range 0-2.7 mg kg^{-1} [181], and an average ≤ 2.74 g kg^{-1} [187]. *Kiser et al.* [188] measured TiO_2NPs concentration in the range of 1.8-6.4 g kg^{-1} in biosolids from WWTPs in Arizona, Colorado, California, Maryland, Iowa, and New York (USA). Johnson *et al.* [189] and Khosravi *et al.* [190] determined an average concentration of 305 mg kg^{-1} and 317.4 mg kg^{-1}, respectively, in biosolids from an activated sludge plant in UK and in sewage sludge from Canada. Moreover, a study conducted in Xiamen Bay, China, reported a TiO_2NPs concentration of 2.74 g kg^{-1} in surface sediments [191].

It is now widely accepted that NMs entering different environmental compartments undergo physicochemical transformations, and that a suite of transformation products–such as dissolved element– will be released. Adam *et al.* [192] assessed the flows of different released forms of NMs throughout the complete system. They categorised NMs as pristine, dissolved, transformed, matrix-embedded, and product-embedded. Modelling suggests that AgNPs are primarily released to surface water and soil as transformed Ag (46 % and 79 %, respectively), whereas release into the air is mostly in the form of pristine and matrix-embedded Ag (42 % and 40 %, respectively). Converely, TiO_2NPs were predominantly released into water, soil, and air in pristine form (97 %, 91 %, and 80 %, respectively). Sediments are recognized as the main environmental sink for AgNPs [193].

NMs in air

There are multiple potential sources of NPs in the atmosphere. They can be directly released into the open air as a result of manufacturing processes, including grinding, mixing and packing, from the application of disinfection sprays, and emitted from waste incineration plants [194]. However, in urban atmospheres, a significant source of NPs in air are diesel- and gasoline-fuelled vehicles [166]. Road transport along with stationary combustion sources contribute to more than 36 % of NPs present in air [195]. Studies have shown that carbon nanotubes (CNTs) and fibres are released ass byproducts during diesel and gas combustion

USC UNIVERSIDADE DE SANTIAGO DE COMPOSTELA

processes. Diesel emissions alone account for over 90 % of carbon-based NPs in the atmosphere [195].

In 2021, respiratory-associated conditions ranked fourth, fifth, and sixth among the global leading causes of death [196]. The World Health Organization (WHO) also released a report on ambient air pollution exposure and global burden of disease in 2016 [197]. Particulate matter (PM_{10}, $PM_{2.5}$) has received considerable attention in air pollution assessment. According to Li *et al.*, ambient $PM_{2.5}$ pollution is responsible for millions of premature deaths annually, and reduces average life expectancy by approximately one year [198].

Once released into the atmosphere, NPs can diffuse and travel long distances due to their small size and slow gravitational settling rate [199]. Besides, they can also form aggregates and eventually enter aquatic and soil compartments by wet and dry deposition [193].

Mueller and Nowack [200] modelled the quantities of ENPs released into the environment considering two possible scenarios, one realistic and the other high emission. Predicted environmental concentrations for nano-Ag were 0.0017 μg m^{-3} (realistic scenario) and 0.0044 μg m^{-3} (high emission scenario), whereas for nano-TiO_2 were 0.0015 μg m^{-3} (realistic scenario) and 0.042 μg m^{-3} (high emission scenario). Gottschalk *et al.* [201] modelled environmental concentration of NMs for different regions–Europe, U.S., and Switzerland. PEC values for Europe territory were within the range of 0.006-0.02 ng m^{-3} for nano-Ag, and < 0.0005 μg m^{-3} for nano-TiO_2. Giese *et al.* predicted air PEC values for Ag-ENMs to be within the range of 0.00-0.49 ng m^{-3} [184]. Differences can be found between the model approaches mainly due to variations in the estimated NMs production volumes and the residence time considered in each model.

3.2 Alleviation of environmental stress by NMs

Apart from being considered contaminants, NMs are also regarded as solutions for alleviation of environmental stress. NMs are used in environmental remediation and water treatment processes for their adsorption capacity and high affinity for other contaminants. The nano-characteristics allow the development of novel materials for water and wastewater treatment processes. NMs are incorporated into membranes, adsorption materials, nanocatalysts, functionalized surfaces, and coatings.

For example, nano iron hydroxide, α-FeO(OH), is a highly robust, abrasion-resistant adsorbent used for the efficient removal of arsenic from contaminated wastewater and drinking water [202]. Another approach for the removal of arsenic is the use of the commercially available $ArsenX^{np}$ (SolmeteX Inc., Philadelphia, PA, USA), a hybrid ion exchange medium comprised of iron oxide NPs and polymers [203]. The use of magnetic NPs–such as magnetite, Fe_3O_4– for the separation of water pollutants has already been documented [204,205]. Application of TiO_2, ZnO, CNTs, GO, nano zero-valent iron (nZVI), and AgNPs for targeting organic pollutants, dyes, pathogens, organic waste, heavy metals (including Pb, Cd, and Hg), organic and inorganic toxins, chlorinated hydrocarbons, and bacteria and viruses in wastewater treatment has been reported [206–208].

USC UNIVERSIDADE DE SANTIAGO DE COMPOSTELA

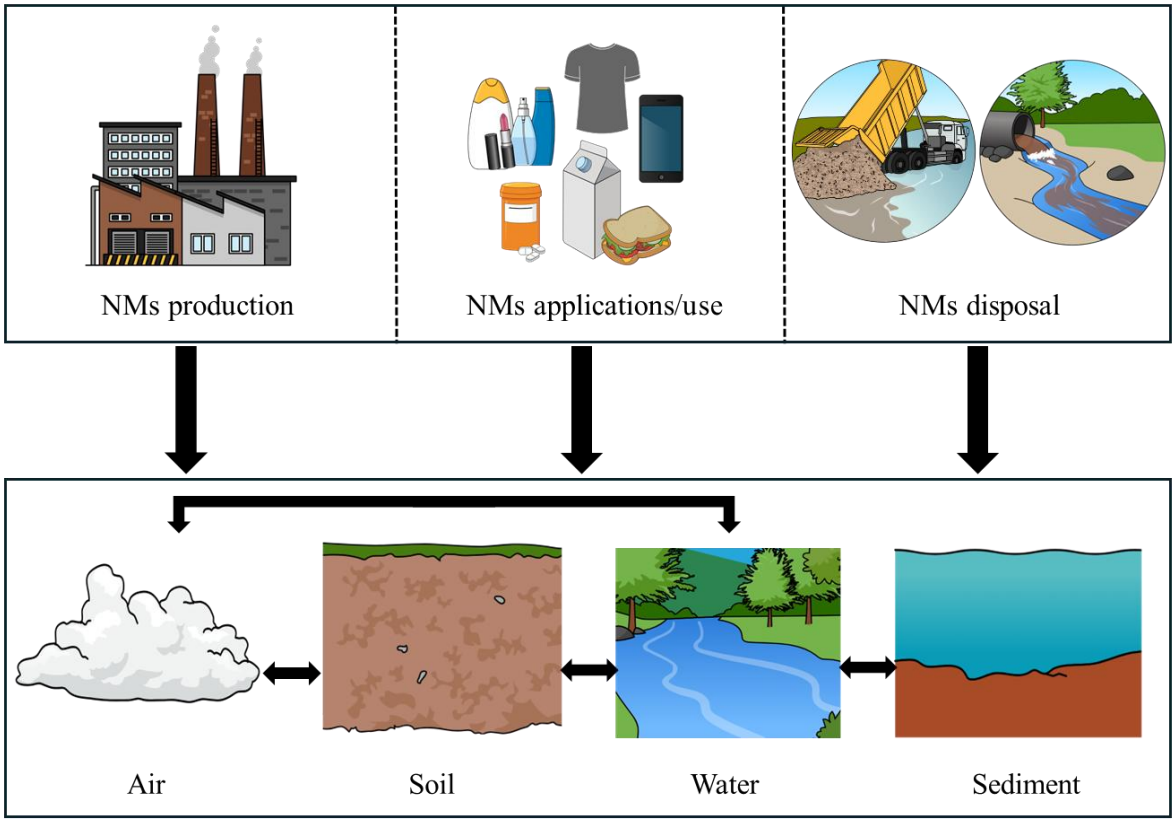

Figure 5. NMs can be released into the environment from different sources, during their production, usage, and disposal.

However, the use of NMs in environmental remediation can pose another source of direct release to ecosystems. Minimizing the environmental impact of NMs production, use and disposal remains a significant challenge. Effective detection and quantification methods of NPs in air, water, and soil are essential, along with the adoption of greener synthesis methods and sustainable manufacturing practices.

USC UNIVERSIDADE DE SANTIAGO DE COMPOSTELA

4 HUMAN BIOMONITORING

4.1 ROUTES OF EXPOSURE

Exposure to NMs can happen either intentionally or unintentionally. NMs can enter the body through different routes, mainly *via* inhalation, ingestion, dermal penetration, direct intravenous/subcutaneous injection, and ocular exposure. The population most at risk of NM exposure is the nanotechnology workforce. A few numbers of epidemiology studies have been focused on occupational exposure at workplace [209–211]. However, the general public is also in direct and daily contact with NMs through NM-based consumer products, medical applications, and environmental exposure. It is important to note that NMs embedded in consumer products can become dislodged or released from the product matrix during use or disposal and behave differently compared to when they were contained within the product. For example, NMs in textiles may be released during laundering, while those in food packaging or containers can leach into the food. Once inside the body, NMs can distribute and translocate to secondary organs different from portal of entry. Therefore, understanding the fate of NMs within the human body requires an integrated assessment of all potential entry routes, alongside the elucidation of dynamics and mechanisms of distribution, including complex biological interactions such as the formation of biomolecular coronas.

Inhalation

Inhalation is considered the main unintentionally entry route of NMs to the body [212–214]. The respiratory system encompasses the nasal cavity, pharynx, larynx, trachea, bronchi, bronchioles, and alveoli [215]. The toxicokinetics of inhaled NPs is predominantly determined by deposition, dissolution, and potential translocation [216]. In this context, particle size, surface characteristics and behaviour in a biological media, are key parameters determining their fate within the respiratory tract. The conduction airways of the lungs and the epithelial tissues are protected by a viscous layer of mucus that functions as a barrier against exogenous elements by retaining them and transporting them back to the oral cavity for clearance. However, moving from the nasal cavity to the inner regions of the lungs, both the airways diameter and the thickness of the mucus layer progressively decrease. In the alveolar region the mucus barrier is absent. Alveoli, which are responsible for the exchange of oxygen and carbon dioxide between the air and the bloodstream, possess a large surface area and high permeability. These characteristics, while essential for efficient gas exchange, also render the alveolar region particularly vulnerable to pathogens and pollutants [215].

Overall, particle size is crucial in determining how deep the particles can penetrate the respiratory system. In simple and general terms, the smaller the particle, the greater the penetration depth [90]. If NMs are not cleared up in the upper airways they can be deposited in different regions of the lungs and introduced into the blood circulation for further distribution

USC

to secondary target organs. Data on translocation from the lung to the liver, spleen, and heart has already been published [217]. Inhaled NPs may also gain access to secondary organs *via* the olfactory bulb, raising significant neurotoxicological concerns due to their potential for direct entry to the central nervous system [218].

Braakhuis *et al.* conducted an *in vivo* study to determine the lung burden and tissue distribution after short-term inhalation exposure of 15 nm and 410 nm-AgNPs [219]. Results confirmed the greater presence of 15 nm-AgNPs in the rat alveolus compared to 410 nm-AgNPs. Similarly, Oberdöster *et al.* reported that, following inhalation exposure in rats, 20 nm-TiO_2NPs exhibited significantly slower clearance and greater translocation to interstitial tissues and regional lymph nodes compared to 250 nm-TiO_2NPs [220].

Ingestion

The gastro-intestinal (GI) route is potentially important for consumers. On the contrary, it is considered less relevant for nanotechnology workers, although they can also be unintentionally exposed by hand-to-mouth transfer [214]. NMs can be ingested directly when used in food, food packaging, drug delivery, and cosmetics [221]. In addition, indirect exposure can occur through the food chain from contaminated environments. Furthermore, a percentage of inhaled NPs can be swallowed into the GI tract after muco-ciliary clearance into the oral cavity.

Broadly, the main parts of the GI tract in anatomical order are the oral cavity, pharynx, oesophagus, stomach, duodenum, small intestine, large intestine, and anus, offering a large surface area for NM interaction [90]. Upon reaching the GI tract, NMs can have diverse fates: (i) secretion back into surroundings, (ii) accumulation, (iii) degradation, and (iv) gain access to the blood and other organs [215]. Emerging evidence suggests that gut microbiota may play a crucial role in modulating both local and systemic biological effects of NMs [222], and has become a key area of study [223,224]. It is also reported that the rate of ingestion of NPs is proportional to the particle size, the larger the particle, the more time it requires to complete the ingestion process [225]. While NM absorption may potentially occur throughout the entire GI tract, it is highly unlikely to take place in the stomach due to its thick mucus layer, underlying connective tissue, and muscular structure [226]. The acidic environment of the stomach (pH 1.5-3.5) may induce NM dissolution or promote their aggregation through surface charge neutralization [227].

Commercial labels consumed by humans including NMs are E551 (silicon dioxide), E171 (titanium dioxide), E174 (silver), E175 (gold), E172 (iron oxides and hydroxides) [228]. The estimated daily uptake of TiO_2 (as E171 food additive) in the United States ranges from approximately 0.2-0.7 mg per kg of body weight per day (mg/kg bw/day), whereas populations in the United Kingdom and Germany are estimated to consume around 1 mg/kg bw/day [229]. However, the EFSA places particular emphasis on children, as they represent the population group with the highest estimated exposure to E171. The maximum exposure levels are observed in children aged 3 to 9 years, who consume an average of 1.9 to 11.5 mg/kg bw/day. For infants (12 weeks to 11 months), mean exposure ranges from 0.06 to 3,6 mg/kg bw/day, while toddlers (12 to 35 months) exhibit a higher range of 0.9 to 12.8 mg/kg bw/day. In adolescents (10 to 17 years), exposure levels decline compared to younger children, ranging from 1.3 to 6.2 mg/kg

bw/day. Estimated intake is lowest among adults (18-64 years) and the elderly (≥ 65 years) [56].

Despite the relevance of ingestion exposure, the number of studies evaluating the hazards associated with ingested NPs remains relatively limited compared to inhaled NPs [215].

Dermal penetration

Dermal exposure has received considerable attention with the introduction of NMs into cosmetic formulations and dermo pharmaceuticals [230]. For example, TiO_2 and ZnONPs are extensively employed as UV blockers in sunscreens. However, such exposure can also occur unintentionally during cleaning activities, as many household cleaning products contain NPs as antimicrobial agents.

Skin is the largest organ in the human body with an estimated surface area of 2 m^2. It is structured in three overlapping layers: the epidermis (outer layer), the dermis (middle layer), and the hypodermis (subcutaneous layer). The epidermis acts as the primary barrier against micrometer-sized particles but is ineffective for particles on the nanometer scale. It is subdivided from innermost to outermost into: the stratum basale (SB), the stratum spinosum (SS), the stratum granulosum (SG) and, most superficially, the stratum corneum (SC) [231].

Three possible routes for NP entry through the skin are described so far: inter-cellular, trans-cellular, and trans-appendageal [232,233]. Although no conclusive evidence is available so far, it seems that some NPs are able to penetrate the dermis, while others may only gain access through skin lesions and wounds. Studies have demonstrated the correlation between skin damage and permeability. For instance, Larese *et al.* in an ex vivo study with human skin, revealed that damaged skin exhibited greater AgNPs permeability through the SC compared to intact skin [234]. Studies involving TiO_2NPs have shown no definitive results. On the one hand, one study using a porcine skin model showed no penetration of 4 nm and 60 nm TiO_2NPs into the dermis after 24 hours of exposure. In contrast, 4 nm TiO_2NPs were detected in the deep layer of the epidermis of a pig's ear following 30 days of exposure [235,236].

Besides particle size, NPs surface properties also dictate skin penetration. Kohli and Alpar demonstrated that negatively charged latex NPs can pass through the SC to reach the viable epidermis in contrast to neutral and positive NPs [237]. Shape also constitutes a key parameter in skin permeability. Rod-shaped AgNMs were reported to have higher skin permeation rates than those of spherical or triangular shapes [238].

Ocular

Studies evaluating ocular exposure risks are very scarce. In fact, some researchers consider it an overlooked potential hazard, given that the eyes are in direct contact with the external environment and can serve as a route of entry into the human body. The ocular surface includes two major parts: the cornea and the conjunctiva. The ocular surface is covered with a thin layer of tear film that is supported by lacrimal [239].

Although limited, few pieces of evidence have been published so far. Sriram *et al.* showed a ROS production increase in bovine retinal cells after exposure to AgNPs [240]. Söderstjerna *et al.* studied the effect of 20 and 80 nm Au and AgNPs using an *in vitro* tissue

USC UNIVERSITADE

culture model of mouse retinas following 72 hours exposure. Results showed that Ag and AuNPs produce adverse effects on the retina causing oxidative stress [241]. Zhu *et al.* reviewed potential NPs toxicity to the eyes, suggesting induced damage on lens, retina, and optic nerve and macula [239].

Intravenous injection

Intentional exposure to NMs can occur through intravenous injection, a method commonly employed in biomedical and clinical settings. Direct injection of NMs is used in advanced medical applications, including targeted drug delivery [242]. Polymeric NPs have been employed in the nanoencapsulation of functional foods (nutraceuticals) to protect them from degradation within the GI tract, or as drug delivery vehicles for the formation of nanoemulsions of omega-3 fatty acids, and oil-in-water nanoemulsions (such as triglycerides with combined with vitamin D or β-carotene) [243].

Figure 6 provides an overview of the possible routes of exposure for NPs into the organism, and the principal target organs after translocation from portal of entry.

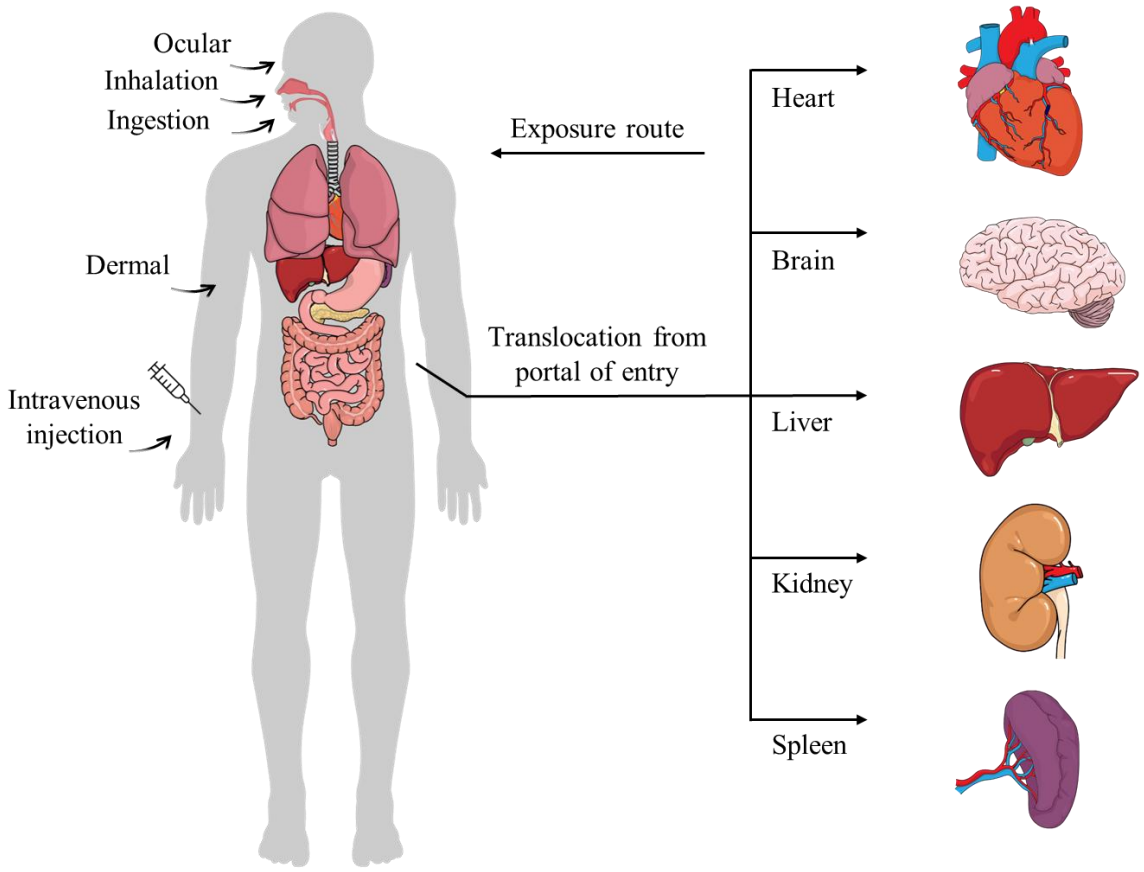

Figure 6. NMs exposure routes and secondary target organs different from portal of entry.

USC UNIVERSIDADE DE SANTIAGO DE COMPOSTELA

4.2 ADME PROCESS

When a substance enters the human body, the processes that follow are absorption, distribution, metabolism and excretion. Together, these constitute the ADME process, which forms the foundation of toxicokinetics [244].

Absorption

Absorption is defined as the process by which NPs proceed from the external site of exposure into an internal biological milieu. After inhalation, ingestion, intravenous injection, ocular, or dermal exposure, NPs have two directions to follow: to be cleared from the body or being absorbed. These are two competitive processes, faster clearance reduces absorption, and *vice versa* [245].

Distribution

Once in systemic circulation, NPs are distributed across various organs and tissues based on their size and interactions with different biological components. The accumulation of NPs in the tissues depends greatly on vascularization and permeability through vascular endothelial and tissue cells [246]. Given that the effective pore size of normal vascular endothelium is around 5 nm, NPs larger than this are generally unable to penetrate the structure of organs like the brain and muscles [247]. Nonetheless, NPs smaller than 60 nm can more easily access tissues with fenestrated endothelium–such as those in glands, kidneys, and digestive mucosa, which have pores around 60 nm–and tissues with discontinuous endothelium, such as the spleen, liver, and bone narrow, where pore sizes range from 50 to 100 nm. After reaching the tissues, NPs may: (i) settle within the extracellular matrix, (ii) adhere to cell surfaces, (iii) be internalized by cells, or (iv) be carried to lymph nodes [246].

The liver and the spleen are known to be the two major organs for systemic distribution of a large number of ENMs. In general terms, smaller particles are more detected in kidney, liver, spleen, lungs and brain, whereas larger particles have a greater tendency to remain in the GI tract. Nonetheless, regardless of the exposure route, the distribution of NPs within the body depends greatly on surface and size properties [244]. Besides, opsonizations, blood flow, vascular permeability, plasma protein corona content, mononuclear phagocytic system, and NP-tissue cells interaction, also modulate biodistribution [248].

Considering AuNPs as an example, it has been reported that larger AuNPs tend to accumulate in the liver and spleen, while smaller ones are more likely to localize in the kidneys [249]. A different study from Faraji and Wipf [250], determined that micron-sized particles remain in the spleen for about two weeks, whereas NPs madre from the same metal are fully cleared from the body within that timeframe.

Metabolism

The metabolism of NPs is defined as any process that alters the original composition and/or physicochemical properties of NPs [245]. Accordingly, dissolution, degradation, opsonization, aggregation, drug release, and formation of biomolecular coronas, are understood as metabolism processes [248].

USC DE SANTIAGO DE COMPOSTELA

Most of the inorganic NPs, such as TiO_2NPs or AuNPs, are relatively stable and undergo minimal or negligible metabolism. In contrast, AgNPs are readily metabolized and can be easily ionized into silver ions (Ag^+) in acidic environments, such as in gastric fluid [248]. On the other hand, organic NPs–like liposomes, micelles, nanogels, and dendrimers–are often biodegraded in the body into hydrophilic metabolites and eventually excreted through urine or bile [251,252].

Small NPs (typically bellow the glomerular filtration threshold ~5.5 nm) are eliminated through renal excretion and cleared via the urine. However, more recent studies have reported the presence of intact NPs in urine that exceed the conventional size limit for kidney filtration. The mechanism remains to be elucidated [248]. Larger and non-biodegradable NPs may be taken up by phagocytes and accumulated within the body for longer periods of time.

Lin *et al.* reviewed the pharmacokinetics of AgNPs [253]. According to most studies, the liver was identified as the primary organ for Ag distribution, followed by the spleen and kidneys, regardless of the exposure route, whether oral, intravenous/subcutaneous, or through inhalation. Within the liver, Ag was detected in Küpffer cells, hepatocytes, and sinusoidal endothelium cells. In the kidneys, Ag deposition was observed in the cortex region, medulla, inner medulla, and cortical glomeruli. In addition to hepatic and renal accumulation, significant distribution to the spleen was also reported. Furthermore, numerous studies showed that AgNPs up to 110 nm can reach the brain, independent of the route of exposure. After oral intake, the acidic environment of the stomach rapidly promotes the oxidative dissolution of AgNPs into Ag^+. In synthetic gastric fluid, about 97 % of the total Ag is released as ions within 6 hours.

Kreyling *et al.* investigated the biokinetics and biodistribution of 70 nm radiolabeled TiO_2NPs across various rat tissues over the period of 1 hour to 28 days. Following intravenous injection, Ti primarily accumulated in the liver within the first hour, with lower concentration in the spleen, carcass, skeleton, and blood. Blood Ti levels decreased rapidly afterward, while concentrations in the other tissues remained constant until day 28. Oral exposure led mostly to fecal elimination, with only 0.6 % of the dose absorbed through the GI tract and distributed to the liver, lungs, kidneys, brain, spleen, uterus, and skeleton. Inhalation via intratracheal instillation resulted in 4 % systemic translocation within 1 hour, predominantly retained in the carcass, which decreased to 0.3 % by day 28. Ti concentration in the liver and kidneys remained constant, while lung clearance through the larynx increased from 5 % to 20 % over time for all translocated particles [254–256].

Excretion

Excretion refers to the elimination of NPs from the living system without decomposition or dramatic alteration in their characteristics from their original forms [245]. Clearance of NMs from the body can happen *via* different pathways. Renal and hepatobiliary clearance were shown to be the major routes for NPs excretion. Although minority excretion can also occur through hair, tears, sweat, saliva, breast milk, and nails [248].

Renal clearance is the most effective excretion pathway. Kidneys are involved in a number of crucial physiological functions, among which is the excretion of foreign substances and waste. Once in the vascular circulation, NMs can be excreted through the kidneys along

USC DE SANTIAGO DE COMPOSTELA

with the urine. The production of urine is performed by three processes of the nephrons and colleting ducts–glomerular filtration, tubular reabsorption, and tubular secretion. However, renal clearance comes with size restrictions (6-8 nm), the reason why many NMs cannot be cleared via this route and undergo biliary excretion [251].

Hepatic clearance involves the elimination of waste products through both the kidneys and the intestinal tract. Within the liver, two key cell types contribute to the clearance of NMs: hepatocytes and phagocytic Kupffer cells. The hepatocytes excrete NMs into the small intestine through the bile, after endocytosis and enzymatic breakdown. Whereas Kupffer cells can internalize larger NMs, often several hundreds of nanometres in size. They are particularly effective at internalizing anionic NPs, while hepatocytes have a preference for cationic ones. Importantly, only NMs processed by hepatocytes can be excreted through the bile and GI tract. In contrast, NPs captured by Kupffer cells tend to remain in the reticuloendothelial system (RES) [245,246,251].

In the above-mentioned study from *Lin et al.* [253], rats were orally dosed with 14 nm AgNPs or silver acetate to evaluate the excretion of silver. In both groups, Ag excretion in urine was negligible. However, the excretion of Ag in faeces was considerably higher–63 % of the daily dose for the AgNPs group and 49 % for the silver acetate group.

According to Cho *et al.* [257], TiO_2NPs were orally administered to rats for 13 weeks, and samples of urine and faeces were collected at necropsy. The results confirmed a significantly higher Ti concentration in faeces compared to urine, suggesting that TiO_2NPs are primarily excreted through the digestive tract.

4.3 BIOFLUIDS UNDER STUDY

4.3.1 Blood

Blood is a body fluid composed of four main components: plasma, red blood cells, white blood cells, and platelets. Blood that circulates through veins, arteries, and capillaries is referred to as whole blood, which consists of approximately 55 % plasma and 45 % blood cells. Blood makes up around 7 % to 8 % of a person's body weight [258]. Due to its diverse functionality, blood is heterogeneous and complex in composition. Main functions of blood include the transport of nutrients and oxygen to all organs, the formation of clots to prevent excessive blood loss, facilitating the removal of waste products *via* the kidneys and liver, the distribution of hormones and other signalling molecules, and the regulation of body temperature [258,259].

Plasma

Plasma represents the aqueous phase of blood that contains water, proteins, peptides, signalling molecules, steroid hormones, and various metabolites–including carbohydrates, amino acids, and lipids–that are absorbed and released by the body's organs [259]. Blood can be withdrawn and treated in several ways to obtain different fluids [260,261]:

– Blood serum. The supernatant obtained after centrifugation of whole blood with no anticoagulants. Blood clot, cells, and platelets have been removed.

USC UNIVERSIDADE DE SANTIAGO DE COMPOSTELA

- Blood plasma. The supernatant obtained after centrifugation of stabilized whole blood (the clotting cascade has been inhibited due to chelation of calcium by EDTA or citrate). Platelets and blood cells have been removed. From a biochemical perspective, plasma is closely identical to the liquid fraction of circulating blood, aside from the presence of anticoagulants.

Together, serum and plasma are the second most commonly used biofluids in metabolomic studies after urine.

Red blood cells (RBCs)

They are also known as erythrocytes. Popular for their bright red colour, RBCs are the most abundant cells in the human blood, accounting for about 40 to 45 % of its volume (haematocrit value) [262]. Normal human RBCs have a biconcave disk shape with a flattened centre, measuring approximately 7-8 μm in diameter and about 2.5 μm in thickness. After around 7 days of maturation, RBCs are released from the bone marrow into the bloodstream. Unlike many other cells–such as white blood cells–RBCs lack a nucleus. This absence enhances their flexibility to circulate through vessels, but also limits their lifespan to an average of 120 days [263,264]. Chemical composition of RBCs consists of approximately 64 % water, 33 % haemoglobin (protein responsible for the red colour), and 3 % erythrocyte stroma, which includes proteins, lipids, enzymes, and inorganic salts [265].

White blood cells (WBCs)

They are also known as leukocytes, and are significantly less abundant than RBCs, making up approximately 1 % of the whole blood. WBCs are composed of granulocytes (neutrophils, eosinophils and basophils), and non-granulocytes (lymphocytes and monocytes). Among these, neutrophils are the most prevalent, accounting for 55 to 70 % of the total white blood cell count. In general terms, WBCs are responsible for the body's protection against infection [258,266].

Platelets

Platelets, also known as thrombocytes, are not completely cells like RBCs and WBCs, but small cytoplasmic cell fragments. Platelets play a key role in blood clotting (coagulation) by accumulating at injury sites, adhering to damaged vessel walls, and forming a fibrin clot. This clot not only stops bleeding but also provides a scaffold for tissue regeneration [258,266].

4.3.2 Urine

Urine constitutes a particularly attractive biofluid for clinical diagnosis and toxicological studies. It is a liquid excretion product made by a complex filtering process in the kidneys [267]. The kidneys are vital organs which basic function is to extract the soluble waste products from the bloodstream and generate urine. Renal blood flow generates approximately 1.5 to 2.0 L of urine per day for an average adult [268,269]. The resulting urine is a transparent, sterile, and amber-coloured fluid. It contains high concentrations of urea (the main nitrogen-containing metabolite of human protein catabolism), inorganic salts, creatinine, ammonia, organic acids, water-soluble toxins and pigmented products of haemoglobin breakdown–including urobilin, which gives urine its characteristic colour [268,270].

Compared to other biofluids, it can be collected non-invasively, in large amounts, and by repeat sampling, which facilitates continuous monitoring [271]. Besides, the concentration of many metabolites is amplified in urine compared to blood [271,272]. Urine contains rich physiological and pathological information about human health, dietary intake, and exposure to chemicals and contaminants.

USC
UNIVERSIDADE
DE SANTIAGO
DE COMPOSTELA

5 ASSESSMENT OF INORGANIC NANOPARTICLES: ADVANCED ANALYTICAL TECHNIQUES

Modern analytical chemistry faces new challenges in the assessment of NPs. Traditional analytical methodologies and instrumentation were developed and validated for conventional analytes–that is, chemical substances that need to be detected, identified, and/or quantified in terms of chemical composition and concentration. In contrast, NPs can be considered sized analytes, thereby requiring characterization not only in chemical terms but also in terms of physical morphology. A comprehensive characterization of NPs demands information on concentration, size and size distribution, shape, chemical composition, crystal structure, surface chemistry and surface area, and the degree of agglomeration/aggregation. The SCENIHR's 2006 report highlighted the limitations in the existing methodologies for assessing NPs and called for the development of specialized tools. The report directly states that "*First, methods are required that reliably detect nanoparticles and measure their physico-chemical properties in the media in which humans and ecosystems are exposed to them, such as air, water, soil, consumer products and nanocomposites. Methods must be also available that support the studies to assess the risk of nanoparticles, such as with toxicological and ecotoxicological studies. Additional tools are required in this case, which are able to detect nanoparticles in the relevant medium, including cells, fluids and plant tissues*" [273].

5.1 METHODS FOR SAMPLE PREPARATION

Sample preparation is a crucial step in the determination of target compounds before instrumental analysis. Accurate detection and quantification of low levels of NMs in complex matrices usually require prior sample cleanup and preconcentration. This type of sample preparation prior to analysis usually involves either removing the matrix or isolating the NMs from the sample matrix.

5.1.1 Surfactant-assisted dispersive liquid-liquid microextraction (SA-DLLME)

Historical development and extraction principles of liquid-phase extraction

Liquid-liquid extraction (LLE) is considered one of the oldest and most extensively employed extraction techniques [274]. In LLE, target compounds are transferred from one liquid phase (the donor phase) to another immiscible or partially immiscible liquid phase (the acceptor phase), which come into contact with one another. In general terms, the isolation of target compounds requires a two (or more)-phase system and a mechanism for phase separation. Initially, the donor phase comes in active contact with the acceptor phase through agitation or dispersion of the system. This interaction facilitates the transfer of analytes between phases. Next, the system must be allowed to settle–by gravity or centrifugation–to recreate the two (or more)-phase system. Finally, a phase separation step is required to collect the phase enriched with the target compounds [274].

The transfer of analytes between phases is driven by differences in their solubility in each phase. For compounds that exist in the same chemical form in both phases and have reached equilibrium, their distribution is governed by the partition constant, K_D°, which defines the ratio of activity of a given species A in the extract to its activity in the other phase with which it is in equilibrium, as described in equation (1):

$$K_D^\circ = a_{A,1} / a_{A,2} \qquad \textit{Equation (1)}$$

Where $a_{A,1}$ is the activity of a compound A in the acceptor phase, and $a_{A,2}$ the activity of the compound in the donor phase. The value of K_D° depends on the choice of standard states and on the temperature (and eventually the pressure). Nevertheless, distribution isotherms are often linear over a broad concentration range, allowing activities to be replaced by concentrations (mol L^{-1}). Under these conditions, the partition ratio, K_D, can be determined. According to IUPAC, K_D is defined as *the ratio of concentration of substance in a single definite form, A, in the extract to its concentration in the same form in the other phase at equilibrium* [275]. K_D is also commonly referred to as the distribution constant. For an aqueous/organic system, equation (1) can thus be rearranged into equation (2):

$$K_D = [A]_{org} / [A]_{aq} \qquad \textit{Equation (2)}$$

Nevertheless, classical LLE has several well-known drawbacks, including emulsion formation, the need for large samples volumes, and the use of toxic organic solvents. These factors contribute negatively to the generation of significant amounts of hazardous waste, making LLE labour-intensive, costly, time-consuming, and environmentally unfriendly.

Back in the 1990s, the development of eco-friendly, miniaturized, and more efficient extraction techniques became the new academic research interest. This interest in green chemistry principles was further supported by the publication of "Green Chemistry: Theory and Practice" by Paul T. Anastas and John C. Warner [276]. As a result, this research-driven area introduced the novel liquid-phase microextraction (LPME) as an alternative miniaturized strategy addressing some of the main disadvantages of classical LLE [277]. In LPME, extraction usually takes place in a very small amount of a water-immiscible solvent–within the microliter range. Progress in liquid-phase microextraction advanced rapidly, leading to the development of several modern derivative techniques. LPME approach can now be divided into three main groups that developed chronologically: (i) single-drop microextraction (SDME), (ii) hollow fibre liquid-phase microextraction (HF-LPME), and the latest (iii) dispersive liquid-liquid microextraction (DLLME) [277,278].

Dispersive liquid-liquid microextraction (DLLME)

DLLME was first introduced by Rezaee and coworkers in 2006 to identify organic compounds in aqueous samples [279]. This technique employs a ternary solvent system including a water-immiscible extraction solvent (typically organic solvents such as chlorobenzene or chloroform), a disperser solvent miscible with both water and the extraction solvent (generally methanol, acetonitrile or acetone), and the aqueous sample solution. The mixture of extractant and disperser is rapidly injected into the sample solution, resulting in the formation of an emulsion. This cloudy solution contains fine droplets of the extractant solvent dispersed throughout the sample solution. The disperser solvent plays a key role in promoting droplet formation and enhancing the contact surface area between the extraction solvent and

the sample solution, thereby improving mass transfer. After the equilibrium is achieved, sample solution is shaken and centrifuged to facilitate phase separation. Most frequently, the extraction solvents employed are denser than water and thus they form the bottom layer after sedimentation [279,280]. The choice of extraction solvent must meet specific criteria: it should differ in density from water to allow phase separation, be immiscible with the aqueous phase, form a cloudy solution when dispersed, and exhibit affinity for the target analytes. Under these conditions, chlorinated solvents are typically the right choice. Alternative brominated and iodinated solvents have been evaluated, but no clear advantages over chlorinated ones have been noted [281].

Since its introduction, the scientific interest in DLLME has only grown. More than 2,500 research articles have thus far been published in this field (www.webofscience.com/wos/). The wider popularity of DLLME in sample preparation is largely attributed to its simplicity, offering high enrichment factors and reduced extraction times. DLLME is predominantly applied for the analysis of food samples (32.3 %), though it is also employed for environmental (6.5 %), biological (9.7 %), and low-alcoholic beverages (12.9 %) matrices [281].

Accordingly to the trends for more efficient and environmentally friendly extraction techniques, DLLME received considerable attention, prompting various modifications and improvements over the classical method [281,282]. Among them, some DLLME modes can be listed: (i) air-assisted (AA)-, (ii) effervescence-assisted (EA)-, (iii) ultrasound-assisted (UA)-, (iv) vortex-assisted (VA)-, (v) ionic liquid (IL)-, (vi) magnetic ionic liquid (MIL)-, (vii), deep eutectic solvent (DES)-, and (viii) surfactant-assisted (SA)-DLLME.

Surfactant-assisted dispersive liquid liquid microextraction (SA-DLLME)

Surfactants are amphiphilic organic compounds with a hydrophobic non-polar hydrocarbon moiety (tail) and a hydrophilic polar headgroup. In its simplest form, the hydrocarbon part consists of a linear, saturated alkane, and its hydrophobic character increases progressively with increasing chain length. Alternatively, branched-chain alkanes and aromatic hydrocarbons are examples of more complex structures. On the other hand, surfactant headgroups exhibit much greater structural diversity [283].

There are different classification systems to categorized surfactants. Probably, the most widely recognized is based on the nature of the surfactant headgroup. In this context, four types of surfactants can be considered [284]:

(i) Non-ionic: with uncharged hydrophilic headgroups that can not be ionized in aqueous solution. They are considered mild surfactants. Typical examples of non-ionic surfactants are the Tween family (Tween-20 and Tween-80) and the Triton family (Triton X-100, Triton X-114).

(ii) Anionic: with anionic hydrophilic headgroups and generally higher critical micelle concentration (CMC) values compared to non-ionic surfactants. They are commonly employed as detergents and foaming agents. Examples include sodium dodecyl sulfate (SDS), sodium deoxycholate and sodium cholate, and sarkosyl (also known as sodium lauroyl sarcosinate).

(iii) Cationic: with cationic hydrophilic headgroups and higher CMC values compared to non-ionic surfactants. Common examples are quaternary ammonium salts and fatty amine salts like dimethyl-benzylammonium chloride and cetyltrimethylammonium bromide (CTAB).

(iv) Zwitterionic or amphoteric: hydrophilic headgroups that contain both positive and negative centres, resulting in a zero net charge. This type of surfactant combines

USC UNIVERSIDADE DE SANTIAGO DE COMPOSTELA

characteristics of both ionic and non-ionic surfactants. Phospholipids and amino acids are natural zwitterionic substances. Other typical examples include sulfobetaines and 3-[(3-cholamidopropyl)dimethylammonio]-1-propanesulfonate, better known as CHAPS.

As previously mentioned, several classifications exist to grasp the complexity and diversity of surfactants. Another conventional classification scheme is based on the hydrophile-lipophile balance number (HLB). This parameter ranges from 0 to 40 and quantifies the relative contributions of the hydrophilic and lipophilic regions of the molecule. Low HLB values (< 10) indicate that the surfactant is predominantly lipophilic and thus not water-soluble. Very high HLB values (> 20) denote highly hydrophilic molecules, which are typically used as stabilizers rather than classical emulsifiers. Moderate HLB values indicate a more balanced amphiphilicity and are associated with strong emulsifier-like characteristics [283]. Triton X-114, with an HLB of 12.4, places in this category [285]. Figure 7 displays the chemical structure and formula of Triton X-114.

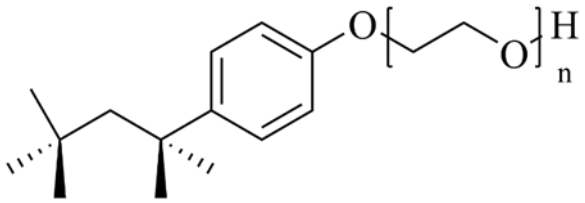

$(C_2H_4O)nC_{14}H_{22}O$, n=7 or 8

Figure 7. Chemical structure and formula of Triton X-114.

In order to avoid the use of organic solvents and promote safer, modern analytical extraction methods, surfactants have received significant attention over the past decades owing to their ability to reduce surface tension. The replacement of the organic dispersing solvent in DLLME with a surfactant has allowed the development of surfactant-assisted dispersive liquid liquid microextraction (SA-DLLME). This approach was first reported by Saraji et al. in 2010 for the determination of herbicides in aqueous samples [286]. In this mode, a mixture of surfactant and extraction solvent is rapidly injected into the sample solution, followed by the conventional DLLME procedure. Schematic diagram of the SA-DLLME extraction process is presented in Figure 8.

Although SA-DLLME was initially applied to the determination of organic compounds in aqueous samples [287,288], it was soon successfully extended to a wider range of target analytes and sample matrices [289–297]. Nonetheless, only few works have been reported so far for the extraction of NPs. Li *et al.* [298] explored the applicability of SA-DLLME combined with electrothermal vaporization inductively coupled plasma mass spectrometry (ETV-ICP-MS) for the analysis of AuNPs in environmental water samples. In the work presented they study the effect of the type of surfactant on extraction efficiency, comparing Triton X-100 and Triton X-114 (non-ionic surfactants), CTAB (cationic surfactant), and SDS (anionic surfactant). Among these, Triton X-114 achieved the highest extraction efficiency.

Selahle *et al.* [299] later reported in 2019 the integration of SA-DLLME with inductively coupled plasma-optical emission spectrometry (ICP-OES) for the extraction and quantification of TiO_2 and ZnONPs in industrial wastewater samples. Triton X-114 was employed as the surfactant during extraction.

USC DE COMPOSTELA

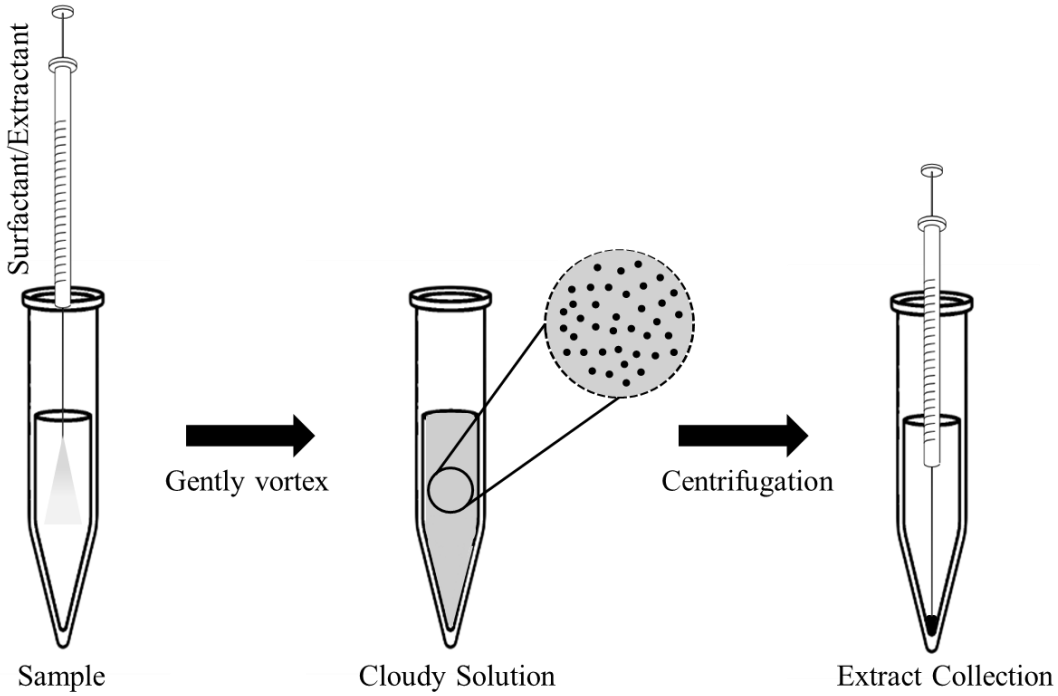

Figure 8. Diagram of the SA-DLLME extraction process.

5.1.2 Enzymatic hydrolysis

Degradation of the sample matrix generally requires the application of acidic, alkaline, or enzymatic digestion methods. However, in NP analysis, acidic digestion–classically employed for elemental analysis–is unsuitable because NP integrity is compromised [300].

Enzymatic hydrolysis refers to the use of enzymes for cleaving macromolecules bonds into smaller, soluble fragments (amino acids, sugars, peptides, fatty acids, etc.). Biological and environmental samples are organic-rich matrices that embed NPs. Hydrolysis depolymerizes and solubilizes these organic barriers [301]. As a result, NPs are released from the sample matrix and remain as undigested fraction. Enzyme specificity allows enzymes to act only on specific substrates and under mild temperature and pH conditions. This scenario minimizes analyte degradation phenomena. Thus, enzymatic hydrolysis selectively removes the biological matrix while preserving NPs physicochemical integrity.

Enzyme selection is dependent on the nature of the sample–high protein, fat, or carbohydrate content. Proteases are a specific type of enzymes that break peptide bonds in proteins, with common examples including pepsin, trypsin, and Proteinase K. Lipases, subclass of esterases, hydrolyse ester bonds and thereby degrade fats. Glycosylases (e.g., amylases, cellulases, and lactase) cleave glycosidic bonds in carbohydrates [301].

In many cases, mixtures of enzymes can be used simultaneously for the hydrolysis of different biomolecules. One popular enzyme combination reported in several literature sources is the pancreatin/lipase mixture.

Taboada-López *et al.* reported several works using pancreatin/lipase for the extraction of TiO_2NPs from bivalve molluscs [302] and surimi (crab sticks) [303], and for the extraction of AgNPs from seafood [304,305]. Chalifoux *et al.* [306]also used this enzyme combination for the extraction of AgNPs from a high fat animal matrix (in-house prepared ground beef reference

material). Later, Suzuki *et al.* [307] compared four different extraction protocols–ultrasonic crushing, alkali-treated hydrolysis, solubilization with surfactant, and enzymatic hydrolysis– for AgNPs in oysters. Results revealed that not only enzymatic hydrolysis had the highest recoveries in terms of particle number concentration and particles mass, but also the smallest effect on particle size.

However, matrix degradation can produce substantial quantities of hydrolysed matrix components in the extract, often requiring additional clean-up steps before analysis, such as filtration, settling, centrifugation, and dilution [300].

5.1.3 Centrifugal ultrafiltration (UF)

Filtration, ultrafiltration (UF), and dialysis have long been used for size fractionation. All three approaches are based on the use of semipermeable membranes of different materials and nominal molecular weight cutoffs (MWCO). However, it has been recently accepted that 0.45 μm filtration is no longer valid to separate dissolved and particulate forms. In contrast, dialysis and UF, which use nanoporous membranes, have been shown to isolate dissolved species from NPs. UF is generally preferred because dialysis relies solely on diffusion and therefore requires significantly longer times to reach equilibrium [308].

UF was first described by Whitlam and Brown in 1981 for the determination of protein binding in serum [309]. Nowadays, UF is successfully applied in pharmaceutical, food engineering, water treatment, and various nano-, bio-, and chemical technologies for concentration, purification, clarification and washing of colloidal suspensions such as proteins, DNA, polymers, and NPs [310–312]. The general principle behind UF is quite straight forward: species with molecular sizes below the MWCO are driven to cross the membrane through the application of centrifugal force. However, in certain cases, depending on NP composition and surface functionality, interactions with the UF membrane may occur, thereby affecting the analytical recovery [313]. Figure 9 illustrates the UF process.

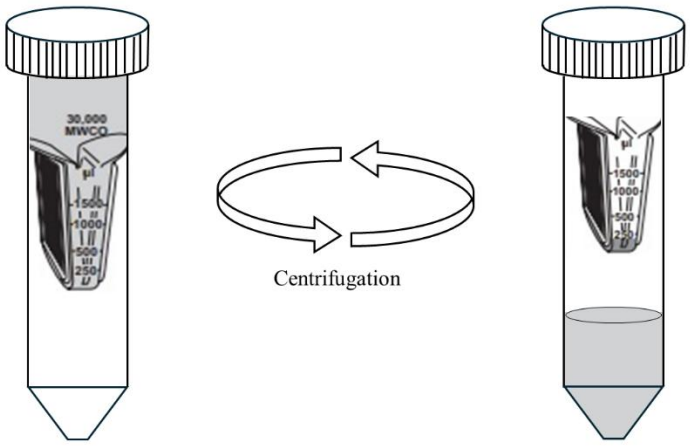

Figure 9. Schematic diagram of UF workflow.

UF has been applied to the analysis of NMs with membranes pore sizes between 3 and 100 kDa, including studies on Ag [314,315], ZnO [314,316], CeO_2 [314,315], TiO_2 [314], CuO [317], quantum dots, and Au [314].

USC DE COMPOSTELA

5.2 QUANTIFICATION AND CHARACTERIZATION OF NPS: ICP-MS-BASED TECHNIQUES

Historical background of inductively coupled plasma

The inductively coupled plasma (ICP) was originally developed by Reed in 1960 for crystal growing [318–320]. Shortly thereafter, its potential as an analytical excitation source was recognized, with the first publications reported in 1964 [321] and 1965 [322]. Although prior knowledge on generation of plasmas by inductive heating of gases at reduced pressure was existing [323].

A plasma is an ionized gas characterized by macroscopic electrical neutrality, with an equal density of positively charged ions and negatively charged electrons. In contrast to a flame, a plasma requires the continuous supply of an external energy in the form of an electrical field, to initiate and sustain gas ionization. The energized plasma then transfers part of its energy to the sample, for atomization and ionization. Plasmas are commonly classified according to the type of electrical field used for their generation and maintenance [324]:

- Direct current plasma (DCP), a direct current field is established across electrodes.
- Microwave-induced plasma (MIP), a microwave field is applied within a resonant cavity.
- Inductively coupled plasma (ICP), a high-frequency electromagnetic field is applied through an induction coil.

Historically, the DCP was the first plasma to be described and commercialized. However, the ICP has become the most widely used since its introduction. Initially, several alternative designations were used before the term ICP was established, including induction-coupled plasma spectrometric excitation source, high-frequency (hf) plasma source, induction plasma, or radio-frequency (rf) plasma torch [324].

Principles of inductively coupled plasma generation

The argon inductively coupled plasma (Ar ICP) is the most widely used [325]. The work of Houk *et al.* [326] is thought to be the first that reports the coupling of an argon-based ICP ion source to a quadrupole-based mass spectrometer for trace elemental analysis. Like any noble gas is a monoatomic element with a high ionization energy (15.76 eV), and is chemically inert. Consequently, Ar has the capability to excite and ionize most of elements of the Periodic Table, and no stable compounds are formed between Ar and analytes [324].

Energy is transferred into the Ar ICP through interactions between ionized argon and the electromagnetic field of the induction coil. First, an argon flow is directed through a quartz torch, around which an induction coil (or load coil) is positioned at the top end and connected to a radio frequency (RF) generator. When a RF power (usually between 750-1700 W) is applied, an alternating current oscillates within the field. These oscillations set up an electromagnetic field at the top of the torch. Plasma initiation begins when a spark is applied to the argon, stripping electrons from some argon atoms. These free electrons are confined and accelerated in the magnetic field through a process known as inductive coupling, and collide with neutral argon atoms triggering a chain collision–induced ionization reaction. This chain reaction process generates extremely high temperatures, typically ranging from 6000 to 10,000 K, depending on the plasma region. Once the sample aerosol is introduced, it undergoes rapid desolvation, vaporisation, atomization, and ionization within the plasma [327,328].

USC UNIVERSIDADE DE SANTIAGO DE COMPOSTELA

Aerosol generation and sample transport

The vast majority of ICP-MS applications are devoted to the analysis of liquid samples, although the technique has been adapted over the years to handle solid samples as well.

The main role of a liquid sample introduction system is to generate a fine aerosol of the sample. Generally, it consists of two components: (i) a nebulizer, that generates an aerosol from the bulk liquid sample, and (ii) a spray chamber, that filters the maximum drop size that will be further introduced into the plasma. The nebulizer generates a primary aerosol, which is coarse and polydisperse, while the spray chamber refines this into a tertiary aerosol, characterized by finer and less polydisperse droplets (8–10 μm) [329]. The sample introduction system is often described as the Achille's heel of ICP-MS, because it is considered the weakest component of the instrument [328]. Some of the main limitations are [329]:

(1) Low analyte transport efficiency (0.5–5 %)
(2) Susceptibility of the nebulizer tip to blockage when analysing high-salt content samples
(3) Pronounced memory effects and long wash-out times
(4) Difficulty in the analysis of very low samples volumes (i.e. < 1mL)

A number of sample introduction devices are commercially available. The most common nebulizers are pneumatic nebulizers (PNs) and ultrasonic nebulizers (USNs), although alternatives such as thermospray and electrothermal nebulizers are also available. Pneumatic nebulizers use mechanical forces of a gas flow to generate the sample aerosol. They have two basic configurations: (i) a high-velocity gas stream directed parallel to the sample capillary, or (ii) the liquid-carrying capillary positioned at a right angle to the gas stream capillary [325]. A typical pneumatic nebulizer for ICP spectrometry operated with a gas flow of 0.6-1.2 L min^{-1}, and a liquid flow rate of 0.5-1.5 mL min^{-1} [330]. Efficient production of a fine primary aerosol requires: (i) a high gas-to-liquid ratio, (ii) a narrow liquid capillary diameter, (iii) low sample viscosity, (iv) low surface tension, and (v) high gas density. Popular pneumatic nebulizer designs include: concentric (similarly for micro-concentric), single bore, direct injection high-efficiency (DIHEN), microflow, Babington (Cone-Spray version), and cross-flow nebulizers [330].

Spray chambers are basically available in two main designs: cyclonic and double-pass (Scott-type) spray chambers, with the market dominated by the latter type. In general terms, the double-pass chamber provides a finer tertiary aerosol, while the cyclonic design offers higher transport efficiency. Both designs are commonly manufactured in glass, silica, or polymer (typically PFA). In addition, in certain ICP-MS configurations, spray chambers are externally cooled to ensure thermal stability of the sample [328,330].

The core of an ICP: the torch

The plasma torch consists of three concentric tubes, typically madre from quartz. The outermost tube carries the plasma gas (argon), typically operated at a flow rate of 11-15 L min^{-1}. The middle tube supplies the so-called auxiliary gas at a flow rate of 0.5-1.5 L min^{-1}. The innermost tube, injector tube, carries the sample in the form of an aerosol from the sample introduction system, this gas flow is often called nebulizer gas flow [327,328,331]. Figure 10 displays a real image of a plasma torch mounted in an instrument.

USC UNIVERSIDADE DE SANTIAGO DE COMPOSTELA

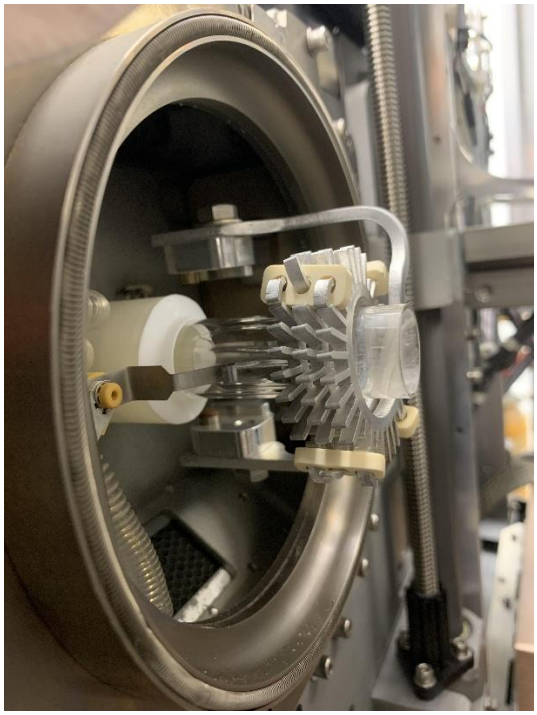

Figure 10. Photograph of a plasma torch mounted in an instrument.

Ion sampling interface

The role of the interface region is to efficiently transport the ions generated in the plasma to the mass spectrometer analyser. This fundamentally involves the transport of analyte ions from a high temperature (~7,500 K), atmospheric pressure (~1,000 mbar) environment to a room temperature (~300 K) and reduced pressure (10^{-5}-10^{-9} mbar) region [327]. This is achieved by directing the analyte ions through a series of small orifices. A comprehensive study on the effect of orifice size and shape has been performed by Campargue [332], and readers are encouraged to consult this work. The interface consists of two metallic cones, typically made of nickel, although other materials such as platinum may be used for greater tolerance to corrosive liquids. After ion generation, the ions pass into the first cone, known as the sampler cone, which has an orifice of 0.8-1.2 mm in diameter, approximately. On passing through this orifice the gas expands adiabatically, causing a decrease in gas density and kinetic temperature. The ions then proceed to the skimmer cone, which is generally more sharply pointed than the sample cone and has a smaller orifice, about 0.4-0.8 mm in diameter [328]. The area between the sampler and the skimmer cones is known as the zone of silence, where the sampled gas is considered to be representative of the plasma gas [333]. To reduce the effect of high-temperature plasma on the cones, the interface is water cooled. Once skimmed, the ions are extracted and focused through a series of ion optics into the mass analyser.

Mass analysers

Various configurations of ICP-MS are commercially available. Among them, the most commonly used are quadrupole (ICP-Q-MS), static sector field with multi-collector detector (MCICP-MS), scanning sector field (SF-ICP-MS), and time of flight (ICP-TOF-MS) [334]. All options present benefits and limitations. In general terms, quadrupole-based ICP-MS are best suited for the analysis of mono-elemental NMs. Triple quadrupole ICP-MS (ICP-QQQ-MS) provides enhanced performance, particularly for the detection of NPs such as SiO_2 and TiO_2 in

complex sample matrices. In contrast, the characterization of nanocomposites, naturally occurring materials, or unknown NMs, usually requires simultaneous multi-element detection, possible with ICP-TOF-MS instruments.

5.2.1 spICP-MS

Due to the rapid development of nanotechnology, interest has grown in analytical methods capable of determining the chemical composition, number concentration, and size distribution of nanoparticles at single-particle resolution. Single particle ICP-MS is a technique able to perform measurements on a "particle by particle" basis. Single particle analysis was first demonstrated in 1986 using ICP optical emission spectrometry, and later coupled with ICP-MS to enhance sensitivity. However, it was not until 2003 that Degueldre and Favarger published the first study outlining the theoretical framework of single particle ICP-MS for the analysis of colloidal and microparticle suspensions. As noted in *1.1 History, scientific story and today's global landscape*, the nanotechnology sector experienced a significant growth beginning in the early 2000s. Consequently, the development and interest within the scientific community in spICP-MS grew in parallel.

Having outlined the process by which a liquid sample is introduced and transport into the plasma, it is important to address two fundamental concepts: (i) soluble forms of an element are homogeneously distributed within the solution and, consequently, within the aerosol droplets. As a result, the flux of the element entering the plasma and reaching the detector produces a constant, stable signal throughout the measurement period. In contrast, (ii) particulate elements within a suspension are not homogeneously distributed but confined to discrete particles. Once the NP is vaporized, it will produce a cloud of ions, resulting in a transient signal of less than 0.5 ms, approximately [335]. Then, if a sufficiently diluted suspension (<10^8 particles L^{-1}) is introduced, and high acquisition frequencies (>100 Hz) are used, the transient signal produced by each individual particle can be recorded [336]. The basic assumption behind spICP-MS is that each recorded event corresponds to only one particle. If this is accepted, then the frequency of events recorded during an acquisition time is directly related to the number concentration of particles [337–339]:

$$n_p = n_{neb} Q_{sam}\, t_i\, C_p \qquad \textit{Equation (3)}$$

Where, n_p is the number of pulses recorded, n_{neb} the nebulization efficiency, Q_{sam} the sample introduction flow rate, t_i the acquisition time, and C_p the number concentration. In addition, the intensity of each pulse (I_p) is proportional to the number of atoms of the element monitored in each detected particle. Therefore, the mass of element (m_p) per particle can be calculated as:

$$I_p = K_{ICPMS}\, K_M\, m_p \qquad \textit{Equation (4)}$$

Where K_{ICPMS} is the detection efficiency, defined as the ratio of amount of analyte detected versus the amount of analyte introduced into the ICP, and K_M is a factor intrinsic to the element measured, calculated as:

$$K_M = A\, N_{AV} / M_M \qquad \textit{Equation (5)}$$

USC UNIVERSIDADE DE SANTIAGO DE COMPOSTELA

Where A is the atomic abundance of the isotope considered, N_{AV} the Avogadro number, and M_M the atomic mass of the element.

Equations (3) and (4) summarize the fundamental principles of spICP-MS. For suspensions of spherical, solid, and pure NPs, eq. (4) can be rearranged to relate to particle size:

$$I_p = \frac{1}{6}\pi\ \rho\ X_p\ K_{ICPMS}\ K_M\ d^3 \qquad \textit{Equation (6)}$$

Where ρ is the density, X_p the mass fraction of the element in the particle, and d the particle diameter.

In this sense, spICP-MS can provide information about: (i) qualitative presence of particulate and/or dissolve forms of specific elements, (ii) characterization about the mass of element per particle, which can be later translated into particle size when composition, shape, and density of the particles are known, and (iii) quantitative information on particle number concentration, and mass concentrations of both particulate and dissolved forms [337].

Detectability and limits of detection

Initially, dwell times were limited to the millisecond range (3-10 ms), which allowed recording particle events as pulses. More recently, fast scanning instruments have become commercially available, allowing the use of dwell times in the microsecond range, and therefore recording particle events as transient signals [340].

The detection of NPs in single particle mode depends on two factors: (i) the number concentration, which should be high enough to allow counting a minimum number of events, and (ii) the element mass per NP (or NP size), which should be large enough to generate a number of ions detectable by the detector. Consequently, two limits of detection (LODs) need to be considered, one in terms of concentration (LOD_{NP}), and the other in terms of size (LOD_{size}). Equations (7) and (8) describe their calculation [341]:

$$LOD_{size} = \left(\frac{30\ \sigma_B}{\frac{2}{w}\pi\rho X_p K_{ICPMS} K_M t_{dwell}}\right)^{1/3} \qquad \textit{Equation (7)}$$

Where σ_B is the standard deviation of the mean baseline signal, w the peak width, and t_{dwell} the dwell time used.

$$LOD_{NP} = \frac{5\sqrt{Y_{N,B}}+3}{n_{neb} Q_{sam} t_i} \qquad \textit{Equation (8)}$$

Where $Y_{N,B}$ is the mean number of particles counted for a blank.

Raw time scans can be processed by plotting the event intensity versus the event intensity frequency, obtaining a histogram. If fully resolved, the first distribution shows the contribution from the background and/or the presence of dissolved element and should fit a Poisson profile, whereas the second one is due to the particles which tends to be lognormal [337].

USC UNIVERSIDADE DE SANTIAGO DE COMPOSTELA

5.2.2 SC-ICP-MS

Single Cell ICP-MS is an emerging analytical technique in the fields of environmental and biological sciences that enables quantification on a single-cell basis. Traditional cell analysis was performed by acid-digestion methods providing an average information of a high number of cells. Nonetheless, cell-to-cell variations were neglected, and cell heterogeneity information was lost. In this context, SC-ICP-MS analysis provides information at a single-cell resolution.

A great amount of fundamental concepts discussed for spICP-MS can be directly applied to SC-ICP-MS, as theoretical basis of single event-ICP-MS apply to different types of entities [342]. In some cases, research groups that initially mastered spICP-MS have later extended their expertise to SC-ICP-MS and considered the latter an evolution of the former. Nonetheless, the evolution of SC-ICP-MS has been largely independent and in parallel, although at a much slower pace in terms of publications. Figure 11 shows the temporal evolution of publications on spICP-MS (solid dark bars) and SC-ICP-MS (dashed bars).

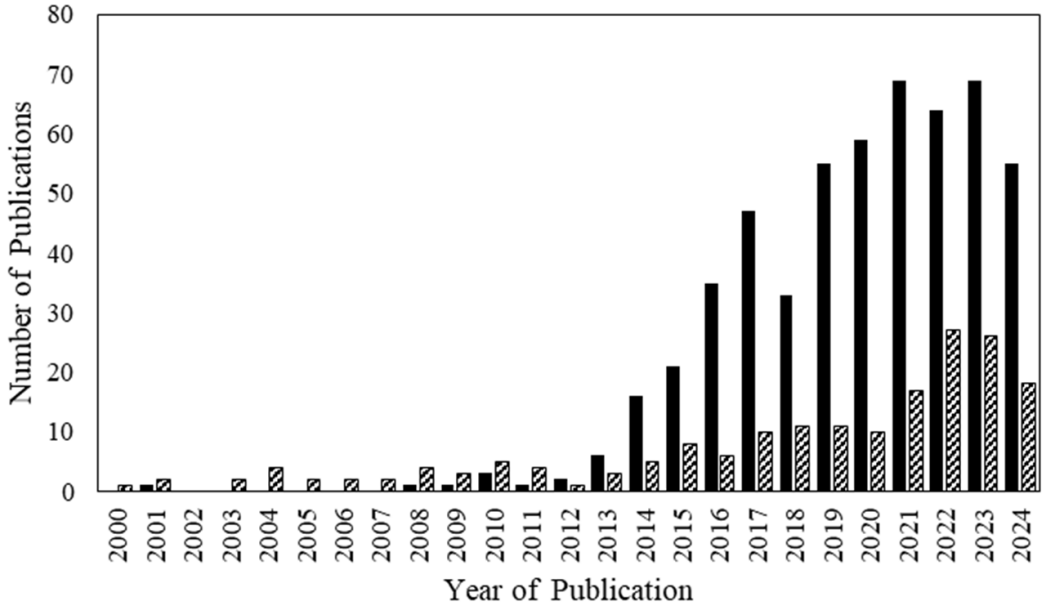

Figure 11. Temporal evolution of spICP-MS (solid dark bars) and SC-ICP-MS (dashed lines) in number of publications since 2000 to 2024, using 'spICP-MS' or 'single particle ICP-MS' and 'SC-ICP-MS' or 'single cell ICP-MS' as keywords. Source Web of Science, September 2025.

Briefly, in SC-ICP-MS, a cell suspension is introduced into the plasma where the droplets containing cells are vaporized and the analytes of interest present in the cell are atomized and ionized, producing and ion plume that is detected as a short transient signal, called cell event. If acquisition conditions are properly selected (i.e. suspension dilution, and dwell time) it may be presumed that each cell event corresponds to one individual cell. Thus, the cell event frequency is proportional to the cell concentration, and the cell event intensity to the mass of the analyte present in the cell [343].

Sample introduction is an aspect where differences between spICP-MS and SC-ICP-MS become more evident. The stability of NPs and cells is not the same. In general terms, cell are more fragile entities, and thus they need special handling. In addition, cells have tendency to adhere to surfaces leading to poor transport efficiencies and high memory effects [344]. Sample preparation strategies prior to SC-ICP-MS usually involve cell fixation with different types of

fixatives, including paraformaldehyde, formaldehyde, or glutaraldehyde. Furthermore, conventional ICP spray chambers are designed to filter large droplets, and the cells dimensions often exceed the droplet sizes allowed by such spray chambers. For this reason, several pieces of literature show the use of direct injection *via* microdroplets for SC-ICP-MS. Although spray chambers have been redesigned and several options are now commercially available. This is the case of the Asperon^{TM} spray chamber shown in Figure 12, which ensures intact delivery of cells. A similar device has been proposed by Glass Expansion, marketed under the name Single-Cell Sample Introduction System (SC-SIS). These spray chambers are typically equipped with a makeup gas to minimize cell deposition onto the chamber walls, and transport efficiencies higher than 30 % have been reported for such designs.

Analytical information that can be obtained by SC-ICP-MS includes: (i) concentration of cells containing specific analytes, (ii) mass of the analyte per cell, and (iii) mass distribution within a cell population [345].

Figure 12. Photograph of an Asperon^{TM} spray chamber for single-cell analysis mounted in an instrument.

5.2.3 LA-ICP-MS

The word *laser* is an acronym for 'light amplification by stimulated emission of radiation', which describes the process of photons being released from energized atoms in these devices. The emitted light of a laser is monochromatic, coherent and directional [327].

The first application of laser ablation for solid sample introduction into an ICP-MS was published in 1985 by Gray *et al.* [346]. Further work was then developed by Arrowsmith [347,348], Tye *et al.* [349], Hager [350], and Mochizuki *et al.* [351,352] using both ruby (wavelength = 694 nm) and Nd:YAG (wavelength = 1064 nm) lasers with commercial ICP-MS.

Shortly after its demonstration, LA-ICP-MS became a powerful tool for the direct analysis of the elemental and isotopic composition of solid (or semisolid) samples. LA refers to the use of an intense burst of energy in the form of a focused laser beam directly onto the sample [327]. As a result, material from the sample surface is sputtered and vaporized. The laser-induced aerosol generated is then transported by an inert gas to the ICP-MS [353].

The general instrumental layout consists of a pulsed laser source, beam delivery optics, an air-tight sampling cell, and an aerosol transport line [353]. Figure 13 displays a common LA-ICP-MS layout.

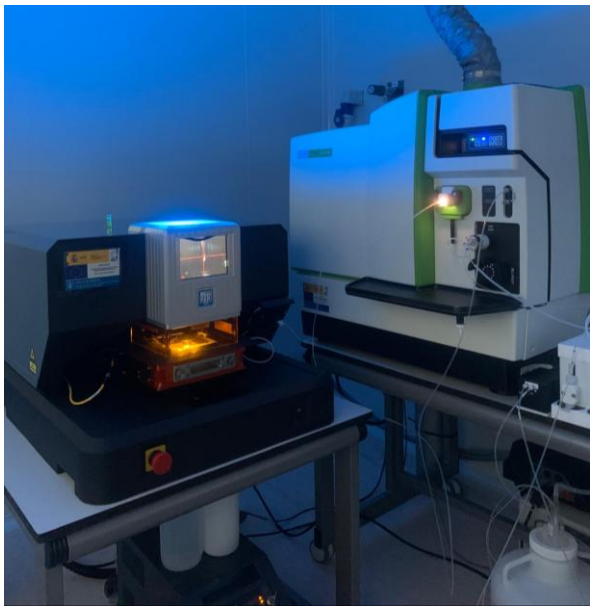

Figure 13. Laser Ablation NWR-213 unit (New Wave Research, Inc., CA, USA) coupled to NexION 2000 ICP-MS (Perkin Elmer, Waltham, MA, USA).

LA-ICP-MS can perform analysis of individual spots, "standard LA-ICP-MS", or two/three-dimensional analysis, "LA-ICP-MS imaging", which in the case of soft tissues, is known as bioimaging [354]. Unlike solution analysis, solid sampling offers the benefit of obtaining information on the spatial distribution of elements within the samples. LA-ICP-MS enables spatially-resolved analysis with lateral resolutions typically within the range of 1-20 μm (sub-cellular resolution can be achieved in some applications, depending on laser characteristics and experimental layout employed), whereas depth resolution can reach up to 300 nm if femtosecond laser systems are used [355].

In recent years, LA-ICP-MS has advanced rapidly and found growing applications in many different fields, including cultural heritage, geochemistry, environmental chemistry, advance materials, provenance studies, forensics, and life sciences–particularly biological and medical research [354].

Laser beam properties

The properties of the laser and the laser instrumentation significantly influence the ablation process. Laser wavelength, pulse energy, pulse frequency, pulse duration, laser beam profile, and spot size are key parameters [327].

Laser wavelength has an enormous impact on the ablation process, ablation rate, fractionation process, and the materials that can be ablated. In general terms, lower laser wavelengths in the ultra-violet (UV) region are preferred. Pulse energy will determine the ablation depth. High power density lead to greater depths, and thus higher absorbance of the energy in the sample. Pulse frequency is an important parameter to consider, as high repetition rates can cause to plasma shielding–a phenomenon where the incident laser beam is absorbed or reflected by a plasma formed close to the sample surface from the previous laser shot. Pulse duration strongly influences the ablation process. When nanosecond laser pulses are used, the ablation mechanism is largely governed by thermal effects; materials with low melting points may melt during ablation, compromising local spatial and/or depth resolution. In contrast,

femtoseconds laser pulses minimize melting effects and prevent thermal diffusion, thereby providing better lateral and depth resolution. The energy profile of the laser beam influences the geometry of the resulting ablation crater, while the spot size determines the achievable lateral resolution. Commonly used spot sizes are between 10 and 400 μm.

Limitations

A major limitation of LA-ICP-MS, as with most laser-based analytical sampling, is that the measured signal does not always represent the true stoichiometric sample composition. This effect, known as elemental fractionation, may occur during the laser ablation, aerosol transport, or subsequent vaporization, atomization, and ionization processes in the ICP [355]. Laser energy and wavelength, pulse duration, and beam profile can influence elemental fractionation.

Moreover, the lack of appropriate standard or certified reference materials–particularly for biological matrices–hinders accurate quantification. Several normalization and calibration strategies, including in-house calibration approaches such as pressed powders or doped gelatine, have been proposed so far, yet a universal calibration method has not been established [355].

USC
UNIVERSIDADE DE SANTIAGO DE COMPOSTELA

II. OBJECTIVES

USC
UNIVERSIDADE
DE SANTIAGO
DE COMPOSTELA

OBJECTIVES

The overarching aim of this thesis was to advance the analytical capabilities required for the reliable detection, characterization, and quantification of ENPs in complex environmental, biological, and cellular systems. Recognizing that the accurate study of NPs depends on both the instrumental platform selected and the suitability of pre-treatment methods, the work aimed to developed nanometrological platforms for sensitive and reproducible NP assessment.

The specific objectives were as follows:

- To design and validate pre-concentration and extraction procedures that enable NP detection in tap water samples, with particular focus on the application of surfactant-assisted dispersive liquid-liquid microextraction (SA-DLLME) combined with spICP-MS for analysis of AgNPs and TiO_2NPs.

- To evaluate and compare different sample preparation strategies, including SA-DLLME and centrifugal UF, for the quantification of AgNPs and TiO_2NPs in human urine. To assess the feasibility of urine as non-invasive biomonitoring fluid.

- To study enzymatic hydrolysis as a gentle pre-treatment for serum samples analysis, avoiding particle dissolution or aggregation, and thereby enabling spICP-MS detection of TiO_2NPs in a protein-rich matrix.

- To apply SC-ICP-MS for the analysis of human red blood cells, quantifying AgNPs uptake at the single-cell level and elucidating cell-to-cell heterogeneity in NP association.

- To develop innovative calibration and cell handling srtategies for future biological LA-ICP-MS applications.

USC
UNIVERSIDADE DE SANTIAGO DE COMPOSTELA

III. METHODOLOGY

USC
UNIVERSIDADE
DE SANTIAGO
DE COMPOSTELA

METHODOLOGY

The thesis employed a combination of sample preparation strategies and (ICP-MS)-based techniques for the detection, characterization, and quantification of ENPs in environmental, biological, and cellular systems. Each chapter focused on a specific matrix and applied a particular analytical approach.

– Chapter 1

Tap water samples were processed using SA-DLLME to pre-concentrate and stabilize AgNPs and TiO_2NPs. A mixture of Triton X-114 and 1,2-dichloroethane in a 49:1 ratio was employed for the extraction. After vortexing and centrifugation, extracts were collected, diluted with 1.0 % (w/v) glycerol and analyzed by spICP-MS to determine particle size distributions, concentrations (in terms of mass and number), and dissolution behaviour.

– Chapter 2

Human urine samples were prepared using two alternative sample extraction methods: SA-DLLME and UF. On the one hand, 1.0 mL of a 49:1 surfactant/extractant (2.5 % (w/v) Triton X-114/1,2-dichloroethane) mixture was employed for the extraction. Diluted urine extracts were analyzed by spICP-MS. On the other hand, the Amicon Ultra units (30 kDa MWCO) were employed for UF pre-treatment. The cleaned extracts were withdrawn from the filter, diluted, and anlysed by spICP-MS under the same operating conditions.

– Chapter 3

Human serum samples were subjected to enzymatic hydrolysis using a mixture containing 0.1 % (w/v) pancreatin and 0.1 % (w/v) lipase to digest proteins and liberate NPs. Enzymatic hydrolysis was carried out for 4 hours at 150 rpm and 37 ºC under orbital-horizontal shaking. After digestion, the hydrolysed serum wass subjected to UF (30 kDa MWCO membranes) to remove residual macromolecules. Diluted extracts were finally analized by spICP-MS.

– Chapter 4

Human red blood cells were isolated from whole blood and exposed in vitro to AgNPs of different sizes and concentrations for 8, 12, and 24 hours. After incubation, all cell cultures were centrifugated and washed twice with 1.0 % (w/v) PBS. The final cell pellets were resuspended in freezing solution and kept at -80 ºC until SC-ICP-MS analysis.

USC
UNIVERSIDADE DE SANTIAGO DE COMPOSTELA

– Chapter 5

Two methodological innovations were developed to improve calibration and cell handling in LA-ICP-MS. On the one hand, ionic and nanoparticle-spiked gelatine microdroplets were prepared as novel calibration strategy. On the other hand, a microwell array master mold was desing in AutoCAD and fabricated through photolitography to later produce negative-PDMS molds for controlled single-cell trapping.

USC
UNIVERSIDADE DE SANTIAGO DE COMPOSTELA

IV. RESULTS

USC
UNIVERSIDADE
DE SANTIAGO
DE COMPOSTELA

IV. PART A: PUBLISHED RESULTS

USC
UNIVERSIDADE
DE SANTIAGO
DE COMPOSTELA

CHAPTER 1. PROSPECTS OF SURFACTANT ASSISTED DISPERSIVE LIQUID-LIQUID MICROEXTRACTION FOR THE SELECTIVE EXTRACTION OF SILVER AND TITANIUM DIOXIDE NANOPARTICLES FROM TAP WATER AND DETERMINATION BY SPICP-MS

USC
UNIVERSIDADE DE SANTIAGO DE COMPOSTELA

CHAPTER 1. PROSPECTS OF SURFACTANT ASSISTED DISPERSIVE LIQUID-LIQUID MICROEXTRACTION FOR THE SELECTIVE EXTRACTION OF SILVER AND TITANIUM DIOXIDE NANOPARTICLES FROM TAP WATER AND DETERMINATION BY SPICP-MS

The results from this chapter have already been published as:
Ana Justo-Vega, Raquel Domínguez-González, Pilar Bermejo-Barrera, and Antonio Moreda-Piñeiro

Group of Trace Elements, Spectroscopy and Speciation (GETEE), Institute of Materials iMATUS, Department of Analytical Chemistry, Nutrition and Bromatology, Faculty of Chemistry, Universidade de Santiago de Compostela, Avenida das Ciencias, s/n., 15782, Santiago de Compostela, Spain.
*Journal of Analytical Atomic Spectrometry, 2024, **39**, 573*
(DOI: 10.1039/d3ja00227f)

GRAPHICAL ABSTRACT

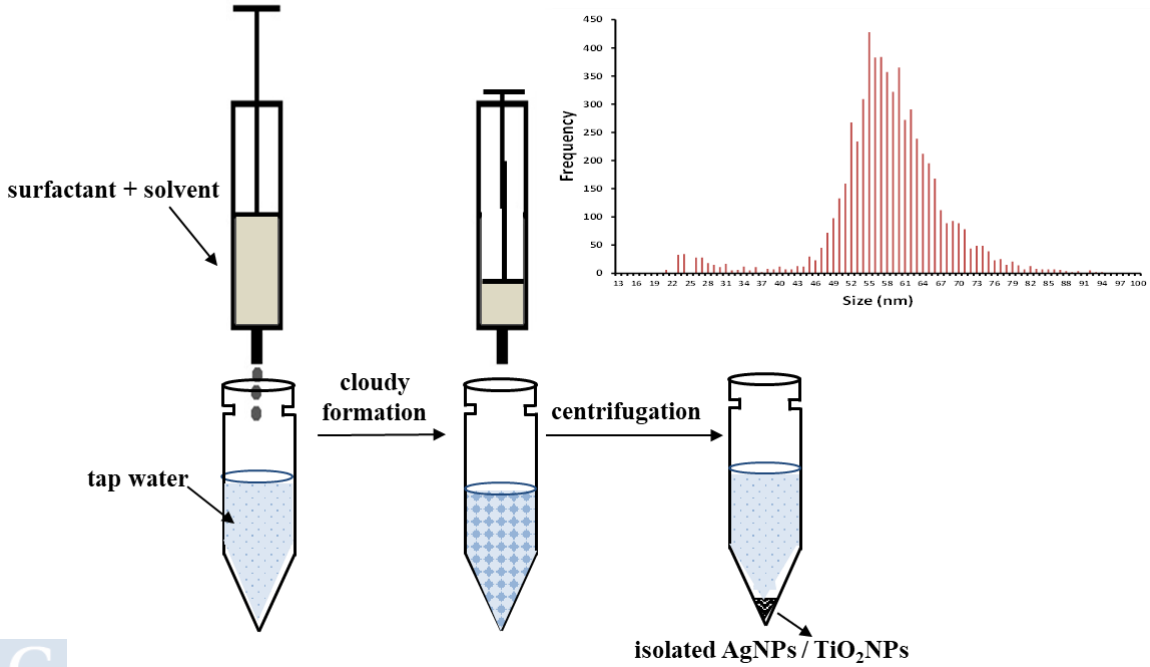

USC UNIVERSIDADE DE SANTIAGO DE COMPOSTELA

ABSTRACT

The widespread use of inorganic nanoparticles (NPs), especially silver (Ag) and titanium dioxide (TiO_2) NPs, has led to growing concern about their impact on human health and the environment. Inorganic nanoparticles are present in a large variety of products including cosmetics, foodstuffs, and medical goods, and NPs releasing from consumers' products into the environment can be therefore expected. Because of the low concentration levels of NPs in water, special care must be taken when developing new reliable analytical methods. In the current research, the possibilities of surfactant-assisted dispersive liquid–liquid microextraction (SA-DLLME) in combination with single-particle inductively coupled plasma mass spectrometry (spICP-MS) have been explored/discussed. Optimum conditions for the preconcentration of TiO_2NPs and AgNPs were 10 mL of water sample, 1.0 mL of the Triton X-114/1,2-dichloroethane (49:1) mixture, vortexing at 1500 rpm for 30 s, and centrifugation at 3500 rpm for 5 min. The collected organic phase was finally diluted to 1–2 mL with 1 % (w/v) glycerol, leading to an enrichment factor within the 5–10 range. The developed procedure (sample pre-treatment and spICPMS) led to a size detection limit (5σ criteria) of 65.8 and 16.7 nm for TiO_2NPs and AgNPs, respectively. The limit of detection in number concentration was 6.06×10^6 L^{-1} for AgNPs and 2.85×10^6 L^{-1} for TiO_2NPs, whereas the limit of detection for dissolved Ag and Ti mass concentrations was found to be 0.435 and 9.82 ng L^{-1}, respectively. The operational simplicity, low cost and less consumption of organic solvents make SA-DLLME a greener and faster choice compared to classical liquid–liquid extraction techniques.

1.1 INTRODUCTION

The scientific interest on nanomaterials (NMs), and mainly on inorganic nanoparticles (NPs), has exponentially increased since early 2000s. Due to the unique and outstanding properties that these NMs exhibit, they are now used for a large variety of applications, and currently they are present in more than 10400 products [1]. However, this widespread use has led to a growing concern about their environmental implications and the potential risk for humans.

Silver nanoparticles or nanosilver (AgNPs) and titanium dioxide nanoparticles or nano-titanium (TiO_2NPs) are nowadays the most widely used NPs. Nanosilver exhibits antibacterial, antiviral, antifungal and anti-inflammatory characteristics, and these properties, as well as their ability to promote wound healing, have been exploited for medic al and biomedical purposes including drug delivery, orthopaedics, pharmaceutics, and dentistry [2-4]. Furthermore, AgNPs are included in many daily consumer products such as cosmetics, deodorants, toothpaste, food packaging, toys, textiles, as well as in goods from the bioelectronics industry [5,6]. Regarding nano-titanium, the main applications are focused on cosmetic preparations and personal care products (foundations, day creams, and lip balms) because of their high refraction index [8] (an estimated 25 % of the total nano-TiO_2 market is used for sunscreen formulations [9]). In addition, TiO_2NPs also find applications in agriculture, building engineering, sewage, and water treatment, as well as in organic synthesis as catalysts. Although E171 (titanium dioxide) is nowadays no longer considered safe in the food industry [12] this food additive, which can contain up to 36 % of nano-titanium [13], was also widely used to enhance the sheen and white colour of certain foods, such as candies or sauces [14], and also as a flavour enhancer for some other nonwhite foodstuffs (soups, beer, nuts and dried vegetables) [8].

The widespread use of NPs has led to their inevitable release and presence in the environment, and NPs have already been considered as emerging pollutants [15]. However, the

levels of NPs in water are expected to be low and measured environmental concentrations (MECs) within the ng L^{-1} to low mg L^{-1} range have been reported of Ti- and Ag-based NPs in tap water [16]. In addition, similar concentration ranges have been also described in surface water [17–20] From the analytical point of view, there are still major challenges to master before understanding NPs and environmental factors and their interplay. Even though a large variety of techniques are available, the existing protocols do not yet fulfil all desirable criteria, and adequate and innovative analytical approaches for the identification, characterization, and quantification of NPs in natural environments are required.

Single-particle inductively coupled plasma mass spectrometry (spICP-MS) in combination with other instrumental techniques such as electronic microscopy and light scattering techniques is a useful nanometrological tool for the determination of NPs [21]. The principle behind the single-particle mode is that only one particle is measured at a given reading time, if a sufficiently diluted sample is introduced. Assuming this, the number of counts of the recorded signal is proportional to the number of atoms in the particle, and the frequency of the pulses relates directly to the number concentration of NPs. The direct relationship between the number of counts (number of events) and the NP number concentration requires the appropriate assessment of transport efficiency (% TE), a key parameter in the equations involved in spICP-MS calculations [22]. In addition to NP number concentration, spICP-MS gives information regarding the particle size and size distribution of the measured NPs [22,23]. However, some limitations of spICP-MS lie in the lack of information regarding the shape of the NP, and in assuming that all NPs are solid and spherical in shape. Moreover, prior knowledge of the density and composition of detected NPs is required, and NP certified reference materials for TE calculation are needed when using the particle size and particle frequency approaches. Critical statements on the advantages and limitations of spICP-MS can be found in various reviews on the topic [21,24].

An additional challenge in nanometrology is the stability of the inorganic NPs during the sample pre-treatment, a step required for isolating and/or pre-concentrating the NPs from the bulk sample. Once NPs enter natural environments, they are subjected to different transformation processes including aggregation, oxidation, dissolution, chlorination and sulfidation [25]. Hence, separation methods that do not modify the physicochemical properties of NPs are imperative, and surfactants have been investigated for NP stabilization purposes in aqueous solutions [26–29]. Therefore, the use of surfactants for assisting extractive processes of NPs could guarantee the integrity of NPs. Surfactants (Triton X-100, Triton X-114, and tween 80) have been used as dispersing agents in dispersive liquid–liquid microextraction (DLLME) procedures due to their dissolution capacity in polar and non-polar media (the extractant in DLLME is an organic solvent) leading to the so-called surfactant assisted dispersive liquid–liquid microextraction (SA-DLLME). As reviewed, applications have been mainly focused on preconcentrating/isolating organic compounds and metallic ions [30–32]; although some developments have been made for gold nanoparticles (AuNPs) in water [33] and TiO_2NPs and zinc oxide nanoparticles (ZnONPs) in wastewater [34]. Analytical techniques such as inductively coupled plasma optical emission spectroscopy (ICP-OES) [34] and electrothermal vaporization inductively coupled plasma-mass spectrometry (ETV-ICP-MS) [33] have been proposed for assessing the metal amount of the isolated NPs. These techniques assess the metal content in NPs but do not determine the number of nanoparticles. Furthermore, the phenomena of degradation (ionization) and/or agglomeration of the isolated nanoparticles during the extraction process will not be detected with the use of these techniques since their detection/determination power does not distinguish the ionic metal (in solution) from the nanoparticle metal, nor the state of aggregation (agglomeration) of the NPs. More robust

USC DE COMPOSTELA

information regarding the stability of the isolated NPs by SA-DLLME can be obtained by using spICP-MS because the number of isolated NPs can be measured and ionization phenomena, mainly for high ionizable NPs such as AgNPs, can be easily detected.

Therefore, the current research aims to study the potential of SA-DLLME as an extractive technique for NPs from tap water by assessing the number of NPs as well as the size distribution of NPs by spICP-MS to prove the stability of the NPs during the extractive process. A comprehensive investigation of the experimental parameters affecting the efficiency of the SA-DLLME process was carried out, and the spotlight has been put on method validation to assess the degree of stability of TiO_2NPs and AgNPs. Since agglomeration, as well as dissolution of NPs, can be influenced by the NPs' environment (sample's components), the studies have been focused on tap water.

1.2 METHODOLOGY

1.2.1 Chemicals and standards

An N8151035 reference PEG-COOH coated gold nanoparticle suspension (49.6 nm determined by TEM, 12.4 ng mL^{-1}, number particle concentration of 9.89×10^6 mL^{-1}, in aqueous 1 mM citrate) was purchased from NanoComposix (San Diego, CA, USA). Silver nanoparticles of a nominal size of 20.8 ± 3.0 nm (0.021 mg mL^{-1}, number particle concentration of 4.2×10^{11} mL^{-1}), 41 ± 5 nm (0.021 mg mL^{-1} and number particle concentration of 5.4×10^{10} mL^{-1}), and 59 ± 6 nm (0.020 mg mL^{-1} and number particle concentration of 1.8×10^{10} mL^{-1}) were also obtained from NanoComposix. Titanium dioxide nanoparticle ethanol dispersion (15 wt %) with a nominal size of 100 nm was supplied by US Research Nanomaterials (Houston, TX, USA). Diluted suspensions of inorganic NPs were prepared in ultrapure water (Milli-Q Gradient A10, Millipore Co., Bedford, USA) by accurately weighing aliquots of the commercially available suspensions after vigorously shaking for 1.0 min. Glycerol and 1,2-dichloroethane (LC Gradient) were both purchased from Merck (Darmstadt, Germany), as well as the silver standard ($AgNO_3$, 1000 mg L^{-1} Ag) and titanium standard ($(NH_4)_2TiF_6$, 1000 mg L^{-1} Ti). Triton X-114 at 2.5 % (v/v) was prepared from laboratory grade Triton X-114 (Sigma-Aldrich, San Luis, MO, USA), and nitric acid (hyperpure, 69 %) from Panreac (Barcelona, Spain). NexIon setup solution (10 mg L^{-1} Be, Ce, Fe, In, Li, Mg, Pb, and U in 1 % HNO_3) was supplied by PerkinElmer (Waltham, MA, USA).

1.2.2 Instrumentation

A PerkinElmer NexION® 300X inductively coupled plasma mass spectrometer (Waltham, MA, USA) was used throughout. The sample introduction system consisted of a Meinhard® nebulizer and a quartz cyclonic spray chamber. Syngistix™ Nano Application software version 2.5 was used for single-particle data processing. A JEOL 2100 transmission electron microscope (TEM, operating at 200 kV) equipped with an energy dispersive X-ray spectrometer (EDS, a solid angle of 0.28 sr in HR configuration with a 50 mm^2 detector) from JEOL, Japan was used for 100 nm TiO_2NPs standard characterization. A Reax vortex agitator from Heidolph (Schwabach, Germany) and a Sigma Laborzentrifugen 2K15 (Osterode, Germany) centrifuge with a cooling system were used during the SA-DLLME process. For weighing purposes, a Mettler Toledo ML204/01 analytical balance (Columbus, OH, USA) was employed.

USC UNIVERSIDADE DE SANTIAGO DE COMPOSTELA

1.2.3 SA-DLLME extraction procedure

An aliquot of 10 mL of tap water was placed in a glass tube with a conical bottom and 1.0 mL of a 49:1 surfactant (2.5 % (w/v) Triton X-114)/extractant (1,2-dichloroethane) mixture was added into the sample solution. The mixture was then vortexed at 1500 rpm for 30 s forming a cloudy solution due to the dispersion of fine droplets of organic solvent into the aqueous sample. The analytes (organic extract) were later collected by centrifugation at 3500 rpm for 5.0 min, and the recovered sedimented phase was diluted to 2.0 mL with 1.0 % (w/v) glycerol (optimization and validation experiments) or to 1 mL with 1.0 % (w/v) glycerol (sample analysis with an enrichment factor of 10). Redissolved extracts were again vortexed before spICPMS measurements.

1.2.4 Operating conditions for spICP-MS measurements

Instrumental conditions

The instrumental and data acquisition parameters are listed in Table 3. The standard operation mode was used for monitoring ^{49}Ti and ^{107}Ag isotopes. The choice of the most abundant isotope for Ti (^{48}Ti) was discarded because of the potential isobaric interference derived from ^{48}Ca. Measurements based on ^{49}Ti have been found to be sensitive enough when assessing Ti in complex samples [35–39]. A tuning solution containing Be, Ce, Fe, In, Li, Mg, Pb, and U (1.0 mg L^{-1}) and Ag or Ti (10 mg L^{-1}) was used to adjust the ICPMS prior to analysis. The flow rate was daily determined by weighing the amount of deionized ultrapure water aspirated by the sample introduction system for 1.0 min (measurements in triplicate).

Table 3. Instrumental spICP-MS conditions.

Parameter	Value/type/mode
Nebulizer	Meinhard
Spray chamber	Cyclonic, quartz
Cones (sampler and skimmer)	Ni
Sample flow rate (mL min^{-1})	0.155 ± 0.001
Operation mode	Standard
Isotopes monitored	^{49}Ti, ^{107}Ag
Scan time (s)	100
Dwell time (µs)	100 (TiO_2NPs), 50 (AgNPs)
Mass (amu)	48.948 (TiO_2NPs), 106.905 (AgNPs)
Density (g cm^3)	4.23 (TiO_2NPs), 10.49 (AgNPs)
Mass fraction (%)	59.90 (TiO_2NPs), 100.00 (AgNPs)

Assessment of transport efficiency

Transport efficiency (% TE), defined as the ratio of the amount of analyte reaching the plasma compared to the amount of analyte aspirated by the sample introduction system, is one of the most critical parameters and its determination is crucial for an accurate NP quantification and size measurement. This parameter has been assessed by the pulse frequency method described by Pace *et al.* [40], which required the daily determination of the flow rate and the analysis of a reference material of nanoparticles of certified (known) particle number

concentration and size. Daily flow rate assessment gave a mean flow rate of 0.1548 ± 0.0098 mL min^{-1} values, which, together with the analysis of a gold nanoparticle suspension (nominal concentration of 9.89×10^4 NPs mL^{-1} and mean size of 49.6 nm), led to a mean % TE of 5.4 ± 0.7.

Calibration

Considering the lack of certified reference materials for the analysis of TiO_2NPs and AgNPs, dissolved standard calibration must be used. This strategy was firstly described by Pace *et al.* [40] and it requires the knowledge of the accurate value of % TE for assuming that the behaviour of dissolved metal and NPs in the plasma (vaporization, atomization, and ionization) is the same. Mass calibration curves were subsequently obtained by covering the 0–10 mg L^{-1} range for both Ti and Ag measurements.

1.3 RESULTS AND DISCUSSION

1.3.1 Optimization of the SA-DLLME experimental parameters

As previously commented, NP agglomeration and/or dissolution are dependent on NPs' environment (sample's matrix). Therefore, tap water was selected for developing the SA-DLLME procedure and for a further method validation.

The effect of the main parameters affecting the extraction efficiency of the SA-DLLME process was investigated. All experiments were performed using 10 mL aliquots from tap water spiked with 25 mg L^{-1} of 100 nm TiO_2NPs and 1.08×10^5 AgNPs (40 nm) L^{-1} for ensuring a right measurement of TiO_2NPs and AgNPs events by spICP-MS. Each set of conditions was tested in triplicate and reagent blanks (10 mL of ultrapure water) were also analysed for each case. Analytical recovery (mass concentration as TiO_2 mg L^{-1} for TiO_2NPs and AgNPs number concentration L^{-1} for AgNPs) was used as analytical response in optimization experiments.

Triton X-114 was selected as a surfactant [33,34], and several preliminary experiments were performed for selecting the best extractant, the concentration of Triton X-114, and the surfactant/extractant ratio (49:1). A proper cloudy solution was observed when using 1,2-dichloroethane as an extractant [33], and a 2.5 % (m/v) Triton X-114/1,2-dichloroethane (49:1) mixture, whereas other surfactant concentrations and/or surfactant/extractant ratios led to transparent solutions and lack of a sedimented phase after centrifugation. In addition, a previous mixture of both reagents (2.5 % (m/v) Triton X-114/1,2-dichloroethane) before addition to the water sample was needed, since the addition of dispersant and extractant separately did not lead to cloudy dispersion. These findings agree with those reported by Selahle and Nomngongo [34] when using the Triton X-114/n-butyl acetate mixture.

1.3.2 Effect of the volume of the 49:1 Triton X-114/1,2-dichloroethane mixture

The volume of the sedimented phase is directly affected by both the volume of extractant and the volume of surfactant, as well as the volume of the sample [41]. An adequate volume of the sedimented phase is needed for ensuring a good enrichment factor (EF). Consequently, the volume of the 49:1 Triton X-114/1,2-dichloroethane mixture was studied at 625 µL, 750 µL, and 1000 µL. The experiment was performed by vortexing at 2000 rpm for 1.0 min, and by isolating the organic phase by centrifugation at 2500 rpm and 4 °C for 3.0 min. The results (Fig. 14 (a)) imply slightly higher extraction efficiencies when using 750 and 1000 µL of the surfactant/extractant mixture, achieving more repeatable results when 1000 mL was used for the extraction of TiO_2NPs. Measured ionic Ti was found to be within the 0.40–0.70 mg L^{-1}

range, whereas ionic Ag varied in the 0.40 to 0.60 mg L^{-1} range. Regarding size distribution (Table 4), a mean size of 36 nm was measured for AgNPs under all conditions (water samples were previously spiked with 41 ± 5 nm AgNPs), which implies that agglomeration and ionization processes are not observed during the extraction process. However, mean sizes for TiO_2NPs were close to 200 nm, which suggests TiO_2NPs agglomeration since water was spiked with 100 nm TiO_2NPs. Therefore, a volume of 1000 µL of 49:1 Triton X-114/1,2-dichloroethane mixture was selected for further experiments. The need for using large dispersant/extractant volumes has been also reported for the Triton X-114/n-butyl acetate system [34], and it contrasts to the low dispersant and extractant volumes reported by Liu *et al.* (50 and 70 µL of dispersant and extractant, respectively, in sequential addition [33]).

Table 4. Mean sizes of AgNPs and TiO_2NPs under several operational conditions.

	Mean size of AgNPs (nm)	Mean size of TiO_2NPs (nm)
Volume of 49:1 Triton X-114/1,2-dichloroethane mixture		
625 µL	36 ± 3	207 ± 9
750 µL	36 ± 1	205 ± 3
1000 µL	36 ± 1	196 ± 5
Vortexing time		
0.5 min	32 ± 3	226 ± 19
1.0 min	37 ± 1	231 ± 17
2.0 min	38 ± 1	232 ± 4
5.0 min	38 ± 1	241 ± 11
Vortexing speed		
500 rpm	30 ± 2	318 ± 9
1000 rpm	36 ± 1	315 ± 3
1500 rpm	35 ± 1	314 ± 3
2000 rpm	24 ± 1	314 ± 5
2500 rpm	25 ± 1	299 ± 1
Centrifugation speed		
2000 rpm	37 ± 4	212 ± 3
2500 rpm	35 ± 2	221 ± 7
3000 rpm	31 ± 3	218 ± 4
3500 rpm	33 ± 1	218 ± 3
Centrifugation time		
1 min	31 ± 1	228 ± 7
3 min	39 ± 3	252 ± 2
5 min	40 ± 2	246 ± 5
10 min	39 ± 1	242 ± 8

1.3.3 Effect of vortex (extraction) time and speed

Stirring time is a factor that influences the extraction efficiency because it influences how fast the equilibrium state is achieved. Once the mixture of the surfactant and extractant is injected into the sample, a cloudy solution is formed. Then, the mixture is gently shaken to speed up the mass transfer of the analytes from the aqueous to the organic phase. In this study, the influence of the vortex time within the 0.5–5.0 min range was tested by using a volume of 1000 µL of the 49:1 Triton X-114/1,2-dichloroethane mixture, and fixing the vortex speed at 2000 rpm and the centrifugation conditions at 2500 rpm and 4 °C for 3.0 min. Results plotted in Fig. 14 (b) show a slight decrease in the analytical recovery of TiO_2NPs for vortexing times

USC UNIVERSIDADE DE SANTIAGO DE COMPOSTELA

higher than 0.5 min, whereas the extracted amounts of AgNPs remain constant. The highest extraction efficiency for both NPs was achieved when using the shortest extraction time (0.5 min), which was finally selected for further studies. Ionic Ti and Ag were below 0.6 mg L^{-1} for all experiments, which suggests that the vortexing time does not lead to NP dissolution.

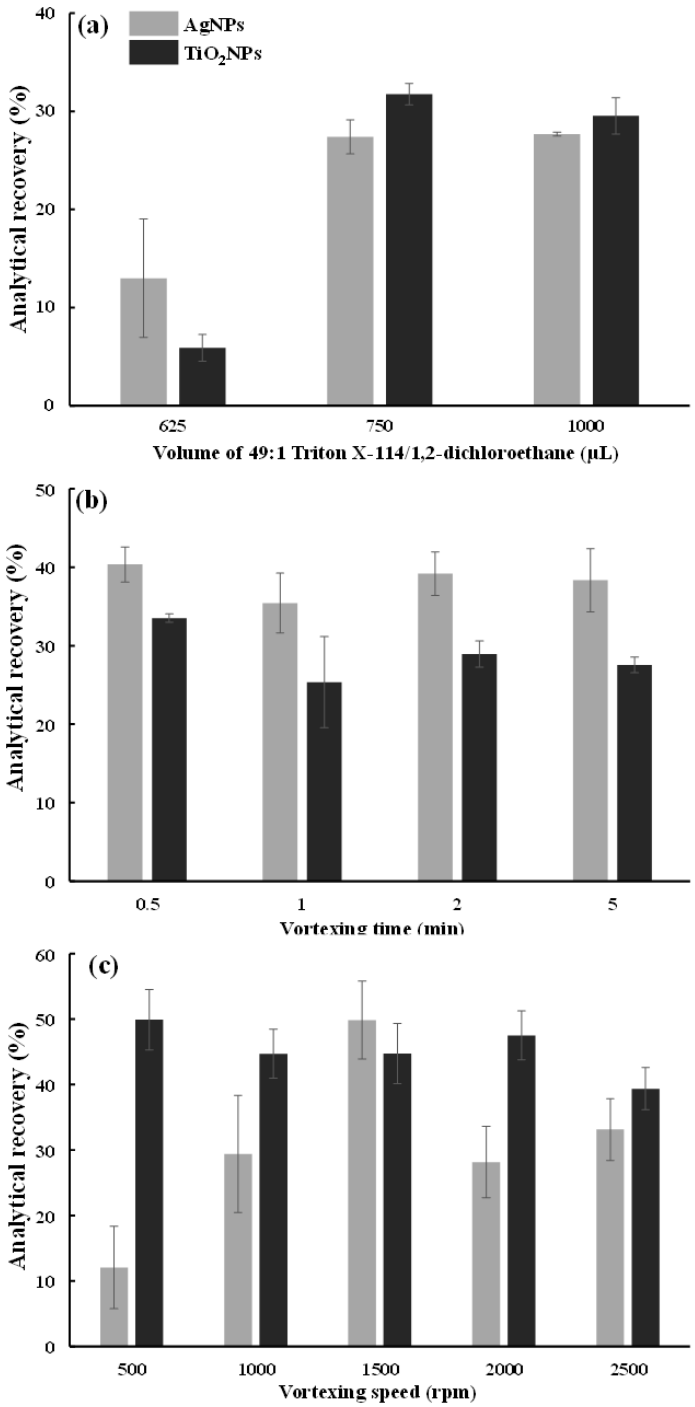

Figure 14. Effect of the volume of 49:1 Triton X-114/1,2-dichloroethane (a), vortexing time (b) and vortexing (c) on the analytical recovery of AgNPs and TiO_2NPs.

USC UNIVERSIDADE DE SANTIAGO DE COMPOSTELA

Regarding size distribution, Table 4 lists the mean sizes for AgNPs and TiO_2NPs under all operational SA-DLLME conditions. Sizes of 36 nm were measured for AgNPs (tap water samples spiked with 41 ± 5 nm AgNPs), whereas mean sizes for TiO_2NPs were close to 200 nm (tap water samples spiked with 100 nm TiO_2NPs). These sizes are higher than the calculated size detection limit by using the 5σ criteria (see section 1.4.2), which were 65.8 nm and 16.7 nm for TiO_2NPs and AgNPs, respectively. Since mean sizes obtained for AgNPs (36 nm) are close to the nominal size of the AgNPs standard used for spiking (41 ± 5 nm), we can conclude that the stability of AgNPs is guaranteed during the SA-DLLME procedure. However, the higher sizes measured for TiO_2NPs (close to 200 nm) suggest TiO_2NPs agglomeration (TiO_2NPs standard of 100 nm), but conclusions regarding TiO_2NPs stability during the SA-DLLME process cannot be attained since the direct analysis of the 100 nm TiO_2NPs standard by transmission electron microscopy (Fig. 15) shows large TiO_2NPs aggregates. Like the time of vortexing, the vortexing speed influences the equilibrium between the donor and the acceptor phases, and consequently, the mass transfer of analytes. The selection of the vortexing speed was limited to the operational range of the vortex device used, and so the influence was studied within the 500–2500 rpm range. Previously selected conditions for 49:1 Triton X-114/1,2-dichloroethane mixture volume (1000 µL) and vortex time (0.5 min), as well as fixed centrifugation conditions (2500 rpm and 4 °C for 3.0 min), were used throughout the experiment. The results in Fig. 14 (c) show that the stirring speed does not have an apparent effect on TiO_2NPs extraction, but AgNPs extraction efficiency is improved when vortexing at moderate speeds (1500 rpm). These findings imply a better AgNPs transfer at moderate speeds and the decrease in AgNPs recovery at higher speeds could be attributed to AgNPs ionization (low mean sizes at high vortexing speed as listed in Table 4). Therefore, a vortexing speed of 1500 rpm was finally selected for an efficient simultaneous co-extraction of AgNPs and TiO_2NPs.

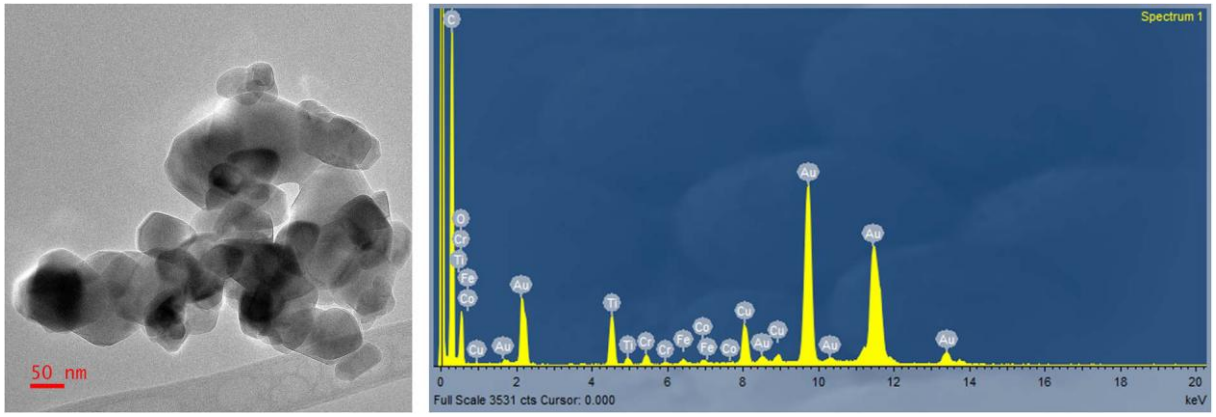

Figure 15. TEM image and EDS spectra of the 100 nm TiO_2NPs standard.

1.3.4 Effect of centrifugation speed and time

Centrifugation is a critical step during the SA-DLLME process due to potential losses of NPs by dissolution and/or agglomeration. Centrifugation is used to speed up phase separation and thus, speed and time need to be carefully investigated. Centrifugation speeds ranging from 2000 to 3500 rpm were tested, and the results are shown in Fig. 16 (a). It can be observed that higher centrifugation speeds promote higher extraction efficiencies for both TiO_2NPs and AgNPs, and 3500 rpm was finally selected as the speed of choice for the centrifugation step. The effect of centrifugation time was tested within the 1.0–10 min range (centrifugation speed at 3500 rpm and vortex conditions at optimum values, section 1.3.3).

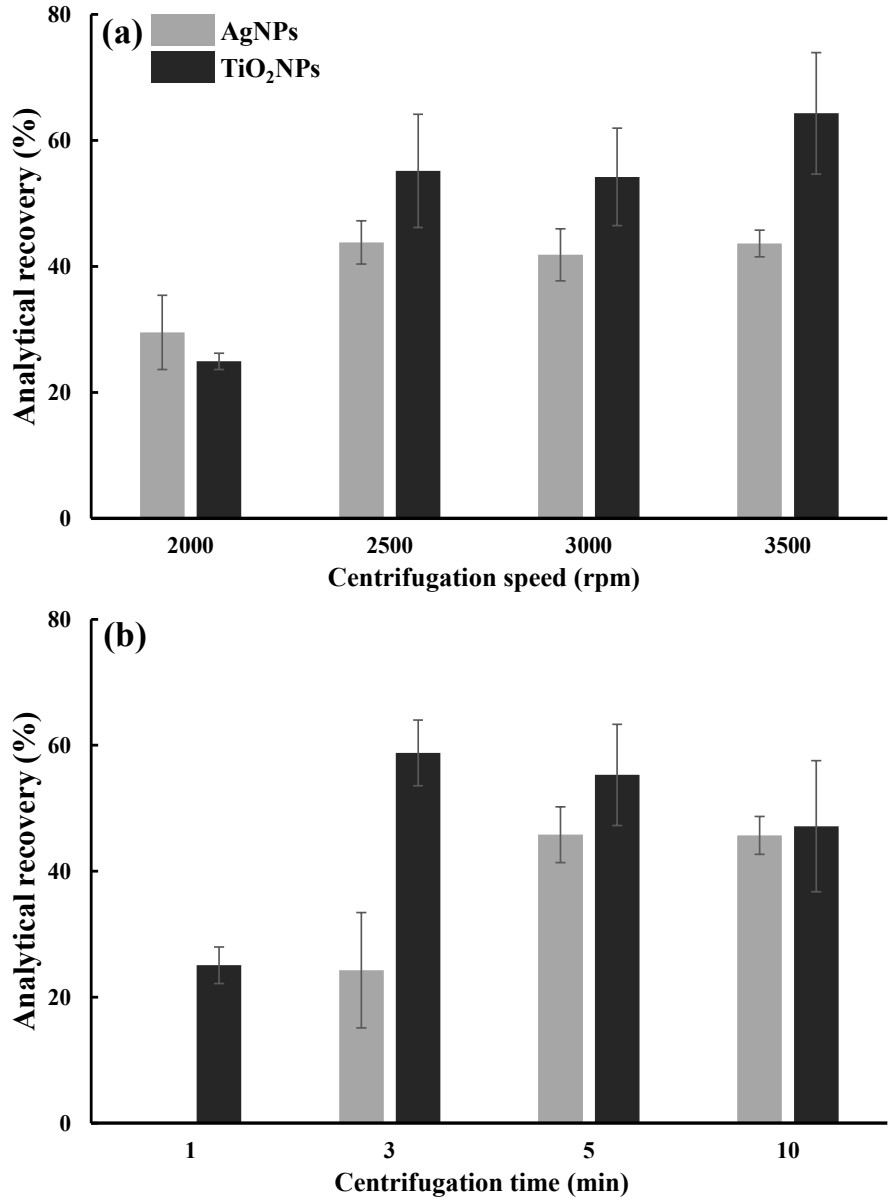

Figure 16. Effect of the centrifugation speed (a) and centrifugation time (b) on the analytical recovery of AgNPs and TiO_2NPs.

Fig. 16 (b) shows higher extraction efficiencies when increasing the centrifugation time, and the highest extraction efficiency for TiO_2NPs is already obtained within the 3.0–5.0 min range; meanwhile, the highest extraction for AgNPs is achieved at times longer than 5.0 min. Differences in the centrifugation time for both types of NPs can be explained by the different sedimentation speeds of each one, a parameter mathematically described by the Svedberg equation [42] and is directly dependent on the density and the radius of the particle:

$$\frac{dx/dt}{\omega^2 x} = \frac{2r^2(\rho_p - \rho_m)}{9\eta}$$

USC UNIVERSIDADE DE SANTIAGO DE COMPOSTELA

Where ω is the angular velocity, x the distance from the rotational axis, r the radius of the particle, ρ_p and ρ_m the densities of the particle and the medium respectively, and η the viscosity. For a joint extraction, centrifugation of the cloudy solution for 5.0 min will be considered as the optimal time. As listed in Table 4, the mean sizes of AgNPs were close to 40 nm under all conditions, whereas the mean sizes for TiO_2NPs varied from 228 to 252 nm.

1.4 Analytical performance

1.4.1 Calibration and matrix effect

In order to verify the presence or absence of the matrix effect, a series of aqueous ionic calibrations (Ag and Ti concentrations within the 0–10 mg L^{-1} range) were performed and the slopes were statistically compared with those obtained by preparing ionic standards (same concentrations) but using reconstituted (2.0 mL with 1 % (w/v) glycerol) sedimented phases obtained after applying the SA-DLLME procedure to 10 mL aliquots of ultrapure water (matrix matched calibration). Counts versus mg $event^{-1}$ were plotted and, in all cases, $r^2 > 0.997$ was achieved. The statistical analysis (90 % confidence interval) revealed that there are statistically significant differences (p-value < 0.1) between the slopes of the aqueous ionic calibration (8.0×10^9 counts events mg^{-1}) and the matrix matched calibration (1.0×10^{10} counts events mg^{-1}) for Ti. However, p-values > 0.1 were obtained when comparing the calibration slopes of Ag (9.0×10^{10} and 1.0×10^{11} counts events mg^{-1} for the aqueous ionic calibration and matrix matched calibration, respectively); hence, there were not statistically significant differences between the slopes of both calibration modes. These findings imply that there is no matrix effect for Ag, but the reagents used for SA-DLLME promote matrix effects when measuring Ti.

1.4.2 Limits of detection and limits of quantification

The detection capabilities of spICP-MS are related not only to concentration but also to the mass of element per particle, which can be translated into particle size. Therefore, two LODs must be considered, a size detection limit (LOD_{SIZE}) and a nanoparticles number concentration limit of detection (LOD_{NP}). The assessment of these features has been performed by applying the calculation Excel tool designed by Laborda *et al.* [43] based on the 3σ (3 × baseline standard deviation) and 5σ (5 × baseline standard deviation) criteria. Table 5 lists the several outputs for number concentration and size, and for dissolved mass concentration (critical value and limit of detection) assessed. The number concentration critical values were 2.67×10^6 NPs L^{-1}, and 5.84×10^6 L^{-1} for TiO_2NPs and AgNPs, respectively. The number concentration limits of detection were 2.85×10^6 NPs L^{-1} (TiO_2NPs) and 6.06×10^6 L^{-1} (AgNPs), which after assuming an EF of 10 led to a number concentration limit of detection referred to the tap water of 2.85×10^5 NPs L^{-1} for TiO_2NPs and 6.06×10^5 L^{-1} for AgNPs. Table 5 also lists the dissolved mass concentration (critical value and limit of detection), values within the 2.94– 5.38 ng L^{-1} range for Ti, and from 0.238 to 0.435 ng L^{-1} for Ag. Regarding the limit of detection in size, values of 65.8 (5σ criteria) and 55.5 nm (3σ criteria) were assessed for TiO_2NPs; whereas the minimum sizes for AgNPs were 16.7 (5σ criteria) and 14.1 nm (3σ criteria). These values imply a mass per particle limit of detection of 631.6 ag (5σ criteria) and 379.0 ag (3σ criteria) for TiO_2NPs; and a mass per particle limit of detection of 25.49 ag (5σ criteria) and 15.30 ag (3σ criteria) for AgNPs. Since the use of a criterion higher than 4σ virtually eliminates the occurrence of false positives when nanoparticle distributions are partially overlapped with the background [44] the 5σ criterion was selected for establishing the size limit of detection (Table 5). These values

USC
DE SANTIAGO
DE COMPOSTELA

match with reported LODs in size by other authors (13–30 nm for AgNPs and 50–100 nm for TiO_2NPs) [45–47].

1.4.3 Selectivity of the SA-DLLME procedure for nanoparticle forms of Ti and Ag

The selectivity of the method (the ability of the SA-DLLME procedure for isolating TiO_2NPs and AgNPs in the presence of ionic Ti and Ag) was tested by subjecting 10 mL aliquots of ionic Ti (25 mg L^{-1}) and Ag (8.0 mg L^{-1}) solutions to the proposed SA-DLLME procedure. Experiments in triplicate showed very low analytical recoveries (4.2 ± 2.4 % and 2.5 ± 0.1 % for dissolved Ti and Ag, respectively). In this way, SA-DLLME proves to be selective for isolating nanoparticle forms of Ti and Ag.

Table 5. Number concentration and size limit of detection of the method.

		3σ criteria		5σ criteria	
		Critical value	Limit of detection	Critical value	Limit of detection
TiO_2NPs	Number concentration / L^{-1}	2.67×10^6	2.85×10^{6a}	2.67×10^6	2.85×10^{6a}
	Dissolved mass concentration / ng L^{-1}	2.94	5.38	2.94	5.38
	Size / nm	55.5	55.5	65.8	65.8
	Mass per particle / ag	379.0	379.0	631.6	631.6
AgNPs	Number concentration / L^{-1}	5.84×10^6	6.06×10^{6b}	5.84×10^6	6.06×10^{6b}
	Dissolved mass concentration / ng L^{-1}	0.238	0.435	0.238	0.435
	Size / nm	14.1	14.1	16.7	16.7
	Mass per particle / ag	15.3	15.3	25.5	25.5

(a) 2.85×10^6 L^{-1} (referred to the tap water sample, EF 10). (b) 6.06×10^6 L^{-1} (referred to the tap water sample, EF 10).

1.4.4 Analytical recovery assays

The accuracy of the spICP-MS measurements was studied through the analytical recovery by combining several extracts from a tap water after applying the proposed SA-DLLME, and spiking extract aliquots with 20 and 60 nm AgNPs at 6.0×10^4 and 12×10^4 mL^{-1}; and with 100 nm TiO_2NPs at 25 and 50 mg L^{-1} (experiments in triplicate for each NP and concentration level). Analytical recovery values were calculated by subtracting the un-spiked concentration values from the spiked extracts and dividing them by the standard concentration used for spiking experiments. As listed in Table 6, analytical recoveries within the 80–120 % range were obtained for all cases, which implies good accuracy for the spICP-MS measurement process.

USC UNIVERSIDADE DE SANTIAGO DE COMPOSTELA

Table 6. Analytical recovery of the spICP-MS measurements and of the over-all procedure (SA-DLLME and spICP-MS).

		spICP-MS			SA-DLLME – spICP-MS	
		Added concentration	Analytical recovery (%)[a]		Added concentration	Analytical recovery (%)[a]
AgNPs	20 nm	6.0×10^4 mL^{-1}	96±6	40 nm	6.0×10^4 mL^{-1}	44±4
		12×10^4 mL^{-1}	114±4		12×10^4 mL^{-1}	53±7
	60 nm	6.0×10^4 mL^{-1}	83±5	60 nm	6.0×10^4 mL^{-1}	50±5
		12×10^4 mL^{-1}	99±6		12×10^4 mL^{-1}	47±5
TiO_2NPs	100 nm	25 µg L^{-1}	104±7	100 nm	25 µg L^{-1}	58±3
		50 µg L^{-1}	88±3		50 µg L^{-1}	47±5

(a) n=3

Similarly, the accuracy of the over-all method (SA-DLLME and spICP-MS) was also assessed through the analytical recovery after applying the SA-DLLME procedure to water samples spiked with AgNPs of two size distributions (40 and 60 nm) at two concentration levels (6.0×10^4 and 12×10^4 mL^{-1}, each one), and with 100 nm TiO_2NPs at 25 and 50 mg L^{-1} each one. Spiked and un-spiked samples, as well as NP standards, were measured in triplicate. Analytical recovery, also calculated by subtracting the un-spiked concentration values from the spiked extracts and using the standard concentrations for spiking experiments as a reference, is listed in Table 6. The obtained TiO_2NPs analytical recoveries ranged from 47 ± 5 to 58 ± 3 %, whereas the analytical recoveries obtained for AgNPs were between 44 ± 4 and 53 ± 7 %. A representative histogram for spiked experiments with 100 nm TiO_2NPs (50 mg L^{-1}) is given in Fig. 17 (a), showing TiO_2NPs sizes larger than 100 nm because of the agglomeration phenomena. In the case of AgNPs (40 nm, 12×10^4 mL^{-1}), a size distribution close to the nominal size (40 nm) was observed (Fig. 17 (b)) together with an additional size distribution (sizes lower than 25 nm) related to AgNPs close to the LOD_{SIZE} (lower than 16.7 nm, 5σ criteria) and ionic silver. In general, dissolved titanium and silver concentrations were found to be lower than 0.80 mg L^{-1} which could imply that the SA-DLLME procedure is a safe methodology for guaranteeing the integrity of AgNPs and TiO_2NPs.

The low analytical recovery assessed when considering the over-all process (SA-DLLME and spICP-MS) is attributed to the equilibrium achieved with the SA-DLLME procedure, which implies analytical recoveries around 50 %. Several experiments were further performed for verifying the non-exhaustive nature of the SA-DLLME process. The first set of experiments consisted of subjecting the residues (tap water) after carrying out the SA-DLLME (first extraction) to a second SA-DLLME (second successive extraction), obtaining analytical recoveries for Ag NP trials of 44 ± 5 and 41 ± 4 % (40 nm AgNPs at 6.0×10^4 and 12×10^4 mL^{-1}, respectively), and 58 ± 4 and 44 ± 5 % (60 nm AgNPs at 6.0×10^4 and 12×10^4 mL^{-1}, respectively). Additionally, new spiking experiments for AgNPs were also developed but using lower Ag NP number concentrations (3.0×10^4 mL^{-1}) and similar analytical recoveries (44 ± 3 and 51 ± 4 % for 40 nm AgNPs and 60 nm AgNPs, respectively) were also obtained. Therefore, a procedural standard calibration consisting of the use of AgNPs/TiO_2NPs at increasing

USC UNIVERSIDADE DE SANTIAGO DE COMPOSTELA

concentrations subjected to the SA-DLLME must be used to assess accurate results (quantitative analytical recoveries).

1.5 CONCLUSIONS

Pre-concentration procedures based on SA-DLLME are reliable sample pre-treatments for assessing AgNPs and TiO_2NPs in tap water. The procedure has been found to be selective for nanoparticle titanium and silver forms (ionic Ag and Ti species are not extracted), and the enrichment factor (5–10) could be improved, when necessary, by using large volumes of sample. Therefore, the SA-DLLME technique can be used as sample pretreatment for the determination of AgNPs and TiO_2NPs by instrumental techniques such as ICP-OES/MS and others because the selective isolation of the nanoparticle forms is achieved. In addition, NP dissolution did not occur during the extraction process since spICP-MS analysis has revealed very low ionic titanium and silver concentrations in the extracts.

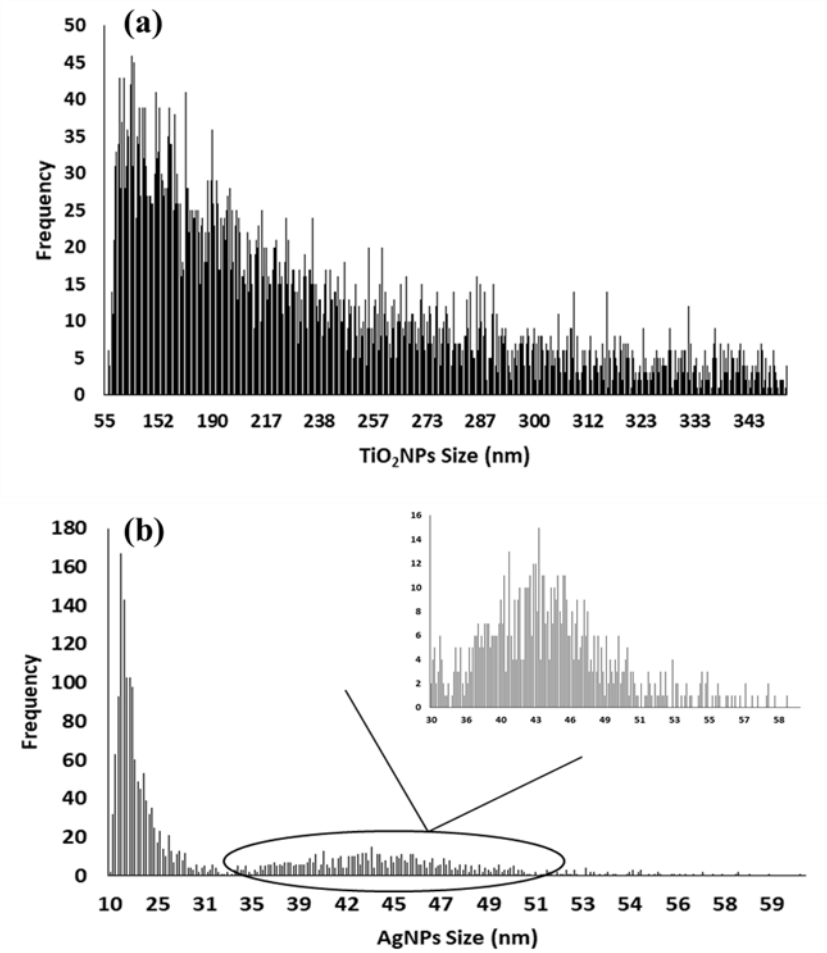

Figure 17. Representative histograms for extracts from a tap water sample spiked with 50 µg L^{-1} of 100 nm TiO_2NPs (a) and 12 $\times 10^4$ mL^{-1} of 40 nm AgNPs (b).

However, spiking experiments for TiO_2NPs have shown agglomeration since TiO_2NPs sizes higher than the nominal sizes of the TiO_2NPs used for spiking were observed. Moreover, SA-DLLME is a technique based on the equilibrium of the targets between the donor (sample)

and the acceptor (extract) phases, and a procedural standard calibration has therefore been required for assessing accurate results.

Finally, although the current research has been focused on tap water, the developed SA-DLLME methodology offers potential applications to other more complex water samples such as environmental water (seawater and riverine water), wastewater, and bottled water. Further studies are needed for verifying the influence of the matrix composition of these water samples on the selectivity (nanoparticle and ionic forms) and analytical recovery when applying SA-DLLME methodologies for the isolation of AgNPs and TiO_2NPs.

1.6 ACKNOWLEDGEMENTS

The authors wish to acknowledge the financial support from the Ministerio de Economía y Competitividad (FOODNANORISK, reference PID2021-125276NB-I00), and Xunta de Galicia (Grupo de Referencia Competitiva, reference ED431C 2022/029).

1.7 REFERENCES

[1] Nanotechnology Products Database, https://product.statnano.com (Accessed 2022 December).

[2] M. Murphy, K. Ting, X. Zhang, C. Soo and Z. Zheng, J. Current Development of Silver Nanoparticle Preparation, Investigation, and Application in the Field of Medicine, *J. Nanomater.*, 2015, 696918, 12 pages, 2015. https://doi.org/10.1155/2015/696918.

[3] S. J. Soenen, W. J. Parak, J. Rejman and B. Manshian, (Intra)Cellular Stability of Inorganic Nanoparticles: Effects on Cytotoxicity, Particle Functionality, and Biomedical Applications, Chem. Rev., 2015, 115, 2109–2135, https://doi.org/10.1021/cr400714j.

[4] L. Rizzello and P. P. Pompa, Nanosilver-based antibacterial drugs and devices: Mechanisms, methodological drawbacks, and guidelines, Chem. Soc. Rev., 2014, 43, 1501–1518, https://doi.org/10.1039/C3CS60218D.

[5] B. A. Weldon, E. M. Faustman, G. Oberdörster, T. Workman, W. C. Griffith, C. Kneuer and I. J. Yu, Occupational exposure limit for silver nanoparticles: considerations on the derivation of a general health-based value, Nanotoxicology, 2016, 10, 945–956, https://doi.org/10.3109/17435390.2016.1148793.

[6] A. Haider and I. K. Kang, Preparation of Silver Nanoparticles and Their Industrial and Biomedical Applications: A Comprehensive Review, Adv. Mater. Sci. Eng., 2015, 65257, https://doi.org/10.1155/2015/165257.

[7] B. Dréno, A. Alexis, B. Chuberre and M. Marinovich, Safety of titanium dioxide nanoparticles in cosmetics, J. Eur. Acad. Dermatol. Venereol., 2019, 33, 34–46, https://doi.org/10.1111/jdv.15943.

[8] R. J. B. Peters, G. Van Bemmel, Z. Herrera-Rivera, H. P. F. G. Helsper, H. J. P. Marvin, S. Weigel, P. C. Tromp, A. G. Oomen, A. G. Rietveld and H. Bouwmeester, Characterization of

USC UNIVERSIDADE DE SANTIAGO DE COMPOSTELA

Titanium Dioxide Nanoparticles in Food Products: Analytical Methods To Define Nanoparticles, J. Agric. Food Chem., 2014, 62, 6285–6293, https://doi.org/10.1021/jf5011885.

[9] S. Heilgeist, R. Sekine, O. Sahin and R. A. Stewart, Finding Nano: Challenges Involved in Monitoring the Presence and Fate of Engineered Titanium Dioxide Nanoparticles in Aquatic Environments, Water, 2021, 13, 734, https://doi.org/10.3390/w13050734.

[10] E. Baranowska-W´ojcik, D. Szwajgier, P. Oleszczuk and A. Winiarska-Mieczan, Effects of Titanium Dioxide Nanoparticles Exposure on Human Health—a Review, Biol. Trace Elem. Res., 2020, 193, 118–129, https://doi.org/10.1007/s12011-019-01706-6.

[11] M. S. Waghmode, A. B. Gunjal, J. A. Mulla, N. N. Patil and N. N. Nawani, Studies on the titanium dioxide nanoparticles: biosynthesis, applications and remediation, SN Appl. Sci., 2019, 1, 310, https://doi.org/10.1007/s42452-019-0337-3.

[12] European Food Safety Agency, Titanium Dioxide: E171 No Longer Considered Safe when Used as a Food Additive. https://www.efsa.europa.eu/en/news/titanium-dioxide-e171-no-longer-considered-safe-when-used-food-additive (Accessed December 2022).

[13] Y. Yang, K. Doudrick, X. Bi, K. Hristovski, P. Herckes, P. Westerhoff and R. Kaegi, Characterization of Food-Grade Titanium Dioxide: The Presence of Nanosized Particles, Environ. Sci. Technol., 2014, 48, 11, 6391–6400, https://doi.org/10.1021/es500436x.

[14] W. Mu, Y. Wang, C. Huang, Y. Fu, J. Li, H. Wang, X. Jia and Q. Ba, Effect of Long-Term Intake of Dietary Titanium Dioxide Nanoparticles on Intestine Inflammation in Mice, J. Agric. Food Chem., 2019, 67, 9382–9389, https://doi.org/10.1021/acs.jafc.9b02391.

[15] B. F. da Silva, S. Pérez, P. Gardinalli, R. K. Singhal, A. A. Mozeto and D. Barceló, Analytical chemistry of metallic nanoparticles in natural environments, Trends Anal. Chem., 2011, 30, 528–540, https://doi.org/10.1016/j.trac.2011.01.008.

[16] J. Zhao, M. Lin, Z. Wang, X. Cao and B. Xing, Engineered nanomaterials in the environment: Are they safe?, Crit. Rev. Environ. Sci. Technol., 2021, 51, 1443–1478, https://doi.org/10.1080/10643389.2020.1764279.

[17] L. J. A. Ellis, M. Baalousha, E. Valsami-Jones and J. R. Lead, Seasonal variability of natural water chemistry affects the fate and behaviour of silver nanoparticles, Chemosphere, 2018, 191, 616–625, https://doi.org/10.1016/j.chemosphere.2017.10.006.

[18] L. Li, M. Sillanpää, and M. Risto, Influences of water properties on the aggregation and deposition of engineered titanium dioxide nanoparticles in natural waters, Environ. Pollut., 2016, 219, 132–138, https://doi.org/10.1016/j.envpol.2016.09.080.

[19] Z. X. Luo, Z. H. Wang, B. Xu, I. L. Sarakiotis, G. Du Laing and C. Z. Yan, Measurement and characterization of engineered titanium dioxide nanoparticles in the environment, J. Zhejiang Univ., Sci., A, 2014, 15, 593–605, https://doi.org/10.1631/jzus.A1400111.

USC UNIVERSIDADE DE SANTIAGO DE COMPOSTELA

[20] F. Gottschalk, T. Sun and B. Nowack, Environmental concentrations of engineered nanomaterials: Review of modeling and analytical studies, Environ. Pollut., 2013, 181, 287–300, https://doi.org/10.1016/j.envpol.2013.06.003.

[21] F. Laborda, E. Bolea, G. Cepriá, M. T. Gómez, M. S. Jiménez, J. Pérez-Arantegui and J. R. Castillo, Detection, characterization and quantification of inorganic engineered nanomaterials: A review of techniques and methodological approaches for the analysis of complex samples, Anal. Chim. Acta, 2016, 904, 10–32, https://doi.org/10.1016/j.aca.2015.11.008.

[22] F. Laborda, J. Jiménez-Lamana, E. Bolea and J. R. Castillo, Selective identification, characterization and determination of dissolved silver(i) and silver nanoparticles based on single particle detection by inductively coupled plasma mass spectrometry, J. Anal. At. Spectrom., 2011, 26, 1362–1371, https://doi.org/10.1039/C0JA00098A.

[23] T. A. Saleh, Trends in the sample preparation and analysis of nanomaterials as environmental contaminants, Trends Environ. Anal. Chem., 2020, 28, 1–10, https://doi.org/10.1016/j.teac.2020.e00101.

[24] D. Mozhayeva and C. Engelhard, A critical review of single particle inductively coupled plasma mass spectrometry – A step towards an ideal method for nanomaterial characterization, J. Anal. At. Spectrom., 2020, 35, 1740–1783, https://doi.org/10.1039/C9JA00206E.

[25] G. R. Tortella, O. Rubilar, N. Durán, M. C. Diez, M. Martínez, J. Parada and A. B. Seabra, Silver nanoparticles: Toxicity in model organisms as an overview of its hazard for human health and the environment, J. Hazard. Mater., 2020, 390, 121974, https://doi.org/10.1016/j.jhazmat.2019.121974.

[26] X. Du, X. Wang, S. You, Q. Wang and X. Gong, A case study of aggregation behaviors of titanium dioxide nanoparticles in the presence of dodecylbenzene sulfonate in natural water, J. Environ. Sci., 2015, 36, 84–92, https://doi.org/10.1016/j.jes.2015.05.011.

[27] K. Raja, P. S. Ramesh, D. Geetha, T. Kokila and R. Sathiyapriya, Synthesis of structural and optical characterization of surfactant capped ZnO nanocrystalline, Spectrochim. Acta, Part A, 2015, 136, 155–161, https://doi.org/10.1016/j.saa.2014.08.092.

[28] Zhao T, Liu F, Zhang C, Chen X. Anions influence the extraction of rutile nanoparticles from synthetic and lake water. RSC Adv. 2019 May 29; 9 (29):16767-16773, https://doi.org/10.1039/C9RA02419K.

[29] I. G. Godinez, C. J. G. Darnault, A. P. Khodadoust and D. Bogdan, Deposition and release kinetics of nano-TiO2 in saturated porous media: Effects of solution ionic strength and surfactants, Environ. Pollut., 2013, 174, 106–113, https://doi.org/10.1016/j.envpol.2012.11.002.

[30] A. Spietelun, Ł. Marcinkowski, M. de la Guardia and J. Namieśnik, Green aspects, developments and perspectives of liquid phase microextraction techniques, Talanta, 2014, 119, 34–45, https://doi.org/10.1016/j.talanta.2013.10.050.

USC UNIVERSIDADE DE SANTIAGO DE COMPOSTELA

[31] V. Azevedo Lemos, J. Alves Barreto, L. Bastos Santos, R. dos Santos de Assis, C. Galvao Novaes and R. J. Cassella, *In-syringe* dispersive liquid-liquid microextraction, Talanta, 2022, 238, 123002, https://doi.org/10.1016/j.talanta.2021.123002.

[32] I. Hagarová, L. Nemček, M. Šebesta, O. Zvěřina, P. Kasak and M. Urík, Preconcentration and Separation of Gold Nanoparticles from Environmental Waters Using Extraction Techniques Followed by Spectrometric Quantification, Int. J. Mol. Sci., 2022, 23, 11465, https://doi.org/10.3390/ijms231911465.

[33] Y. Liu, M. He, B. Chen and B. Hu, Ultra-trace determination of gold nanoparticles in environmental water by surfactant assisted dispersive liquid liquid microextraction coupled with electrothermal vaporization-inductively coupled plasma-mass spectrometry, Spectrochim. Acta, Part B, 2016, 122, 94–102, https://doi.org/10.1016/j.sab.2016.04.009.

[34] S. K. Selahle and P. N. Nomngongo, Quantification of TiO_2 and ZnO nanoparticles in wastewater using inductively coupled plasma optical emission spectrometry, Toxicol. Environ. Chem., 2019, 101, 204–214, https://doi.org/10.1080/02772248.2019.1686151.

[35] M. V. Taboada-López, S. Iglesias-López, P. Herbello-Hermelo, P. Bermejo-Barrera and A. Moreda-Piñeiro, Ultrasound assisted enzymatic hydrolysis for isolating titanium dioxide nanoparticles from bivalve mollusk before sp-ICP-MS, Anal. Chim. Acta, 2018, 1018, 16–25, https://doi.org/10.1016/j.aca.2018.02.075.

[36] M. V. Taboada-López, P. Herbello-Hermelo, R. Domínguez-González, P. Bermejo-Barrera and A. Moreda-Piñeiro, Enzymatic hydrolysis as a sample pre-treatment for titanium dioxide nanoparticles assessment in surimi (crab sticks) by single particle ICP-MS, Talanta, 2019, 195, 23–32, https://doi.org/10.1016/j.talanta.2018.11.023.

[37] K. Badalova, P. Herbello-Hermelo, P. Bermejo-Barrera and A. Moreda-Piñeiro, Possibilities of single particle-ICP-MS for determining/characterizing titanium dioxide and silver nanoparticles in human urine, J. Trace Elem. Med. Biol., 2019, 54, 55–61, https://doi.org/10.1016/j.jtemb.2019.04.003.

[38] M. V. Taboada-López, G. Vázquez-Expósito, R. Domínguez-González, P. Herbello-Hermelo, P. Bermejo-Barrera and A. Moreda-Piñeiro, Biopersistence rate of metallic nanoparticles in the gastro-intestinal human tract (stage 0 of the EFSA guidance for nanomaterials risk assessment), Food Chem., 2021, 360, 130002, https://doi.org/10.1016/j.foodchem.2021.130002.

[39] M. V. Taboada-López, B. H. Leal-Martínez, R. Domínguez-González, P. Bermejo-Barrera, P. Taboada-Antelo and A. Moreda-Piñeiro, Caco-2 *in vitro* model of human gastrointestinal tract for studying the absorption of titanium dioxide and silver nanoparticles from seafood, Talanta, 2021, 233, 122494, https://doi.org/10.1016/j.talanta.2021.122494.

[40] H. E. Pace, N. J. Rogers, C. Jarolimek, V. A. Coleman, C. P. Higgins and J. F. Ranville, Determining Transport Efficiency for the Purpose of Counting and Sizing Nanoparticles via Single Particle Inductively Coupled Plasma Mass Spectrometry, Anal. Chem., 2011, 83, 9361–9369, https://doi.org/10.1021/ac201952t.

[41] M. Saraji and M. K. Boroujeni, Recent developments in dispersive liquid-liquid microextraction, Anal. Bioanal. Chem., 2014, 406, 2027–2066, https://doi.org/10.1007/s00216-013-7467-z.

[42] J. D. Castle, Overview of cell fractionation, Curr. Protoc. Cell Biol., 1998, 69, 3.1.1–3.1.9, https://doi.org/10.1002/0471143030.cb0301s00.

[43] F. Laborda, A. C. Gimenez-Ingalaturre, E. Bolea and J. R. Castillo, About detectability and limits of detection in single particle inductively coupled plasma mass spectrometry, Spectrochim. Acta, Part B, 2020, 169, 105883, https://doi.org/10.1016/j.sab.2020.105883.

[44] F. Laborda, J. Jiménez-Lamana, E. Bolea and J. R. Castillo, Critical considerations for the determination of nanoparticle number concentrations, size and number size distributions by single particle ICP-MS, J. Anal. At. Spectrom., 2013, 28, 1220–1232, https://doi.org/10.1039/C3JA50100K.

[45] F. Laborda, E. Bolea and J. Jiménez-Lamana, Single particle inductively coupled plasma mass spectrometry for the analysis of inorganic engineered nanoparticles in environmental samples, Trends Environ. Anal. Chem., 2016, 9, 15–23, https://doi.org/10.1016/j.teac.2016.02.001.

[46] F. Laborda, E. Bolea and J. Jiménez-Lamana, Single Particle Inductively Coupled Plasma Mass Spectrometry: A Powerful Tool for Nanoanalysis, Anal. Chem., 2014, 86, 2270–2278, https://doi.org/10.1021/ac402980q

[47] R. Peters, Z. Herrera-Rivera, A. Undas, M. Van Der Lee, H. Marvin, H. Bouwmeester and S. Weigel, Single particle ICP-MS combined with a data evaluation tool as a routine technique for the analysis of nanoparticles in complex matrices, J. Anal. At. Spectrom., 2015, 30, 1274–1285, https://doi.org/10.1039/C4JA00357H.

USC UNIVERSIDADE DE SANTIAGO DE COMPOSTELA

CHAPTER 2. SURFACTANT-ASSISTED DISPERSIVE LIQUID-LIQUID MICROEXTRACTION AND CENTRIFUGAL ULTRAFILTRATION AS POTENTIAL EXTRACTION PROCEDURES FOR SILVER AND TITANIUM DIOXIDE NANOPARTICLES FROM HUMAN URINE

USC
UNIVERSIDADE DE SANTIAGO DE COMPOSTELA

CHAPTER 2. SURFACTANT-ASSISTED DISPERSIVE LIQUID-LIQUID MICROEXTRACTION AND CENTRIFUGAL ULTRAFILTRATION AS POTENTIAL EXTRACTION PROCEDURES FOR SILVER AND TITANIUM DIOXIDE NANOPARTICLES FROM HUMAN URINE

The results from this chapter have already been published as:

Ana Justo-Vega, Claudia Torrente-Seco, Lidia Janza-Candal, Manuel Aboal-Somoza, Raquel Domínguez-González, Pilar Bermejo-Barrera, and Antonio Moreda-Piñeiro

Group of Trace Elements, Spectroscopy and Speciation (GETEE), Institute of Materials iMATUS, Department of Analytical Chemistry, Nutrition and Bromatology, Faculty of Chemistry, Universidade de Santiago de Compostela, Avenida das Ciencias, s/n., 15782, Santiago de Compostela, Spain.

*Microchemical Journal, 2025, **211**, 113072*
(DOI: 10.1016/j.microc.2025.113072)

GRAPHICAL ABSTRACT

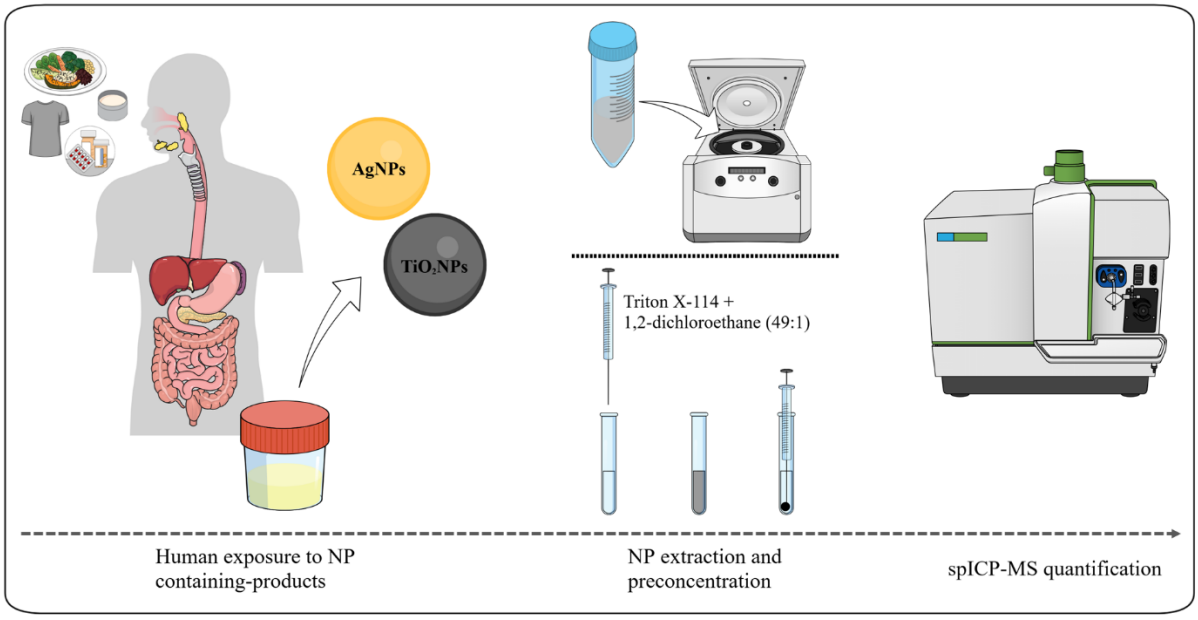

ABSTRACT

Inorganic nanoparticles (NPs) hold great promise in nanomedicine, cosmetics, the food industry and other human-related sectors, raising concerns about their safety and effects on biological systems. Urine shows great potential as a biological compartment for biomonitoring,

but the presence of NPs in urine (basal levels) is expected to be very low and requires advanced instrumentation as well as sample pretreatment. This study reports on the use of single particle inductively coupled plasma mass spectrometry (spICP-MS) as a tool for the assessment of silver nanoparticles (AgNPs) and titanium dioxide nanoparticles (TiO_2NPs) in urine, previously extracted/preconcentrated by two different approaches: surfactant-assisted dispersive liquid–liquid microextraction (SA-DLLME) and centrifugal ultrafiltration (UF). Optimal experimental conditions for SA-DLLME were: 10 mL urine, 1.0 mL surfactant/extractant mixture, vortexing at 2000 rpm for 30 s and a final centrifugation step at 3500 rpm for 10 min. Centrifugal ultrafiltration (molecular weight cut-off (MWCO) of 30 kDa, 5000×g, 25 min, 1 rinsing cycle with 1.0 % (v/v) glycerol) showed improved results for NP preconcentration using up to 30 mL of urine. An improved limit of detection (number concentration) was achieved with UF (3.1 × 102 and 2.9 × 10^2 particle mL^{-1} for TiO_2NPs and AgNPs, respectively), while the analytical recovery of both methods was similar for TiO_2NPs (in the range of 77–97 % for SA-DLLME and between 74 and 99 % for UF) and from 81 to 88 %, and from 90 to 115 % for AgNPs when using SA-DLLME and UF, respectively.

Keywords: silver nanoparticles, titanium dioxide nanoparticles, human urine, SA-DLLME, Centrifugal UF, spICP-MS

2.1 INTRODUCTION

Since the boom of nanomaterials (NMs) in the early 2000s, their use and exploitation has grown exponentially [1], and more than 11,000 nano-based products are currently available on the market [2]. Focusing on inorganic nanoparticles (NPs), the demonstrated powerful and tunable chemical, mechanical, electrical and magnetic properties make these innovative materials attractive for several industrial sectors. For example, silver nanoparticles (AgNPs) can be found in medical devices, disinfectants, cosmetics, textiles, household appliances and food [3–6], while titanium dioxide nanoparticles (TiO_2NPs) are used in water and wastewater treatment, construction materials (self-cleaning roof tiles, windows, paints), in cosmetics (sunscreens), and as a component of the food additive E171 [7–10].

With the proliferation and increasing use of TiO_2NPs and AgNPs in consumer products and biomedical applications, human exposure to these new nanomaterials is increasing, as are concerns about their potential toxicity. There is evidence in the literature that NPs are able to cross the glomerular filtration barrier and be excreted in the urine [11,12]. However, low concentrations of NPs can be expected due to the biotransformation processes that NPs undergo in the organism. Overcoming the problems arising from the high salt content and low concentration of NPs in urine is a challenge in nanometrology, requiring sensitive analytical methods for detection/quantification and reliable sample pre-treatments.

Several analytical tools are available for the determination/characterization of NPs, such as transmission electron microscopy (TEM), dynamic light scattering (DLS), separation techniques such as hydrodynamic chromatography (HDC), field flow fractionation (FFF), mainly asymmetric flow FFF (AF4), and ion exchange chromatography (IEC) combined with, among others, inductively coupled plasma mass spectrometry (ICP-MS) and multiple angle light scattering (MALS) [1,13–15]. However, the development of single particle ICP-MS (spICP- MS) for suspension analysis has attracted attention since its introduction in 2003 by Degueldre and Favarger [16]. The attraction of spICP-MS is that the technique provides data on number concentration, size, size distribution and information on dissolved metal concentration. Recent literature focusing on in-depth discussions of the basic principles of

USC DE COMPOSTELA

spICP-MS (including advantages, potential pitfalls and cautions, and applications) can be found elsewhere [17–23].

There are limited reports on the determination of NPs in urine [24–28], and direct determination by spICP-MS [24–28]and AF4- MALS/UV/ICP-MS [24] was performed after urine dilution. Ultrapure water as a diluent was used by Bocca *et al.* [24,25] for the assessment of AgNPs and gold nanoparticles (AuNPs), while other authors have reported the use of other diluents such as dilute nitric acid (0.1 %(v/v)) for the assessment of TiO_2NPs [26], and glycerol (1.0 % (v/v)) for the quantification of AgNPs and TiO_2NPs [27]. A more complex diluent composition, such as that proposed by Cabré *et al.* [28], has consisted of ethylenediaminetetraacetic acid (EDTA), isopropyl alcohol, ammonia solution, and Triton-X-100 mixture for Au NPs.

Given the low basal levels of NPs in urine, the drawbacks associated with low sensitivity and the presence of concomitant substances could be overcome by the development of advanced sample preparation for urine analysis, a scenario that has not yet been explored. In this context, centrifugal ultrafiltration (UF), first described by Whitlam and Brown for the determination of protein binding in serum [29], has been used mainly for the concentration and purification of macromolecular species, and some applications can be found for colloids and nanoparticle colloids [30,31]. On the other hand, the use of surfactants to assist dispersive liquid–liquid microextraction (DLLME), the so-called surfactant-assisted dispersive liquid–liquid microextraction (SA-DLLME) [32], has been shown to be a useful sample pretreatment for isolating/preconcentrating organic compounds, and some developments have recently been applied to the extraction of AuNPs from environmental water [33,34], AgNPs and TiO_2NPs from tap water [35]and TiO_2NPs and ZnONPs from wastewater [36]. Therefore, the current work aims to explore the possibilities of new isolation/preconcentration sample pretreatments to improve sensitivity and for purification purposes in the determination of AgNPs and TiO_2NPs in urine. The variables affecting the proposed UF (molecular weight cut-off (MWCO) of 30 kDa) and SA-DLLME methods were fully investigated, and the strengths and weaknesses of the proposed methods were discussed. The determination/characterization of AgNPs and TiO_2NPs was performed by spICP- MS.

2.2 EXPERIMENTAL

2.2.1 Instrumentation

Single particle data acquisitions were performed with a NexION® 300X ICP-MS (Perkin Elmer, Waltham, MA, USA) equipped with a Meinhard® nebulizer and a quartz cyclonic spray chamber termostatized by a Peltier refrigerator as the sample introduction system. The Syngistix™ Nano Application software version 2.5 (Perkin Elmer) allowed the NPs assessment in terms of quantification and size distribution. A Sigma Laborzentrifugen 2 K15 (Osterode, Germany) centrifuge equipped with a cooling system, and a Consul 22R (Ortoalresa, Madrid, Spain) refrigerated centrifuge were used during the SA-DLLME and the UF processes, respectively. A Reax Top vortex vibrational shaker (Heidolph, Schwabach, Germany) was used throughout the SA-DLLME extraction procedure.

Additional instrumentation to perform the analysis include a Mettler Toledo ML204/01 analytical balance (Columbus, OH, USA) for weighing purposes, and an USC-TH ultrasound water bath (45 Hz, 80 W) from VWR International Eurolab S.L (Barcelona, Spain) to disperse the NPs suspension prior to use.

USC UNIVERSIDADE DE SANTIAGO DE COMPOSTELA

2.2.2 Materials and reagents

Ultrapure water (18.2 MΩ cm resistivity) was obtained from a Milli-Q® Gradient A10 purification system (Millipore Co., Bedford, MA, USA). Argon (99.998 %) was from Nippon Gases (Madrid, Spain). Ionic 1000 mg L^{-1} silver ($AgNO_3$) and titanium [$(NH_4)_2TiF_6$] stock standard solutions were purchased from Merck (Darmstadt, Germany). NexIon Setup Solution (1.0 μg L^{-1} of Be, Ce, Fe, In, Li, Mg, Pb, and U in 1 % HNO_3) as tuning solution for ICP-MS was from Perkin Elmer. A reference material PEG-COOH Gold Nanospheres (49.6 nm determined by TEM, 12.4 ng mL^{-1}, particle number concentration 9.89 $\times 10^6$ mL^{-1}, in 1 mM aqueous citrate) was supplied by NanoComposix (San Diego, CA, USA). TiO_2 nanopowder (rutile, 99.9 %) of 50 and 100 nm was from US Research Nanomaterials (Houston, TX, USA). AgNPs standard suspensions (in 1 mM aqueous citrate) of 60 nm (0.020 mg mL^{-1}, 1.8 $\times 10^{10}$ particles mL^{-1}), and 40 nm (0.021 mg mL^{-1}, 5.4 $\times 10^{10}$ particles mL^{-1}) were from NanoComposix. The standards were analyzed by high resolution transmission electronic microscopy (HRTEM) and the mean sizes for AgNPs standards were found to be in agreement with those reported by the manufacturer (Fig. 23 and 24, Electronic Supplementary information, ESI). However, a high degree of agglomeration was observed for TiO_2 NPs standards (Fig. 25, ESI), resulting in mean sizes higher than those reported by the manufacturer.

Other consumables were glycerol (99.5 %) and 1,2-dichloroethane (LC Gradient) from Merck, laboratory grade Triton X-114 from Sigma- Aldrich (San Luis, MO, USA), hyperpure nitric acid (69 %) from Panreac (Barcelona, Spain), Minisart NML 5.0 μm filters (Sartorius, Goettingen, Germany), and Amicon® Ultra-15 centrifugal filter units (regenerated cellulose membrane, 30 kDa MWCO from Merck.

To prevent metal contamination, all glassware was cleaned and kept in 10 % (v/v) nitric acid for 48 h, thoroughly rinsed with ultrapure water, and dried in a laboratory drying oven before use.

2.2.3 Urine sample collection

Sample collection was conducted according to the guidelines provided by the Galician Ethics Committee for Clinical Research (Registration Code: CEIC de Galicia 2010/372). All urine samples from healthy participants, were collected in 50 mL polypropylene vials and kept at 4 ºC (for no more than 24 h) before sample processing and analysis.

2.2.4 Surfactant assisted – DLLME extraction procedure

All urine samples were firstly filtered (NML 5.0 μm filters). Surfactant-assisted DLLME was carried out according to Justo-Vega *et al.* [35] with some modifications. Briefly, an aliquot of 10 mL filtered urine was placed in a conical centrifuge glass tube, and 1.0 mL of a 49:1 surfactant/extractant (2.5 % (w/v) Triton X-114/1,2-dichloroethane) mixture was rapidly injected, followed by a vortexing step at 2000 rpm for 30 s (cloudy emulsion formation). Centrifugation at 3500 rpm for 10 min (4 ºC) was carried out and the organic phase containing the NPs as bottom-layer was withdrawn and diluted to 2.0 mL with 1.0 % (w/v) glycerol. Diluted urine extracts were again vortexed for 1 min right before spICP-MS analysis (operating conditions listed further below).

USC UNIVERSIDADE DE SANTIAGO DE COMPOSTELA

2.2.5 Centrifugal UF conditions

The Amicon Ultra units were filled with 15 mL urine aliquot and subsequently centrifuge using a fixed-angle rotor, optimized for *g* force (5000 × *g*). Once the centrifugation was completed (25 min), another 15 mL urine aliquot was added, and the filter units were subjected to the same centrifugation conditions. Finally, the preconcentrated remaining in the filter was washed with 15 mL 1.0 % (v/v) glycerol (under identical centrifugation conditions). The cleaned extract was then withdrawn from the filter and diluted with 1.0 % (w/v) glycerol to a final volume of 2.0 mL. Extracts were vortexed prior to spICP-MS measurements.

2.2.6 spICP-MS analysis

Instrumental and data acquisition parameters for spICP-MS analysis are reported in Table 7. ICP-MS operating conditions were set automatically (Syngistix™ Nano Application software version 2.5) by daily monitoring of Be, In, U, Ce (Ce++/Ce and CeO/Ce ratios) in the NexIon setup solution and background (*m*/*z* at 220) until the values recommended by the ICP-MS manufacturer were reached. It is well accepted now that the duration of the pulse generated by a single particle in the ICP-MS only lasts for a few hundreds of seconds.

Furthermore, to avoid simultaneous counting of NPs during a specific dwell time, a short integration dwell time of 100 µs was selected. Transport efficiency (% TE) assessment was performed following the particle frequency method described by Pace *et al.* [19]. For this aim, it is needed: (1) the determination of the flow rate by weighing the volume of ultrapure water aspirated for 1 min (in triplicate), and (2) the analysis of a certified gold nanoparticles suspension (PEG-COOH gold nanospheres 49.6 nm, 9.89 × 10^6 mL^{-1}). The TE, daily determined, was in the range of 4–7 % throughout the work.

Table 7. Default instrumental and data acquisition parameters.

PARAMETER	TYPE/VALUE/MODE
RF Power	1600 W
Plasma Flow Rate	15 L min^{-1}
Auxiliary Gas Flow Rate	1.2 mL min^{-1}
Nebulizer Gas Flow Rate	1.15 mL min^{-1}
Sample uptake rate	0.15 mL min^{-1}
Nebulizer	Meinhard
Spray chamber	Cyclonic, quartz
Cones (sampler and skimmer)	Nickel
Measuring Mode	Standard
Dwell Time	100 µs
Scan Time	100 s
Number of Readings	25,000
Replicates	3
Isotopes	^{49}Ti, ^{107}Ag, ^{197}Au (for %TE)

USC UNIVERSIDADE DE SANTIAGO DE COMPOSTELA

2.3 RESULTS AND DISCUSSION

2.3.1 Optimization extraction/preconcentration procedures

Surfactant-assisted DLLME

There are several factors which affect the efficiency of the extraction process and were considered for optimization, including the volume of the extraction solvent/surfactant mixture, the speed and time of vortexing, and the speed and time of centrifugation. Typically, the sample's pH is a critical parameter for improving the extraction efficiency of most analytes. Normal human urine pH values are between pH 4.6 and pH 8.0 [37,38]. The point of zero charge (PZC) for TiO_2NPs (rutile) is around pH 5.5, and for AgNPs can vary from nearly neutral pH [39] to pH 8.6 [40]. The effect of the pH was not taken into consideration for optimization purposes as both nanoparticles were in the range of their points of zero charge, and a pH adjustment would benefit one and compromise the other. Moreover, preliminary studies were conducted to select the appropriate extraction solvent as well as the surfactant, and the optimum surfactant/extract ratio, a parameter of high impact [34,36].

Experiments have been performed with urine samples (10 mL) spiked at 64 ng L^{-1} AgNPs and 25.0 µg L^{-1} TiO_2NPs in triplicate. At least two reagent blanks were prepared and analysed for each set of conditions.

Several volumes of the surfactant (TX-114)/extractant ($C_2H_4Cl_2$) mixture (625, 750 and 1000 µL) were added to the sample to investigate the effect on extraction efficiency. The results are plotted in Fig. 18, which shows that the volume of the surfactant/extractant mixture had a greater effect on the extraction of AgNPs (Fig. 18 (A)), and a high mass transfer to the sedimented phase was obtained when using the highest volume tested (1000 µL). For TiO_2NPs (Fig. 18 (B)), little effect of the volume of the surfactant/extractant mixture was observed and similar TiO_2NP concentrations were obtained in the 750–1000 µL range. Therefore, a volume of 1000 µL (980 µL TX-114 and 20 µL $C_2H_4Cl_2$) was chosen to perform a simultaneous extraction of both NPs.

Another significant factor during the extraction process is the centrifugation step (speed and time) since the organic phase rich in AgNPs and TiO_2NPs as bottom layer was separated by centrifugation. The influence of centrifugation speeds ranging from 2000 rpm up to 3500 rpm was evaluated, and results (Fig. 26, SI) showed that the signal intensity remains constant for both analytes when using centrifugation speeds higher than 2500 rpm. However, high centrifugation rates benefit the extraction recoveries in terms of relative standard deviation (% RSD), and lower percentages of RSD were achieved when centrifugation was carried out at 3500 rpm (10 % and 9 % for TiO_2NPs and AgNPs, respectively), and the highest centrifugation rate was finally selected.

The impact of centrifugation time was studied within the 3–10 min range at three levels: 3, 5, and 10 min. As Fig. 27 (B) (SI) shows, the extraction recoveries for TiO_2NPs remained nearly constant throughout the range studied. Nonetheless, centrifugation time had a greater effect on the extraction efficiency of AgNPs, and the analytical signal intensity for AgNPs, and thus extraction recovery (Fig. 27 (A), ESI) was steady from 3 to 5 min, and then increased with further increase of the centrifugation time to 10 min. Therefore, the selected optimal centrifugation time for both analytes was 10 min.

The last parameter considered for optimization was the vortex time and speed. Vortexing affects the extraction equilibrium and accelerates the mass transfer of the analytes from the aqueous phase into the fine organic solvent droplets. The effect of vortex time was evaluated at four levels within the 0.5–5 min range. Results in Fig. 28 (ESI) show the same tendency (an

efficiency decreases when increasing the vortex time) for both NPs, with maximum signals at 30 s. These findings imply that the equilibrium state is reached rapidly because the contact surface between the aqueous and organic phases is highly enhanced with the addition of the surfactant. Moreover, large vortex times may lead to the dissolution of NPs and/or assisting the formation of aggregates and agglomerates.

Vortex speed along with vortex time influences how fast the equilibrium state is achieved. The study of this parameter was conducted within the 500–2500 rpm range, and Fig. 29 (A) (ESI) indicates that the vortex speed has a slight effect on the extraction efficiency AgNPs, although higher values (2000 and 2500 rpm) benefit NPs extraction. This phenomenon is much more heightened for TiO_2NPs (Fig. 29 (B), ESI) and mass transfer into extraction solvent was found to be higher as the vortex speed was increased up to 2000 rpm (optimum value for extraction efficiency). Results of a 95 % Least Significant Difference (LSD) for a multiple comparison test showed no statistically significant differences between 2000 rpm and 2500 rpm for AgNPs extraction, and thus 2000 rpm was finally selected as the optimum vortex speed.

Centrifugal UF

According to the manufacturer's instructions, the ultrafiltration membranes were firstly prepared and rinsed with ultrapure water before use. Specifications of the membrane include active membrane area, 7.6 cm^2; membrane material, low binding regenerated cellulose; filter device dimensions, 72 mm length, 29.7 mm diameter. To improve UF efficiency, two parameters were considered for optimization, the number of washing cycles and the type of washing solvent. At least two reagent blanks were prepared and analysed for each set of conditions.

Initially, the effect of performing 1, 2, and 3 washing cycles was evaluated. Following the conditions described in section 2.2.5, the preconcentrated obtained was washed once, twice or three times with ultrapure water and results were compared based on analytical recovery (%) for the case of AgNPs (the standard suspension certifies a concentration based on number of particles), whereas the results for TiO_2NPs were assessed based on number of particles from spICP-MS measurements. Fig. 19 shows that UF efficiency is comparable when performing one and two washing cycles, but it drastically decreases when a third washing step is carried out. AgNPs analytical recoveries (%) were 84 ± 10, 89 ± 2, and 7 ± 5 for one, two, and three washing steps, respectively. Hence, to minimize the extraction time, one washing cycle was selected as optimum condition.

Optimization of the washing solvent was conducted considering ultrapure water and 1.0 % (v/v) glycerol. Results are presented in Fig. 20, and it can be observed that the impact of both solvents on UF efficiency is virtually the same. Nevertheless, upon closer examination, reduced standard deviation values were obtained for both analytes when 1.0 % (v/v) glycerol was used as a rinsing solvent, and additionally, there is a slight increase in the number of extracted TiO_2NPs when using 1.0 % (v/ v) glycerol. Analytical recoveries (%) for AgNPs were 110 ± 6, and 115 ± 7, for 1.0 % (v/v) glycerol and ultrapure water, respectively. Considering the aforementioned, 1.0 % (v/v) glycerol will be used as the solvent of choice for the washing step.

USC UNIVERSIDADE DE SANTIAGO DE COMPOSTELA

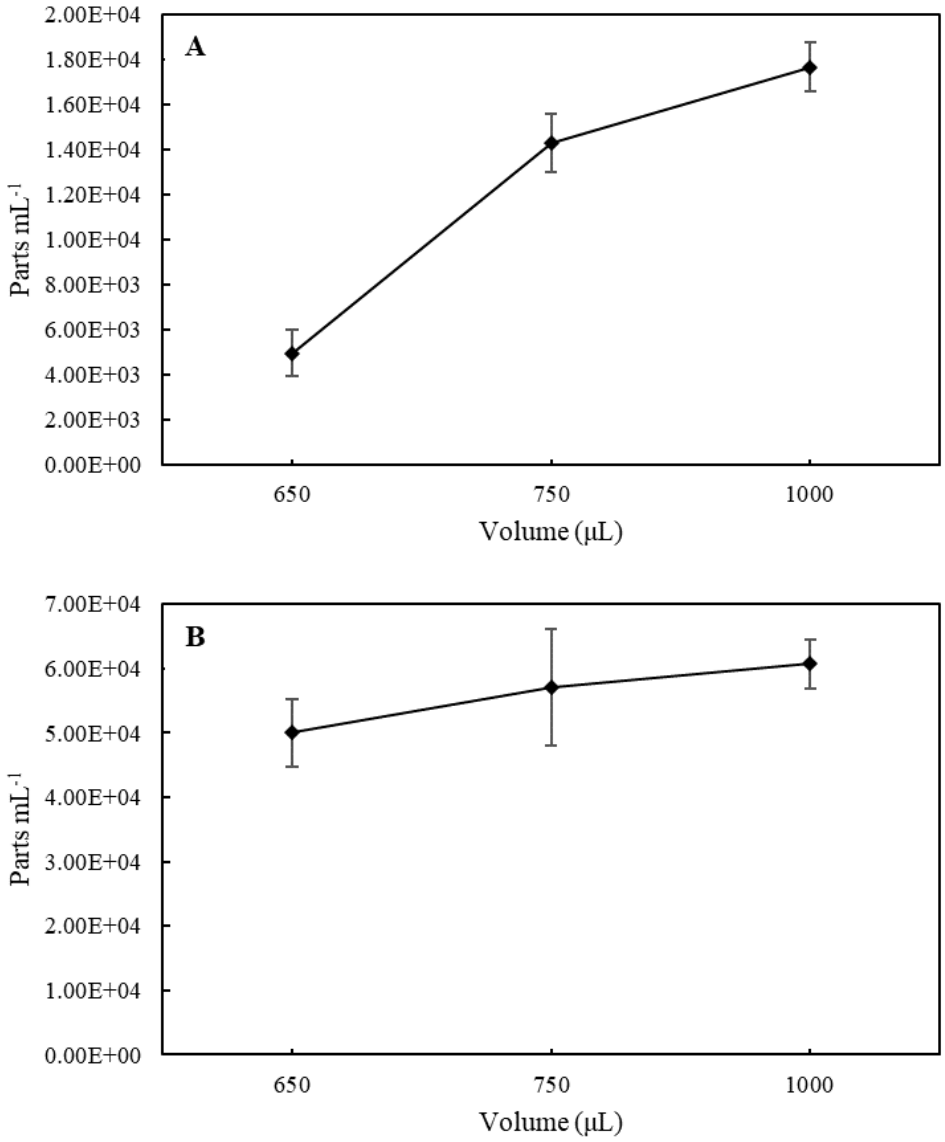

Figure 18. Effect of the volume of the 49:1 surfactant (TX-114)/extractant ($C_2H_4Cl_2$) mixture. Conditions: AgNPs, 64 ng L^{-1}(A), TiO_2NPs 25 µg L^{-1} (B); centrifugation time, 5 min; centrifugation speed, 2500 rpm; centrifugation temperature, 4 °C; vortex time, 30 s; vortex speed, 1500 rpm; error bars correspond to the SD of 3 experimental replicates (n=9 spICP-MS measurements).

USC
UNIVERSIDADE DE SANTIAGO DE COMPOSTELA

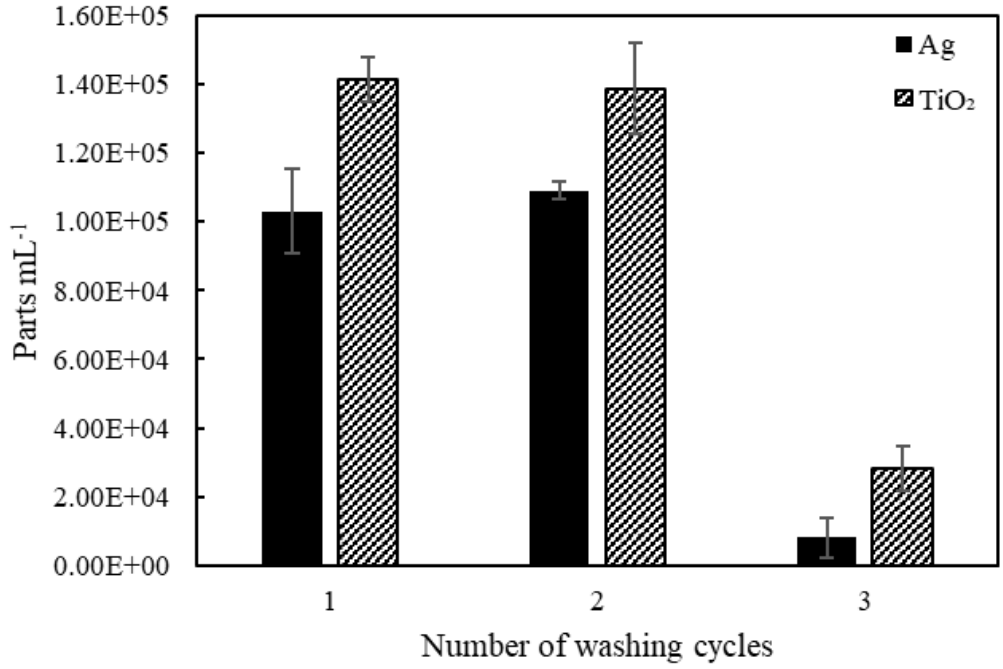

Figure 19. Optimization of the number of washing cycles. Conditions: AgNPs (40nm, 1.23x10^5 NPs mL^{-1}), TiO_2NPs (100 nm, 26.7 µg L^{-1}); error bars correspond to the SD of 2 experimental replicates (n=6 spICP-MS measurements).

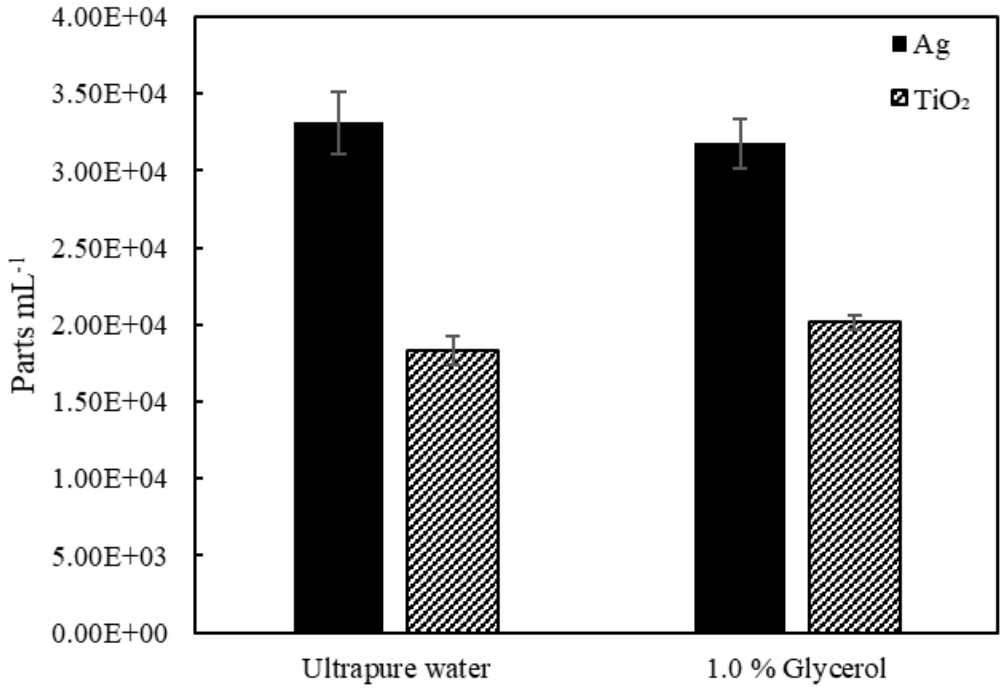

Figure 20. Selection of the appropriate washing solvent. Conditions: AgNPs (60 nm, 2.75x10^4 NPs mL^{-1}), TiO_2NPs (100 nm, 1.6 µg L^{-1}); error bars correspond to the SD of 2 experimental replicates (n=6 spICP-MS measurements)

USC UNIVERSIDADE DE SANTIAGO DE COMPOSTELA

2.3.2 Analytical performance

Matrix effect assessment

An aqueous silver/titanium ionic calibration was compared to silver/titanium matrix matched calibrations prepared with a pool of urine extracts (after the SA-DLLME or UF). Plotting counts versus μg event^{-1} revealed strong linearity ($R^2 > 0.996$) for all calibration graphs (Ag and Ti concentration levels at 1, 2, 5, and 10 μg L^{-1}). Statistical analysis (ANOVA test, 5 % significance level) showed no statistically significant differences (p-value > 0.05) between the slopes of the aqueous ionic silver calibration (5×10^{11} counts event μg^{-1}) and the matrix matched calibration (5×10^{11} counts event μg^{-1}) for the SA-DLLME approach. The application of SA-DLLME to tap water for the isolation of AgNPs and TiO_2NPs [35] gave the same result, suggesting that SA-DLLME is an effective sample pretreatment for the removal of matrix components.

However, significant differences (p-value < 0.05) were found between the slopes of the two calibration strategies (1×10^{11} and 2×10^{11} counts event μg^{-1} for the aqueous and the matrix matched calibration, respectively) for the UF approach. In the case of Ti, both experimental approaches revealed the presence of matrix effect ($p < 0.05$). The slopes of the aqueous and the matrix matched calibration resulted in 3×10^9 and 5×10^9 counts event μg^{-1}, for UF approach respectively, and 5×10^{10} and 1×10^{11} counts event μg^{-1}, for SA-DLLME. These findings suggest that the aqueous ionic silver calibration would be only justified if we follow the SA-DLLME approach for AgNPs quantification. In all other cases, a matrix-matched calibration is required and this type of calibration will be used from now on.

Limits of detection

The spICP-MS detection capabilities are influenced not only by concentration but also by the particle size (expressed as mass per particle). The assessment of the limit of detection in size (LOD_{size}) and in particle concentration (LOD_{number}) was conducted following the Microsoft Excel Tool by Laborda *et al.* [41]. LOD_{size} based on the 5-sigma criterion, was calculated using Eq. (1), where σ_B corresponds to the net mean baseline signal, ω is the peak width, ρ and Fp are the density of the element (10.49 and 4.23 g cm^{-3} for AgNPs and TiO_2NPs, respectively) and the mass fraction of the particle (1.0 and 0.6 for AgNPs and TiO_2NPs, respectively), K_{ICPMS} is the detection efficiency, K_M (=AN_{AV}/ M_M) is a factor related to the element, where A is the atomic abundance of the monitored isotope, N_{AV} the Avogadro number, and M_M the atomic mass, and t_{dwell} is the dwell time.

$$LOD_{SIZE} = \left(\frac{30\ \sigma_B}{\frac{2}{\omega}\pi\rho F_p K_{ICPMS} K_M t_{dwell}} \right)^{1/3} \quad (1)$$

The LOD_{number} was evaluated using Eq. (2), where $Y_{N,B}$ is the number of particles counted for a blank, η_{neb} the analyte transport efficiency, Q_{sample} the sample flow rate, and t_i the acquisition time.

$$LOD_{number} = \frac{5\sqrt{Y_{N,B}}+3}{\eta_{neb} Q_{sample} t_i} \quad (2)$$

USC UNIVERSIDADE DE SANTIAGO DE COMPOSTELA

Table 8 lists the limit of detection (particle concentration and size) for the two proposed techniques, calculated using unspiked urine samples (blank) subjected to the extraction procedure and measured eleven times. The 5-sigma criterion gave LOD_{size} values of 51 nm and 77 nm (SA-DLLME and UF technique, respectively) for TiO_2NPs, and 18 nm and 17 nm (SA-DLLME and UF technique, respectively) for AgNPs. Additionally, following the 3-sigma criterion, the LOD_{size} was 43 nm and 65 nm (SA-DLLME and UF technique, respectively) for TiO_2NPs, and 15 nm (both SA-DLLME and UF technique) for AgNPs. Table 9 summarizes the LOD_{size} and other analytical performances reported by other authors. There may be discrepancies in the LOD_{size} values as the LOD_{size} value is highly dependent on the calculation criteria used. The use of the calculation method described by Lee *et al.* [42] for LOD calculation has been used previously by many authors [24–27] and may result in a small LOD_{size}. The criteria used in the current study are those proposed by Laborda *et al.* [41], based on the quantile of the standard normal distribution.

Table 8. Number concentration and size detection limits (5-sigma criterion) (n=11).

		SA-DLLME	UF
TiO_2NPs	Number concentration/L^{-1}	1.5 x 10^{7a}	3.1 x 10^{5b}
	Size/nm	51	77
AgNPs	Number concentration/L^{-1}	3.1 x 10^{6a}	2.9 x 10^{5b}
	Size/nm	18	17

[a]concentration referred to the sample (EF 5), [b]concentration referred to the sample (EF 15)

Table 9. Analytical performances of the proposed method and reported methodologies for AgNPs and TiO_2NPs in urine.

NP	Sample pretreatment	Analytical technique	LOD_{number} (part mL^{-1})	LOD_{size} (nm)	Analytical recovery (%)	Ref.
AgNPs	Dilution[a]	spICP-MS	0.0006[b]	11	89–100	[25]
AgNPs	Dilution[a]	AF4	0.09[c]	5.6	55–76	[25]
AgNPs	Dilution[a]	spICP-MS	0.001[b]	12.1	80–97	[26]
TiO_2NPs	Dilution[d]	spICP-MS	0.05[b]	50	84–98	[27]
AgNPs	Dilution[e]	spICP-MS	5.7×10^3	8–9	104–106	[28]
TiO_2NPs	Dilution[e]	spICP-MS	4.3×10^3	15–18	96–98	[28]
AgNPs	SA-DLLME	spICP-MS	3.1×10^3	18	81–98	[This work]
AgNPs	UF	spICP-MS	2.9×10^2	17	90–115	[This work]
TiO_2NPs	SA-DLLME	spICP-MS	1.5×10^4	51	72–90	[This work]
TiO_2NPs	UF	spICP-MS	3.1×10^2	77	74–99	[This work]

(a) Ultrapure water as a diluent; (b) mass concentration as ng mL^{-1}; (c) mass concentration as µg mL^{-1}; (d) 0.1 %/(v/v) nitric acid as a diluent; (e) 1.0 %(v/v) glycerol as a diluent

USC UNIVERSIDADE DE SANTIAGO DE COMPOSTELA

Precision and analytical recovery

The accuracy of the method was studied by analytical recovery assays at two different concentration levels for 60 nm AgNPs standards, and for 50 and 100 nm TiO_2NPs standards. Experiments were performed in triplicate (SA-DLLME) and duplicate (UF), and the analytical recovery was calculated following Eq. (3), where $[NP]_{spiked}$ is the concentration in the spiked urine (parts mL^{-1}), $[NP]_{unspiked}$ is the concentration in the urine blank (parts mL^{-1}), and $[NP]_{standard}$ is the concentration of the NP standard suspension used for spiking experiments.

$$\% AR = \frac{[NP]_{spiked} - [NP]_{unspiked}}{[NP]_{standard}} \times 100 \quad (3)$$

Results are summarized in Table 10 (AgNPs) and Table 11 (TiO_2NPs) for both extraction techniques. The average analytical recovery following SA-DLLME approach was 91 ± 8 % and 85 ± 8 % (expressed as mean ±SD) for 40 nm AgNPs and 60 nm AgNPs, respectively; and 94 ± 8 % and 75 ± 8 for 50 nm TiO_2NPs and 100 nm TiO_2NPs, respectively. On the other hand, UF approach gave a mean analytical recovery of 103 ± 2 % (expressed as mean ±SD) for 60 nm AgNPs. TiO_2NPs analytical recovery values were in the range of 74 ± 1 % and 99 ± 1 %. Analytical recoveries for AgNPs and TiO_2NPs after SA-DLLME and UF were found to be in agreement with those reported by other authors (urine dilution as sample pretreatment, Table 9). Furthermore, relative standard deviations (RSD) reported in percentages were lower than 9 %, indicating that both methods had low variability and excellent precision (see Table 11).

Table 10. AgNPs analytical recoveries and relative standard deviation (%) for both extraction techniques.

	Particle Size (nm)	Concentration (NPs mL^{-1})	Analytical Recovery ± RSD (%) (n=9)
SA-DLLME	60	2.9×10^7	88 ± 9
	60	5.8×10^7	81 ± 6
	Particle Size (nm)	**Concentration (NPs mL^{-1})**	**Analytical Recovery ± RSD (%) (n=6)**
UF	60	1.4×10^4	90 ± 2
	60	2.8×10^4	115 ± 1

AgNPs and TiO_2NPs characterization

In order to have a closer insight into the NP stability through the extraction and preconcentration processes, size distribution profiles were assessed. The mean and the most frequent sizes were calculated and displayed in Fig. 21 and Fig. 22 (dataset used for this analysis was obtained from experiments from section *Precision and analytical recovery*). We can observe a good agreement between the sizes determined by spICP-MS following UF approach and those certified in the certificate of analysis for the commercial standards. Moreover, 40 nm AgNPs and 60 nm AgNPs showed a normal distribution with mean size (40 and 59 nm,

respectively) and most frequent size (37 and 54 nm, respectively) values very close to each other even with increasing concentration (low concentration level -L-, and high concentration level -H-). However, following the SA-DLLME extraction technique, AgNPs showed skewed distributions, with both the mean size and the most frequent size consistently lower than the theoretical standard, and the two values diverging significantly from each other (most frequent size of 25 nm and mean size of 35 nm for 40 nm AgNPs, and most frequent size of 21 nm and mean size of 47 nm for 60 nm AgNPs).

Table 11. TiO_2NPs analytical recoveries and relative standard deviation (%) for both extraction techniques.

	Particle Size (nm)	Concentration (μg L^{-1})	Analytical Recovery ± RSD (%) (n=9)
SA-DLLME	50	20	90 ±9
	100	20	77 ± 8
	50	40	97 ± 7
	100	40	72 ± 7
	Particle Size (nm)	**Concentration (μg L^{-1})**	**Analytical Recovery ± RSD (%) (n=6)**
UF	50	0.84	77 ± 3
	100	0.84	74 ± 1
	50	1.60	99 ± 12
	100	1.60	78 ± 1

This significant change in size distribution may indicate that AgNPs undergo partial dissolution during the SA-DLLME process. A previous HRTEM analysis of the AgNPs standards used for the spiking assays (Fig. 23 and 24, ESI) showed mean sizes in good agreement with the reported values, so the changes in size distributions upon application of SA-DLLME indicate that AgNPs undergo dissolution during this extraction process. Several studies have shown that the dissolution of AgNPs is favored in the presence of chloride ions [43,44], and therefore the urine matrix must be responsible for the partial dissolution of AgNPs due to the high chloride ion content. These results are in good agreement with previous experience on SA-DLLME for the isolation of AgNPs from tap water [35], a matrix with a low chloride content and for which SA-DLLME led to similar AgNPs mean sizes and most common sizes.

Regarding the size distributions of TiO_2NPs, more repeatable mean and most frequent sizes were obtained using the UF approach compared to the standard (96 nm and 64 nm as mean and most frequent size, respectively, for 50 nm TiO_2NPs; and 102 nm and 79 nm as mean and most frequent size, respectively, for 100 nm TiO_2NPs). However, larger differences between the mean and most frequent size values were observed when using the SA-DLLME method [mean and most frequent sizes were in all cases higher than 145 nm (regardless of the standard used, 50 or 100 nm TiO_2NPs)]. This finding can be attributed to the strong tendency of TiO_2NPs to

USC UNIVERSIDADE DE SANTIAGO DE COMPOSTELA

agglomerate and/or form aggregates, phenomena favored in the presence of large molecules and electrolytes (chloride ions, among others) [43,45,46].

Therefore, the SA-DLLME process compromises NP integrity for a complex matrix such as urine because matrix components (mainly chloride ions) promote AgNPs dissolution and also promote TiO_2NPs agglomeration (organic molecules and salts).

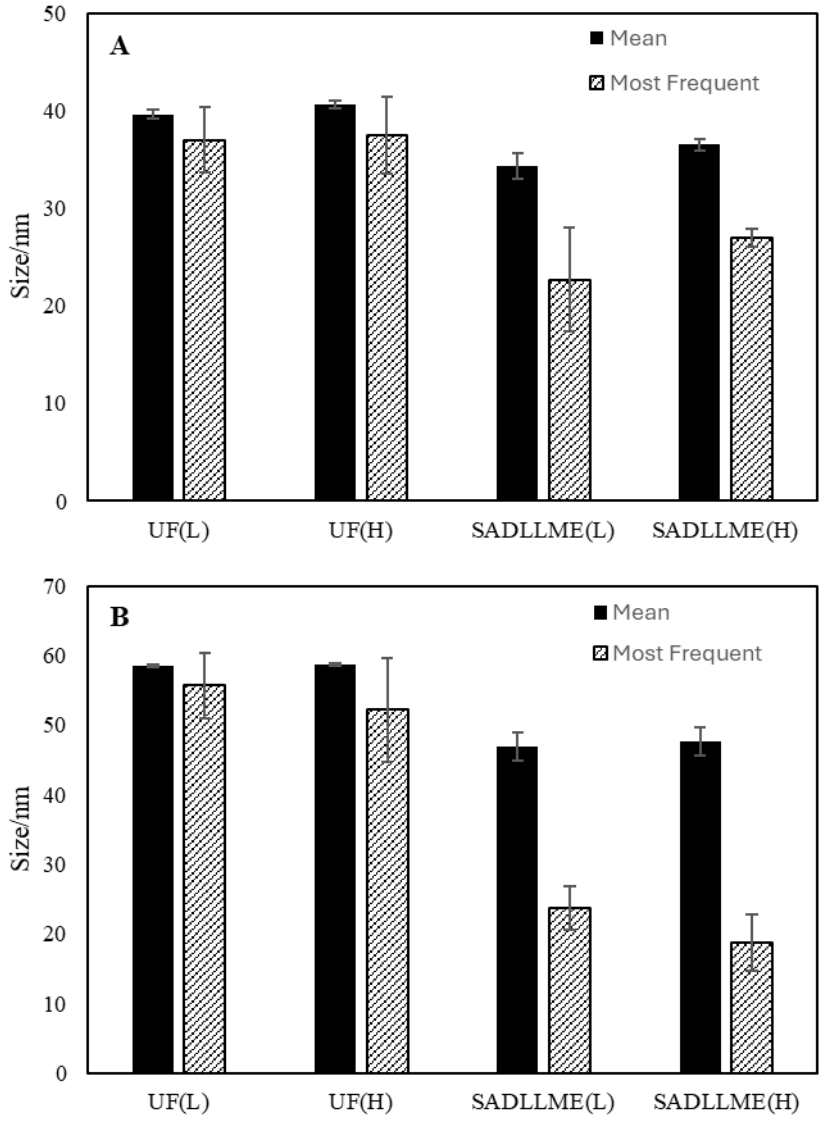

Figure 21. Values of mean and most frequent sizes for 40nm-AgNPs (A) and 60nm-AgNPs (B) at low spiking level* (L) and high spiking level* (H); error bars correspond to the SD of 3 experimental replicates (n=9 spICP-MS measurements).*See table 10 for concentrations.

2.4 CONCLUSIONS

Two analytical methodologies (SA-DLLME and centrifugal UF) have been proposed as sample pre-treatments for the quantification and characterization (size distribution) of AgNPs and TiO_2NPs in complex clinical matrices such as human urine. Both techniques are more time-

consuming than dilution-based pre-treatments but since the low concentration of NPs expected in urine, problems of number concentration detectability due to dilution are avoided. When comparing SA-DLLME with UF, it can be said that SA-DLLME is a multi-step process that requires samples to be processed manually one at a time. Although the processing time for each sample is less than that required by UF, approximately 15 min for SA-DLLME, the manual nature of the process makes it lengthy. On the other hand, UF allows the simultaneous processing of several samples (depending on the centrifuge rotor, in our case 8 samples at a time) and although it is a long process (about 25 min for loading and 25 min for washing) it requires less manual effort.

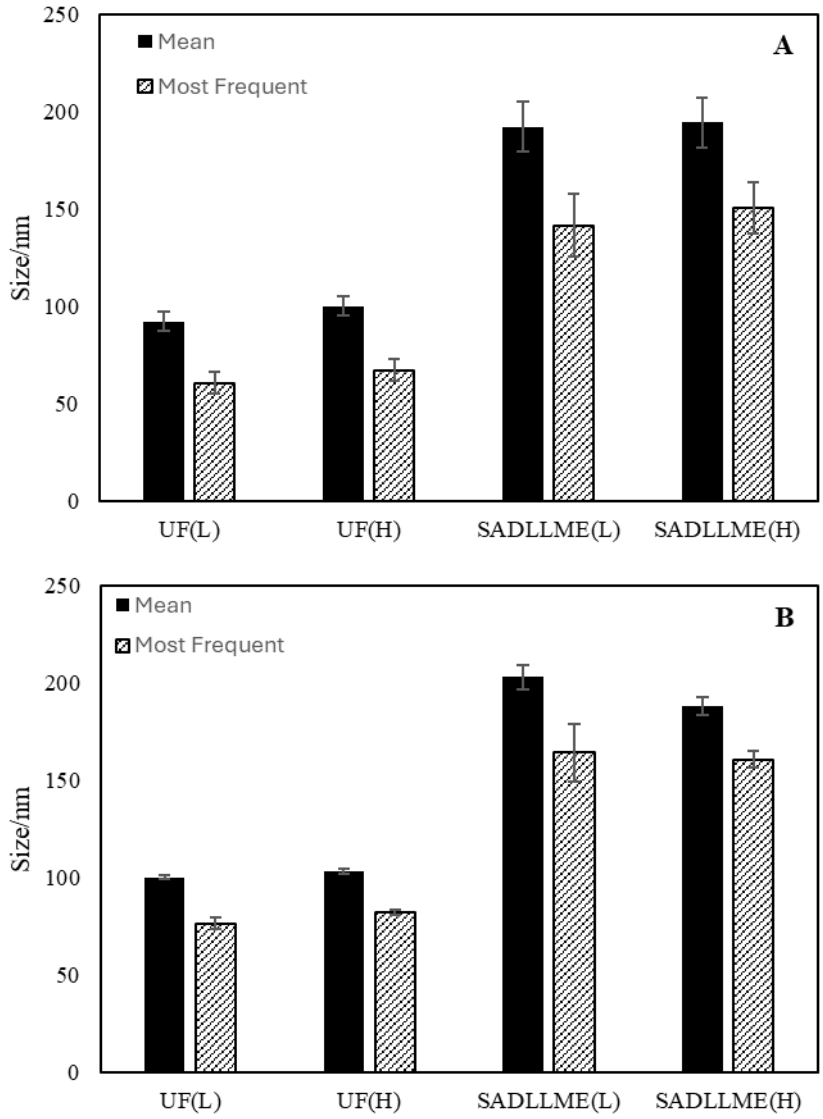

Figure 22. Values of mean and most frequent sizes for 50nm-TiO_2NPs (A) and 100nm-TiO_2NPs (B) at low spiking level* (L) and high spiking level* (H). error bars correspond to the SD of 3 experimental replicates (n=9 spICP-MS measurements). *See table 11 for concentrations.

Regarding analytical performances, SA-DLLME was found to provide good sensitivity and analytical recoveries. However, the integrity of the NPs after SA-DLLME was

compromised, and particle sizes differed significantly from those reported in the commercial standards (manufacturer's sizes) used for the spiking assays, and the extraction process can lead to NPs dissolution and particle aggregation/agglomeration. Finally, the results of this work highlight the applicability of spICP-MS for the determination of NPs in human urine, but further studies are needed to develop sample pre-treatments that guarantee the integrity and accuracy of NPs.

2.5 FUNDING SOURCES

Grant FOODNANORISK (reference PID2021-125276NB-I00) funded by MICIU/AEI/ 10.13039/501100011033 Spain. and *Grupo de Referencia Competitiva* (reference ED431C 2022/029) funded by Consellería de Educación, Ciencia, Universidades y Formación Profesional, Xunta de Galicia, Spain. A. J.-V. acknowledges Xunta de Galicia, Spain, for a pre-doctoral grant.

2.6 REFERENCES

[1] F. Laborda, E. Bolea, G. Cepriá, M.T. Gómez, M.S. Jiménez, J. Pérez-Arantegui, J. R. Castillo, Detection, characterization and quantification of inorganic engineered nanomaterials: A review of techniques and methodological approaches for the analysis of complex samples, Anal. Chim. Acta 904 (2016) 10–32, https://doi.org/10.1016/j.aca.2015.11.008.

[2] Nanotechnology Products Database, (n.d.). https://statnano.com/ (accessed November 6, 2024).

[3] M. Rai, K. Kon, A. Ingle, N. Duran, S. Galdiero, M. Galdiero, Broad-spectrum bioactivities of silver nanoparticles: the emerging trends and future prospects, Appl. Microbiol. Biotechnol. 98 (2014) 1951–1961, https://doi.org/10.1007/s00253-013-5473-x.

[4] S.S.D. Kumar, N.K. Rajendran, N.N. Houreld, H. Abrahamse, Recent advances on silver nanoparticle and biopolymer-based biomaterials for wound healing applications, Int. J. Biol. Macromol. 115 (2018) 165–175, https://doi.org/10.1016/j.ijbiomac.2018.04.003.

[5] R.A. Bapat, T.V. Chaubal, C.P. Joshi, P.R. Bapat, H. Choudhury, M. Pandey, B. Gorain, P. Kesharwani, An overview of application of silver nanoparticles for biomaterials in dentistry, Mater. Sci. Eng. C 91 (2018) 881–898, https://doi.org/10.1016/j.msec.2018.05.069.

[6] S.P. Deshmukh, S.M. Patil, S.B. Mullani, S.D. Delekar, Silver nanoparticles as an effective disinfectant: A review, Mater. Sci. Eng. C 97 (2019) 954–965, https://doi.org/10.1016/j.msec.2018.12.102.

[7] J. Theron, J.A. Walker, T.E. Cloete, Nanotechnology and water treatment: Applications and emerging opportunities, Crit. Rev. Microbiol. 34 (2008) 43–69, https://doi.org/10.1080/10408410701710442.

[8] R.J.B. Peters, G. Van Bemmel, Z. Herrera-Rivera, H.P.F.G. Helsper, H.J.P. Marvin, S. Weigel, P.C. Tromp, A.G. Oomen, A.G. Rietveld, H. Bouwmeester, Characterization of

USC UNIVERSIDADE DE SANTIAGO DE COMPOSTELA

titanium dioxide nanoparticles in food products: analytical methods to define nanoparticles, J. Agric. Food Chem. 62 (2014) 6285–6293, https://doi.org/10.1021/jf5011885.

[9] F. Fiordaliso, P. Bigini, M. Salmona, L. Diomede, Toxicological impact of titanium dioxide nanoparticles and food-grade titanium dioxide (E171) on human and environmental health, Environ. Sci. Nano 9 (2022) 1199–1211, https://doi.org/10.1039/d1en00833a.

[10] B. Faure, G. Salazar-Alvarez, A. Ahniyaz, I. Villaluenga, G. Berriozabal, Y.R. De Miguel, L. Bergström, Dispersion and surface functionalization of oxide nanoparticles for transparent photocatalytic and UV-protecting coatings and sunscreens, Sci. Technol. Adv. Mater. 14 (2013), https://doi.org/10.1088/1468-6996/14/2/023001.

[11] T. Skotland, T.G. Iversen, A. Llorente, K. Sandvig, Biodistribution, pharmacokinetics and excretion studies of intravenously injected nanoparticles and extracellular vesicles: possibilities and challenges, Adv. Drug Deliv. Rev. 186 (2022) 114326, https://doi.org/10.1016/j.addr.2022.114326.

[12] V. Naumenko, A. Nikitin, K. Kapitanova, P. Melnikov, S. Vodopyanov, A. Garanina, M. Valikhov, A. Ilyasov, D. Vishnevskiy, A. Markov, S. Golyshev, D. Zhukov, I. Alieva, M. Abakumov, V. Chekhonin, A. Majouga, Intravital microscopy reveals a novel mechanism of nanoparticles excretion in kidney, J. Control. Release 307 (2019) 368–378, https://doi.org/10.1016/j.jconrel.2019.06.026.

[13] A. Lapresta-Fernández, A. Salinas-Castillo, S. Anderson De La Llana, J.M. Costa-Fern´andez, S. Domínguez-Meister, R. Cecchini, L.F. Capitán-Vallvey, M.C. Moreno- Bondi, M.P. Marco, J.C. Sánchez-López, I.S. Anderson, A general perspective of the characterization and quantification of nanoparticles: Imaging, spectroscopic, and separation techniques, Crit. Rev. Solid State Mater. Sci. 39 (2014) 423–458, https://doi.org/10.1080/10408436.2014.899890.

[14] Z. Gajdosechova, Z. Mester, Recent trends in analysis of nanoparticles in biological matrices, Anal. Bioanal. Chem. 411 (2019) 4277–4292, https://doi.org/10.1007/s00216-019-01620-9.

[15] R.M. Galazzi, K. Chacón-Madrid, D.C. Freitas, L.F. da Costa, M.A.Z. Arruda, Inductively coupled plasma mass spectrometry based platforms for studies involving nanoparticle effects in biological samples, Rapid Commun. Mass Spectrom. 34 (2020) 1–14, https://doi.org/10.1002/rcm.8726.

[16] C. Degueldre, P.Y. Favarger, Colloid analysis by single particle inductively coupled plasma-mass spectroscopy: A feasibility study, Colloids Surf., A Physicochem. Eng. Asp. 217 (2003) 137–142, https://doi.org/10.1016/S0927-7757(02)00568-X.

[17] F. Laborda, E. Bolea, J. Jiménez-Lamana, Single particle inductively coupled plasma mass spectrometry for the analysis of inorganic engineered nanoparticles in environmental samples, Trends Environ. Anal. Chem. 9 (2016) 15–23, https://doi.org/10.1016/j.teac.2016.02.001.

USC UNIVERSIDADE DE SANTIAGO DE COMPOSTELA

[18] F. Laborda, J. Jiménez-Lamana, E. Bolea, J.R. Castillo, Critical considerations for the determination of nanoparticle number concentrations, size and number size distributions by single particle ICP-MS, J. Anal. At. Spectrom. 28 (2013) 1220–1232, https://doi.org/10.1039/c3ja50100k.
[19] H.E. Pace, N.J. Rogers, C. Jarolimek, V.A. Coleman, C.P. Higgins, J.F. Ranville, Determining transport efficiency for the purpose of counting and sizing nanoparticles via single particle inductively coupled plasma mass spectrometry, Anal. Chem. 83 (2011) 9361–9369, https://doi.org/10.1021/ac201952t.

[20] A.R. Montoro Bustos, K.P. Purushotham, A. Possolo, N. Farkas, A.E. Vladár, K. E. Murphy, M.R. Winchester, Validation of single particle ICP-MS for routine measurements of nanoparticle size and number size distribution, Anal. Chem. 90 (2018) 14376–14386, https://doi.org/10.1021/acs.analchem.8b03871.

[21] D. Mozhayeva, C. Engelhard, A critical review of single particle inductively coupled plasma mass spectrometry-A step towards an ideal method for nanomaterial characterization, J. Anal. At. Spectrom. 35 (2020) 1740–1783, https://doi.org/10.1039/c9ja00206e.

[22] B. Meermann, V. Nischwitz, ICP-MS for the analysis at the nanoscale-a tutorial review, J. Anal. At. Spectrom. 33 (2018) 1432–1468, https://doi.org/10.1039/c8ja00037a.

[23] M.D. Montaño, J.W. Olesik, A.G. Barber, K. Challis, J.F. Ranville, Single particle ICP-MS: advances toward routine analysis of nanomaterials, Anal. Bioanal. Chem. 408 (2016) 5053–5074, https://doi.org/10.1007/s00216-016-9676-8.

[24] B. Bocca, B. Battistini, F. Petrucci, Silver and gold nanoparticles characterization by SP-ICP-MS and AF4-FFF-MALS-UV-ICP-MS in human samples used for biomonitoring, Talanta 220 (2020) 121404, https://doi.org/10.1016/j.talanta.2020.121404.

[25] B. Bocca, B. Battistini, V. Leso, L. Fontana, S. Caimi, M. Fedele, I. Iavicoli, Occupational exposure to metal engineered nanoparticles: a human biomonitoring pilot study involving Italian nanomaterial workers, Toxics. 11 (2023), https://doi.org/10.3390/toxics11020120.

[26] S. Salou, D. Larivière, C.M. Cirtiu, N. Fleury, Quantification of titanium dioxide nanoparticles in human urine by single-particle ICP-MS, Anal. Bioanal. Chem. 413 (2021) 171–181, https://doi.org/10.1007/s00216-020-02989-8.

[27] K. Badalova, P. Herbello-Hermelo, P. Bermejo-Barrera, A. Moreda-Piñeiro, Possibilities of single particle—ICP-MS for determining/characterizing titanium dioxide and silver nanoparticles in human urine, J. Trace Elem. Med. Biol. 54 (2019) 55–61, https://doi.org/10.1016/j.jtemb.2019.04.003.

[28] M. Cabré, G. Fernández, E. Gonz´alez, J. Abellà, A. Verdaguer, Single particle ICP- MS: a tool for the characterization of gold nanoparticles in nanotheranostics applications, J. Anal. At. Spectrom. (2024) 2508–2513, https://doi.org/10.1039/d4ja00141a.

[29] J.B. Whitlam, K.F. Brown, Ultrafiltration in serum protein binding determinations, J. Pharm. Sci. 70 (1981) 146–150, https://doi.org/10.1002/jps.2600700208.

USC UNIVERSIDADE DE SANTIAGO DE COMPOSTELA

[30] M. Loginov, F. Samper, G. Gésan-Guiziou, T. Sobisch, D. Lerche, E. Vorobiev, Centrifugal ultrafiltration for determination of filter cake properties of colloids, J. Memb. Sci. 536 (2017) 59–75, https://doi.org/10.1016/j.memsci.2017.04.064.

[31] V.J. Pansare, D. Tien, P. Thoniyot, R.K. Prud'homme, Ultrafiltration of nanoparticle colloids, J. Membr. Sci. 538 (2017) 41–49, https://doi.org/10.1016/j.memsci.2017.03.041.

[32] M. Saraji, A.A.H. Bidgoli, Dispersive liquid-liquid microextraction using a surfactant as disperser agent, Anal. Bioanal. Chem. 397 (2010) 3107–3115, https://doi.org/10.1007/s00216-010-3894-2.

[33] I. Hagarová, L. Nemˇcek, M. ˇSebesta, O. Zvˇeˇrina, P. Kasak, M. Urík, Preconcentration and separation of gold nanoparticles from environmental waters using extraction techniques followed by spectrometric quantification, Int. J. Mol. Sci. 23 (2022), https://doi.org/10.3390/ijms231911465.

[34] Y. Liu, M. He, B. Chen, B. Hu, Ultra-trace determination of gold nanoparticles in environmental water by surfactant assisted dispersive liquid liquid microextraction coupled with electrothermal vaporization-inductively coupled plasma-mass spectrometry, Spectrochim. Acta - Part B At. Spectrosc. 122 (2016) 94–102, https://doi.org/10.1016/j.sab.2016.04.009.

[35] A. Justo-Vega, R. Domínguez-González, P. Bermejo-Barrera, A. Moreda-Piñeiro, Prospects of surfactant assisted dispersive liquid-liquid microextraction for the selective extraction of silver and titanium dioxide nanoparticles from tap water and determination by spICP-MS, J. Anal. At. Spectrom. 39 (2023) 573–581, https://doi.org/10.1039/d3ja00227f.

[36] S.K. Selahle, P.N. Nomngongo, Quantification of TiO2 and ZnO nanoparticles in wastewater using inductively coupled plasma optical emission spectrometry, Toxicol. Environ. Chem. 101 (2019) 204–214, https://doi.org/10.1080/02772248.2019.1686151.

[37] D.O.F. Kidney, Laboratory Assessment of Kidney Disease, Pocket Companion to Brenner Rector's Kidney. (2011) 21–41. https://doi.org/10.1016/b978-1-4160-6640-8.00002-6.

[38] ˙I. Yıldırım, H. Koçan, The pH of drinking water and its effect on the pH of urine, Cureus 15 (2023), https://doi.org/10.7759/cureus.47437.

[39] K. Dastafkan, M. Khajeh, M. Bohlooli, M. Ghaffari-Moghaddam, N. Sheibani, Mechanism and behavior of silver nanoparticles in aqueous medium as adsorbent, Talanta 144 (2015) 1377–1386, https://doi.org/10.1016/j.talanta.2015.03.065.

[40] F.A. Dawodu, C.U. Onuh, K.G. Akpomie, E.I. Unuabonah, Synthesis of silver nanoparticle from Vigna unguiculata stem as adsorbent for malachite green in a batch system, SN Appl. Sci. 1 (2019), https://doi.org/10.1007/s42452-019-0353-3.

[41] F. Laborda, A.C. Gimenez-Ingalaturre, E. Bolea, J.R. Castillo, About detectability and limits of detection in single particle inductively coupled plasma mass spectrometry,

USC UNIVERSIDADE DE SANTIAGO DE COMPOSTELA

Spectrochim. Acta - Part B At. Spectrosc. 169 (2020) 105883, https://doi.org/10.1016/j.sab.2020.105883.

[42] S. Lee, X. Bi, R.B. Reed, J.F. Ranville, P. Herckes, P. Westerhoff, Nanoparticle size detection limits by single particle ICP-MS for 40 elements, Environ. Sci. Technol. 48 (2014) 10291–10300, https://doi.org/10.1021/es502422v.

[43] D.M. Mitrano, J.F. Ranville, A. Bednar, K. Kazor, A.S. Hering, C.P. Higgins, Tracking dissolution of silver nanoparticles at environmentally relevant concentrations in laboratory, natural, and processed waters using single particle ICP-MS (spICP-MS), Environ. Sci. Nano 1 (2014) 248–259, https://doi.org/10.1039/c3en00108c.

[44] B.A. Chambers, A.R.M.N. Afrooz, S. Bae, N. Aich, L. Katz, N.B. Saleh, M.J. Kirisits, Effects of chloride and ionic strength on physical morphology, dissolution, and bacterial toxicity of silver nanoparticles, Environ. Sci. Technol. 48 (2014) 761–769, https://doi.org/10.1021/es403969x.

[45] F. Xu, Review of analytical studies on TiO2 nanoparticles and particle aggregation, coagulation, flocculation, sedimentation, stabilization, Chemosphere 212 (2018) 662–677, https://doi.org/10.1016/j.chemosphere.2018.08.108.

[46] S.V. Jenkins, H. Qu, T. Mudalige, T.M. Ingle, R. Wang, F. Wang, P.C. Howard, J. Chen, Y. Zhang, Rapid determination of plasmonic nanoparticle agglomeration status in blood, Biomaterials 51 (2015) 226–237, https://doi.org/10.1016/j.biomaterials.2015.01.072.

USC UNIVERSIDADE DE SANTIAGO DE COMPOSTELA

SUPPLEMENTARY INFORMATION

- *Ag NPs standard 60 nm*

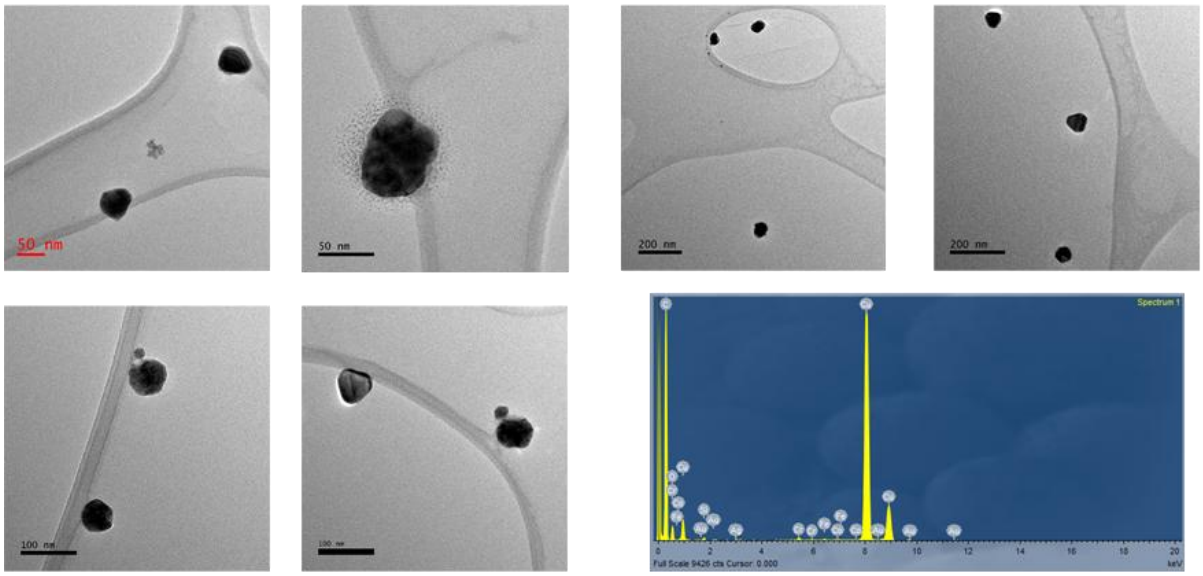

Figure 23. HRTEM image and EDX spectrum of 60 nm AgNPs standard.

- *Ag NPs standard 40 nm*

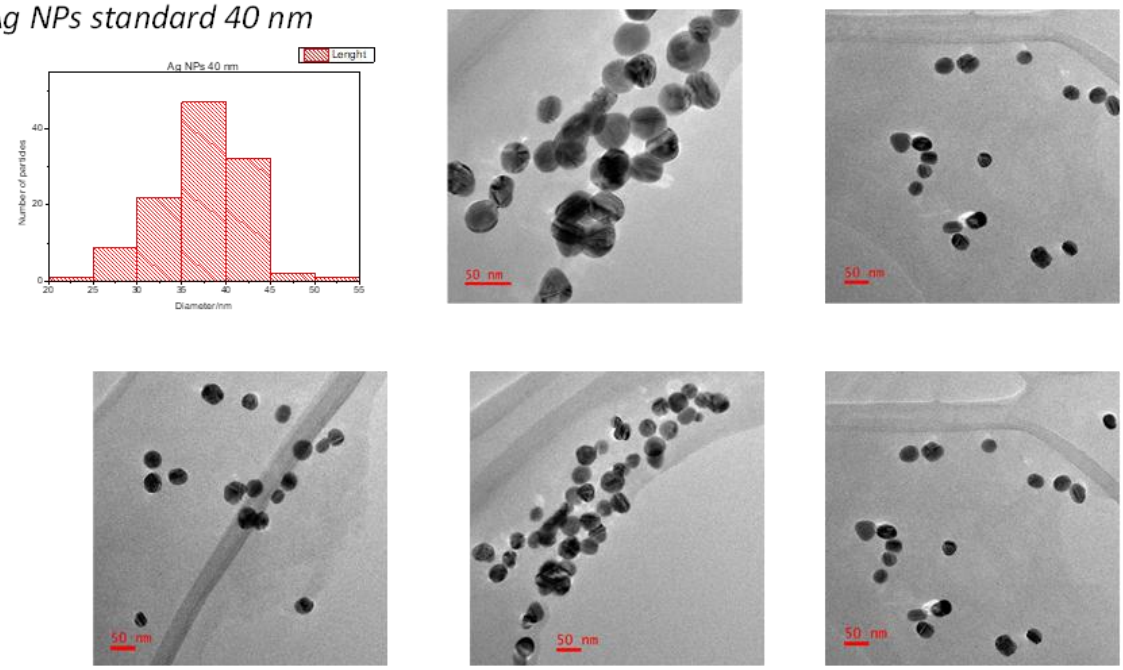

Figure 24. HRTEM image and EDX spectrum of 40 nm AgNPs standard.

- *TiO_2 NPs standard 100 nm*

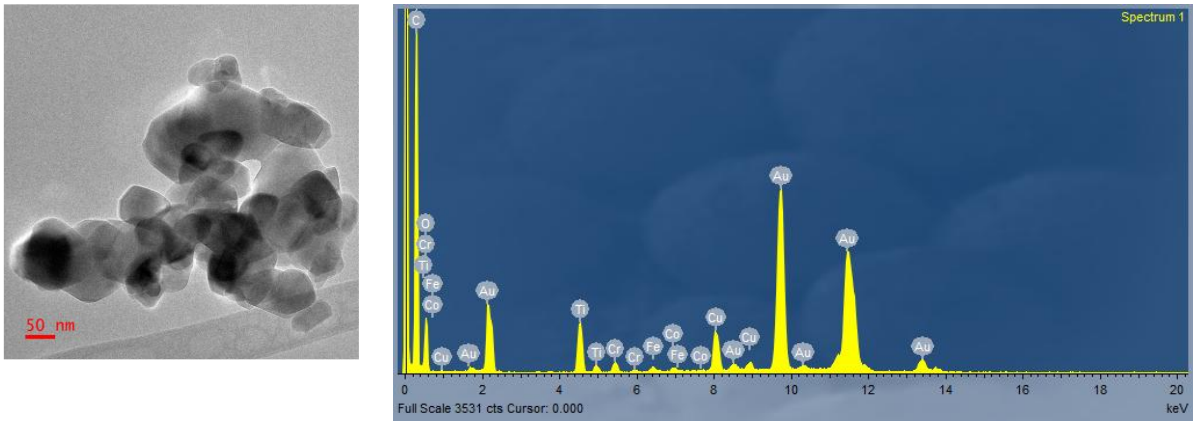

Figure 25. HRTEM image and EDX spectrum of 100 nm TiO_2NPs standard.

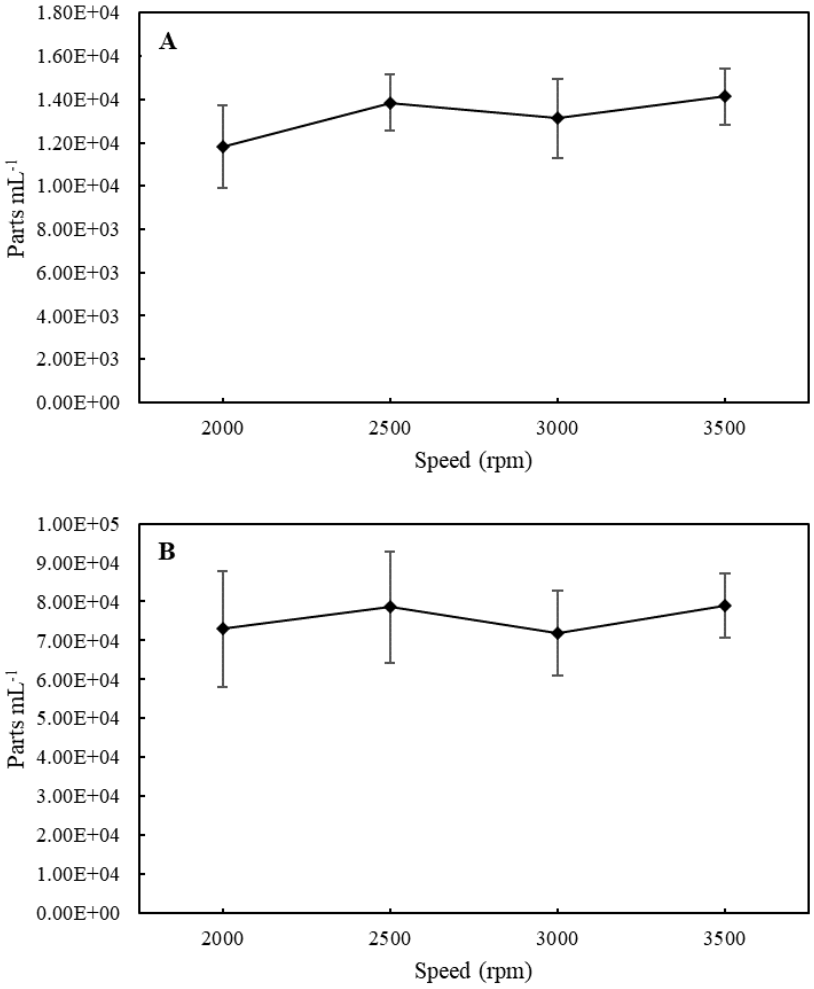

Figure 26. Effect of the centrifugation speed on the extraction efficiency. Conditions: AgNPs, 64 ng L^{-1}(A), TiO_2NPs 1 µg L^{-1} (B); volume of the 49:1 surfactant (TX-114)/extractant ($C_2H_4Cl_2$) mixture, 1 mL; centrifugation time, 5 min; centrifugation temperature, 4 ºC, vortex time, 30 s; vortex speed, 1500 rpm; error bars correspond to the SD of 3 experimental replicates (n=9 spICP-MS measurements).

USC
DE SANTIAGO
DE COMPOSTELA

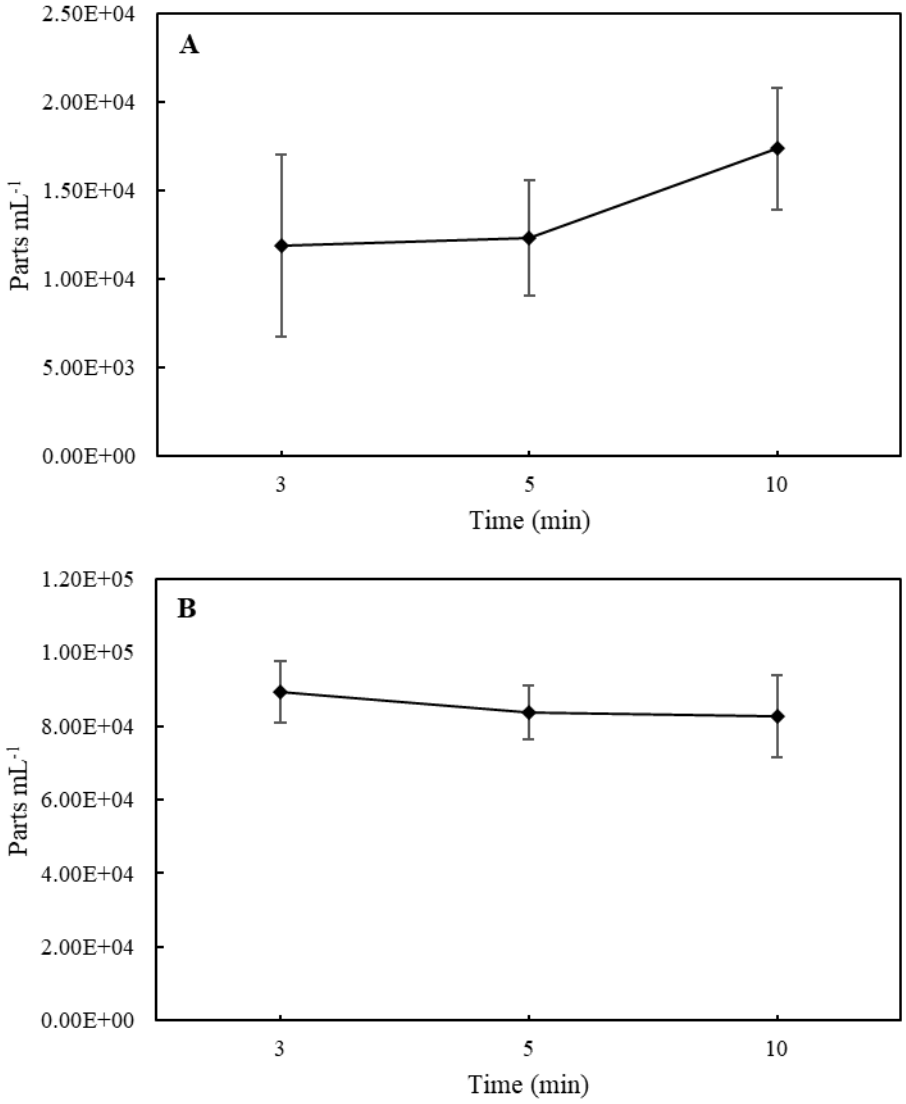

Figure 27. Effect of the centrifugation time on the extraction efficiency. Conditions: AgNPs, 64 ng L^{-1}(A), TiO_2NPs 1 µg L^{-1} (B); volume of the 49:1 surfactant (TX-114)/extractant ($C_2H_4Cl_2$) mixture, 1 mL; centrifugation speed, 3500 rpm; centrifugation temperature, 4 °C; vortex time, 30 s; vortex speed, 1500 rpm; error bars correspond to the SD of 3 experimental replicates (n = 9 spICP-MS measurements).

USC UNIVERSIDADE DE SANTIAGO DE COMPOSTELA

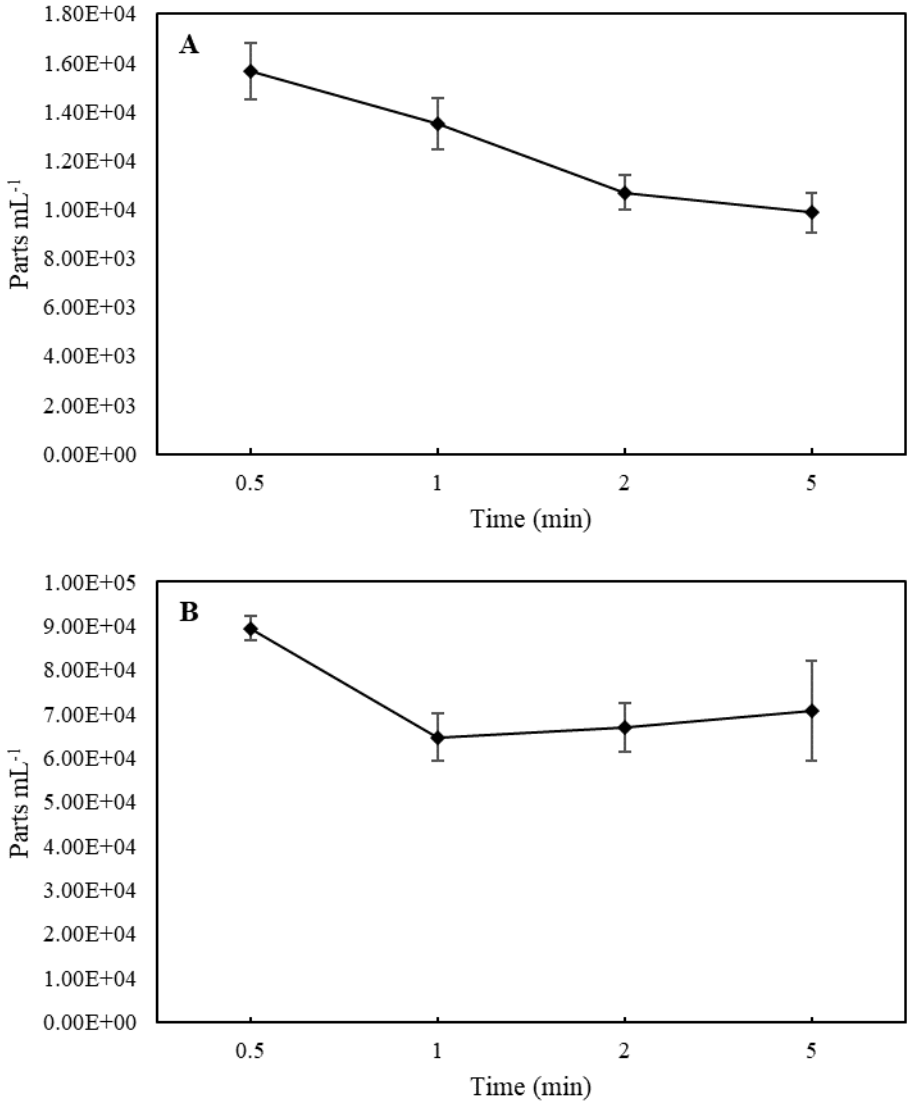

Figure 28. Effect of the vortex time on the extraction efficiency. Conditions: AgNPs, 64 ng L^{-1}(A), TiO_2NPs 1 µg L^{-1} (B); volume of the 49:1 surfactant (TX-114)/extractant ($C_2H_4Cl_2$) mixture, 1 mL; centrifugation speed, 3500 rpm; centrifugation time, 10 min; centrifugation temperature, 4 °C; vortex speed, 1500 rpm; error bars correspond to the SD of 3 experimental replicates (n = 9 spICP-MS measurements).

USC UNIVERSIDADE DE SANTIAGO DE COMPOSTELA

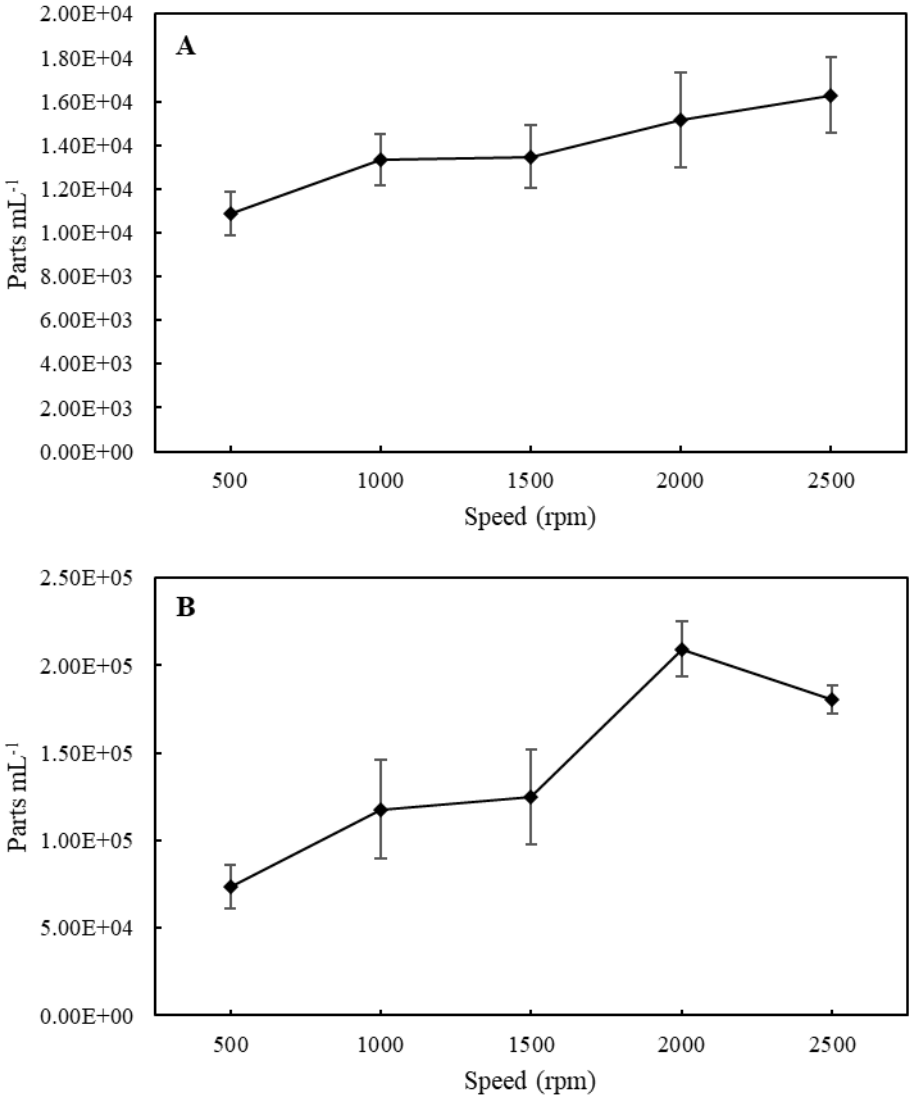

Figure 29. Effect of the vortex speed on the extraction efficiency. Conditions: AgNPs, 64 ng L^{-1}(A), TiO_2NPs 1 µg L^{-1} (B); volume of the 49:1 surfactant (TX-114)/extractant ($C_2H_4Cl_2$) mixture, 1 mL; centrifugation speed, 3500 rpm; centrifugation time, 10 min; centrifugation temperature, 4 °C; vortex time, 30 s; error bars correspond to the SD of 3 experimental replicates (n = 9 spICP-MS measurements).

USC
UNIVERSIDADE DE SANTIAGO DE COMPOSTELA

CHAPTER 3. ENZYMATIC HYDROLYSIS FOR PRE-TREATING HUMAN SERUM BEFORE TITANIUM DIOXIDE NANOPARTICLES ASSESSMENT BY spICP-MS

USC
UNIVERSIDADE DE SANTIAGO DE COMPOSTELA

CHAPTER 3. ENZYMATIC HYDROLYSIS FOR PRE-TREATING HUMAN SERUM BEFORE TITANIUM DIOXIDE NANOPARTICLES ASSESSMENT BY SPICP-MS

The results from this chapter have already been published as:

Ana Justo-Vega, Sara Vázquez-Pérez, Raquel Domínguez-González, Pilar Bermejo-Barrera, and Antonio Moreda-Piñeiro

Group of Trace Elements, Spectroscopy and Speciation (GETEE), Institute of Materials iMATUS, Department of Analytical Chemistry, Nutrition and Bromatology, Faculty of Chemistry, Universidade de Santiago de Compostela, Avenida das Ciencias, s/n., 15782, Santiago de Compostela, Spain.

*Talanta, 2025, **291**, 127766*
(DOI: 10.1016/j.talanta.2025.127766)

GRAPHICAL ABSTRACT

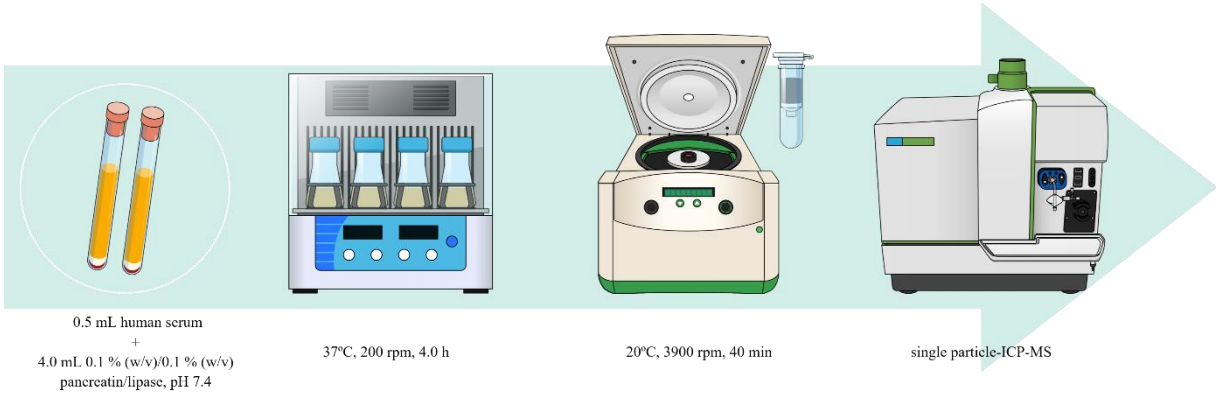

ABSTRACT

The current use of inorganic nanoparticles (NPs) in many industrial sectors, particularly in the food industry, has led to growing concerns about the toxicity of these emerging materials to humans. Therefore, NPs assessment in foodstuff, environmental materials and biological fluids is becoming an important topic, and the development of reliable quantification/characterization analytical methods is needed. The presence of NPs in blood and urine can be expected because of the bioavailability/assimilation of these entities by the organism. However, the determination of NPs in biofluids is a challenge mainly due to the complexity of the sample and the low levels of NPs (basal levels). The research on new methodologies for sample treatment is therefore needed.

The possibilities of enzymatic hydrolysis followed by centrifugal ultrafiltration for isolating titanium dioxide nanoparticles (TiO_2NPs) from serum samples have been explored in

USC DE COMPOSTELA

the current research. Hydrolysis of serum′s matrix components was performed with a pancreatin-lipase mixture (0.1 % (w/v) each one) operating at pH 7.4 and 37 ºC for 4.0 h under orbital - horizontal shaking at 150 rpm. In addition, centrifugal ultrafiltration (30 kDa molecular weight cutoff (MWCO) membrane) was optimised for removing enzymes residues and other matrix′s components. The developed method showed a limit of detection of 6.89×10^3 NPs mL^{-1}, and a limit of detection in size of 36 nm, whereas analytical recovery for spiking assays with 100 nm TiO_2NPs were within the 103−114 % range.

Keywords: Titanium dioxide nanoparticles, serum, enzymatic hydrolysis, ultra centrifugal filtration, spICP-MS

3.1 INTRODUCTION

Titanium dioxide has long been used in paint formulations and coatings due to the bright white colour achieved in the final products. In addition, this pigment is also used as a white colorant in pharmaceuticals and foodstuff (referred as food additive E171 in the food industry), and in personal care products, mainly sunscreens, since the exhibited UV filter properties [1]. The food additive E171 has been demonstrated to contain up to 50 % titanium dioxide in nanometric state (titanium dioxide nanoparticles, TiO_2NPs) [2], and the European Food Safety Authority (EFSA) has recently stated that E171 is not a safe food additive and hence, the use of E171 in the food industry is no longer authorized in the European Union [3]. The EFSA has also published a guidance for assessing the risk of the presence of nanomaterials (NMs) in the food/feed chain [4], and several studies have demonstrated the high bio-persistence of TiO_2NPs in human gastro-intestinal tract [5–7], and hence the potential distribution of TiO_2NPs in several organs. In addition to ingestion (food chain), inhalation [8,9] and dermal and mucosal surface exposure [10] there are other exposure pathways for NMs, and several studies have been focused on occupational hygiene studies [8,9]. Therefore, the determination of NMs, mainly inorganic nanoparticles (NPs), in consumer products (foodstuff) and environmental materials is a challenging analytical problem which requires advances on analytical methodologies [11]. In addition, innovative analytical methods, including sample pretreatment, are required in nanotoxicological studies to determine the degree of NMs impregnation and bioavailability in humans.

Inductively coupled plasma-mass spectrometry (ICP-MS), mainly operating in the so-called single particle mode (spICP-MS) and single cell mode (SC-ICP-MS), as well as other several ICP-MS-based systems, such as laser ablation-ICP-MS (LA-ICP-MS) and hyphenated ICP-MS techniques with hydrodynamic chromatography (HDC), capillary electrophoresis (CE) and flow field flow fractionation (FFFF) techniques, mainly asymmetrical FFFF (AF4), has been found to offer great potential for determining and characterizing NPs in toxicological studies [12]. Several spICP-MS and ICP-MS-based methods for NPs assessment can be found in the literature [13–15], but applications focused on human biological fluids are scarce. The low concentration of NPs (basal levels) in biofluids, as well as he complexity of the sample, is a challenge in nanometrology, and robust and reliable sample pre-treatments and cleaning and/or preconcentration processes are needed. Developments have been mainly found for gold nanoparticles (Au NPs) in blood [16], blood serum and urine [17,18], and silver nanoparticles (AgNPs) in blood [16,17,19], blood plasma [20], and urine [21]. Other developments have been performed for assessing platinum nanoparticles (Pt NPs) in human urine and blood serum [22], TiO_2NPs in urine [21,23], and superparamagnetic iron oxide nanoparticles (SPIONs) [24] and carbon-coated iron carbide nanoparticles (C/Fe_3C NPs) [25] in simulated biological fluids.

Sample pre-treatment methods for isolating NPs from complex samples requires a soft environment for avoiding NPs degradation. Proposals for blood and blood serum have therefore consisted of using tetramethylammonium hydroxide (TMAH) at concentrations within the 1.0–5.0 % (v/v) range combined with 0.1 % (v/v) Triton X-100 [16,17,19,20,22] to digest the samples at room temperature [17,19] or at 4 ºC [22] for 24 h. On other occasions, TMAH at 0.1 % (v/v) combined with 0.1 % (v/v) Triton X-100 and 2.8 % (v/v) NH_4OH 2.8 % (w/w) was also used for pre-treating blood under controlled temperature (37 ºC) [20]. In addition, the analysis of blood and urine samples was conducted after dilution of the samples with a solution comprising ethylenediaminetetraacetic acid (EDTA), isopropyl alcohol, ammonia solution, and Triton-X-100 [18]. Direct dilution with 1.0 % (v/v) glycerol for AgNPs and TiO_2NPs assessment [21] and 0.1 % (v/v) nitric acid for TiO_2NPs [23] was also proposed for urine analysis.

Enzymes operate at mild temperatures and pH levels, promoting an extractive environment that ensures the integrity of the NPs. Combinations of pancreatin and lipase, as well as a multi-component enzyme mixture containing cellulose, hemicellulose and pectinase (Macerozyme R-10), have been proposed for isolating NPs from materials rich in proteins and fat such as seafood [26–29], and carbohydrates such as terrestrial plants and seaweed [30–32]. The aim of the current research has been the novel evaluation of enzymatic hydrolysis based on pancreatin and lipase mixtures for releasing TiO_2NPs from serum structures. The extraction conditions of moderate pH and temperature minimise the degradation of TiO_2NPs and the proposed sample pre-treatment may be useful for the extraction of other NPs that can be easily ionized. In addition, an additional step based on the centrifugal ultrafiltration (UF) has been originally used as a cleaning stage for removing degradation components from the enzymatic process. Characterization of TiO_2NPs (particle size distribution) and quantification (particle number concentration) have been finally performed by spICP-MS.

3.2 Materials and methods

3.2.1 Instrumentation

Determinations were performed with a NexIon 2000 triple quadrupole ICP-MS system with dynamic reaction cell (DRC) technology from PerkinElmer (Waltham, MA, USA). The instrument is equipped with a Single Cell Micro DX autosampler (PerkinElmer), concentric Meinhard nebulizer attached to a cyclonic spray chamber (Glass Expansion, Inc., Melbourne, Australia), quartz torch with a quartz injector tube (2.5 mm i.d.), and triple cone system (nickel sampler cone, skimmer cone and hyperskimmer cone). Automatic data acquisition/management was performed with PerkinElmer Syngistix™ Nano Application 2.5 version software. Enzymatic hydrolysis was performed with a Rotabit orbital- rocking platform shaker (J.P. Selecta, Barcelona, Spain) placed inside a Boxcult temperature-controlled incubation chamber (Stuart Scientific, Surrey, UK). A Laborcentrifugen 2K15 centrifuge (Sigma, Osterode, Germany) equipped with a 12072 fixed-angle rotor was used for centrifugal filtration by using Amicon Ultra-4 centrifugal filter units (regenerated cellulose, 30000 NMWL) from Millipore (Cork, Irland). The same centrifuge equipped with a 12139-H fixed-angle rotor was used for solid removal when preparing enzymes solution. A F200-CF (Jeol, Tokyo, Japan) coupled to a Jeol JED-2300T were used for high resolution transmission electron microscopy (HRTEM) and energy dispersive X-rays spectrometry (EDX) analysis, respectively. A Kunft KMW-4459 domestic microwave oven (Shenzhen, China), with a microwave power of 700 W and programmable for time, was used for pre-treating the enzymatic extracts before TEM analysis.

USC UNIVERSIDADE DE SANTIAGO DE COMPOSTELA

The poly(tetrafluoroethylene) (PTFE) bombs were laboratory-made with hermetically sealed and resulted adequate to work at low pressures.

Other pieces of equipment were a Basic20 pH-meter (Crison, Barcelona, Spain), a Raypa UCI–150 ultrasonic cleaner water-bath (ultrasound frequencies of 17 and 35 kHz, power 325 W) from R. Espinar S.L. (Barcelona, Spain), a Reax orbital vortex stirrer (Heidolph, Schwabach, Germany), and a BP1215 analytical balance (Sartorius, Barcelona, Spain).

3.2.2 Reagents

All solutions/suspension were prepared with ultrapure water 18 MΩ cm of resistivity obtained from an IQ 7003 Milli-Q purification device (Millipore Co., Bedford, MA, USA). In addition, all glassware and plasticware were washed with ultrapure water, kept in 10 % (v/v) nitric acid for 48 h, and fully rinsed with ultrapure water before use for avoiding metal contamination.

Nanoparticle stock suspensions were prepared from 100 nm TiO_2 (nanopowder, rutile, 99.9 %) from US Research Nanomaterials (Houston, TX, USA). Gold nanoparticles suspensions used for assessing transport efficiency was prepared from a N8151035 standard (nanoComposix, San Diego, CA, USA) consisted of Au NPs covered by PEG carboxyl in aqueous 1.0 mM citrate with a certified particle diameter of 49.6 ±2.1 nm, Au mass concentration of 12.4 ng mL^{-1}, and particle concentration of 9.89 $\times 10^6$ Au NPs mL^{-1}. Ionic titanium [$(NH_4)_2TiF_6$ 1000 mg L^{-1}] and ionic gold ($AuCl_4$, 1000 mg Au L^{-1}) standard solutions were from Merck (Darmstadt, Germany) whereas, a NexION Setup Solution of Be, Ce, Fe, In, Li, Mg, Pb, and U at 10 μg L^{-1} (used for instrument tunning) was from PerkinElmer (Waltham, MA, USA). The enzymatic solution was prepared from porcine pancreatin and lipase from *Candida rugose* (Sigma Aldrich, Osterode, Germany) and using a 0.2 M sodium dihydrogen phosphate (NaH_2PO_4) solution prepared from NaH_2PO_4 (Merck) and adjusting the pH to 7.4 using a 0.2 M sodium hydroxide (NaOH) solution prepared from NaOH (Merck). Diluted glycerol solutions (1 % (v/v)) were prepared from 99.5 % glycerol from Sigma Aldrich.

3.2.3 Human serum samples

Serum samples (30 samples of approximately 2.0 mL each from different patients) were supplied by the Central Laboratory at the Santiago de Compostela University Hospital Complex (CHUS) in compliance with the ethical criteria stablished by the centre regarding patient anonymity. Several pooled serum samples were prepared by combining four-five serum samples before freezing at –20 ºC. Each pooled serum sample ensures matrix homogeneity and the same basal TiO_2NPs content for further optimization experiments.

3.2.4 Enzyme mixture preparation

A solution containing 0.1 % (w/v) pancreatin and 0.1 % (w/v) lipase was prepared by dissolving/suspending the appropriate amounts of enzymes in a 0.2 M NaH_2PO_4 solution (pH adjusted at 7.4 with a 0.2 M NaOH solution). The mixture was further sonicated (35 kHz, 325 W) for 5.0 min to ensure enzymes dissolution. Pancreatin was found to be slightly soluble, and undissolved enzyme was removed by centrifugation (3900 rpm, 10 min) for preventing TiO_2NPs agglomeration as consequence of pancreatin slurries and avoiding obstruction of the ultrafiltration membrane. The dissolved portion of the enzyme's mixture was used for further experiments.

3.2.5 Enzymatic hydrolysis process

Serum samples (0.5 mL) were mixed with 4.0 mL of an enzyme's solution at 0.1 % (w/v) pancreatin and lipase each one (prepared in 0.2 M NaH_2PO_4, pH at 7.4 with 0.2 M NaOH) and subjected to orbital – horizontal shaking at 150 rpm and at 37 ºC for 4.0 h. Three replicates were performed for each set of conditions together with a reagent blank.

3.2.6 Centrifugal ultrafiltration process

The hydrolysed serum is charged into ultrafiltration tubes (30 kDa NMWL) and centrifugation at 3900 rpm (2364 g) and 20 ºC is performed for 40 min. This stage ensures TiO_2NPs retention whereas, hydrolysed serum components are removed by passing through the membrane. The concentrate in the filter container was recovered by placing the filter container upside down in a clean microcentrifuge tube and centrifuging at 3900 rpm (2364 g) and 20 ºC for 2 min. The recovered hydrolysed serum (around 50–100 µL) was further diluted to 2.0 mL and 1.0 mL with a glycerol solution at 1 % (v/v) for optimization and validation assays, respectively. The experimental workflow for the overall method (enzymatic hydrolysis and UF) is given in Fig. 30.

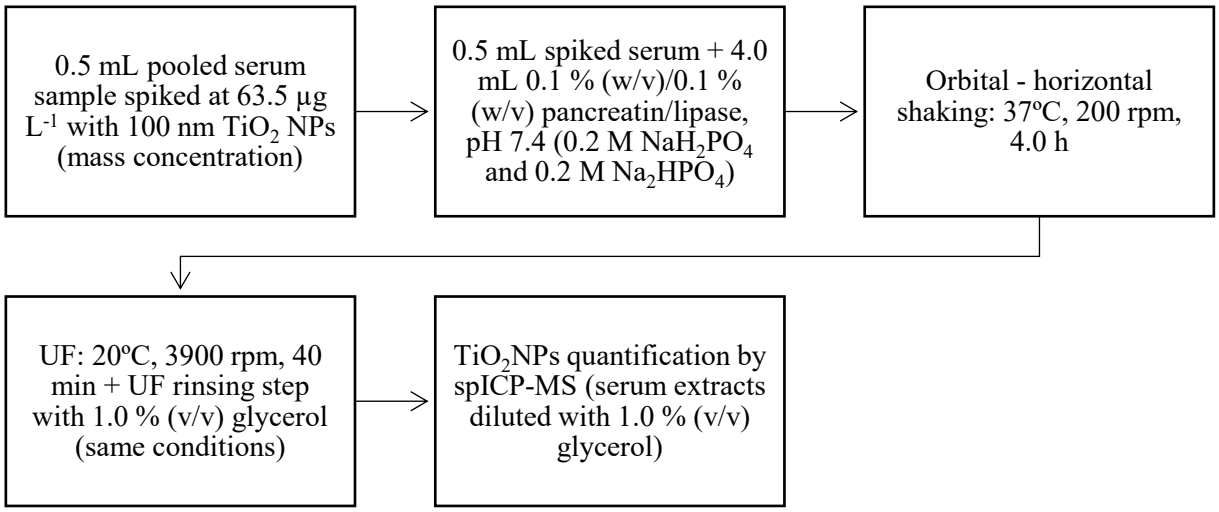

Figure 30. Schematic diagram of the experimental workflow followed.

3.2.7 Operating conditions for spICP-MS determination of TiO_2NPs

Daily performance of the ICP-MS instrument was assessed by monitoring Be, In, U, Ce (Ce++/Ce and CeO/Ce ratios) and background in accordance with ICP-MS manufacturer. Determinations were performed using ammonia (flow rate of 1.0 mL min^{-1}) as a reaction gas (Table 12) to monitor an ammonia cluster at m/z 131 ($^{48}Ti(NH)(NH_3)_4$) [33]. Therefore, the quadrupole ion deflector (axial field voltage, AFT at 350 V), RPa (high-mass cut-off) and RPq (low-mass cut-off) rejection parameters were fixed at optimised values (Table 12) for a better focusing of the mass-to-charge ratio of the ammonia adduct.

USC UNIVERSIDADE DE SANTIAGO DE COMPOSTELA

Table 12. Operating conditions for spICP-MS analysis.

Analyte (m/z)	Ti (131)
Density (g cm^{-3})	4.23
Mass Fraction	59.90 %
Sample Flow Rate (mL min^{-1})	0.18–0.21
Transport efficiency (%)	8.0–10
Dwell time (µs)	100
Mode	Dynamic Reaction Cell Technology
Ammonia flow rate (mL min^{-1})	0.75
Ion-product registered	$^{48}Ti(NH)(NH_3)_4$
Rejection parameter q	0.20
Quadrupole ion deflector (V)	Set for maximum ion transmission

The particle frequency method [34] was used for assessing the transport efficiency (% TE). Therefore, the sample flow rate (obtained values within the 0.19–0.21 mL min^{-1} range) was calculated by aspirating ultrapure water and weighing the solution before and after aspiration at the selected pump conditions). In addition, an aqueous ionic Au calibration (within the 0.5–10 µg L^{-1} range), and the measurement of an Au NPs suspension (9.89×10^4 particles mL^{-1}) were performed. Transport efficiency (% TE) values, directly calculated by PerkinElmer Syngistix™ Nano Application 2.5, were between 7.8 and 10.3 %.

Calibrations were performed using ultrapure water and covering dissolved (ionic) titanium concentrations of 2.5, 5.0, 10.0, 15.0, and 20.0 µgL^{-1}. The enzymatic digests were conveniently diluted with 1.0 % (v/v) glycerol (dilutions varied from 5 to 10), and solutions were subjected to ultrasounds (ultrasound water-bath, 37 kHz) for 2.0–3.0 min before spICP-MS measurements (operating conditions summarized in Table 1). TiO_2NPs particle number concentration and size distribution were directly obtained from PerkinElmer Syngistix™ Nano Application 2.5 considering the TiO_2 mass fraction of 59.90 % and TiO_2 density of 4.23 g cm^{-3} (Table 12) and by assuming a spherical nature of the TiO_2NPs.

3.2.8 High resolution transmission electronic microscopy and EDX analysis

The high organic matter content in the enzymatic extracts from serum samples impair the HRTEM-EDX analysis of extracts, and a procedure for removing organic matter is needed before analysis. Therefore, the enzymatic extracts from spiked serum samples were subjected to an oxidative procedure involving 33 % (v/v) hydrogen peroxide and microwave heating in accordance with Taboada-López *et al.* [27]. Then, the cleaned enzymatic digests (10 µL) were dropped onto a copper grid, wicked on filter paper, and air-dried at room temperature before HRTEM-EDX analysis.

Regarding 100 nm TiO_2NPs standard, a suspension at 250 mg L^{-1} (TiO_2NPs mass concentration) of the material was dispersed under ultrasound, and 10 µL were dropped onto a copper grid (also wicked on filter paper and air-dried at room temperature) before direct HRTEM-EDX measurement.

USC UNIVERSIDADE DE SANTIAGO DE COMPOSTELA

3.3 RESULTS AND DISCUSSION

3.3.1 Optimization of the enzymatic hydrolysis process

In addition to various substances such as nutrients, hormones and metabolic waste, the main components of serum are ions acting as electrolytes, proteins (including antibodies) and lipids (cholesterol) [35]. Therefore, a proteolytic enzyme (pancreatin) and lipase were selected to hydrolyse the serum matrix and release TiO_2NPs. Inherent variables affecting pancreatin and lipase activity, such as temperature and pH, were fixed at the optimum (recommended) values of 37 ºC and 7.4 for maximum hydrolysis efficiency. Ionic strength, another important parameter in enzymatic hydrolysis procedures, was settled by the concentration of the buffer's components used for fixing the pH (0.2 M NaH_2PO_4 and 0.2 M Na_2HPO_4). The effect of other variables that can influence the hydrolysis process, such as enzyme (pancreatin plus lipase) concentration, hydrolysis time, and shaking rate, have been conveniently studied. Since the direct serum analysis gave TiO_2NPs number concentrations lower than the limit of detection (LOD) of the method, spiked serum samples were used for optimization proposals. Spiking experiments have consisted of adding a convenient volume of a 100 nm TiO_2NPs suspension to pooled serum sample to achieve a spiked concentration of 63.5 μg L^{-1}. Then, 0.5 mL of the spiked serum samples were mixed with 4.0 mL of the enzymes solution (variable concentrations depending on the tested condition). Experiments were performed in triplicate.

Recovered TiO_2NPs contents used for discussing the optimization and validation assays (also TiO_2NPs contents displayed in plots) throughout this research were based on TiO_2 mass concentration instead of TiO_2 particle number concentration. A spherical shape of TiO_2NPs using the mean diameter of the particle size distribution (given by spICP-MS), and the TiO_2 particle number concentration (also given by spICP-MS) was assumed for obtaining TiO_2 mass concentrations (expressed as μg L^{-1}). The effect of TiO_2 agglomeration (changes on the mean sizes) is therefore minimised by considering TiO_2 mass concentrations rather than TiO_2 number concentrations. Finally, the cleaned extracts after UF were diluted to 2.0 mL with 1.0 % (v/v) glycerol.

An additional remark is referred to the size distribution of the 100 nm TiO_2NPs standard used in the current research. As it can be seen in the HRTEM image (Fig. 31 (a)), the material shows a high degree of agglomeration, and the right particle size assessment is quite difficult. Data obtained by applying the spICP-MS methodology (see next sections) will reveal most frequent sizes around 150 nm and mean sizes 160–180 nm. The EDX analysis (Fig. 31 (b)) shows the characteristic peaks at 4.50 keV (TiKa) and 5.0 keV (TiKb) which implies the presence of Ti.

Effect of the pancreatin/lipase concentration

A first set of experiments were conducted to select the amounts of enzymes (pancreatin and lipase) by preparing buffered solutions at pH 7.4 containing 0.100, 0.250, 0.375, and 0.500 % (w/v) of each enzyme. The mixtures (0.5 mL of serum and 4.0 mL of enzymes solution) were subjected to an orbital-horizontal shaking at 150 rpm and at 37 ºC for 14 h. After hydrolysis, the enzymatic digests were subjected to a UF step followed by with two UF rinsings stages with 1.0 % (v/v) glycerol. The retentate solution was recovered and diluted to 2.0 mL with 1.0 % (v/v) glycerol.

USC UNIVERSIDADE DE SANTIAGO DE COMPOSTELA

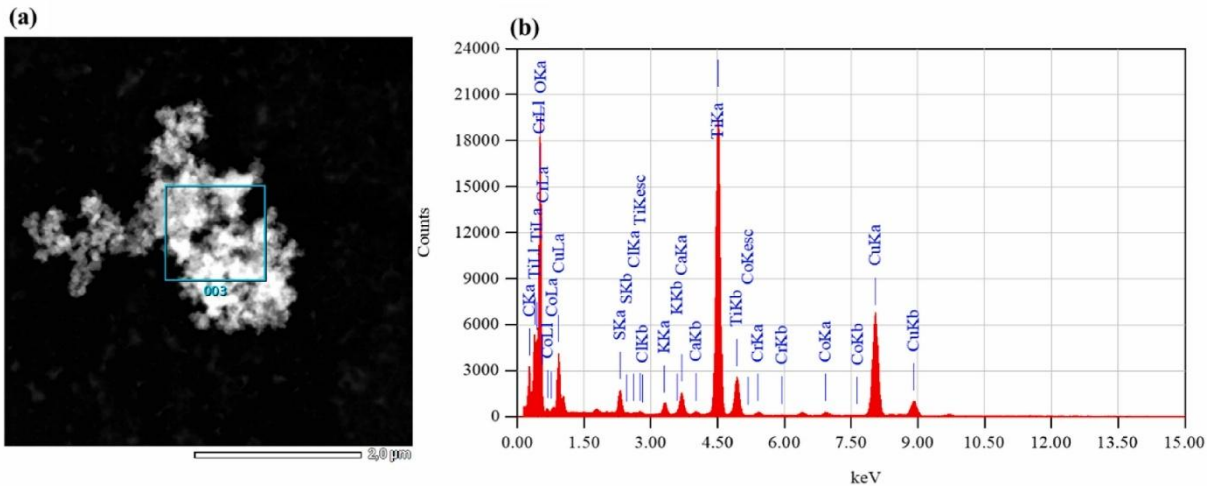

Figure 31. HRTEM image (a) and EDX spectrum showing Ti characteristics peaks at 4.5 keV (TiK_a) and 5.0 keV (TiK_b) (b) of a slurry containing 100 nm TiO_2NPs standard at 10 mg L^{-1} TiO_2NPs.

Results (mean TiO_2NPs mass concentration and mean size) of three replicates after blank subtraction are plotted in Fig. 32(a) and a gradual decreased on the TiO_2 mass concentration was obtained when increasing the enzymes concentration. In parallel, hydrolysis using high enzyme concentrations leads to a gradual increased on the measured sizes (Fig. 32(a)). These findings can be explained considering the agglomeration phenomena. Aggregation of TiO_2NPs has been reported to be affected by pH, ionic strength, and dissolved (inorganic and organic) compounds [36–38]. Elevated enzyme concentrations have been demonstrated to result in increased enzyme residue concentrations, a factor that has been hypothesized to promote the agglomeration of TiO_2NPs. In addition, the best results when using low extractant (enzyme) concentrations agree with previous papers regarding the use of low TMAH concentrations for TiO_2NPs extraction from seafood [39] and also for PtNPs, AuNPs and AgNPs from biofluids [16,17,19,20,22], as well as low enzyme concentrations for isolating TiO_2NPs and AgNPs from seafood [26–29,31,32]. Therefore, pancreatin and lipase concentration was fixed at 1.0 % (w/v), experiments which led to a TiO_2NPs mass concentration of 23.8 ± 1.7 TiO_2 µg L^{-1} (value quite lower than the TiO_2NPs mass concentration used for spiking experiments, 63.5 TiO_2 µg L^{-1}).

Effect of the hydrolysis time and the orbital-horizontal shaking rate

After fixing the concentration of pancreatin and lipase at 0.1 % (w/v), spiked serum samples were subjected to enzymatic hydrolysis (orbital-horizontal shaking at 150 rpm) for several times (from 1.0 to 14 h). Also, the enzymatic digest was subjected to UF and two UF rinsing stages (use of 1.0 % (v/v) glycerol). Fig. 32(b) shows that recovered TiO_2NPs remains constant for hydrolysis times higher than 4.0 h (TiO_2NPs mass concentrations of 26.0 ± 1.3, 24.0 ± 2.4, and 25.3 ± 2.2 TiO_2 µg L^{-1} for 4.0, 6.0, and 14.0 h, respectively). Therefore, a hydrolysis time of 4.0 h was selected.

USC UNIVERSIDADE DE SANTIAGO DE COMPOSTELA

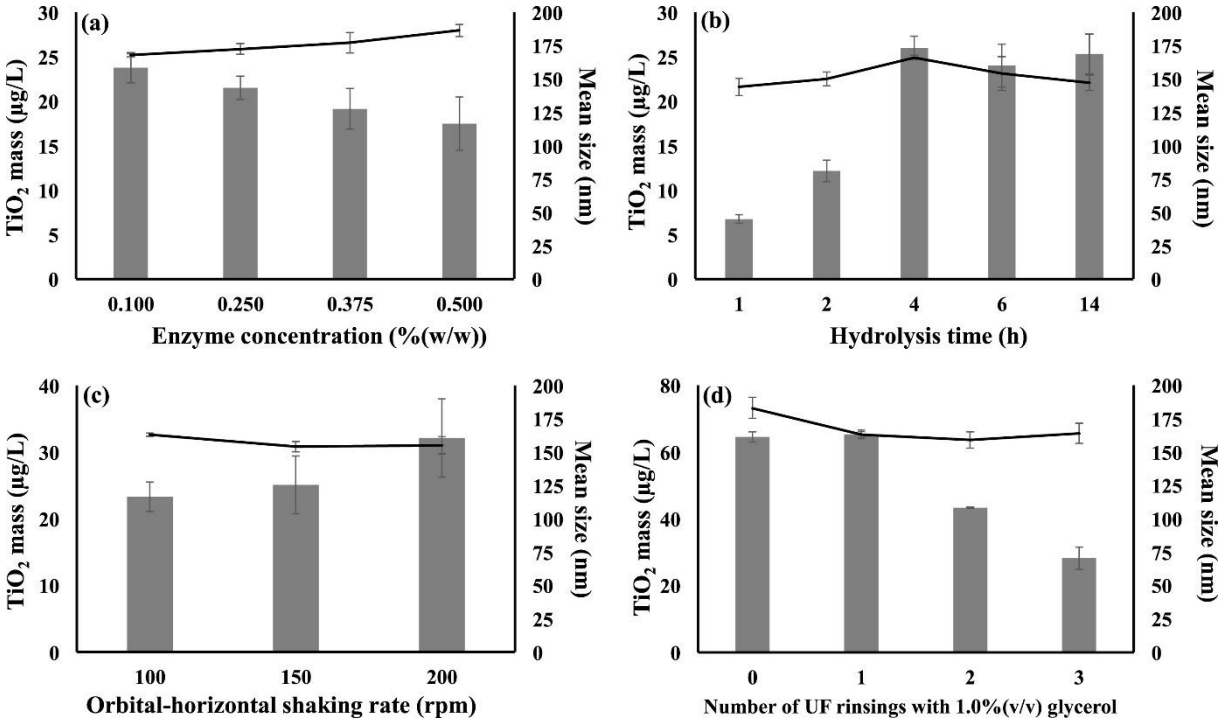

Figure 32. Effect of the enzyme (pancreatin plus lipase) concentration (a), hydrolysis time (b), orbital-horizontal shaking rate (c), and number of UF rinsings (d) on the TiO_2NPs mass concentration and mean size for serum samples spiked with 63.5 µg L^{-1} TiO_2NPs (n=9).

By fixing the hydrolysis time at 4.0 h and the enzymes amount (0.1 % (w/v)), the effect of the orbital-horizontal shaking rate was evaluated. An UF stage followed by two UF rinsings with 1.0 % (v/v) glycerol was performed in triplicate for spiked serum samples, and results after spICP-MS analysis are plotted in Fig. 32(c). The orbital-horizontal shaking rate was found to slightly increase the recovered TiO_2 NPs mass concentration up to 32.1 ± 1.9 TiO_2 µg L^{-1} when using the highest orbital-horizontal shaking rate tested (200 rpm). Furthermore, similar TiO_2NPs size distributions were observed in the 154–163 nm range as shown in Fig. 32(c). The slightly better increase on recovery could be attributed to better mixing at high shaking rates.

Effect of the number of UCF rinsings

After fixing the parameters involved in the enzymatic hydrolysis process, the effect of the number of 1.0 % (v/v) glycerol UF rinsings was evaluated. Fig. 32(d) shows that two successive rinses UF promotes TiO_2NPs losses, and the highest TiO_2NPs mass concentrations were achieved when omitting the 1.0 % (v/v) glycerol rinsing or at least when using only one glycerol UF rinsing (TiO_2NPs mass concentrations of 65.3 ± 1.3 TiO_2 µg L^{-1} for one UF rinsing and 64.5 ± 1.5 TiO_2 µg L^{-1} without UF rinsing). These findings suggest that TiO_2NPs losses can occur during the UF cleaning stage, and further investigations would be necessary to establish whether TiO_2NPs loss is due to retention by adsorption on the cut-off membrane and/or TiO_2NPs passage of NPs through the cut-off membrane.

Regarding TiO_2NPs size distribution, higher mean sizes (183 ± 8 nm) were achieved in absence of UF rinsings, whereas the mean values decrease within the 159–164 nm when performing the glycerol rinsings. Therefore, one UF rinsing with 1.0 % (v/v) glycerol was

USC DE COMPOSTELA

finally selected to clean the enzymatic extract and to diminish TiO_2NPs agglomeration since the presence of biomolecules residues.

3.3.2 Analytical performance

A preliminary study for % TE assessment was performed by preparing AuNPs slurries (9.89×10^4 parts mL^{-1}) in ultrapure water and in 0.1 % (w/v) pancreatin and 0.1 % (w/v) lipase. Values for % TE were found to be quite similar (9.18 ± 0.95 %, within the 7.77–10.30 % range, n = 9, for AuNPs slurries in ultrapure water, and 8.57 ± 0.77 %, within the 7.58–9.40 % range, n = 4, for AuNPs slurries in 0.1 % (w/v) pancreatin and 0.1 % (w/v) lipase).

Similarly, a comparison between calibration slopes and recovered TiO_2NPs when using ionic Ti calibrations in ultrapure water and in 0.1 % (w/v) pancreatin and 0.1 % (w/v) lipase was also tested. Ionic Ti concentration ranged from 2.5 to 20.0 μg L^{-1} (TiO_2NPs mass concentration) for all cases, and good linearity ($R^2 > 0.9947$) was observed. Calibration slopes of nine aqueous calibration curves and four matched enzymes (pancreatin plus lipase 0.1 % (w/v) each one) were 0.413 ± 0.0506, and 0.330 ± 0.082, respectively, which implies that aqueous Ti standards can be used for measurements. This fact has been verified after analysing by sextuplicate TiO_2NPs slurries at 127.0 μg L^{-1} (TiO_2NPs mass concentration) by using both calibration methods since measured/ recovered TiO_2NPs were 126.7 ± 3.5 μg L^{-1} for aqueous standards and 129.4 ± 3.4 μg L^{-1} for matched calibrations. Similarly to % TE, enzymatic digest composition, even at high enzyme concentrations as 0.1 % (w/v), and matrix effect can be considered negligible after diluting the enzymatic digests with 1.0 % (w/w) glycerol.

The limit of detection for particle size (LOD_{SIZE}) and particle number concentration (LOD_{NP}) was stablished in accordance with Laborda *et al.* [40] by considering the 5σ (5 × baseline standard deviation) criterion, which guarantees the avoidance of false positives (NP distributions partially overlapped with the background) [41]. Values of 36 nm and 5.70×10^3 particles mL^{-1} were obtained for LOD_{SIZE} and LOD_{NP}, respectively. The LOD_{size} after applying this criterion was quite close to the LOD_{SIZE} daily given by Syngistix™ Nano Application 2.5 version software (LOD_{size} within the 34–41 nm range).

The precision was studied with spiked serum samples at two different 100 nm TiO_2NPs mass concentrations (63.5 and 127.0 μg L^{-1}) which were subjected to the enzymatic hydrolysis and UF process in triplicate followed by spICP-MS analysis also in triplicate. Precision, expressed as the relative standard deviation (% RSD) for nine measurements, was 14 and 7 % for spiked samples at 63.5 and 127.0 μg L^{-1}, respectively.

Accuracy of the method was assessed through analytical recovery by spiking serum samples with 100 nm TiO_2NPs at 63.5 and 127.0 μg L^{-1} (spiking experiments in triplicate) and subjecting the spiked serum samples to the enzymatic hydrolysis and UF procedures. Replicated measurements (n = 3) of the un-spiked and spiked serum samples were used for calculating the analytical recovery in accordance with equation (1):

$$\%AR = \frac{[TiO_2\ NP]_{spiked} - [TiO_2\ NP]_{unspiked}}{[TiO_2\ NP]_{standard}} \times 100 \quad (1)$$

Where *[TiO₂ NP]spiked* is the TiO_2NPs concentration in the spiked serum (part mL^{-1}), *[TiO₂ NP]unspiked* is the TiO_2NPs concentration in the serum blank (part mL^{-1}), and *[TiO₂ NP]standard* is the TiO_2NPs concentration of the standard suspension used for spiking experiments.

USC
DE SANTIAGO
DE COMPOSTELA

It should be noted that un-spiked serum samples gave TiO_2 NPs mass concentrations lower than the LOD_{NP} of the method. Values, expressed as mean ± standard deviation, were 105 ± 11 % and 113 ± 8 % for spiked serum samples at 63.5 and 127.0 μg L^{-1}, respectively.

3.3.3 Applications

Four different serum samples were subjected to the optimised procedure in triplicate, but TiO_2NPs number concentrations were found to be lower than the LOD_{NP} of the method (5.70 × 10^3 particles mL^{-1}) for all cases. A further application was then performed by spiking in triplicate a serum sample with 100 nm TiO_2NPs (63.5 μg L^{-1}, TiO_2NPs mass concentration). Determinations by spICP-MS in triplicate were performed after enzymatic hydrolysis for 4.0 h and UF and without enzymatic hydrolysis (enzymes mixture was added but the serum samples were immediately subjected to UF – referred as time 0 h in Table 13). Determinations of TiO_2NPs were found to be improved after applying the enzymatic hydrolysis procedure (51.6 ± 5.2 μg L^{-1} without enzymatic hydrolysis and 61.1 ± 2.1 μg L^{-1} with enzymatic hydrolysis) which led to enhanced analytical recoveries (82 ± 8 % without enzymatic hydrolysis and 97 ± 3 % with enzymatic hydrolysis).

Regarding size distributions, TiO_2NPs sizes remained unchanged since the calculated most frequency size was 146 ± 15 and 146 ± 7 nm in absence and presence of enzymatic hydrolysis, respectively. However, a little difference has been observed in the mean sizes which varied from 169 ± 15 nm in absence of enzymatic hydrolysis to 180 ± 7 nm when applying the enzymatic process (Table 13). Since the most frequent sizes are smaller than the mean sizes, a positively skewed size distribution was observed (Fig. 33) and the most frequency size is preferable because it is unaffected by extreme outliers. Additionally, HRTEM images and EDX analysis for TiO_2NPs in spiked serum samples without enzymatic hydrolysis and with UF, and after enzymatic hydrolysis and UF are given in Fig. 34.

Table 13. TiO_2NPs mass concentration and mean size, and analytical recovery for a serum sample subjected to UF and to enzymatic hydrolysis (4.0 h) and UF.

	TiO_2NPs mass concentration (μg L^{-1})[a]	AR (%)[a,b]	TiO_2NPs mean size (nm)[a]
0 h	51.6 ± 5.16	82 ± 8	169 ± 11
4.0 h	61.1 ± 2.10	97 ± 3	180 ± 7

(a) n=3

(b) TiO_2NPs mass concentration added 63.0 μg L^{-1}

3.4 CONCLUSIONS

Enzymatic hydrolysis and UF have been found to be reliable sample pre-treatments for TiO_2NPs assessment in serum samples. The soft digestion of serum's components by the action of the pancreatin/lipase mixture allows an efficient TiO_2NPs release so that the extract can be easily analysed by spICP-MS after a previous UF cleaning stage. The mild pH and temperature conditions of enzymatic hydrolysis procedures are very promising for extracting other NPs which could be easily ionized. Therefore, the potential of enzymes as sample pre-treatment tools in nanometrology must be fully realised. Results have demonstrated that the tested UF conditions do not affect TiO_2NPs size distributions as well as TiO_2NPs mass concentrations. Although TiO_2NPs were undetected in the analysed serum samples, our findings show the

applicability of spICP-MS for TiO_2NPs determination/characterization after reliable sample pre-treatments that guarantee the integrity of the TiO_2NPs. Further research on developing pre-concentration methods is needed for assessing very low TiO_2NPs number concentration in biofluids. Therefore, the proposed method is a good option for future nanometrological applications in clinical samples.

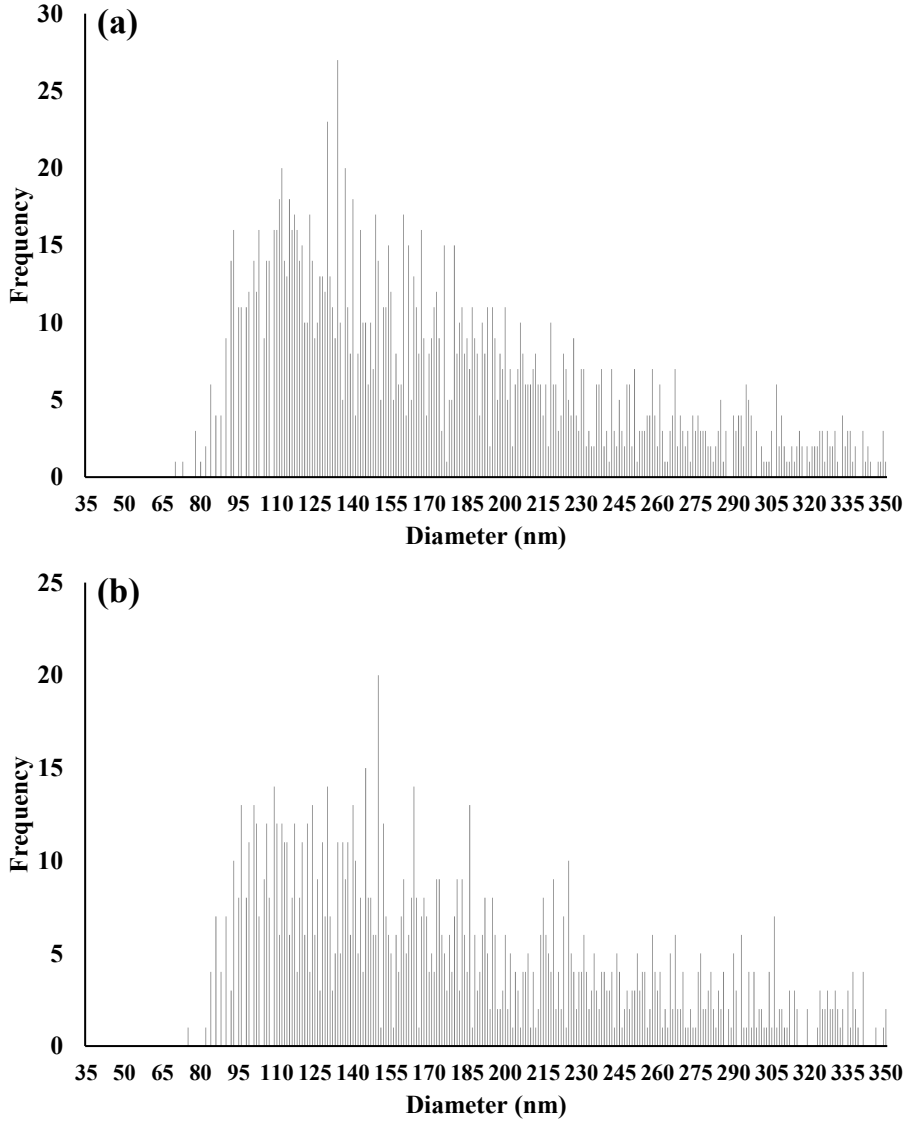

Figure 33. Histograms for TiO_2NPs size distribution in a spiked serum sample at 63.5 µg L^{-1} (TiO_2NPs mass concentration) without enzymatic hydrolysis and with UF (a) and after enzymatic hydrolysis and UF (b).

USC UNIVERSIDADE DE SANTIAGO DE COMPOSTELA

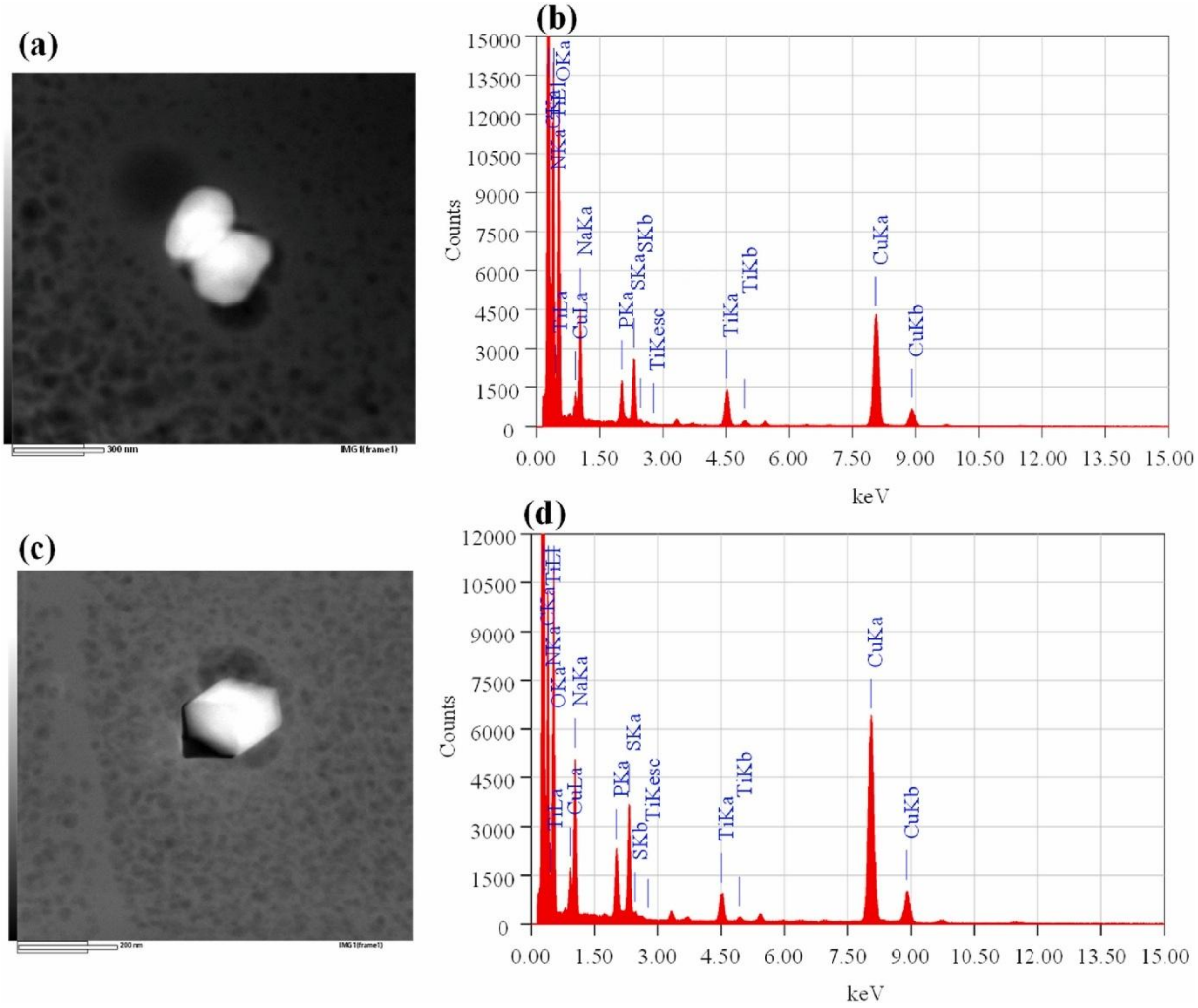

Figure 34. HRTEM image for spiked serum samples at 63.5 TiO_2NPs µg L^{-1} without enzymatic hydrolysis and with UF (a) and after enzymatic hydrolysis and UF (c) and EDX spectrum showing Ti characteristics peaks at 4.5 keV (TiK_a) and 5.0 keV (TiK_b) for spiked serum samples at 63.5 TiO_2NPs µg L^{-1} without enzymatic hydrolysis and with UF (b) and after enzymatic hydrolysis and UF (d).

3.5 Funding sources

Grant FOODNANORISK (reference PID2021-125276NB-I00) funded by MICIU/AEI/ 10.13039/501100011033 Spain. and Grupo de Refer encia Competitiva (reference ED431C 2022/029) funded by Consellería de Educación, ‘Ciencia, Universidades y Formacion Profesional’, Xunta de Galicia, Spain. A. J.-V. acknowledges Xunta de Galicia, Spain, for a pre doctoral grant.

3.6 Acknowledgements

The authors also wish to María José Pazos-Guldrís from Electronic and Confocal Microscopy and Support for Biological Specialities Unit at the University of Santiago de Compostela for HRTEM-EDX technical support.

USC UNIVERSIDADE DE SANTIAGO DE COMPOSTELA

3.7 REFERENCES

[1] M.E. Vance, T. Kuiken, E.P. Vejerano, S.P. Mcginnis Jr., M.F. Hochella, D. Rejeski, M.S. Hull, Nanotechnology in the real world: redeveloping the nanomaterial consumer products inventory, J. Nanotechnol. 6 (2015) 1769–1780, https://doi.org/10.3762/bjnano.6.181.

[2] European Food Safety Authority, Safety Assessment of Titanium Dioxide (E171) as a Food Additive, 2021, https://doi.org/10.2903/j.efsa.2021.6585, 01st May. (Accessed 15 March 2024).

[3] European Food Safety Authority, Titanium Dioxide: E171 No Longer Considered Safe when Used as a Food Additive, 2021, 1st May, https://www.efsa.europa.eu/en/news. (Accessed 15 March 2024).

[4] EFSA Scientific Committee, Guidance on risk assessment of nanomaterials to be applied in the food and feed chain: human and animal health, EFSA J. 19 (2021) 6768, https://doi.org/10.2903/j.efsa.2021.6768.

[5] M.V. Taboada-López, G. Vázquez-Expósito, R. González-Domínguez, P. Herbello-Hermelo, P. Bermejo-Barrera y A. Moreda-Piñeiro, Biopersistence rate of metallic nanoparticles in the gastro-intestinal human tract (stage 0 of the EFSA guidance for nanomaterials risk assessment), Food Chem. 360 (2021) 130002, https://doi.org/10.1016/j.foodchem.2021.130002.

[6] M. Ferrante, A. Grasso, G. Giuberti, M. Dall'Asta, E. Puglisi, G. Arena, A. Nicosia, M. Fiore, C. Copat, Behaviour and fate of Ag-NPs, TiO2-NPs and ZnO-NPs in the human gastrointestinal tract: biopersistence rate evaluation, Food Chem. Toxicol. 176 (2023) 113779, https://doi.org/10.1016/j.fct.2023.113779.

[7] E. Espada-Bernabé, G. Moreno-Martín, B. Gómez-Gómez, Y. Madrid, Assessing the behaviour of particulate/nanoparticulate form of E171 (TiO2) food additive in colored chocolate candies before and after in vitro oral ingestion by spICP-MS, TEM and cellular in vitro models, Food Chem. 432 (2024) 13720, https://doi.org/10.1016/j.foodchem.2023.137201.

[8] M. Hemmendinger, G. Squillacioti, T. Charreau, G. Garzaro, F. Ghelli, R. Bono, J.- J. Sauvain, G. Suarez, N.B. Hopf, P. Wild, A. Progiou, C. Fito, E. Bergamaschi, I. G. Canu, Occupational exposure to nanomaterials and biomarkers in exhaled air and urine: insights from the NanoExplore international cohort, Environ. Int. 179 (2023) 108157, https://doi.org/10.1016/j.envint.2023.108157.

[9] B. Bocca, B. Battistini, V. Leso, L. Fontana, S. Caimi, M. Fedele, I. Iavicoli, Occupational exposure to metal engineered nanoparticles: a Human biomonitoring pilot study involving Italian nanomaterial workers, Toxics 11 (2023) 120, https://doi.org/10.3390/toxics11020120.

[10] N. Hadrup, A.K. Sharma, Katrin Loeschner, Toxicity of silver ions, metallic silver, and silver nanoparticle materials after in vivo dermal and mucosal surface exposure: a review, Regul. Toxicol. Pharmacol. 98 (2018) 257–267, https://doi.org/10.1016/j.yrtph.2018.08.007.

USC UNIVERSIDADE DE SANTIAGO DE COMPOSTELA

[11] C. Contado, Nanomaterials in consumer products: a challenging analytical problem, Front. Chem. 3 (2015) 48, https://doi.org/10.3389/fchem.2015.00048.

[12] S. Fernández-Trujillo, M. Jim´enez-Moreno, N. Rodríguez-Fariñas, R.C. Rodríguez Martín-Doimeadios, Critical evaluation of the potential of ICP-MS-based systems in toxicological studies of metallic nanoparticles, Anal. Bioanal. Chem. 416 (2024) 2657–2676, https://doi.org/10.1007/s00216-024-05181-4.

[13] X. Tian, H. Jiang, L. Hu, M. Wang, W. Cui, J. Shi, G. Liu, Y. Yin, Y. Cai, G. Jiang, Simultaneous multi-element and multi-isotope detection in single-particle ICP-MS analysis: principles and applications, Trends Anal. Chem. 157 (2022) 116746, https://doi.org/10.1016/j.trac.2022.116746.

[14] D. Mozhayeva, C. Engelhard, A critical review of single particle inductively coupled plasma mass spectrometry – a step towards an ideal method for nanomaterial characterization, J. Anal. At. Spectrom. 35 (2020) 1740–1783, https://doi.org/10.1039/c9ja00206e.

[15] K. Loeschner, M.E. Johnson, A.R. Montoro Bustos, Application of single particle ICP-MS for the determination of inorganic nanoparticles in food additives and food: a short review, Nanomaterials 13 (2023) 2547, https://doi.org/10.3390/nano13182547.

[16] M. Witzler, F. Küllmer, K. Günther, Validating a Single-particle ICP-MS method to measure nanoparticles in human whole blood for nanotoxicology, Anal. Lett. 51 (2018) 587–599, https://doi.org/10.1080/00032719.2017.1327538.

[17] B. Bocca, B. Battistini, F. Petrucci, Silver and gold nanoparticles characterization by SP-ICP-MS and AF4-FFF-MALS-UV-ICP-MS in human samples used for biomonitoring, Talanta 220 (2020) 121404, https://doi.org/10.1016/j.talanta.2020.121404.

[18] M. Cabré, G. Fernández, E. Gonz´alez, J. Abellà, A. Verdaguer, Single particle ICP- MS: a tool for the characterization of gold nanoparticles in nanotheranostics applications, J. Anal. At. Spectrom. 39 (2024) 2508, https://doi.org/10.1039/d4ja00141a.

[19] I. Abad-Alvaro, D. Leite, D. Bartczak, S. Cuello-Nunez, B. Gomez-Gomez, Y. Madrid, M. Aramendia, M. Resano, H. Goenaga-Infante, An insight into the determination of size and number concentration of silver nanoparticles in blood using single particle ICP-MS (spICP-MS): feasibility of application to samples relevant to in vivo toxicology studies, J. Anal. At. Spectrom. 36 (2021) 1180, https://doi.org/10.1039/d1ja00068c.

[20] M. Roman, C. Rigo, H. Castillo-Michel, I. Munivrana, V. Vindigni, I. Mi˘ceti´c, F. Benetti, L. Manodori, W.R.L. Cairns, Hydrodynamic chromatography coupled to single-particle ICP-MS for the simultaneous characterization of AgNPs and determination of dissolved Ag in plasma and blood of burn patients, Anal. Bioanal. Chem. 408 (2016) 5109–5124, https://doi.org/10.1007/s00216-015-9014-6.

[21] K. Badalova, P. Herbello-Hermelo, P. Bermejo-Barrera, A. Moreda-Piñeiro, Possibilities of single particle—ICP-MS for determining/characterizing titanium dioxide and silver nanoparticles in human urine, J. Trace Elem. Med. Biol. 54 (2019) 55–61, https://doi.org/10.1016/j.jtemb.2019.04.003.

[22] S. Fernández-Trujillo, M. Jiménez-Moreno, Á. Ríos, R.C. Rodríguez Martín- Doimeadios, A simple analytical methodology for platinum nanoparticles control in complex clinical matrices via SP-ICP-MS, Talanta 231 (2021) 122370, https://doi.org/10.1016/j.talanta.2021.122370.

[23] S. Salou, D. Larivière, C.-M. Cirtiu, N. Fleury, Quantification of titanium dioxide nanoparticles in human urine by single-particle ICP-MS, Anal. Bioanal. Chem. 413 (2021) 171–181, https://doi.org/10.1007/s00216-020-02989-8.

[24] J. Kruszewska, J. Sikorski, J. Samsonowicz-G´orski, M. Matczuk, A CE-ICP-MS/MS method for the determination of superparamagnetic iron oxide nanoparticles under simulated physiological conditions, Anal. Bioanal. Chem. 412 (2020) 8145–8153, https://doi.org/10.1007/s00216-020-02948-3.

[25] K. Mehrabi, M. Dengler, I. Nilsson, M. Baumgartner, C.A. Mora, D. Günther, A. Gundlach-Graham, Detection of magnetic iron nanoparticles by single-particle ICP-TOFMS: case study for a magnetic filtration medical device, Anal. Bioanal. Chem. 414 (2022) 6743–6751, https://doi.org/10.1007/s00216-022-04234-w.

[26] M.V. Taboada-López, S. Iglesias-López, P. Herbello-Hermelo, P. Bermejo-Barrera, A. Moreda-Piñeiro, Ultrasound assisted enzymatic hydrolysis for isolating titanium dioxide nanoparticles from bivalve mollusk before sp-ICP-MS, Anal. Chim. Acta 1018 (2018) 16–25, https://doi.org/10.1016/j.aca.2018.02.075.

[27] M.V. Taboada-López, P. Herbello-Hermelo, R. Domínguez-Gonz´alez, P. Bermejo-Barrera, A. Moreda-Piñeiro, Enzymatic hydrolysis as a sample pre-treatment for titanium dioxide nanoparticles assessment in surimi (crab sticks) by single particle ICP-MS, Talanta 195 (2019) 23–32, https://doi.org/10.1016/j.talanta.2018.11.023.

[28] M.V. Taboada-López, N. Alonso-Seijo, P. Herbello-Hermelo, P. Bermejo-Barrera, A. Moreda-Piñeiro, Determination and characterization of silver nanoparticles in bivalve molluscs by ultrasound assisted enzymatic hydrolysis and sp-ICP-MS, Microchem. J. 148 (2019) 652–660, https://doi.org/10.1016/j.microc.2019.05.023.

[29] C. Suárez-Oubiña, P. Herbello-Hermelo, N. Mallo, M. Vázquez, S. Cabaleiro, R. Domínguez-Gonz´alez, A. Moreda-Piñeiro, P. Bermejo-Barrera, Bioaccumulation and human risk assessment of inorganic nanoparticles in aquaculture species, Environ. Sci. Nano 11 (2024) 2937–2947, https://doi.org/10.1039/D4EN00167B.

[30] Y. Dan, W. Zhang, R. Xue, X. Ma, C. Stephan, H. Shi, Characterization of gold nanoparticle uptake by tomato plants using enzymatic extraction followed by single-particle inductively coupled plasma-mass spectrometry analysis, Environ. Sci. Technol. 49 (2015) 3007–3014, https://doi.org/10.1021/es506179e.

[31] J.J. López-Mayán, B. Álvarez-Fernández, E. Peña-Vázquez, M.C. Barciela-Alonso, A. Moreda-Piñeiro, P. Bermejo-Barrera, Ultrasonication followed by enzymatic hydrolysis as a sample pre-treatment for the determination of Ag nanoparticles in edible seaweed by SP-ICP-MS, Talanta 247 (2022) 123556, https://doi.org/10.1016/j.talanta.2022.123556.

USC DE COMPOSTELA

[32] J.J. López-Mayán, B. Álvarez-Fernández, E. Peña-Vázquez, M.C. Barciela-Alonso, A. Moreda-Piñeiro, J. Maguire, M. Mackey, M. Quarato, I. Pinheiro, B. Espiña, L. Rodríguez-Lorenzo, P. Bermejo-Barrera, Bioaccumulation of titanium dioxide nanoparticles in green (*Ulva sp.*) and red (*Palmaria palmata*) seaweed, Microchim. Acta 190 (2023) 287, https://doi.org/10.1007/s00604-023-05849-1.

[33] C. Suárez-Oubiña, P. Herbello-Hermelo, P. Bermejo-Barrera, A. Moreda-Piñeiro, Single-particle inductively coupled plasma mass spectrometry using ammonia reaction gas as a reliable and free-interference determination of metallic nanoparticles, Talanta 242 (2022) 123286, https://doi.org/10.1016/j.talanta.2022.123286.

[34] H.E. Pace, N.J. Rogers, C. Jarolimek, V.A. Coleman, C.P. Higgins, J.F. Ranville, Determining transport efficiency for the purpose of counting and sizing nanoparticles via single particle inductively coupled plasma mass spectrometry, Anal. Chem. 83 (24) (2011) 9361–9369, https://doi.org/10.1021/ac201952t.

[35] A. Poletaev, Composition of the blood and reflection of the health state of human body, Biomed. Pharmacol. J. 11 (2018) 1797–1800, https://doi.org/10.13005/bpj/1551.

[36] V.R. Sharma, Aggregation and toxicity of titanium dioxide nanoparticles in aquatic environment—a Review, J. Environ. Sci. Health, Part A 44 (2009) 1485–1495, https://doi.org/10.1080/10934520903263231.

[37] G.E. Schaumann, A. Philippe, M. Bundschuh, G. Metreveli, S. Klitzke, D. Rakcheev, A. Grün, S.K. Kumahor, M. Kühn, T. Baumanng, F. Lang, W. Manz, R. Schulz, H.- J. Vogel, Understanding the fate and biological effects of Ag- and TiO2- nanoparticles in the environment: the quest for advanced analytics and interdisciplinary concepts, Sci. Total Environ. 535 (2015) 3–19, https://doi.org/10.1016/j.scitotenv.2014.10.035.

[38] F. Xu, Review of analytical studies on TiO2 nanoparticles and particle aggregation, coagulation, flocculation, sedimentation, stabilization, Chemosphere 212 (2018) 662–677, https://doi.org/10.1016/j.chemosphere.2018.08.108.

[39] J.J. López-Mayán, S. del-Ángel-Monroy, E. Peña-Vázquez, M.C. Barciela-Alonso, P. Bermejo-Barrera, A. Moreda-Piñeiro, Titanium dioxide nanoparticles assessment in seaweeds by single particle inductively coupled plasma – mass spectrometry, Talanta 236 (2022) 122856, https://doi.org/10.1016/j.talanta.2021.122856.

[40] F. Laborda, A.C. Gimenez-Ingalaturre, E. Bolea, J.R. Castillo, About detectability and limits of detection in single particle inductively coupled plasma mass spectrometry, Spectrochim. Acta, Part B 169 (2020) 105883, https://doi.org/10.1016/j.sab.2020.105883.

[41] F. Laborda, J. Jiménez-Lamana, E. Bolea, J.R. Castillo, Critical considerations for the determination of nanoparticle number concentrations, size and number size distributions by single particle ICP-MS, J. Anal. At. Spectrom. 28 (2013) 1220–1232, https://doi.org/10.1039/C3JA50100K.

USC UNIVERSIDADE DE SANTIAGO DE COMPOSTELA

CHAPTER 4. SILVER NANOPARTICLES BEHAVIOUR IN EXPOSED HUMAN RED BLOOD CELLS BY SINGLE CELL – INDUCTIVELY COUPLED PLASMA – MASS SPECTROMETRY

USC
UNIVERSIDADE DE SANTIAGO DE COMPOSTELA

CHAPTER 4. SILVER NANOPARTICLES BEHAVIOUR IN EXPOSED HUMAN RED BLOOD CELLS BY SINGLE CELL – INDUCTIVELY COUPLED PLASMA – MASS SPECTROMETRY

The results from this chapter have already been published as:

Ana Justo-Vega[1,2], Raquel Domínguez-González[1], Pilar Bermejo-Barrera[1], Antonio Moreda-Piñeiro[1], and Javier Jiménez-Lamana[2]

[1]Group of Trace Elements, Spectroscopy and Speciation (GETEE), Institute of Materials iMATUS, Department of Analytical Chemistry, Nutrition and Bromatology, Faculty of Chemistry, Universidade de Santiago de Compostela, Avenida das Ciencias, s/n., 15782, Santiago de Compostela, Spain.
[2]Université de Pau et des Pays de l'Adour, E2S UPPA, CNRS, Institut des Sciences Analytiques et de Physico-Chimie pour l'Environnement et les Matériaux (IPREM), UMR5254, Hélioparc, Pau 64053, France

Talanta, 2026, ***298****, 128972*
(DOI: 10.1016/j.talanta.2025.128972)

GRAPHICAL ABSTRACT

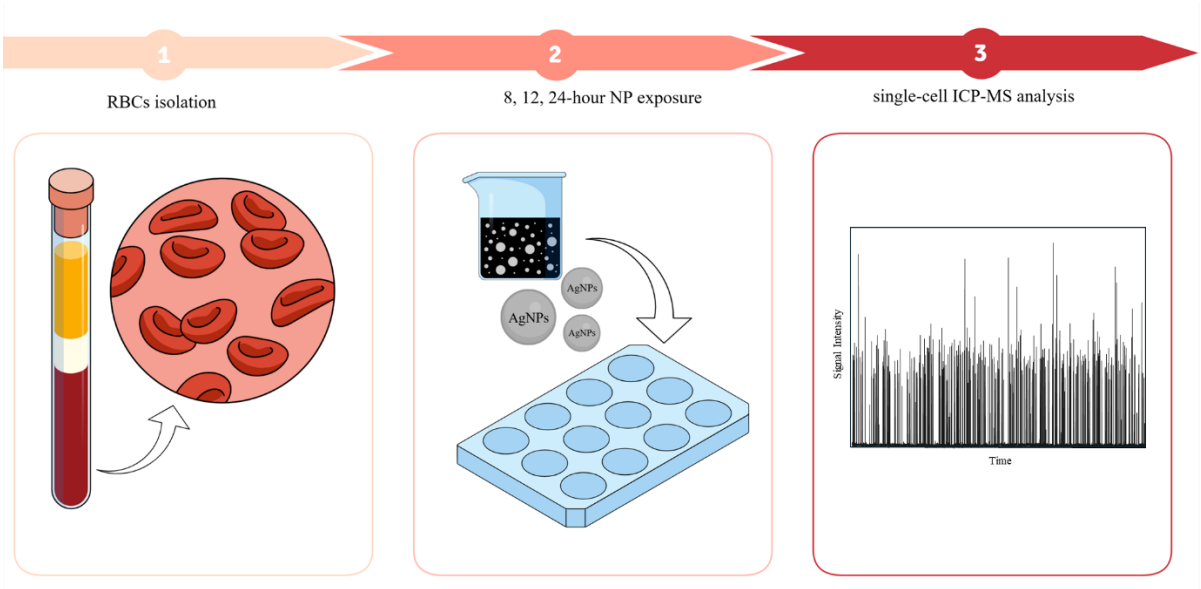

ABSTRACT

Research concerning nanoparticles, NPs, at the single cell level is at the forefront of recent investigations. With the widespread use of silver nanoparticles (AgNPs) in fields like nanomedicine and nanobiotechnology, human exposure has increased. Investigating cellular

response to NP exposure in terms of NPs distribution within a cell population is essential. In this sense, single cell (SC)-ICP-MS is a powerful and promising technique that provides quantitative information on a cell-to-cell basis. The present work, in a proof-of-principle experiment, investigates the feasibility of SC-ICP-MS for the determination of surface-adsorbed and intracellular AgNPs in exposed human red blood cells (RBCs). Firstly, RBCs were isolated from whole blood and subsequently incubated with AgNPs suspensions. The exposure was conducted at two dosing concentrations in a low cell:NP ratio of 1:1, and a higher cell:NP ratio of 1:50, for 8, 12, and 24 hours. Results showed that the low AgNPs dose concentration had a negligible effect on the uptake by cells, whereas higher doses exhibited a time-dependent uptake. Under specific conditions, the quantification yielded an estimate of 3 AgNPs cell^{-1} after 8 hours of exposure, 5 AgNPs cell^{-1} after 12 hours of exposure, and 8 AgNPs cell^{-1} after 24 hours of exposure. SC-ICP-MS methodology proved to be an excellent tool to track and confirm the presence of AgNPs-containing cells.

Keywords: silver nanoparticles, single cell ICP-MS, red blood cells, erythrocytes, human biomonitoring

4.1 INTRODUCTION

Nanoparticles (NPs) are encountered in a large variety of personal care products, including cosmetics, deodorants, toothpastes, lip balms, and suncreams, as well as in textiles, food items, and pharmaceuticals [1–4]. Moreover, the fields of nanomedicine and nanobiotechnology are gaining special attention [5–7]. Silver nanoparticles (AgNPs) stand out for their antimicrobial and antiviral properties, chemical stability, catalytic activity, and good conductivity, reason why they have been widely used for biomedical device coatings and drug delivery [8,9]. The use of NPs in areas closely connected to our daily lives is growing, and thus human exposure is increasing likewise. To date, the real impact of NPs on human health has not been fully elucidated yet. However, there is growing evidence reporting toxic effects of AgNPs at the cellular level [10–12], even though it is important to determine whether in vitro results translate to *in vivo* human toxicity. Munger *et al.* [13] reported no clinically significant changes in metabolic, hematologic, urine measures, physical findings, or imaging morphology after nanoscale silver ingestion in a human *in vivo* exposure design.

Red blood cells (RBCs), or erythrocytes, constitute the primary cells in the human circulatory system, representing 40 to 45 % of the whole blood volume (hematocrit value) [14]. Non-nucleated cells with discoid shape and a 120-day lifespan [15], human RBCs are known as transporters of oxygen and carbon dioxide. However, they are also involved in tissue protection and regulation of cardiovascular homeostasis, among other essential biological functions [16–19]. Chemical composition of RBCs is about 64 % water, 33 % hemoglobin, and 3 % erythrocyte stroma (proteins, lipids, enzymes, and inorganic salts – Na, K, Cu, Fe, and Zn).

After exposure to NPs, the cells will interact and behave differently showing great heterogeneity. NPs are suspected to induce cytotoxicity, oxidative stress, cellular proliferation or differentiation, and even apoptosis in some cases within a biological environment [8,20]. The NP-cell interaction mechanisms are still lacking, and hence, a better understanding is needed. Traditionally, the methods used for the analysis of cell populations rely on providing average information over a large number of cells after lysis, extraction, or acid-digestion, and the cell-to-cell variations have been neglected so far. However, it is widely accepted that even cells with the same genotype may exhibit different responses to the same environmental stimuli.

USC UNIVERSIDADE DE SANTIAGO DE COMPOSTELA

Therefore, the study of NP uptake by single cells is crucial and analytical techniques that allow for the discrimination of individual cells are of meaningful interest.

Various analytical methods for quantitative and imaging analysis of single cells have been used to the moment [21–23], such as inductively coupled plasma atomic emission spectrometry (ICP-AES) [24,25], X-ray fluorescence [26], transmission electron microscopy (TEM), nanoSIMS [27] and several ICP-MS-based techniques including LA-ICP-MS [28–30], mass cytometry, or microfluidic injection (μFI) ICP-MS [31]. More recently, single cell (SC) ICP-MS is receiving considerable attention [32,33]. The principles and theoretical basis supporting the technique can be conceptually derived from the consolidated single particle (sp)ICP-MS [34–37]. When a cell suspension is introduced into the plasma, each individual cell is vaporized, atomized, and ionized producing and ion plume that will be detected as a discrete event (cell event). Unlike homogeneous solutions that produce a constant signal throughout readings, the individual cells will cause a spike in the signal intensity. Once the dwell time selected is appropriate and the cell suspension introduced is sufficiently diluted, it may be presumed that each cell event signal corresponds to only one individual cell. In this case, the signal frequency is proportional to cell concentration, and the signal intensity is proportional to the mass of the element in each cell. Thus, SC-ICP-MS provides information about concentration of cells containing specific analytes, mass of the analyte per cell, and mass distribution within a cell population [38–40]. Ever since the pioneering work published by Li *et al.* in 2005 [41], SC-ICP-MS has been applied to the analysis of different NPs in numerous bioparticles such as cells, bacteria [42], microalgae [43] or yeasts [44,45]. So far, only a few studies have been devoted to AgNPs. López-Serrano *et al.* [46] evaluated the uptake of 50 nm AgNPs by human THP-1 monocytes, Rasmussen *et al.* [38] studied the AgNPs and yeast cell interactions, Suárez-Oubiña *et al.* [47] assessed the association of PVP-AgNPs in cell lines derived from aquaculture species, and more recently, Gimenez-Ingalaturre *et al.* [44] performed quantitative biodistribution studies on bacteria (E. Coli) exposed to Ag (I) and 10 nm AgNPs.

Although SC-ICP-MS shows promising potential in numerous applications, the technique possesses some shortcomings: (i) conventional sample introduction systems are not suitable for cells and led to extremely low transport efficiencies, (ii) inability to differentiate between internalized analytes and analytes retained at the cell membrane. So far, a great deal of effort has been made to overcome these limitations, and the scientific community is focused on contributing to the development of single-cell analysis. For example, new cell introductions systems based on total consumption spray chambers and very flow rates in order to preserve the cell intact have been recently developed.

The aim of the present work is the application of SC-ICP-MS to quantitatively measure intracellular and/or membrane adsorbed AgNPs in exposed human RBCs. Moreover, the extent to which the dosage level and exposure time influence the NP-cell interplay has been investigated. To the best of the author's knowledge, this is the first study to examine AgNPs and RBCs interactions following an analytical methodology based on SC-ICP-MS.

4.2 EXPERIMENTAL

4.2.1 Instrumentation

Single-cell analysis have been performed using a NexION 5000 multi-quadrupole-based inductively coupled plasma mass spectrometer (PerkinElmer, Waltham, MA). The instrument was equipped with a Single Cell Micro DX autosampler module, a microflow high-efficiency Meinhard Cytoneb nebulizer with PFA gas line, and an AsperonTM spray chamber

USC UNIVERSIDADE DE SANTIAGO DE COMPOSTELA

(PerkinElmer). Data acquisition was performed using the Syngistix™ Single Cell Application Software version 2.5 (Perkin Elmer).

Cell exposure assays were carried out in a Memmert INCO108 incubator (Memmert, Schwabach, Germany). A Teslar BIO-II-A/P Class II microbiological safety cabinet was used for cell manipulation and handling. Cell counting was performed in a Neubauer chamber bright-line (Brand, Wertheim, Germany) and with a Nikon Eclipse TS100 optical microscope equipped with a digital camera DXM1200 (Nikon Instruments Inc., New York, NY). A Heraeus Megafuge 1.0R and 5415R (Eppendorf, Hamburg, Germany) centrifuges were used. Additional instrumentation for the analysis included a Mettler Toledo ML204/01 analytical balance (Columbus, OH), a USC-TH ultrasonic water bath (45 Hz, 80 W) from VWR International Eurolab (Barcelona, Spain) for dispersing the NP standards before use, and an U101 Innova ultra-low freezer from New Brunswick Scientific (Edison, NJ).

4.2.2 Reagents and consumables

Diluted solutions/suspensions were prepared in ultrapure water (18.2 MΩ cm^{-1} resistivity) obtained from a Milli-Q® IQ 7003 purification system (Millipore Co., Bedford). A 50 nm gold nanospheres suspension (Nanocomposix, San Diego, CA), 9.89×10^{6} particles mL^{-1} (obtained by spICP-MS), 49.6±2.1 nm (TEM diameter), PEG carboxyl particle surface, suspended in aqueous 1 mM citrate, was employed to determine the transport efficiency (% TE). Mono-elemental standards of ionic gold and silver (1000 µg mL^{-1}, in 2 % HNO_3) from SCP Science (Québec, Canada) were employed for calibration purposes. NP suspension containing 40-nm AgNPs (5.4×10^{10} particles mL^{-1} obtained by spICP-MS, nominal diameter 41 ± 5 nm obtained by TEM, and a mass concentration of 0.021 mg mL^{-1}) was used for cell exposure. NP suspension containing 20-nm AgNPs (5.2×10^{11} particles mL^{-1} obtained by spICP-MS, nominal diameter 19.9 ± 2.8 nm obtained by TEM, and a mass concentration of 0.022 mg mL^{-1}) was used for feasibility studies. Glutaraldehyde solution, Grade II, 25 % in ultrapure water, osmium tetroxide solution, and sodium cacodylate buffer were purchased from Sigma-Aldrich (St. Louis, MO). In addition, sterile fetal bovine serum (FBS), and sterile-filtered dimethyl sulfoxide (DMSO, ≥ 99.7 %) as cell freezing solution, were also from Sigma-Aldrich. Phosphate buffered saline solution (1X) pH 7.4, was purchased from Life Technologies Limited (Paisley, UK). Eponate was from Ted Pella (Redding, CA). Nitric acid (69 %, ppb-trace analysis grade) was purchased from Scharlab (Barcelona, Spain), and 30 % hydrogen peroxide (analytical reagent grade) was purchased from Fisher Scientific (Loughborough, UK). NexION Setup solution containing 200 ng L^{-1} Be, Ce, Fe, In, Li, Mg, Pb, U in 1 % HNO_3 was obtained from PerkinElmer. BioLite 12 well multidish from Thermo Fisher Scientific (Rochester, NY) were used for cell exposure.

4.2.3 Red Blood Cells Sample Collection and Isolation Protocol

Human blood samples were provided by the Central Laboratory at University Clinical Hospital of Santiago de Compostela (CHUS). All samples were collected from healthy volunteers in accordance with the centre's ethical criteria with regard to patient anonymity. Blood was sampled with EDTA additive to prevent coagulation, and a pool sample was prepared mixing ten to twelve individuals' blood to ensure matrix homogeneity and representativeness.

USC UNIVERSIDADE DE SANTIAGO DE COMPOSTELA

The RBCs isolation procedure involved mixing 1500 µL of fresh blood (from the pool sample), 1500 µL of 1.0 % PBS, and 9.0 mL of 2.5 % glutaraldehyde (prepared in 1.0 % PBS). In a horizontal shaker, the mixture was steadily stirred for 1 hour at 200 rpm and 37 ºC. The treated samples were then centrifuged (1200 rpm, 23 ºC) for 4 minutes to discard the supernatant (plasma and other blood components). The cell pellets were rinsed three times with 10 mL of 1.0 % PBS (under the same centrifugation conditions) before being suspended in 10 mL of 1.0 % PBS. Finally, RBCs concentration was assessed using a Neubauer chamber and a Nikon Eclipse TS100 optical microscope.

4.2.4 Red Blood Cells Exposure Protocol

For the exposure assay the BioLite 12 well multidish were used. The exposure concentration was selected at two levels: one low-concentrated level in a ratio close to 1:1 (cell/NP ratio), and one high-concentrated level in a ratio close to 1:50 (cell/NP ratio). The AgNPs suspension was sonicated before addition to avoid aggregation. RBCs were exposed to AgNPs for 8, 12 and 24 hours at 39 ºC, 94.5 % relative humidity, and 5.0 % CO_2. Control samples (RBCs not exposed to AgNPs) followed the same experimental conditions. All experiments were performed in triplicate. After incubation, all cell cultures were centrifugated (400 g, 4 min, room temperature) and the cell pellets collected and washed twice with 1.0 % PBS under the same centrifugation conditions to remove free-floating AgNPs in the media. In the case of *4.3.1 Feasibility studies,* supernatants from the first and second centrifugation were also analyzed. The final cell pellets were resuspended in freezing solution (90 % FBS/10 % DMSO) and kept at -80 ºC until analysis.

4.2.5 Single-cell ICP-Ms analysis

RBCs obtained from AgNPs exposure experiments were analyzed by SC-ICP-MS. Daily instrument performance for optimal analysis was performed according to the following criteria: Be intensity > 2500 counts s^{-1}, In intensity > 40,000 counts s-1, U intensity > 30,000 counts s^{-1}, background intensity ≤ 3, Ce++/Ce ratio ≤ 0.05, and CeO/Ce ratio ≤ 0.04. Operating conditions and data acquisition parameters are listed in Table 14. Standard mode was used for the measurement of silver. Right before analysis, all samples were thawed and diluted with 1.0 % PBS.

Table 14. Instrumental conditions and data acquisition parameters for SC-ICP-MS analysis.

Parameter (units)	Value
RF Power (W)	1600
Plasma gas flow rate (L min^{-1})	16.0
Make up gas flow rate (L min^{-1})	0.70
Auxiliary gas flow rate (L min^{-1})	1.20
Nebulizer gas flow rate (L min^{-1})	0.35
Sample flow rate (µL min^{-1})	10.0
Sample loop (µL)	100
Mode	Standard
Scan Time (s)	100
Dwell Time (µs)	100
Analyte (m/z)	Ag (107)
Density (g cm^{-3})	10.49
Mass Fraction (%)	100

USC UNIVERSIDADE DE SANTIAGO DE COMPOSTELA

Transport Efficiency

Compared to NPs, cells are larger, heterogeneous and more fragile entities. In this context, the conventional sample introduction systems led to very poor transport efficiencies as traditional spray chambers were designed to filter and remove larger particles. To overcome this limitation, and to ensure intact transportation of cells into the plasma, new high-efficiency low-flow nebulizers and spray chambers are marketed. In this work, an Asperon™ spray chamber and a low-flow nebulizer (10 µL min^{-1}) were employed to introduce diluted RBCs into the plasma. This system allowed the analysis of RBCs with an approximate mean diameter of 7.5 µm avoiding clogging and blockages. Since certified bioparticle standards are not yet available, strategies based on spICP-MS for transport efficiency calculation were followed. The % TE, obtained by analyzing 50-nm Au NPs suspensions at 1.00×10^8 Parts L^{-1} following the particle frequency method [48], was found to be within the 28.9-34.9 % range (31.3 % average TE).

Calibration

The calibration strategy involved the use of dissolved mono-elemental standards at concentrations 0, 2, 4, and 10 µg L^{-1} prepared in ultrapure water. The R-squares obtained for all calibration curves were above 0.996 in every case. The mass of silver present in red blood cells was calculated using *Equation 1* [49]:

$$m = \frac{\varepsilon \times Q \times t_{dwell} \times (I - I_{bkg})}{s} \qquad (1)$$

Where m is the mass of the element, ε is the transport efficiency, Q is the sample uptake rate, t_{dwell} is the selected dwell time, I and I_{bkg} are the analyte and background signal intensities, respectively, and s is the slope of the calibration curve.

Data processing

The data acquisition and collection were performed using the Syngistix™ Single Cell Application Software Module. Raw data was extracted and processed afterwards using Excel software (Microsoft, Washington) and SPCal version 1.1.6, an open-source Python-based processing platform for single particle and single cell ICP-MS [50]. Description of mathematical operations for signal filtering, processing and calibration of the software is available.

Processing SC-ICP-MS data follows the same principles as spICP-MS, i.e. discrimination between analyte events (AgNPs containing RBCs in the case of this study) and the baseline produced by the background is the first step in data evaluation. If the dissolved and NP distributions are fully resolved, the former one exhibits a Poisson profile, whereas the latter one tends to follow a log-normal distribution [35,51]. Ideally, the threshold (Y_C) should ensure an accurate discrimination between the two distributions. However, the selection of a certain threshold brings with it a certain probability α that an event is falsely detected as a particle or, in this case, as a cell. The threshold, or critical value, can be represented as follows:

$$Y_C = Y_B + k\sigma_B \qquad (2)$$

USC UNIVERSIDADE DE SANTIAGO DE COMPOSTELA

Where Y_B represents the mean baseline signal and σ_B its standard deviation, and k represents the (1- α) quantile of the standard normal distribution. As the counting of particle events is governed by Poisson statistics, it can be assumed that $\sigma_B = \sqrt{Y_B}$, and Equation (2) can be transformed into Equation (3) [51]:

$$Y_C = Y_B + k\sqrt{Y_B} \quad (3)$$

Using the Syngistix Single Cell software, the selection of the threshold is automatic and there is limited disclosure regarding information related to the mathematical calculations followed to obtain it. However, SPCal offers an advantage in this respect thanks to its multiple threshold selection options, which makes the application of a given threshold more transparent. All data curation and processing using SPCal software was conducted following a Poisson detection threshold method (α (Type I) = 0.001) as discrimination between cell events and baseline.

4.2.6 Preparation of RBCs sections for TEM analysis

The cell pellets obtained were fixed with 500 µL of 1.5 % (w/v) glutaraldehyde, embedded in an agar pellet, and fixed again with 1 % (w/v) osmium tetroxide in a 0.1 M sodium cacodylate buffer solution. Finally, an epoxy resin (eponate) was added to form a pellet, and cell sections were obtained using an ultramicrotome. The cell sections were analysed by TEM.

4.3 RESULTS AND DISCUSSION

In this study, SC-ICP-MS has been employed to perform AgNPs uptake profiling on individual RBCs. The uptake, accumulation, and association of AgNPs with RBC were investigated and information regarding the occurrence of RBCs containing silver, the mass per cell distributions, and the total silver concentration accumulated was obtained.

4.3.1 Feasibility studies

On a first approach, the potential uptake of AgNPs by RBCs was evaluated. Cells (4.8×10^{11} cells L^{-1}) were dosed with 20 nm-AgNPs at a cell-to-NP concentration ratio of 1:50 (2.4×10^{13} NPs L^{-1} initial concentration) for 8, 12, and 24 hours. Experiments were all performed in triplicate.

Table 15 shows the number of events detected (RBCs containing AgNPs), the mean signal intensity in counts, the median mass (ag), and the calculated number concentration (L^{-1}) for the RBCs exposed to AgNPs. The overall observation is that the standard deviations are consistently high in all cases, which would be evidence of the heterogeneous nature of the cell population. Moreover, distributions obtained (data not shown) are non-symmetrical and right-skewed with median or mode (most frequent value) mass values lower than the mean mass obtained. In such cases, where positively skewed distributions are observed, the median is generally the most representative measure of central tendency. Based on these results, the amount of silver in the RBCs was determined.

USC UNIVERSIDADE DE SANTIAGO DE COMPOSTELA

Table 15. Detected events, mean signal, median mass and number concentration of RBCs containing AgNPs (number concentration referred to the ICP-MS). Values expressed as mean ± standard deviation (n=6).

Sample	Detected events	Mean signal (counts)	Median mass (ag)	Number concentration (L^{-1})
8h	554 ± 161	104.3 ± 39.4	228.7 ±19.0	$9.24 \pm 2.69 \times 10^7$
12h	1643 ± 680	115.2 ± 6.6	246.9 ± 11.2	$2.74 \pm 1.13 \times 10^8$
24h	1725 ± 468	156.8 ± 14.2	253.9 ± 31.6	$2.87 \pm 0.78 \times 10^8$

Table 18 (supplementary information) illustrates the AgNPs concentration in terms of silver mass for 8, 12, and 24 h of incubation. An increase in the assimilation of AgNP by the cells is observed with increasing exposure time from 8 to 12 h. However, no further increase is observed from 12 to 24 h. The same trend was observed for the number of RBCs containing AgNPs (detected events, Table 15). This might indicate that most of the assimilation would occur in the period between 8 and 12 h suggesting a rapid uptake rate, or that cells gradually eliminate NPs over prolonged exposure. Moreover, the 12-hour and 24-hour exposure experiments exhibit larger standard deviations, suggesting that NP assimilation occurs unevenly across the cell population and that cell-to-cell variability is a significant factor to consider. The silver concentration derived from mean mass values is comparatively higher than that based on median mass values. As previously mentioned, the distribution obtained is right-tailed and the median would generate more representative results.

Additionally, the quantification of silver in the first and second supernatants (collected from the first and second centrifugations after incubation) was performed. Figure 40 (supplementary information) illustrates the silver concentration (sum of both supernatants) after 8, 12, and 24 h of exposure. As the uptake of AgNPs by RBCs increases with increasing exposure time, the concentration in the supernatant decreases as time increases, obtaining silver concentrations of 4.70 ± 0.01, 2.58 ± 0.01, and 1.37 ± 0.01 μg L^{-1} for 8, 12, and 24 hours respectively. Figure 41 A-D (supplementary information) shows the time resolved ICP-MS profiles for a RBCs sample incubated with 20-nm AgNPs, ratio 1:50 cell/NP, for 24 h (A), along with the corresponding control (B), first (C), and second (D) supernatants. A higher dissolved silver concentration, and consequently a higher background, was observed during supernatant (Figure 41 C and D) analysis, suggesting that cells may play a crucial role in NP stabilization and that significant AgNP dissolution occurs when cells are removed from the media. The absence of Ag spikes in the control sample indicates that spectral interferences did not limit the single cell detection and determination. Conversely, numerous Ag spikes exceeding the background level were detected in the RBCs sample exposed to AgNPs (Figure 41 A). It can be observed how the spikes recorded substantially decrease from Fig. 41 C to 41 D. Given that an additional washing step is performed and that samples are 2000-fold diluted prior to acquisition, the Ag spike signals in Fig. 41 A are entirely attributed to AgNPs associated with RBCs, although no distinction between internalized AgNPs and surface-adsorbed AgNPs can be made.

The potential of SC-ICP-MS to evaluate the uptake of 20 nm-AgNPs by RBCs has been demonstrated. To investigate the impact of dose concentration, 40 nm-AgNPs will be employed, as it is necessary to examine low cell:NP ratio. The use of 20 nm-AgNPs standards would result in a very low silver mass concentration and challenges in detection/quantification might reasonably be expected.

USC UNIVERSIDADE DE SANTIAGO DE COMPOSTELA

4.3.2 Effect of dose concentration and incubation time

To evaluate the impact of dose concentration and incubation time on AgNPs uptake by RBCs, cells (6.7×10^{11} cells L^{-1}) were exposed to two concentrations of 40 nm-AgNPs in a cell:NP ratio close to 1:1 (5.1×10^{11} NPs L^{-1} initial concentration) and 1:50 (2.5×10^{13} NPs L^{-1} initial concentration) for 8, 12, and 24 hours. Each set of experiments was performed in triplicate and control samples (RBCs not exposed to AgNPs) were subjected to the same experimental procedure.

The uptake of AgNPs at the lowest dose concentration (ratio 1:1) was minimal and a proper quantification was not possible even for the longest incubation time tested. Rasmussen *et al*. [38] studied the AgNP-yeast cell interactions and estimated that the optimal dosing particle concentration for highest uptake were approximately 1820, 1000, and 300 AgNPs $cell^{-1}$ for 10, 20, and 40 nm-AgNPs, respectively. Consequently, a ratio 1:1 might have been too low, although studies with 1:1 and 1:3 cell:NP ratio have been conducted for AuNPs in freshwater algae [43].

On the other hand, Figure 36 illustrates the effect of exposure time on AgNPs uptake by RBCs for the higher dose concentration (ratio 1:50) tested.

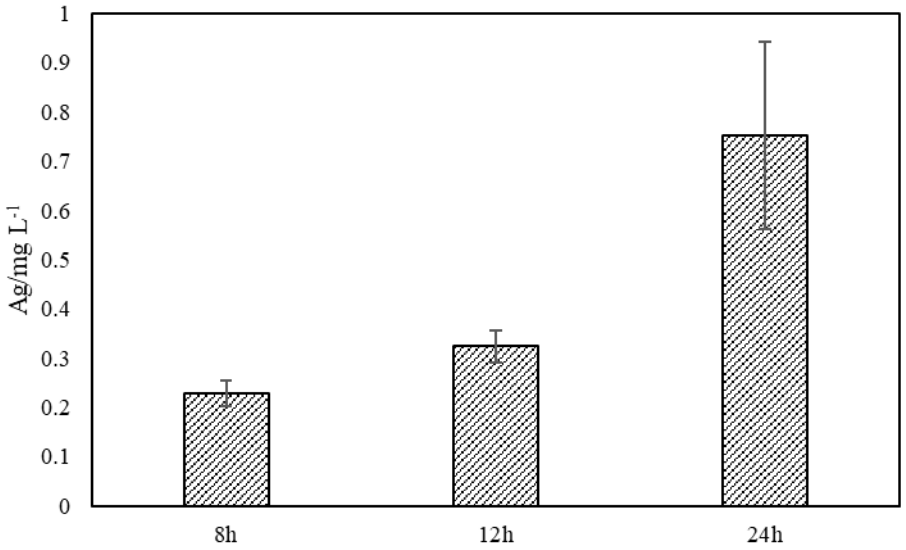

Figure 35. Effect of exposure time (8, 12, and 24 hours) on 40 nm-AgNPs uptake by RBCs. Conditions: concentration ratio 1:50 cell/NP, 39 ºC, 94.5 % relative humidity, 5.0 % CO_2; error bars correspond to the standard deviation of 3 experimental replicates (n=6 ICP-MS measurements).

In this case, a clear time-dependent relationship can be observed. The AgNPs concentration (expressed as silver mass concentration, mg L^{-1}) increases with increasing time of exposure. The 24-hour incubation experiment also exhibits the highest standard deviation, suggesting that prolonged exposure times may trigger a process of NP elimination in the cells and lead to greater cell-to-cell variability within the cell population. Table 16 displays the number concentration of RBCs (L^{-1}), the silver mass concentration (mg L^{-1}), and the calculated AgNPs per cell based on median mass values. It is important to note that Table 16 only includes data from RBCs that accumulated AgNPs (RBCs that did not accumulate AgNPs were not detected by SC-ICP-MS, as the Ag signal was monitored). The total RBC population considered for

USC UNIVERSIDADE DE SANTIAGO DE COMPOSTELA

subsequent calculations was determined through Neubauer chamber counting at the start of the incubation experiment.

Table 16. Number concentration of RBCs containing 40 nm-AgNPs, silver mass concentration, and the calculated AgNPs per cell. (Conditions: dose concentration ratio 1:50 cell/NP, results expressed as mean ± standard deviation, n=6).

Exposure time (h)	Number concentration (L^{-1})	Ag (mg L^{-1})	AgNPs $cell^{-1}$	CV (%)
8	$1.3 \pm 0.09 \times 10^{11}$	0.228 ± 0.026	3	4
12	$1.3 \pm 0.11 \times 10^{11}$	0.324 ± 0.032	5	8
24	$1.7 \pm 0.45 \times 10^{11}$	0.751 ± 0.190	8	3

After 8 and 12 h of exposure, approximately 20 % of the cell population contains AgNPs. This percentage rises to 25 % when the exposure time is extended to 24 h, showing that 75-80 % of cells do not accumulate AgNPs under these conditions. Also note that the reported percentages are calculated relative to the initial RBCs concentration and therefore do not account for potential losses in RBCs count during exposure–either due to AgNPs-related toxicity or to natural cell mortality. Although the fraction of cells containing AgNPs remains virtually constant over the tested time, the number of AgNPs associated with RBCs increases over time, indicating a strong time-dependent interaction. To calculate the number of AgNPs per cell, the median of the mass distribution (ag) of the cell population determined by SC-ICP-MS is divided by the mass (ag) corresponding to one AgNPs of the standard suspension used for cell exposure (determined knowing the nominal size, density and considering a spherical particle). Therefore, by knowing the mass of a single particle, it is possible to correlate to how many particles correspond the median mass of the sample measured. Specifically, cells exposed to AgNPs for 8 hours exhibited an average internalization/surface adherence of approximately 3 AgNPs per cell. This number increased to about 5 AgNPs per cell following 12 hours of exposure and further rose to an average of 8 NPs per cell after 24 hours. These observations suggest that prolonged exposure significantly enhances the extent of AgNPs assimilation, likely due to extended interaction time between NPs and the cellular membrane.

Figure 37 shows the Ag mass distributions in RBCs histograms after several exposure times. All mass distributions show a noticeable right-hand tail, indication of cells accumulating larger amounts of silver (AgNPs), this effect is even more acute in RBCs exposed for the longer incubation time (24 h, Figure 37C). The tailing observed in the mass distributions is a characteristic feature of a cell population and strengthens the concept of cell-to-cell variability. As time increases a shift in the mass distributions to higher mass values can be observed due to an increase in the AgNPs association with cells. Therefore, the mass distributions obtained for the 8 h exposure (Figure 37A) present a mean mass value of 2.3 fg, a median mass value of 1.6 fg, and a most frequent mass of 1.4 fg, whereas the mass distributions for 12 h (Figure 37B) show a mean mass value of 2.8 fg, a median mass value of 2.3 fg, and a most frequent mass of 2.4 fg, and the mass distributions for 24 h (Figure 37C) exhibit a mean mass value of 4.7 fg, a median mass value of 4.5 fg, and a most frequent mass of 3.3 fg. Colored dashed lines correspond to the median mass values of the distributions, the grey line represents the 8 h (corresponding to the mass of 3 AgNPs), the light-blue line the 12 h (5 AgNPs), and the dark-blue line the 24 h (8 AgNPs). Fig. 37A shows how most cells cluster around the mass corresponding to 3 AgNPs (grey dashed line) and insignificant events are recorded beyond the dark-blue line, being the narrower distribution observed of all. After 12 h (Fig. 37B), the

distribution widens, the number of cells accumulating less than 3 AgNPs decreases and the assimilation of AgNPs clusters between 3 and 8. Fig. 37C exhibits the wider distribution of all, indicating higher NP uptake variability at longer exposure times. The number of cells accumulating less than 5 NPs becomes negligible, while a growing number of cells begin to accumulate higher quantities of AgNPs, potentially influenced by AgNPs aggregation effects.

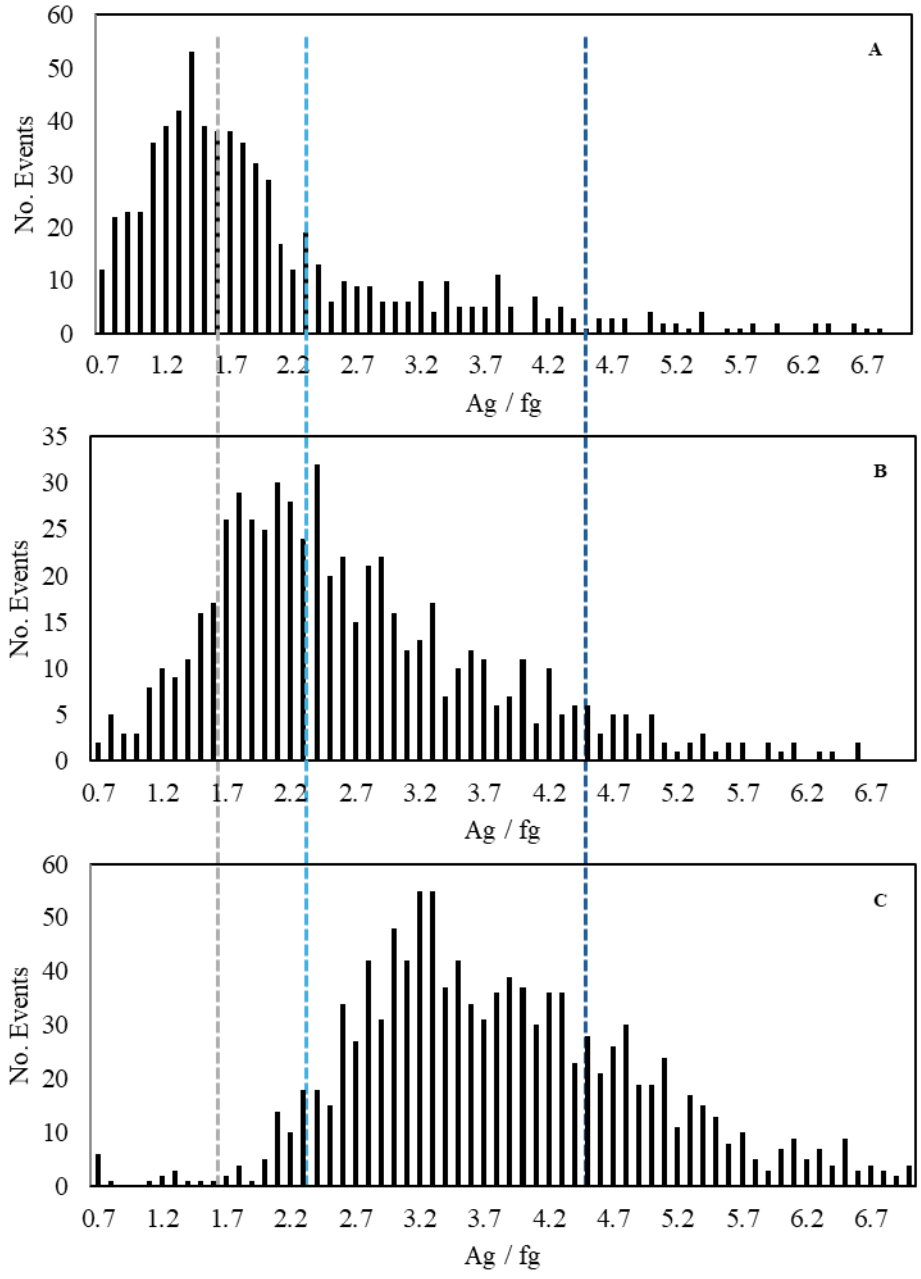

Figure 36. Ag mass distribution histogram after exposure times of 8 h (A), 12 h (B), and 24 h (C) in detected RBCs. Coloured dash lines correspond to the median mass values of the distribution, the grey line represents the 8 h-corresponding to the mass of 3 AgNPs, the light-blue line the 12 h-5 AgNPs, and the dark-blue line the 24 h-8 AgNPs. (Conditions: 40 nm-AgNPs, concentration ratio 1:50 cell/NP, histograms correspond to one biological sample replicate).

USC UNIVERSIDADE DE SANTIAGO DE COMPOSTELA

Considering the mean mass values from the histogram, the estimated average number of AgNPs per cell would be 4, 5, and 9 for the 8-hour, 12-hour, and 24-hour exposure assays, respectively. However, most frequent mass values would give results of 3, 4, and 6 AgNPs per cell for exposure times of 8, 12 and 24 h, respectively. Thus, after 8 hours of exposure most of the cells within the 20 % of the cell population containing silver would accumulate 3 AgNPs. After 12 hours, most cells within the 20 % of the cell population containing silver, would accumulate 4 AgNPs, and after 24 h, the majority of cells within the 25 % of the cell population containing silver would accumulate 6 AgNPs.

The presence of Ag-containing RBCs was further confirmed by transmission electron microscopy (TEM), as illustrated in Figure 38. Across the magnification range–from 38A (2 μm) to 38D (100 nm)–the presence of solid black dots within the RBC population is visible. Presumably, AgNPs appear as high-contrast features due to their high atomic number, which enhances electron scattering under TEM. At higher magnification (Fig. 38D), individual spherical particles with diameters below 100 nm can be distinguished, with particle size estimated using the scale bar. Lower magnification image (Fig. 38A) facilitates the general observation of the heterogeneous distribution above mentioned, with some cells exhibiting NP association while others do not. TEM images of a control RBCs sample can be found in the supplementary information (Figure 42).

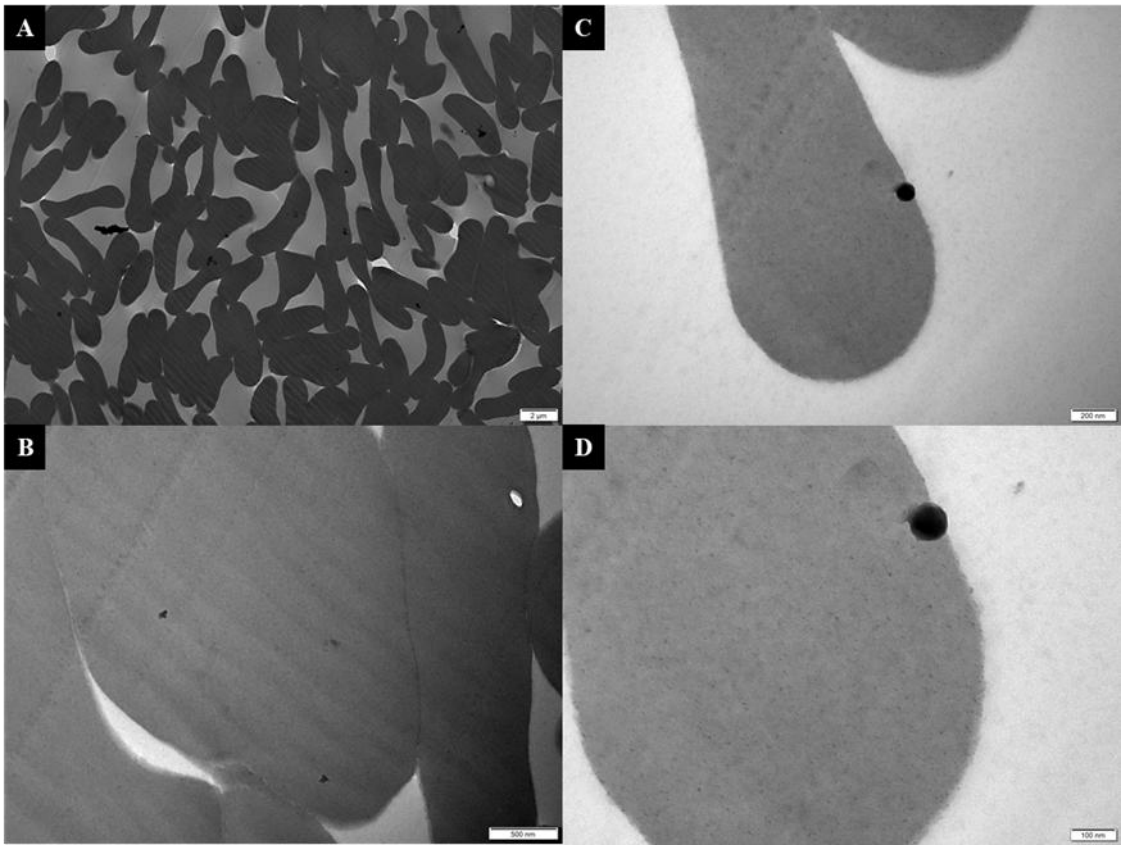

Figure 37. TEM images of a section of a RBCs sample exposed to 40 nm-AgNPs for 24 hours, from lower (A) to higher (D) magnification range. Panels C and D display the same region at different magnifications, while panels A and B depict separate regions.

USC UNIVERSIDADE DE SANTIAGO DE COMPOSTELA

In summary, the results obtained in this part of the study suggest that: (i) exposure time is a significant factor in the AgNP-cell interaction, shorter exposure times may be insufficient for a complete association while longer exposure times may trigger some type of NP elimination mechanism from the cells; (ii) 40 nm-AgNPs exhibit a time-dependent uptake by cells; (iii) it could not be confirmed whether AgNPs dose concentration is a significant parameter in the NP-cell interplay; (iv) only a 20-25 % of the cell population accumulated AgNPs; and (v) AgNP uptake occurs heterogeneously within the cell population, resulting in long-tailed distributions.

The results obtained in this study can be compared to those reported in the literature by López-Serrano *et al* [46] who investigated the uptake of 50 nm-AgNPs by human THP-1 monocytes. In their study, THP-1 cells were incubated with AgNPs at concentrations of 0.1 and 1 μg mL^{-1} for 4 and 24 hours (dose concentration in our study expressed in silver mass were 0.20 μg mL^{-1} and 9.72 μg mL^{-1}). The results revealed a negligible AgNP uptake at the lower dose concentration and a time-dependent uptake at the higher dose concentration, with approximately 3 and 7 AgNPs per cell calculated for the 4-hour and 24-hour incubation experiments, respectively. Although some differences can be noted, these results are in good agreement with those obtained in our study.

4.3.3 Influence of nanoparticle size on AgNPs-RBCs association

Table 17 collects the concentration of RBCs associated with 20 nm-AgNPs in terms of number concentration (L^{-1}), percentage of RBCs containing silver, and the estimated AgNPs per cell.

Table 17. Number concentration of RBCs containing 20 nm-AgNPs, percentage of RBCs containing 20 nm-AgNPs, and calculated AgNPs per cell. (Conditions: dose concentration ratio 1:50 cell/NP, results expressed as mean ± standard deviation, n=6).

Exposure time (h)	Number concentration (L^{-1})	% Ag-containing RBCs	AgNPs $cell^{-1}$	CV (%)
8	$1.9 \pm 0.5 \times 10^{11}$	40	2	8
12	$5.5 \pm 2.3 \times 10^{11}$	114	2	5
24	$5.8 \pm 1.6 \times 10^{11}$	121	2	12

A sharp increase in the number concentration from 8 to 12 hours can be observed, followed by no significant increase from 12 to 24 hours, which is ultimately reflected in the percentage of Ag-containing RBCs. After 8 h of exposure, 40 % of cell population contains silver, this rises to 114 % after 12 h, and 121 % after 24 h. However, the calculated number of AgNPs associated with RBCs remains virtually constant regardless of the time. The accumulation of AgNPs in RBCs for 8, 12, and 24 hours of exposure would be 2 AgNPs. Therefore, exposure time proves to have an impact on the number of cells containing AgNPs, but not on the number of particles accumulated. This would stand in marked contrast to the effect observed for 40-nm AgNPs (ratio 1:50 cell/NP). To facilitate visual interpretation, Figure 39 compares 20 nm- and 40 nm-AgNPs in terms of number concentration (L^{-1}) and percentage (%) of silver-containing RBCs. Although exposure time is critical for both AgNPs size, and an increase in the silver concentration accumulated is observed, the distribution of AgNPs within the cell population varies between 20 nm and 40 nm NPs. In the case of 20 nm-AgNPs, the great majority of cells is able to accumulate NPs, most likely due to their smaller size. After the appropriate exposure time, an homogeneous AgNPs uptake is observed across the cells and an increase in the

USC UNIVERSIDADE DE SANTIAGO DE COMPOSTELA

exposure time does not lead to an increase in the number of particles accumulated. In contrast, for 40 nm-AgNPs, only a small percentage (around 25 %) of cells is capable of accumulating NPs. After long exposure times (12 and 24 h) the RBCs population exhibits uneven AgNPs uptake, with some cells accumulating no particles and others accumulating up to 9 NPs. These findings emphasize that AgNPs uptake is governed by multiple factors, and is not only dependent on exposure time but also significantly influenced by the NP size.

It should be noted that the cell/NP ratio was arbitrarily selected, and the comparison results between 20 nm- and 40 nm-AgNPs are based on this ratio, which does not translate into the same silver mass for both NPs. Ratio 1:50 cell/NP expressed in terms of silver mass for 20 nm-AgNPs would be 1.02 mg L^{-1}, whereas for 40 nm-AgNPs would be 9.72 mg L^{-1}.

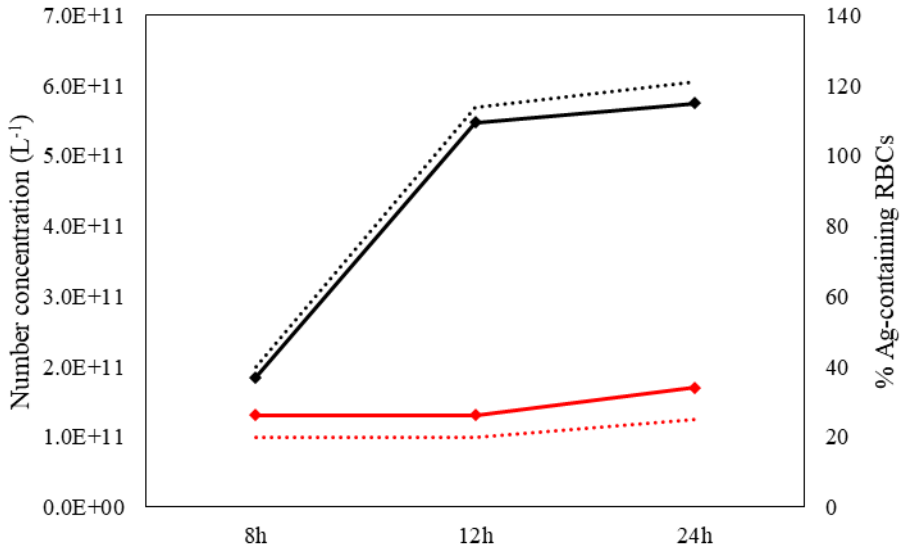

Figure 38. Comparison between 20 nm-AgNPs (black lines) and 40 nm-AgNPs (red lines). Solid lines represent the calculated RBCs number concentration (L^{-1}) for 8, 12, and 24 h of exposure; whereas dash lines stand for the percentage (%) of silver-containing RBCs.

4.4 CONCLUSIONS

The study presented here demonstrates for the first time the application of SC-ICP-MS methodology for the quantification of AgNPs uptake by human RBCs after exposure for 8, 12, and 24 hours. SC-ICP-MS is a powerful and promising tool that was able to detect and confirm the presence of silver-containing cells. Quantification in terms of cell concentration, mass of silver per cell, and silver mass distribution within the cell population was conducted. These features are of great benefit to investigate the NP-cell interaction at the single cell level and taking into consideration the cell-to-cell variability. As shown in this study, cells behave differently after NP exposure. Under specific conditions, some cells are able to accumulate exclusively one NP, whereas others may accumulate up to 8 NPs. These differences are key when elucidating the NP-cell interplay in nanotoxicological and biomedical studies. Additionally, AgNPs uptake was also monitored in the supernatant concentration, where it was shown how dissolved silver level increased in the absence of cells, suggesting that cells may play a role in NP stabilization. Only a small percentage of the total cell population (20-25 %)

accumulated 40 nm-AgNPs; whereas under specific exposure time, the great majority of cells accumulated 20 nm-AgNPs. Exposure time proved to have a greater effect on the number of NPs internalized or surface-adhered to the cell than on the proportion of cells that contained silver for 40 nm-AgNPs and *vice versa* for 20 nm-AgNPs.

The feasibility of the proposed strategy to track, assess, and quantify AgNPs in exposed RBCs by SC-ICP-MS has been demonstrated.

4.5 ACKNOWLEDGEMENTS

Grant FOODNANORISK (reference PID2021-125276NB-I00) funded by MICIU/AEI/ 10.13039/501100011033 Spain, and *Grupo de Referencia Competitiva* (reference ED431C 2022/029) funded by *Consellería de Educación, Ciencia, Universidades e Formación Profesional*, *Xunta de Galicia*, Spain. Authors also acknowledge Albina Roman-Castro from Electronic and Confocal Microscopy and Support for Biological Specialities Unit at the University of Santiago de Compostela for TEM technical assistance. Ana Justo-Vega acknowledges *Xunta de Galicia*, Spain, for a predoctoral grant.

4.6 REFERENCES

[1] L.M. Katz, K. Dewan, R.L. Bronaugh, Nanotechnology in cosmetics, Food Chem. Toxicol. 85 (2015) 127–137. https://doi.org/10.1016/j.fct.2015.06.020.

[2] E. Villena de Francisco, R.M. García-Estepa, Nanotechnology in the agrofood industry, J. Food Eng. 238 (2018) 1–11. https://doi.org/10.1016/j.jfoodeng.2018.05.024.

[3] A. Haider, I.K. Kang, Preparation of silver nanoparticles and their industrial and biomedical applications: A comprehensive review, Adv. Mater. Sci. Eng. 2015 (2015). https://doi.org/10.1155/2015/165257.

[4] K. Pathakoti, M. Manubolu, H.M. Hwang, Nanostructures: Current uses and future applications in food science, J. Food Drug Anal. 25 (2017) 245–253. https://doi.org/10.1016/j.jfda.2017.02.004.

[5] J. Noireaux, R. Grall, M. Hullo, S. Chevillard, C. Oster, E. Brun, C. Sicard-Roselli, K. Loeschner, P. Fisicaro, Gold nanoparticle uptake in tumor cells: Quantification and size distribution by sp-ICPMS, Separations. 6 (2019) 1–13. https://doi.org/10.3390/separations6010003.

[6] S.J.H. Soenen, N. Nuytten, U. Himmelreich, M. De Cuyper, The possible side-effects of iron oxide nanoparticles on cell functionality, AIP Conf. Proc. 1275 (2010) 106–111. https://doi.org/10.1063/1.3505056.

[7] K.S. Butler, B.J. Casey, G.V.M. Garborcauskas, B.J. Dair, R.K. Elespuru, Assessment of titanium dioxide nanoparticle effects in bacteria: Association, uptake, mutagenicity, co-mutagenicity and DNA repair inhibition, Mutat. Res. - Genet. Toxicol. Environ. Mutagen. 768 (2014) 14–22. https://doi.org/10.1016/j.mrgentox.2014.04.008.

USC UNIVERSIDADE DE SANTIAGO DE COMPOSTELA

[8] S.J. Soenen, W.J. Parak, J. Rejman, B. Manshian, (Intra)cellular stability of inorganic nanoparticles: Effects on cytotoxicity, particle functionality, and biomedical applications, Chem. Rev. 115 (2015) 2109–2135. https://doi.org/10.1021/cr400714j.
[9] L. Rizzello, P.P. Pompa, Nanosilver-based antibacterial drugs and devices: Mechanisms, methodological drawbacks, and guidelines, Chem. Soc. Rev. 43 (2014) 1501–1518. https://doi.org/10.1039/c3cs60218d.

[10] B. Bocca, B. Battistini, F. Petrucci, Silver and gold nanoparticles characterization by SP-ICP-MS and AF4-FFF-MALS-UV-ICP-MS in human samples used for biomonitoring, Talanta. 220 (2020). https://doi.org/10.1016/j.talanta.2020.121404.

[11] T. Ishizaka, K. Nagano, I. Tasaki, H. Tao, J.Q. Gao, K. Harada, K. Hirata, S. Saito, H. Tsujino, K. Higashisaka, Y. Tsutsumi, Optimization and Evaluation of Pretreatment Method for sp-ICP-MS to Reveal the Distribution of Silver Nanoparticles in the Body, Nanoscale Res. Lett. 14 (2019). https://doi.org/10.1186/s11671-019-3016-9.

[12] M. Witzler, F. Küllmer, K. Günther, Validating a Single-Particle ICP-MS Method to Measure Nanoparticles in Human Whole Blood for Nanotoxicology, Anal. Lett. 51 (2018) 587–599. https://doi.org/10.1080/00032719.2017.1327538.

[13] M.A. Munger, P. Radwanski, G.C. Hadlock, G. Stoddard, A. Shaaban, J. Falconer, D.W. Grainger, C.E. Deering-Rice, *In vivo* human time-exposure study of orally dosed commercial silver nanoparticles, Nanomedicine Nanotechnology, Biol. Med. 10 (2014) 1–9. https://doi.org/10.1016/j.nano.2013.06.010.

[14] R. Dejonghe, E. Bolea-Fernandez, A. Lores-Padin, T. Van Acker, A. Rua-Ibarz, O. De Wever, F. Vanhaecke, An evaluation of the analytical and biological robustness of a method for quantifying iron in individual red blood cells via single-cell tandem ICP-mass spectrometry, Microchem. J. 207 (2024). https://doi.org/10.1016/j.microc.2024.112013.

[15] N. Mohandas, P.G. Gallagher, Red cell membrane: Past, present, and future, Blood. 112 (2008) 3939–3948. https://doi.org/10.1182/blood-2008-07-161166.

[16] V. Pretini, M.H. Koenen, L. Kaestner, M.H.A.M. Fens, R.M. Schiffelers, M. Bartels, R. Van Wijk, Red blood cells: Chasing interactions, Front. Physiol. 10 (2019) 1–17. https://doi.org/10.3389/fphys.2019.00945.

[17] M.R. Farag, M. Alagawany, Erythrocytes as a biological model for screening of xenobiotics toxicity, Chem. Biol. Interact. 279 (2018) 73–83. https://doi.org/10.1016/j.cbi.2017.11.007.

[18] A. Bogdanova, L. Kaestner, G. Simionato, A. Wickrema, A. Makhro, Heterogeneity of Red Blood Cells: Causes and Consequences, Front. Physiol. 11 (2020) 1–11. https://doi.org/10.3389/fphys.2020.00392.

[19] V. Kuhn, L. Diederich, T.C.S. Keller, C.M. Kramer, W. Lückstädt, C. Panknin, T. Suvorava, B.E. Isakson, M. Kelm, M.M. Cortese-Krott, Red Blood Cell Function and

USC UNIVERSIDADE DE SANTIAGO DE COMPOSTELA

Dysfunction: Redox Regulation, Nitric Oxide Metabolism, Anemia, Antioxidants Redox Signal. 26 (2017) 718–742. https://doi.org/10.1089/ars.2016.6954.

[20] L. Narciso, L. Coppola, G. Lori, C. Andreoli, A. Zjino, B. Bocca, F. Petrucci, A. Di Virgilio, A. Martinelli, A. Tinari, F. Maranghi, R. Tassinari, Genotoxicity, biodistribution and toxic effects of silver nanoparticles after in vivo acute oral administration, NanoImpact. 18 (2020) 100221. https://doi.org/10.1016/j.impact.2020.100221.

[21] L. Mueller, H. Traub, N. Jakubowski, D. Drescher, V.I. Baranov, J. Kneipp, Trends in single-cell analysis by use of ICP-MS, Anal. Bioanal. Chem. 406 (2014) 6963–6977. https://doi.org/10.1007/s00216-014-8143-7.

[22] A.B.S. da Silva, M.A.Z. Arruda, Single-cell ICP-MS to address the role of trace elements at a cellular level, J. Trace Elem. Med. Biol. 75 (2023). https://doi.org/10.1016/j.jtemb.2022.127086.

[23] D. Schaumlöffel, R. Hutchinson, J. Malherbe, P. Le Coustumer, E. Gontier, M.P. Isaure, Novel Methods for Bioimaging Including LA-ICP-MS, NanoSIMS, TEM/X-EDS, and SXRF, Met. Anal. Tech. Speciat. Methods. (2016) 83–116. https://doi.org/10.1002/9783527694907.ch4.

[24] H. Haraguchi, A. Ishii, T. Hasegawa, H. Matsuura, T. Umemura, Metallomics study on all-elements analysis of salmon egg cells and fractionation analysis of metals in cell cytoplasm, Pure Appl. Chem. 80 (2008) 2595–2608. https://doi.org/10.1351/pac200880122595.

[25] Y. Ishihara, M. Aida, A. Nomura, H. Miyahara, A. Hokura, A. Okino, Development of desolvation system for single-cell analysis using droplet injection inductively coupled plasma atomic emission spectroscopy, Anal. Sci. 31 (2015) 781–785. https://doi.org/10.2116/analsci.31.781.

[26] E. Mathieu, A.S. Bernard, N. Delsuc, E. Quévrain, G. Gazzah, B. Lai, F. Chain, P. Langella, M. Bachelet, J. Masliah, P. Seksik, C. Policar, A Cell-Penetrant Manganese Superoxide Dismutase (MnSOD) Mimic Is Able to Complement MnSOD and Exerts an Antiinflammatory Effect on Cellular and Animal Models of Inflammatory Bowel Diseases, Inorg. Chem. 56 (2017) 2545–2555. https://doi.org/10.1021/acs.inorgchem.6b02695.

[27] J.N. Audinot, A. Georgantzopoulou, J.P. Piret, A.C. Gutleb, D. Dowsett, H.N. Migeon, L. Hoffmann, Identification and localization of nanoparticles in tissues by mass spectrometry, Surf. Interface Anal. 45 (2013) 230–233. https://doi.org/10.1002/sia.5099.

[28] A.J. Managh, S.L. Edwards, A. Bushell, K.J. Wood, E.K. Geissler, J.A. Hutchinson, R.W. Hutchinson, H.J. Reid, B.L. Sharp, Single cell tracking of gadolinium labeled CD4+ T cells by laser ablation inductively coupled plasma mass spectrometry, Anal. Chem. 85 (2013) 10627–10634. https://doi.org/10.1021/ac4022715.

[29] H.A.O. Wang, D. Grolimund, C. Giesen, C.N. Borca, J.R.H. Shaw-Stewart, B. Bodenmiller, D. Günther, Fast chemical imaging at high spatial resolution by laser ablation

USC UNIVERSIDADE DE SANTIAGO DE COMPOSTELA

inductively coupled plasma mass spectrometry, Anal. Chem. 85 (2013) 10107–10116. https://doi.org/10.1021/ac400996x.

[30] T. Büchner, D. Drescher, H. Traub, P. Schrade, S. Bachmann, N. Jakubowski, J. Kneipp, Relating surface-enhanced Raman scattering signals of cells to gold nanoparticle aggregation as determined by LA-ICP-MS micromapping, Anal. Bioanal. Chem. 406 (2014) 7003–7014. https://doi.org/10.1007/s00216-014-8069-0.

[31] X. Yu, B. Chen, M. He, H. Wang, B. Hu, 3D Droplet-Based Microfluidic Device Easily Assembled from Commercially Available Modules Online Coupled with ICPMS for Determination of Silver in Single Cell, Anal. Chem. 91 (2019) 2869–2875. https://doi.org/10.1021/acs.analchem.8b04844.

[32] L. Amable, C. Stephan, S. Smith, R. Merrifield, An Introduction to Single Cell ICP-MS Analysis, White Pap. (2017) 1–5. https://www.perkinelmer.com/lab-solutions/resources/docs/WHT-Introduction-to-Single-Cell-ICP-MS-012774A_01.pdf.

[33] H. Wang, B. Chen, M. He, B. Hu, A Facile Droplet-Chip-Time-Resolved Inductively Coupled Plasma Mass Spectrometry Online System for Determination of Zinc in Single Cell, Anal. Chem. 89 (2017) 4931–4938. https://doi.org/10.1021/acs.analchem.7b00134.

[34] C. Degueldre, P.Y. Favarger, Colloid analysis by single particle inductively coupled plasma-mass spectroscopy: A feasibility study, Colloids Surfaces A Physicochem. Eng. Asp. 217 (2003) 137–142. https://doi.org/10.1016/S0927-7757(02)00568-X.

[35] F. Laborda, E. Bolea, J. Jimenez-Lamana, Powerful Tool for Nanoanalysis, Anal. Chem. 86 (2014) 2270–2278, https://doi.org/10.1021/ac402980q.

[36] M.D. Montaño, J.W. Olesik, A.G. Barber, K. Challis, J.F. Ranville, Single Particle ICP-MS: Advances toward routine analysis of nanomaterials, Anal. Bioanal. Chem. 408 (2016) 5053–5074. https://doi.org/10.1007/s00216-016-9676-8.

[37] A.R. Montoro Bustos, K.P. Purushotham, A. Possolo, N. Farkas, A.E. Vladár, K.E. Murphy, M.R. Winchester, Validation of Single Particle ICP-MS for Routine Measurements of Nanoparticle Size and Number Size Distribution, Anal. Chem. 90 (2018) 14376–14386. https://doi.org/10.1021/acs.analchem.8b03871.

[38] L. Rasmussen, H. Shi, W. Liu, K.B. Shannon, Quantification of silver nanoparticle interactions with yeast Saccharomyces cerevisiae studied using single-cell ICP-MS, Anal. Bioanal. Chem. 414 (2022) 3077–3086. https://doi.org/10.1007/s00216-022-03937-4.

[39] X. Yu, M. He, B. Chen, B. Hu, Recent advances in single-cell analysis by inductively coupled plasma-mass spectrometry: A review, Anal. Chim. Acta. 1137 (2020) 191–207. https://doi.org/10.1016/j.aca.2020.07.041.

[40] J. Jiménez-Lamana, J. Szpunar, R. Łobinski, New Frontiers of Metallomics: Elemental and Species-Specific Analysis and Imaging of Single Cells, Adv. Exp. Med. Biol. 1055 (2018) 245–270. https://doi.org/10.1007/978-3-319-90143-5_10.

[41] F. Li, D.W. Armstrong, R.S. Houk, Behavior of bacteria in the inductively coupled plasma: Atomization and production of atomic ions for mass spectrometry, Anal. Chem. 77 (2005) 1407–1413. https://doi.org/10.1021/ac049188l.

[42] B. Gomez-Gomez, M. Corte-Rodríguez, M.T. Perez-Corona, J. Bettmer, M. Montes-Bayón, Y. Madrid, Combined single cell and single particle ICP-TQ-MS analysis to quantitatively evaluate the uptake and biotransformation of tellurium nanoparticles in bacteria, Anal. Chim. Acta. 1128 (2020) 116–128. https://doi.org/10.1016/j.aca.2020.06.058.

[43] R.C. Merrifield, C. Stephan, J.R. Lead, Quantification of Au Nanoparticle Biouptake and Distribution to Freshwater Algae Using Single Cell - ICP-MS, Environ. Sci. Technol. 52 (2018) 2271–2277. https://doi.org/10.1021/acs.est.7b04968.

[44] A.C. Gimenez-Ingalaturre, I. Abad-Álvaro, P. Goñi, K. Billimoria, H. Goenaga-Infante, F. Laborda, Performance of single-cell ICP-MS for quantitative biodistribution studies of silver interactions with bacteria, J. Anal. At. Spectrom. 39 (2024) 743–753. https://doi.org/10.1039/d3ja00378g.

[45] M. Corte-Rodríguez, R. Álvarez-Fernández, P. García-Cancela, M. Montes-Bayón, J. Bettmer, Single cell ICP-MS using on line sample introduction systems: Current developments and remaining challenges, TrAC - Trends Anal. Chem. 132 (2020). https://doi.org/10.1016/j.trac.2020.116042.

[46] A. López-Serrano Oliver, S. Baumgart, W. Bremser, S. Flemig, D. Wittke, A. Grützkau, A. Luch, A. Haase, N. Jakubowski, Quantification of silver nanoparticles taken up by single cells using inductively coupled plasma mass spectrometry in the single cell measurement mode, J. Anal. At. Spectrom. 33 (2018) 1256–1263. https://doi.org/10.1039/c7ja00395a.

[47] C. Suárez-Oubiña, P. Herbello-Hermelo, N. Mallo, M. Vázquez, S. Cabaleiro, I. Pinheiro, L. Rodríguez-Lorenzo, B. Espiña, P. Bermejo-Barrera, A. Moreda-Piñeiro, Single-cell ICP-MS for studying the association of inorganic nanoparticles with cell lines derived from aquaculture species, Anal. Bioanal. Chem. 415 (2023) 3399–3413. https://doi.org/10.1007/s00216-023-04723-6.

[48] H.E. Pace, N.J. Rogers, C. Jarolimek, V.A. Coleman, C.P. Higgins, J.F. Ranville, Determining transport efficiency for the purpose of counting and sizing nanoparticles via single particle inductively coupled plasma mass spectrometry, Anal. Chem. 83 (2011) 9361–9369. https://doi.org/10.1021/ac201952t.

[49] H. Wang, B. Wang, M. Wang, L. Zheng, H. Chen, Z. Chai, Y. Zhao, W. Feng, Time-resolved ICP-MS analysis of mineral element contents and distribution patterns in single cells, Analyst. 140 (2015) 523–531. https://doi.org/10.1039/c4an01610f.

[50] T.E. Lockwood, R. Gonzalez De Vega, D. Clases, An interactive Python-based data processing platform for single particle and single cell ICP-MS, J. Anal. At. Spectrom. 36 (2021) 2536–2544. https://doi.org/10.1039/d1ja00297j.

USC UNIVERSIDADE DE SANTIAGO DE COMPOSTELA

[51] F. Laborda, A.C. Gimenez-Ingalaturre, E. Bolea, J.R. Castillo, Single particle inductively coupled plasma mass spectrometry as screening tool for detection of particles, Spectrochim. Acta - Part B At. Spectrosc. 159 (2019) 105654. https://doi.org/10.1016/j.sab.2019.105654.

USC
UNIVERSIDADE DE SANTIAGO DE COMPOSTELA

SUPPLEMENTARY INFORMATION

Table 18. Silver concentration in detected RBCs, expressed as mean ± standard deviation (n=6).

Exposure time (h)	Silver Concentration (mg L^{-1})[a]	Silver Concentration (mg L^{-1})[b]
8	0.10 ± 0.03	0.04 ± 0.01
12	0.24 ± 0.10	0.14 ± 0.06
24	0.25 ± 0.08	0.15 ± 0.06

[a]*Silver content concentration calculated based on Mean Mass values,* [b]*silver content concentration calculated based on Median Mass values.*

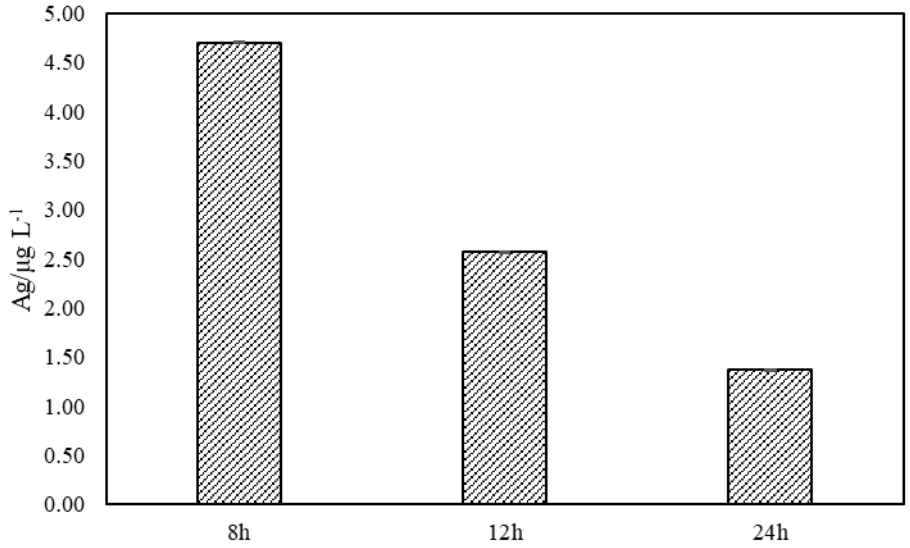

Figure 39. Supernatant silver concentration (µg L^{-1}) after 8, 12, and 24 hours of exposure. Concentration expressed as the sum of the first (3 replicates) and second (3 replicates) supernatants (n=12 ICP-MS measurements).

USC UNIVERSIDADE DE SANTIAGO DE COMPOSTELA

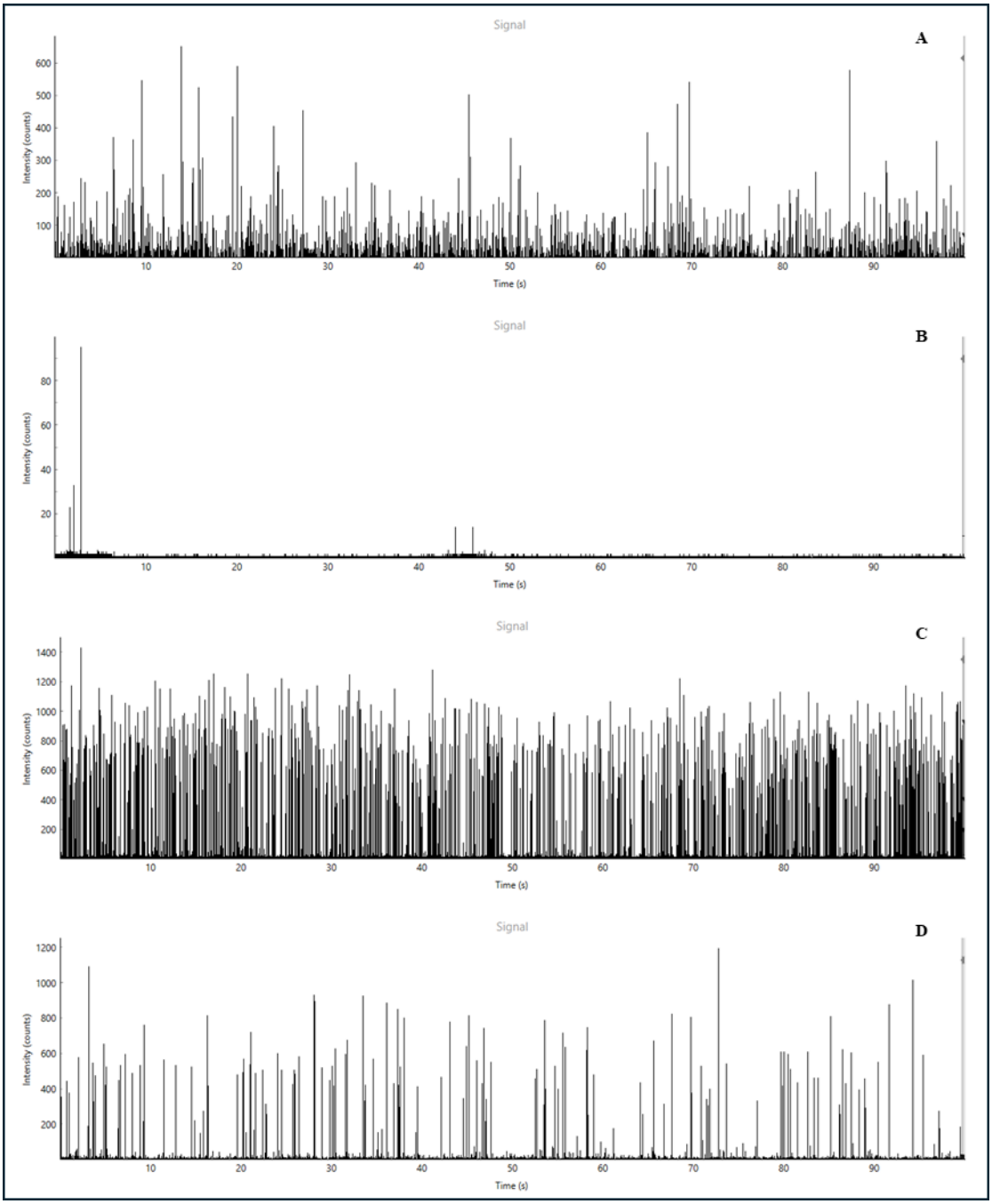

Figure 40. Time resolved ICP-MS profiles obtained with SPCal software for a RBCs sample exposed to 20 nm-AgNPs, ratio 1:50 cell/NP, for 24 hours (A), the corresponding control sample (B), the first supernatant collected (C), and the second supernatant collected after the first wash with 1.0 % PBS (D) (Conditions: (A) and (B) 2000-fold diluted, (C) and (D) no dilution).

USC UNIVERSIDADE DE SANTIAGO DE COMPOSTELA

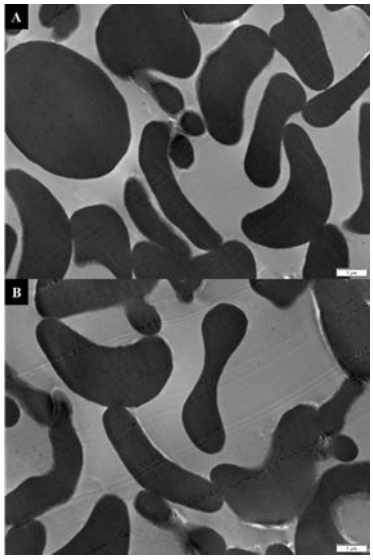

Figure 41. TEM images of a RBCs control sample (not exposed to AgNPs). Panels A and B display the same magnification but different regions of the sample.

USC
UNIVERSIDADE DE SANTIAGO DE COMPOSTELA

IV. PART B: UNPUBLISHED RESULTS

USC
UNIVERSIDADE
DE SANTIAGO
DE COMPOSTELA

CHAPTER 5. ADVANCEMENTS IN LA-ICP-MS: PRELIMINARY INSIGHTS INTO THE OPTIMIZATION OF A NEW CALIBRATION APPROACH AND A MICROWELL ARRAY DESIGN FOR SINGLE-CELL TRAPPING

USC
UNIVERSIDADE DE SANTIAGO DE COMPOSTELA

CHAPTER 5. ADVANCEMENTS IN LA-ICP-MS: PRELIMINARY INSIGHTS INTO THE OPTIMIZATION OF A NEW CALIBRATION APPROACH AND A MICROWELL ARRAY DESIGN FOR SINGLE-CELL TRAPPING

ABSTRACT

In this study, we report advancements for the application in LA-ICP-MS: (a) an innovative calibration approach based on gelatine microdroplets, and (b) the design of a polydimethylsiloxane (PDMS)-based microwell array for controlled single-cell trapping. Gelatine microdroplets were prepared as spiked standards with both ionic and NP solutions, enabling complete ablation ad mitigating issues of representativeness and heterogeneity typical of conventional droplet-based approaches. Parallel, efforts focused on the fabrication and optimization of microwell arrays tailored for Caco-2 cells, ensuring efficient single-cell trapping under controlled CO_2 atmosphere. Key parameters influencing trapping efficiency– including settling time, cell concentration, cell resuspension medium, and NP exposure– were systematically evaluated. Collectively, these findings provide preliminary insights into practical calibration solutions and cell-handling strategies that advance the reliability of LA-ICP-MS, with broad implications for nanotoxicology, bioimaging, and nanomedicine.

5.1 INTRODUCTION

Single-cell analysis has emerged as one of the most powerful approaches in modern biomedical and toxicological research. It is widely accepted now that even cells with the same genotype and phenotype can respond very differently when exposed to the same environmental stimuli, like NP exposure. This heterogeneity highlights the limitations of studying cell populations in bulk, as average concentrations obtained after traditional acid digestion methods would be biased and will neglect the cell-to-cell variations. In this sense, single-cell analysis provides a deeper understanding of cellular diversity [1].

NPs are now extensively employed in both scientific research and industry [2]. They are widely used in nanomedicine for drug delivery, imaging, and diagnostics, while also being incorporated into cosmetics, food products, and other consumer items [3,4]. With such widespread applications, interactions between cells and NPs are to be expected. Therefore, elucidating cellular behaviour and possible mechanisms of interaction between NP and cells is essential for predicting potential risks and ensuring their safe use. Ultimately, integrating single-cell technologies into nanotoxicology and nanomedicine research offers a more precise and comprehensive framework for understanding cellular behaviour. This, in turn, can guide regulatory decisions, improve safety standards, and foster the responsible development of NP-based innovations.

Several works have already been published that highlighted the potential of laser ablation (LA) ICP-MS for NP assessment in individual cells [5]. As a direct sampling system, LA can

be coupled to ICP-MS for quantitative analysis and spatial imaging of single cells, offering unique insights into NP distribution at cellular and subcellular resolution [6]. Recent applications of LA-ICP-MS in cellular studies have primarily focussed on mapping the distribution of endogenous elements as well as tracking spiked elements to elucidate the uptake and metabolism of metal-based NPs [7]. Despite the promising advances, the application of LA-ICP-MS in single-cell analysis remains at an early stage of development, with several critical challenges yet to be addressed. A major limitation that continues to hinder the broader use of this technique is the lack of suitable calibration standards that ensure accurate quantitative analysis and reproducibility of results.

Among the calibration strategies explored, the most reliable approaches rely on the use of matrix-matched standards. However, due to the lack of certified reference materials (CRMs), researchers are often forced to prepare in-house solutions. Different proposals have been published for such purpose, including the use of pressed pellets spiked with powdered samples or standards, homogenized biological tissues enriched with standards, deposition of standards onto nitrocellulose membranes, incorporation of standards into gelatine matrices, and fused glassed beads [8]. For example, Drescher *et al.* [9] developed a method using nitrocellulose membranes spiked with NPs suspensions for the quantification of AuNPs and AgNPs in eukaryotic cells. Arakawa *et al.* [10] refined the method by employing a microarray spotter, enabling the deposition of smaller dried droplets of NPs suspensions. Similarly, Wang *et al.* [11] introduced a technique based on dried residues of picodroplets generated by a commercial inkjet printer to quantify AuNPs.

Calibration strategies based on the use of gelatine proved to be suitable, as its properties partially resembles those of the fibrous protein collagen of biological matrices. Both gelatine sections and gelatine droplets have been utilized in the preparation of calibration standards for LA-ICP-MS analysis [12]. However, challenges remain: (i) ablating only part of a gelatine section can compromise representativeness, while (ii) complete ablation of entire section or droplets is often time-consuming due to large dimensions. In addition, in droplet-based approaches, analyte distributions can be heterogeneous due to coffee stain effect and/or Marangoni effect during the drying process [13].

In light of the challenges outlined above, the present study aims to: (i) investigate an innovative calibration approach based on gelatine microdroplets, reducing the time required for ablation and eliminate the representativeness problems by complete ablation of the microdroplet, and (ii) design a microwell array for single cell deposition and LA-ICP-MS application that provides a controlled and regular distribution of individual cells for easily ablation in a grid pattern.

5.2 EXPERIMENTAL

5.2.1 Instrumentation

Part A: Feasibility studies of a gelatine-based microdroplet calibration approach

Analyses were carried out using an Agilent 8800 Triple Quadrupole ICP-MS (Santa Clara, CA,USA) in combination with a Tofwerk ICP-TOF 2R-MS (Thun, Switzerland) for high-resolution mass spectrometry measurements. Sample introduction was performed via Teledyne Photon Machines Iridia laser ablation-system (ArF* 193 nm, equipped with the patented Cobalt Cell) (Thousand Oaks, CA, USA). Ultrapure water used throughout the procedures was obtained from a Direct-Q® 3 UV water purification system (Merck Millipore, Burlington, MA, USA). For sample preparation, weighing was conducted using analytical balances and

microbalances from Sartorius (Göttingen, Germany), and homogenization was assisted by a Branson 5510 ultrasonic bath (Gemini b.v., Apeldoorn, The Netherlands).

Part B: Feasibility studies of a microwell array design for single-cell deposition

Cell culture experiments were conducted in a Memmert model icoMed incubator (Memmert, Schwabach, Germany) and handled under a Teslar BIO-II-A/P Class II microbiological safety cabinet. Cell counting was performed using a Neubauer chamber bright-line (Brand, Wertheim, Germany) and a Nikon Eclipse TS100 optical microscope equipped with a digital camera DXM1200 (Nikon Instruments Inc., New York, USA). Centrifugation was performed with Heraeus Megafuge 1.0R and 4115R (Eppendorf, Hamburg, Germany). An ML204/01 analytical balance from Mettler Toledo (Columbus, OH, USA) was used for weighing purposes. PDMS deposition was carried out using a WS-650 MZ-23 spin coater (Laurel Technologies, USA). Thermal curing was performed in a laboratory oven (J.P. Selecta, Barcelona, Spain). Optical and fluorescence imaging was performed with a Leica DMI6000 B microscope (Wetzlar, Germany).

5.2.2 Materials and Reagents

Part A: Feasibility studies of a gelatine-based microdroplet calibration approach

Gelatine powder derived from porcine skin (gel strength 300, Type A) was obtained from Sigma-Aldrich (Madrid, Spain). Nanoparticles standards, including 80 nm AgNPs, 30 nm AuNPs, and 100 nm AuNPs, were purchased from NanoComposix (San Diego, CA, USA). Microscope slides (Superfrost® Plus) were supplied by Thermo Scientific (Waltham, MA, USA). Ionic standard solutions of Au and Ag (1,000 μg mL^{-1}) were acquired from Chem-Lab NV (Zedelgem, Belgium), while In ionic standard solutions (1,000 μg mL^{-1}) was obtained from Inorganic Ventures (Christianburg, VA, USA). Nitric acid (S.G. 1.42, <68 %) and hydrochloric acid (S.G. 1.18, ~37 %), both trace analysis grade, were supplied by Fischer Scientific (Madrid, Spain). Hydrogen peroxide (30 %, analytical grade) was purchased from Merck.

Part B: Feasibility studies of a microwell array design for single-cell deposition

Dulbecco's Modified Eagle Medium (DMEM) from Cytiva, HyCLoneTH (Utah, USA) was used for cell culture. Human colorectal adenocarcinoma-drecived Caco-2 cells (Cell Biolabs, San Diego, CA, USA) were maintained in DMEM supplemented with 10 % (v/v) fetal bovine serum (FBS), 1.0 % (v) penicillin/streptomycin, and 1.0 % (v/v) essential amino acids (EAA), all supplied by Thermo Fischer Scientific (Waltham, MA, USA). Phosphate buffered saline solution (PBS, 1X, pH 7.4), was purchased from Life Technologies Limited (Paisley, UK). Cell exposure was carried in BioLite 6-well multidish (Thermo Fischer Scientific). Trypsin from porcine pancreas and sodium pyruvate were obtained from Sigma-Aldrich (St. Louis, MO, USA), as well as Sylgard 184 (761036-5EA). Invitrogen, NucBlue™ Live Cell Stain ReadyProbes™ reagent for cell stain was from Thermo Fischer Scientific. High-purity CO_2 (99.995 %) was supplied by Carburos Metálicos S.A. (Barcelona, Spain). Gold Nanospheres (AuNPs) of a nominal size 30 ± 3 nm by TEM (0.053 mg mL^{-1}, and number particle concentration 2.0×10^{11} particles mL^{-1}), and 61 ± 6 nm by TEM (0.055 mg mL^{-1}, 2.4×10^{10} particles mL^{-1}) were obtained from NanoComposix (San Diego, CA, USA).

USC UNIVERSIDADE DE SANTIAGO DE COMPOSTELA

5.2.3 Protocol to prepare gelatine microdroplets

Two types of gelatine microdroplets (MDs) were prepared: ionic-spiked MDs for external calibration and nanoparticle-spiked MDs for the assessment of transport efficiency. Both followed the same experimental procedure. Briefly, 0.1 g of gelatine powder was weighed into an Eppendorf tube and spiked with the appropriate volume of either multielement stock or intermediate solution to achieve the desired concentrations (Table 19). The volume was then adjusted to 1 mL with ultrapure water. The spiked gelatine solutions were homogenized by manual mixing with a pipette tip, avoiding bubble formation, followed by incubation in a water bath at 55 ºC until complete dissolution; sonication was applied when possible to further improve mixing. Microdroplets (<0.1 mg) of the resulting solution were deposited onto microscope slides using a pipette tip previously wetted with the gelatine solution. Since a microbalance was employed for weighing, standard slides were cut in half prior to spotting by marking, incising with a glass cutter, and applying gentle pressure to break along the marks. Finally, the slides were left to dry at room temperature and subsequently stored at 4 ºC until use.

Table 19. Spiked concentrations for the gelatine solutions.

	Spiked Concentrations (NPs mL^{-1})			
	AuNPs-30nm	**AuNPs-100nm**	**AgNPs-80nm**	**Ionic (Au and Ag)**
P0	0	0	0	0
P1	2.00E+04	5.60E+04	8.00E+04	1 mg L^{-1}
P2	2.00E+05	5.60E+05	8.00E+05	10 mg L^{-1}
P3	2.00E+06	5.60E+06	8.00E+06	50 mg L^{-1}
P4	2.00E+07	5.60E+07	8.00E+07	-
P5	2.00E+08	5.60E+08	8.00E+08	-

Figure 42 displays an image of some of the MDs prepared, exported directly from Chromium 3 software.

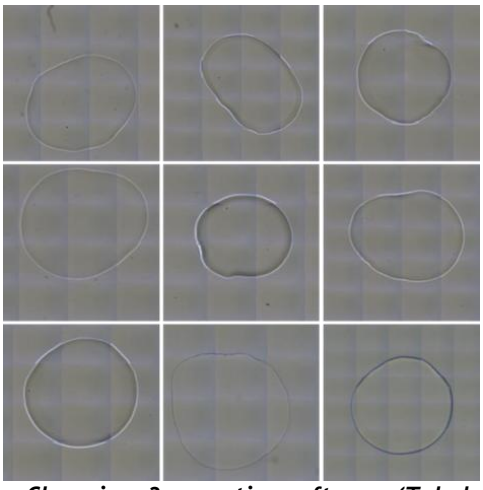

Figure 42. Exported images from Chromium 3 operating software (Teledyne Photon Machines) of some of the MDs prepared.

USC UNIVERSIDADE DE SANTIAGO DE COMPOSTELA

5.2.4 Design and manufacturing of a microwell array master mold by photolithography

The microwell array master mold was designed in AutoCAD (Autodesk Inc. San Francisco, CA) and fabricated though photolithography using a 200 mm silicon wafer as the substrate. Briefly, the fabrication of the silicon master mold started with a 2500 nm SiO_2 coating by SPTS plasma enhanced chemical vapor deposition (SPTS CVD MPX, Newport, RI, USA). The wafer was then coated with a 1035 nm AZ1505 positive photoresist and patterned using direct write laser (DWL 2000, Heidelberg, Germany). After development with AZ400K, the exposed areas were removed. SPTS Advanced Plasma System (SPTS APS LPX, Newport, RI, USA) was then used to etch the exposed SiO_2 layer, followed by plasma Asher (PVA TEPLA, Wettenberg, Germany) to remove the remaining photoresist. The exposed silicon substrate was etched through deep reactive ion etching (SPTS Pegasus, Newport, RI, USA) in steps of 2.5 min, measuring the trench depth after each step using optical profilometry (OPM Hyperion, Ettlingen, Germany), until reaching 50 μm. To remove residues, an oxygen plasma step was performed in the SPTS Pegasus, followed by hydrofluoric acid (HF) vapor etching (SPTS Primaxx, Newport, RI, USA) to remove any remaining SiO_2. Finally, the wafer was cut using an automatic dicing saw (Disco DAD 3350, Tokyo, Japan) to separate the silicon master. Master mold was then rinsed with 2-propanol, deionized water and dried with a N_2 gun, and visually inspected using FEI Quanta scanning electron microscope (SEM) (Hillsboro, OR, USA). Figure 43 shows the characterization of the silicon master mold, a square section of 5.0 × 5.0 cm divided into different regions.

5.2.5 Negative-PDMS mold from the master mold

From the master mold, a polydimethylsiloxane (PDMS) mold was produced. PDMS prepolymer and cross-linker were mixed at a ratio 10:1, degassed, and 2.0 g of the mixture was poured onto the master mold. Thereafter, the master mold with the PDMS layer was spincoated at 200 rpm for 45 s to ensure uniform distribution and cured at 100 ºC for 35 min. After curing, the PDMS mold containing microwells was carefully peeled off the master mold and stored at room temperature for subsequent experiments. PDMS molds were single-use only.

5.2.6 Cell culture and exposure

Human epithelial Caco-2 cells, derived from a colorectal adenocarcinoma, were used. Cells were grown in DMEM medium supplemented with 10 % (v/v) FBS, 1.0 % (v/v) penicillin/streptomycin, and 1.0 % (v/v) essential amino acids (EAA), at 37 ºC in a 5.0 % CO_2 humidified (95 %) air incubator.

For the exposure assay the BioLite 6-well multidish were used. Cells were exposed to 30 nm and 60 nm AuNPs at a cell:NP ratio of 1:50 for 24 hours. AuNPs suspensions were sonicated before use to avoid aggregation/agglomeration. Following exposure, cells were trypsinized, collected, centrifuged (400 g, 4 min, room temperature), washed twice with normal saline solution, and resuspended in DMEM medium.

USC UNIVERSIDADE DE SANTIAGO DE COMPOSTELA

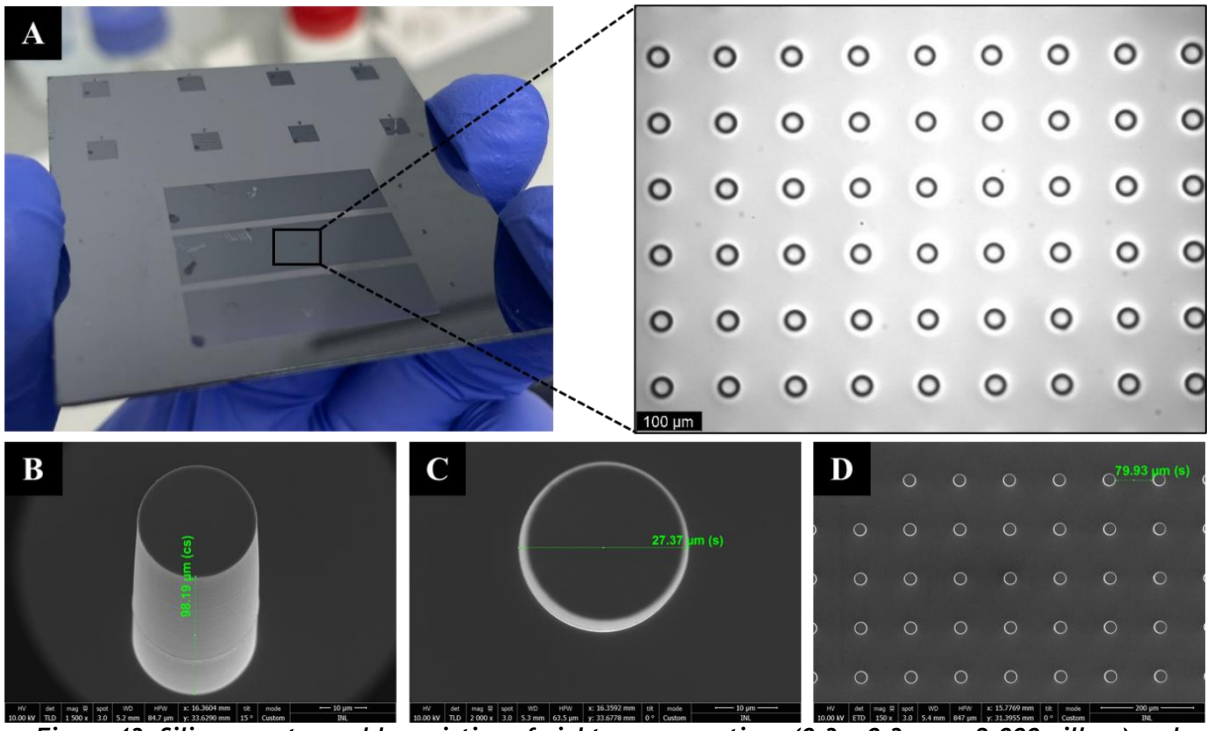

Figure 43. Silicon master mold consisting of eight square sections (0.3 x 0.3 cm, ~2,000 pillars) and three rectangular sections (0.6 x 2.5 cm, ~15,000 pillars) (A). Pillar characterization included measurements of height (B), diameter (C), and inter-well distance (D).

5.3 Results and Discussion

Part A: Feasibility studies of a gelatine-based microdroplet calibration approach

ICP-MS Bulk Analysis

Default instrumental and data acquisition parameters for ICP-MS analysis are reported in Table 20. A Setup Solution was used for daily tunning the ICP-MS before analysis. Internal standard calibration curve (In as IS) was used for quantification.

Table 20. Instrumental ICP-MS parameters.

Parameter	Value
RF Power	1550 W
RF Matching	1.80 V
Smpl Depth	4.5 mm
Nebulizer Gas	1.12 L min^{-1}
Scan Type	MS/MS
Resolution	Standard
Isotopes Monitored	^{107}Ag, ^{115}In, ^{197}Au

An aliquot of 0.05 g of the gelatine solutions prepared was subjected to acid digestion overnight. The conditions for AgNPs and ionic gelatines include a 4:1 mixture of 65 % (m/v) HNO_3 and 30 % (v/v) H_2O_2; whereas AuNPs gelatines were treated with Aqua Regia as a stronger oxidation process to ensure complete digestion was needed. All experiments were performed in

triplicate and digestion blanks were also prepared/measured. Gelatine quantification results are shown in Table 21.

Table 21. Gelatine quantification by ICP-MS.

Sample Name	[Gelatin] µg kg^{-1}	Sd (n=3)	RSD (%)
AgNPs 80 nm-P0	4.6	0.2	4.3
AgNPs 80 nm-P1	2.5	0.2	8.0
AgNPs 80 nm-P2	2.6	0.1	3.9
AgNPs 80 nm-P3	29.0	4.0	13.8
AgNPs 80 nm-P4	252.0	6.0	2.4
AgNPs 80 nm-P5	2384.0	61.0	2.6
AuNPs 30 nm-P0	n.d.	-	-
AuNPs 30 nm-P1	n.d.	-	-
AuNPs 30 nm-P2	n.d.	-	-
AuNPs 30 nm-P3	0.56	0.05	8.9
AuNPs 30 nm-P4	6.4	0.2	3.1
AuNPs 30 nm-P5	73.0	6.0	8.2
AuNPs 100 nm-P0	n.d.	-	-
AuNPs 100 nm-P1	n.d.	-	-
AuNPs 100 nm-P2	6.3	0.2	3.2
AuNPs 100 nm-P3	76.0	4.0	5.3
AuNPs 100 nm-P4	745.0	3.0	0.4
AuNPs 100 nm-P5	6,808.0	19.0	0.3
Ionic Ag-P0	1.32	0.22	16.30
Ionic Ag-P1	245.67	2.64	1.07
Ionic Ag-P2	1,937.78	624.72	32.24
Ionic Ag-P3	9,914.49	3,175.43	32.03
Ionic Au-P0	n.d.	-	-
Ionic Au-P1	1,585.83	249.42	15.73
Ionic Au-P2	9,251.35	299.95	3.24
Ionic Au-P3	45,612.27	3,969.28	8.70

LA-ICP-TOF-MS Analysis

The Standard Reference Material (SRM 612, trace elements in glass) from NIST was used for tunning purposes in terms of sensitivity (In, U, Co), fractionation (U/Th), and level of oxides (ThO/Th). LA-ICP-TOF-MS tune conditions included: 4 J cm^{-2}, laser fluence; 50 Hz, repetition rate; 10 µm circle, beam size; and 20, dosage.

– Laser Fluence Optimization

The effect of the laser fluence was evaluated along the range 0.2-3 J cm^{-2}. The optimum laser fluence value needs to be below the glass slide ablation threshold and must ensure the minimal degradation of NPs. For this purpose, it is essential to calculate the correct dosage for each laser fluence value. For that, two unspiked MDs (only IS) were selected, and the number of shots (particle count, for the case) needed for a complete ablation of the gelatine were calculated. Results are presented in Table 22 and Figure 44.

USC UNIVERSIDADE DE SANTIAGO DE COMPOSTELA

Table 22. Number of shots per laser fluence value.

	Laser Fluence J cm^{-2}										
MD-1	**0.2**	**0.3**	**0.4**	**0.5**	**0.6**	**0.8**	**1.0**	**1.5**	**2.0**	**2.5**	**3**
Particle Count	43	44	41	40	29	35	30	25	24	24	21
Sd	7	7	6	6	5	6	5	5	5	5	5
Detection Threshold	8	8	8	8	8	8	10	8	8	8	8
MD-2	**0.2**	**0.3**	**0.4**	**0.5**	**0.6**	**0.8**	**1**	**1.5**	**2**	**2.5**	**3**
Particle Count	31	28	24	26	24	25	19	13	9	7	9
Sd	6	5	5	5	5	5	4	4	3	3	3
Detection Threshold	20	20	20	20	20	20	20	20	20	20	20

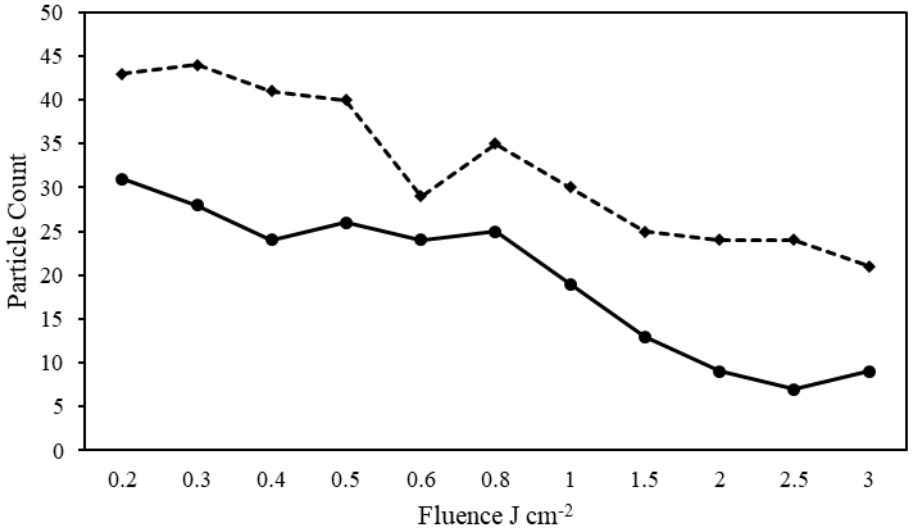

Figure 44. Graphical representation of the particle count per laser fluence value in microdroplet 1 (dashed black line) and microdroplet 2 (solid black line).

A fixed dosage of 50 would ensure a complete gelatine ablation even at the lowest applied fluence (0.2 J cm^{-2}). Nevertheless, the ablation threshold of the glass must also be considered. As illustrated in Figure 45, the glass signal contribution becomes evident at a laser fluence of 1 J cm^{-2} (B), when compared with a lower fluence, 0.8 J cm^{-2} (A). This effect was also visible from 1.5 J cm^{-2} onwards, as it is shown in Figure 46.

Finally, using a fixed dosage of 50 and excluding laser fluences greater than 2 J cm^{-2}, the influence of laser fluence (0.2 – 2.0 J cm^{-2}) on NP degradation was evaluated. For this purpose, a MD containing 100 nm-AuNPs was selected and subjected to line scanning. Figure 47 shows a zoom-in gold intensity time scan using two different laser fluences, and the corresponding signal histogram for each of them. From this figure, it can be seen how the use of a high laser fluence (2.0 J cm^{-2}) decreases the mean intensity of the distribution, which could be translated into NP degradation. Therefore, using high laser fluence not only affects the ablation process (in terms of having a contribution from the glass slide), but also has an impact on the NP's integrity, which would ultimately affect the particle size determination.

USC UNIVERSIDADE DE SANTIAGO DE COMPOSTELA

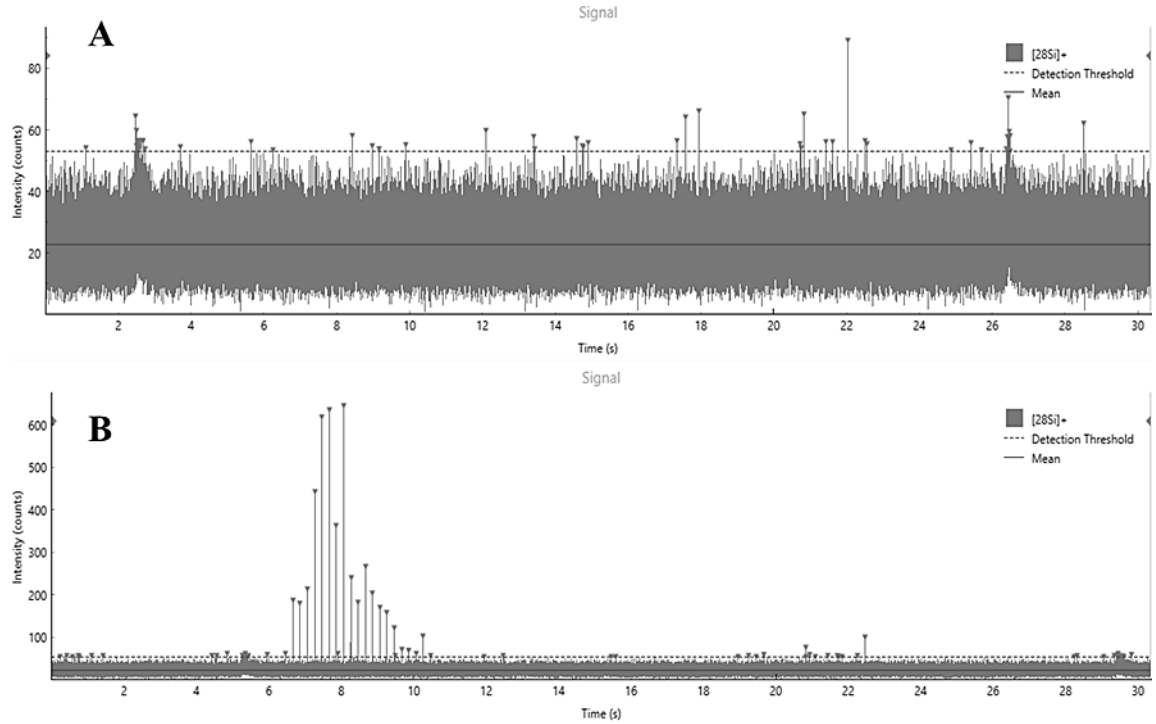

Figure 45. Signal contribution from the glass slide in B, compared to the background signal in A.

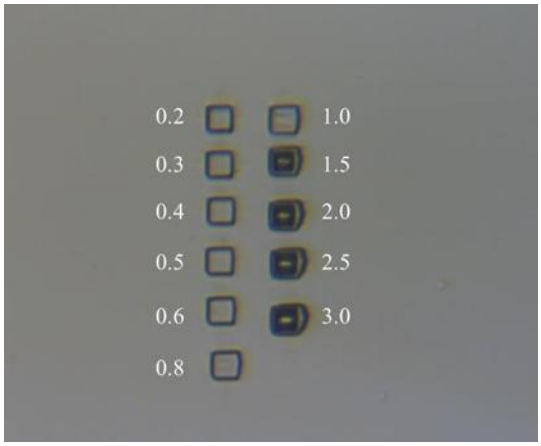

Figure 46. Effect of the laser fluence upon ablation.

For all the above mentioned, and taking into consideration the available literature on NP analysis in biomaterials using LA-ICP-MS, the selected laser fluence was 0.4 J cm^{-2}. The LA-ICP-MS operating conditions employed in subsequent experiments include: 0.4 J cm^{-2}, laser fluence; 1000 Hz, repetition rate; 20 µm square, beam size; 50, dosage; 250 µm s^{-1}, scan speed.

USC
UNIVERSIDADE DE SANTIAGO DE COMPOSTELA

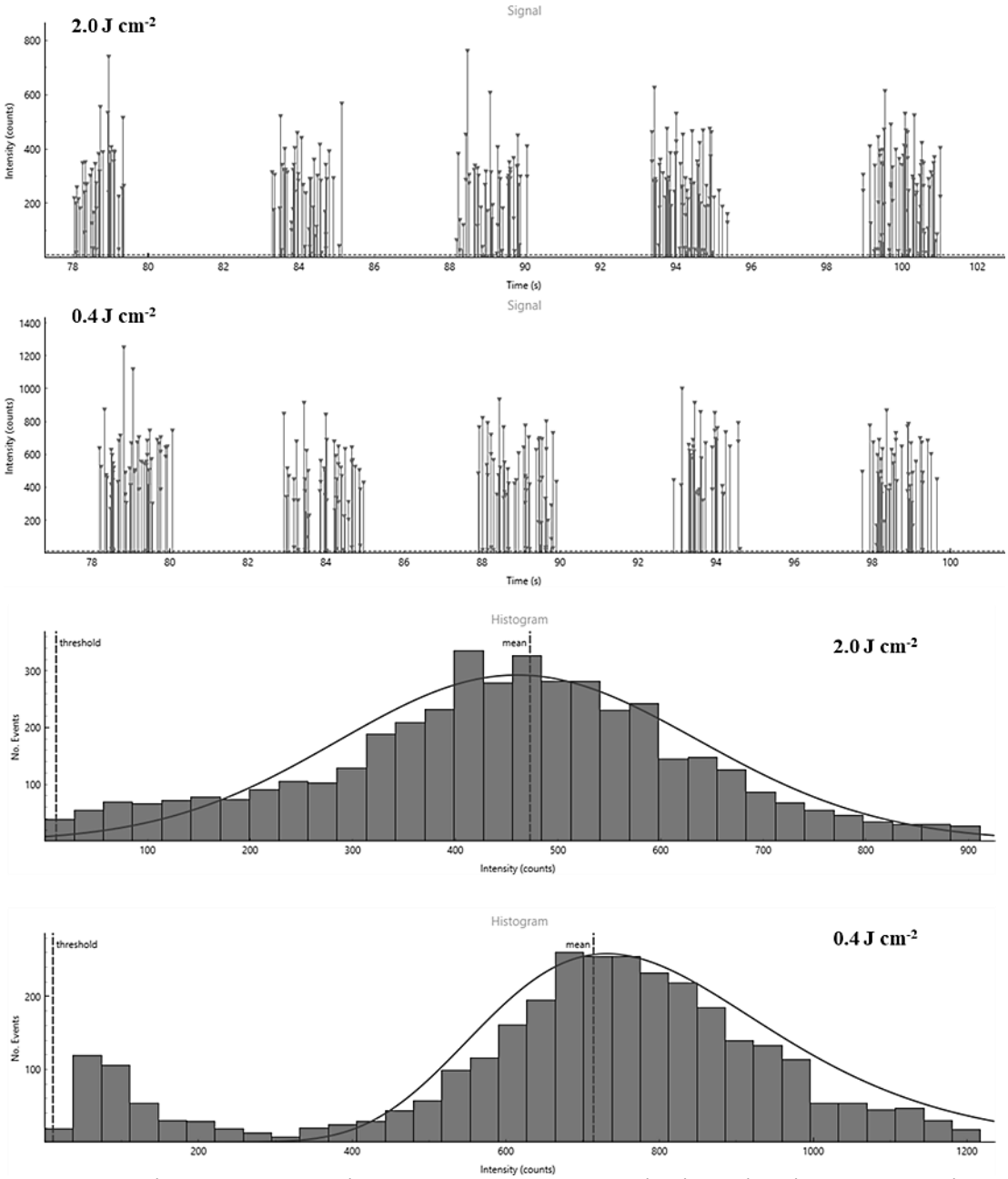

Figure 47. Comparison between the time scan and the corresponding intensity histogram of a high (2.0 J cm^{-2}) and low (0.4 J cm^{-2}) laser fluence.

– Homogeneous/Heterogeneous character of the MDs prepared

The microdroplet approach opens a new possibility for the complete analysis of a droplet within a short scan time, and would solve the problem of representativeness when dealing with heterogenous samples. To assess the homogeneous/heterogenous nature of the prepared MDs, the number of laser shots required for complete gelatine ablation was determined by monitoring the indium (In) signal (used as IS) under different laser fluence conditions. Results are presented in Figure 48.

USC UNIVERSIDADE DE SANTIAGO DE COMPOSTELA

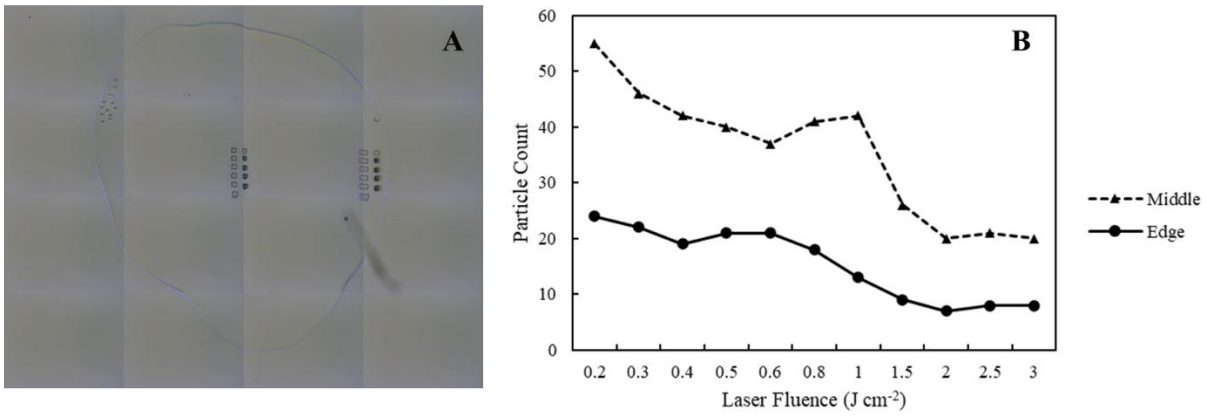

Figure 48. Image obtained from the Chromium software with the middle and edge positions ablated (A), and the particle count of In in those positions under different laser fluences applied (B).

From the Figure 48 it can be seen that the number of shots needed for a complete ablation in the middle position within a MD is higher compared to the edge position, which can be translated into a higher concentration in the middle compared to the edge. The distribution of the IS (ionic) within the droplet is expected to be nearly homogeneous. However, variations in the distribution have been found and this effect can be assumed to be more severe for the case of NPs distribution. For this reason, the use of microdroplets would be an attractive and advantageous approach to follow.

– Evaluation of the Transport Efficiency (TE)

Transport efficiency, % TE, also known as detection-efficiency factor, can be defined as the ratio of the amount of analyte reaching the plasma (and ultimately the detector) compared to the amount of analyte introduced to the system by the sample introduction system. This means that this parameter considers the losses induced by ablation, condensation in the ablation chamber, transport, ionization, and counting. Originally, the study of this parameter was not closely monitored, and it was assumed to be 100 % when using laser ablation as introduction system. However, more recently, some authors have reported transport efficiencies lower than 100 %, pointing to sample deposition and condensation upon ablation as the primary source of sample losses. To study this parameter, we analysed MDs containing 100 nm-AuNPs and 30 nm-AuNPs. Experiments were performed in triplicate. TE was calculated as follows:

$$\%\,TE = \frac{Number\ of\ particles\ by\ LA-SP-ICP-TOF-MS}{Mean\ number\ of\ particles\ from\ bulk\ analysis\ by\ ICP-MS} \times 100$$

Results based on the bulk analysis for the gelatine concentration determination are presented in Table 23. SPCal Software (version 1.1.6) was used to obtain the Number Particle Count, with a threshold of 280 counts. Based on these results, the mean transport efficiency (% TE) was approximately 102 % and 101 % for 100 nm-AuNPs, and 30 nm-AuNPs, respectively.

USC UNIVERSIDADE DE SANTIAGO DE COMPOSTELA

Table 23. TE (%) calculation for 100 nm and 30 nm AuNPs (n=3).

	LA-ICP- TOF-MS Counts	Sd	ICP-MS Counts	Sd	% TE	% RSD
			100 nm-AuNPs			
MD-1	3293	62	3150	12	104	2
MD-2	5379	73	5512	21	98	1
MD-3	4138	64	3937	15	105	2
			30 nm-AuNPs			
MD-1	1475	38	1545	46	95	4
MD-2	1497	39	1452	49	103	5
MD-3	1217	35	1159	42	105	5

– High resolution mapping and spatial biodistribution of gold and silver within a MD

Laser settings for the mapping analysis include: 10 ms Signal Pulse Response, dosage 1, 100 Hz repetition rate, 10 µm x 10 µm X, Y spot size. Data produced from this experiment can be visualized in Figure 50, 51, and 52. HDIP software was used to produce the images.

Manually spotting microdroplets onto a microscope slide can not be considered easily reproducible, the mass and shape of the MDs vary from one to the other. These fluctuations would eventually affect the distribution of the analytes within the MD. In Figure 49, the MD obtained had a very uniform and regular shape and the distribution of both, silver and indium, was essentially homogeneous. However, taking a closer look to the ^{115}In map intensity, it can be appreciated how the MD perimeter has a lower concentration compared to the core area.

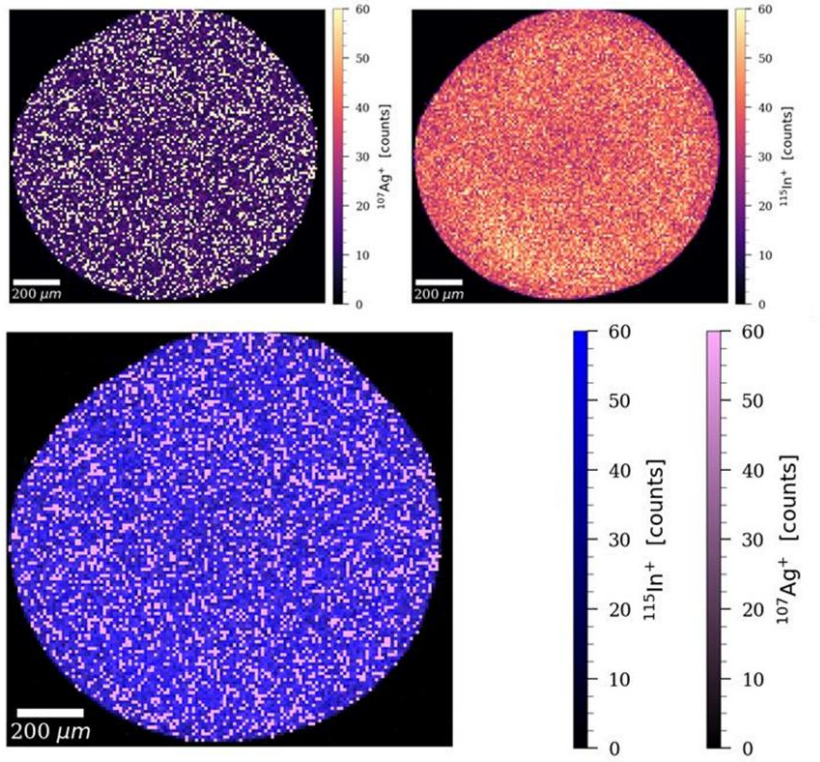

Figure 49. Images showing ^{115}In (used as IS) and ^{107}Ag map intensities within a MD.

USC UNIVERSIDADE DE SANTIAGO DE COMPOSTELA

Meanwhile, for the case of gold (Figures 50 and 51), the MDs spotted had a more inconsistent shape, which led to a more irregular and heterogeneous distribution of the analytes. Figure 50 shows the ^{197}Au map intensity for a MD spiked at P5 concentration level (see Table 19), and the ^{115}In map intensity (used as IS). Figure 51 highlights in yellow the 100 nm-AuNPs within a MD spiked at P3 concentration level (see Table 19).

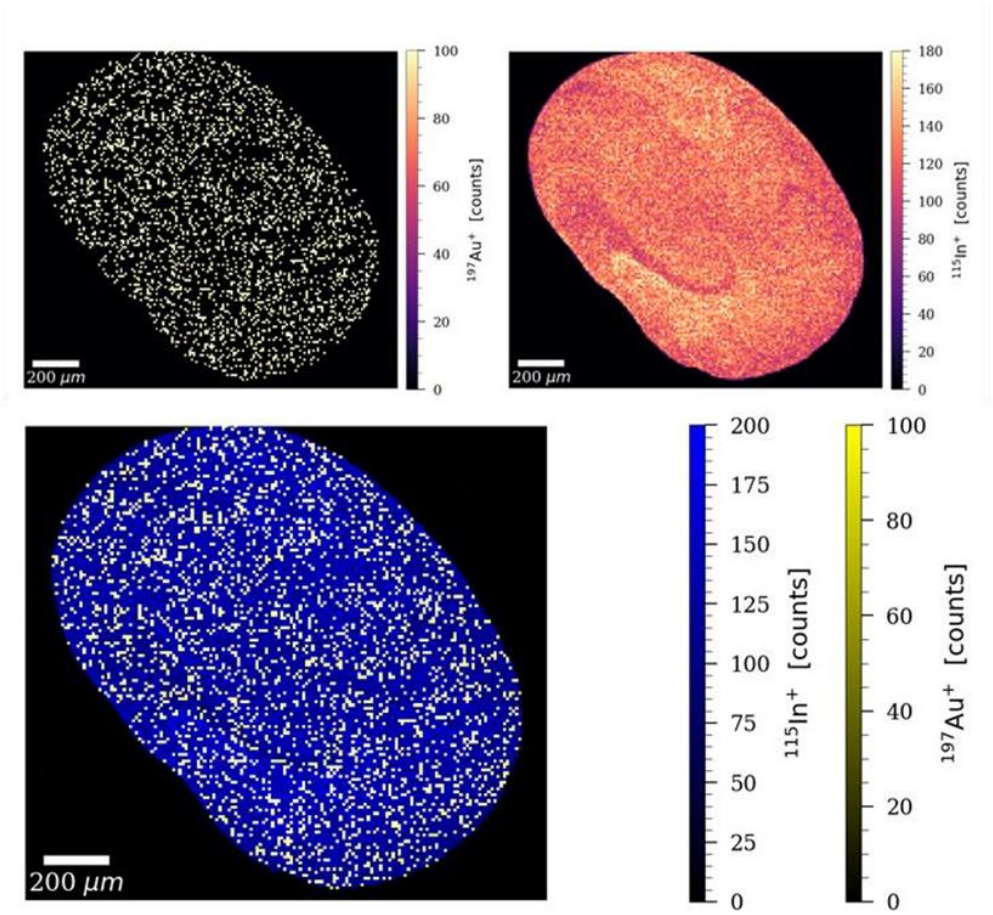

Figure 50. Images showing ^{115}In (used as IS) and ^{197}Au map intensities within a MD.

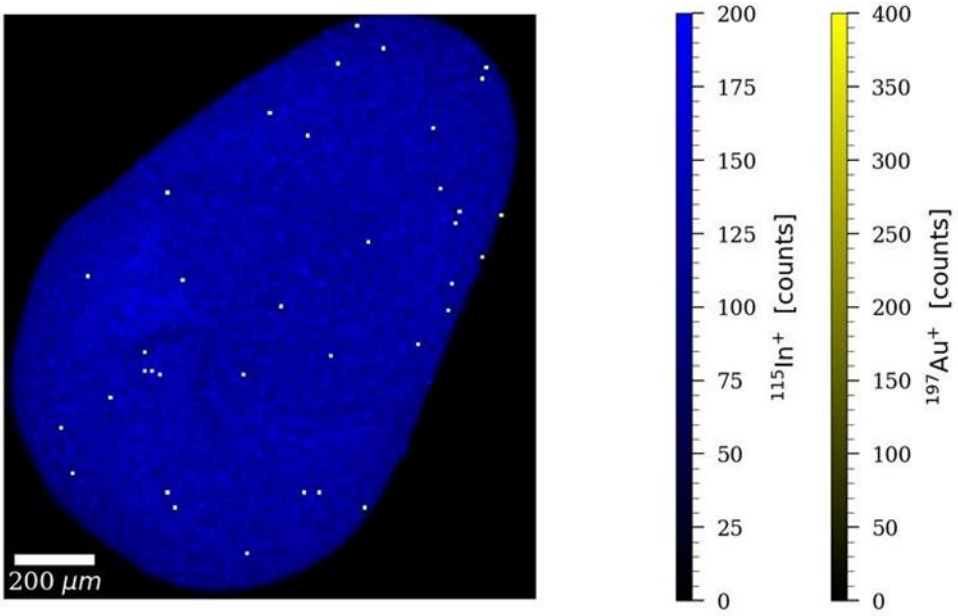

Figure 51. Map intensity of a less concentrated 100 nm-AuNPs gelatine standard (In used as IS).

Part B: Feasibility studies of a microwell array design for single-cell trapping– Optimization

The process of cell trapping within microwell arrays needs to be carefully investigated to maximize single-cell occupancy. Several parameters influence trapping including efficiency, settling time, cell concentration, cell resuspension media, the presence or absence of a CO_2 atmosphere, and differential behaviour of exposed *versus* unexposed cells. The overarching aim is to develop and optimize a strategy that can be subsequently applied to LA-ICP-MS as a single-cell approach. In this context, microwell dimensions play a crucial role, as they must be tailored to accommodate only one cell per microwell.

The optimization process consisted in maximizing the percentage of microwells occupied by a single cell relative to those that contained multiple cells or remained empty. To enable microscopic evaluation, cells (Caco-2) were stained after culture and immediately prior to deposition. Since the staining agent employed specifically targeted the cell nucleus, it was possible to visually discriminate between single- and multi-cell occupancy. For each experimental parameter, more than 500 microwells were considered to ensure statistical reliability. All experiments were performed in duplicate.

In-house CO_2 chamber

Due to the hydrophobic character of PDMS, air bubbles were present inside the microwells. When the cell suspension was poured onto the PDMS mold, these trapped air bubbles created significant resistance to cell entry and settlement. To overcome this limitation, an in-house CO_2 chamber was fabricated to locate the PDMS mold inside during the cell trapping process. The chamber comprises four inlets: (i) two for CO_2 gas introduction, (ii) one for cell suspension delivery, and (iii) one for pressure release. Initially, the chamber containing the PDMS mold is purge at a CO_2 flow rate of 280 mL min^{-1}. During cell trapping, CO_2 flow is maintained at a reduced flow rate of 28 mL min^{-1}.

In experiments conducted without a CO_2 atmosphere, no cells were observed within the microwells. This may be attributed to the fact that air bubbles would not be displaced or dissolve in DMEM, thereby preventing cell entry. In contrast, CO_2 readily dissolves in the medium, avoiding resistance and facilitating effective cell entry and deposition. Therefore, all subsequent experiments will be performed under a CO_2–controlled atmosphere to ensure efficient cell entry and deposition.

Settling time

Settling time can be defined as the time required for a cell to settle inside a microwell. This parameter is critical because very short times may be insufficient for an optimum cell occupancy; whereas longer times may increase the likelihood of multiple cells occupying the same microwell. In the present study, the influence of settling times of 15, 30, and 60 min was evaluated using unexposed Caco-2 cells.

Results are presented in Table 24 and Figure 52. It can be observed that the percentage of well occupancy by only one cell remained virtually constant across all time intervals, with only a slight increase observed at 60 min. However, this increase does not justify extending the deposition period to four times longer, given the negligible improvement in single-cell occupancy. Therefore, 15 min was selected as the optimum settling time. Figure 55 (SI) illustrates real microscope images taking under natural lighting and using a DAPI filter.

Table 24. Total number of microwells considered, number of occupied microwells, and percentage of microwell occupancy for different time intervals.

Time (min)	Total number of microwells	Number of occupied microwells				% Microwell occupancy				
		Total	1 cell	2 cell	> 2 cell	Total	1 cell	2 cell	> 2 cell	> 1 cell
15	654	307	185	72	50	46.9	60.3	23.5	16.3	39.7
30	673	403	223	126	54	59.9	55.3	31.3	13.4	44.7
60	728	393	249	114	30	54.0	63.4	29.0	7.6	36.6

Cell concentration

Cell concentration is a critical parameter in the optimization process. The suspension must provide an adequate number of cells relative to the total number of microwells to ensure efficient occupancy. However, excessively high concentrations may induce either cell aggregation and agglomeration, or multiple-cell occupancy, thereby compromising single-cell trapping efficiency.

The influence of cell concentration was evaluated at 100,000 cells mL^{-1}, 200,000 cells mL^{-1}, and 400,000 cells mL^{-1}. The highest concentration tested resulted in high agglomeration/aggregation phenomena. Results for 100,000 cells mL^{-1} and 200,000 cells mL^{-1} are presented in Table 25 and Figure 53. Considering the percentage of microwell occupancy, no statistically significant differences are found between the two levels of concentration tested. However, the percentage of single-cell microwells occupancy is higher for the lower concentration (55.3 %), as it could be expected. Increasing the concentration leads to an increase in the percentage of multi-cell microwell occupancy, which should be avoided. Therefore, 100,000 cells mL^{-1} was selected as the optimum cell concentration.

USC UNIVERSIDADE DE SANTIAGO DE COMPOSTELA

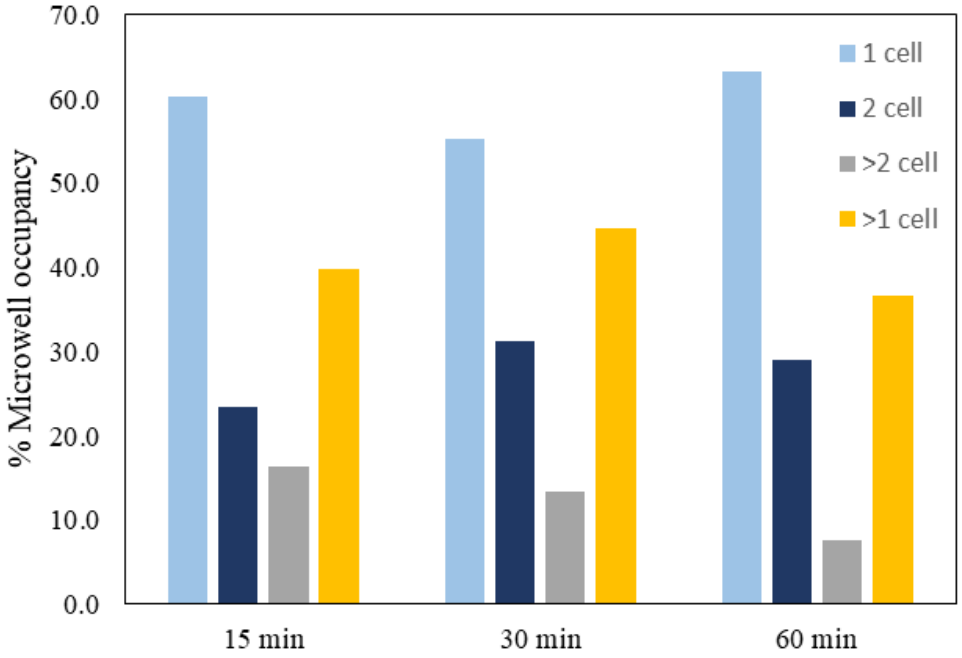

Figure 52. Influence of the settling time on the percentage of microwell occupancy based on single-cell or multiple-cell occupancy. Conditions: CO_2 atmosphere, 100,000 cells mL^{-1} cell concentration, DMEM resuspension medium.

Table 25. Total number of microwells considered, number of occupied microwells, and percentage of microwell occupancy for different cell concentrations.

Cell Concentration (cells mL^{-1})	Total number of microwells	Number of occupied microwells				% Microwell occupancy			
		Total	1 cell	2 cell	> 2 cell	Total	1 cell	2 cell	> 2 cell
100,000	673	403	223	126	54	59.9	55.3	31.3	13.4
200,000	792	477	214	127	98	60.2	44.9	26.6	20.5

Resuspension media: DMEM/PBS

To investigate strategies for improving cell dispersion, a 1.0 % PBS solution was evaluated as potential resuspension medium. Contrary to the initial hypothesis, PBS did not promote homogeneous suspension; instead, it induced cellular aggregation and agglomerate formation, as it was previously observed under high cell concentrations. This fact may be attributed to differences in composition. DMEM is a nutrient-rich, protein-supplemented medium, where proteins and other macromolecules can adsorb onto cell membranes, creating steric hindrance and electrostatic stabilization. In contrast, PBS is a simple salt solution that contains phosphate and chloride ions at relatively high concentrations. This increases ionic strength, which can screen the negative surface charges of cells, thereby facilitating membrane-membrane contact and promoting aggregation.

USC UNIVERSIDADE DE SANTIAGO DE COMPOSTELA

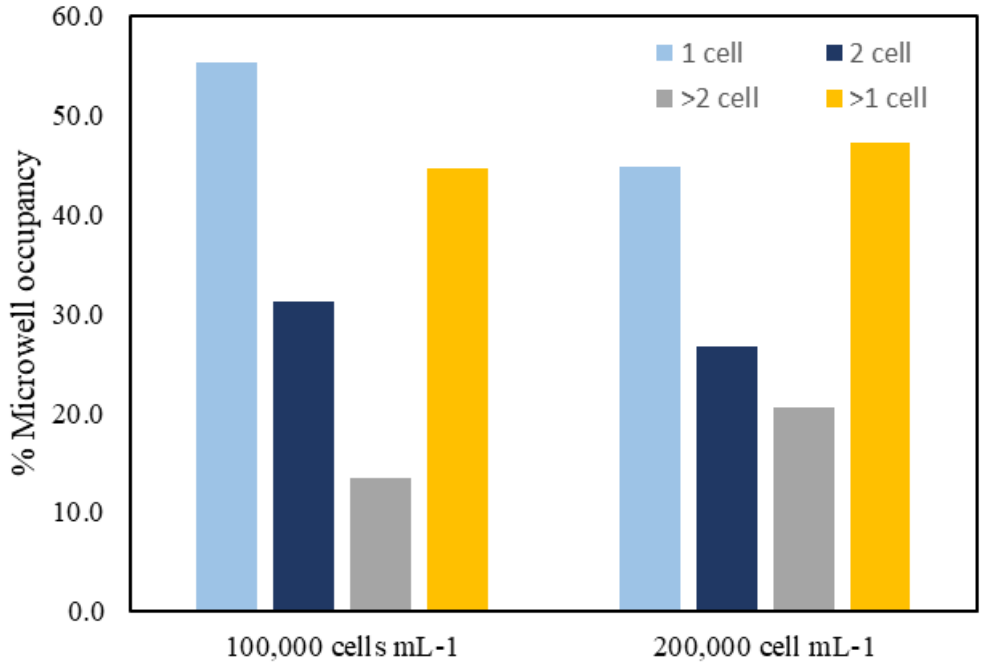

Figure 53. Influence of cell concentration on the percentage of microwell occupancy based on single-cell or multiple-cell occupancy. Conditions: CO_2 atmosphere, 30 min settling time, DMEM resuspension medium.

Cell trapping behaviour between exposed and unexposed Caco-2 cells

The final parameter evaluated was the behaviour of Caco-2 cells under NP exposure compared with unexposed controls. This assessment is particularly relevant since, as previously noted, the microwell dimensions were optimized to accommodate a single cell. Thus, NP-induced alterations in cell size could directly influence trapping efficiency. To investigate this, Caco-2 cells were exposed for 24 hours to AuNPs at a cell-to-NP ratio of 1:50, employing 30 nm and 60 nm AuNPs standards. Control cells, not subjected to NP exposure, underwent the same experimental conditions to ensure comparability. All experiments were conducted in duplicate, and the resulting data are presented in Table 26 and Figure 54.

Table 26. Percentage of microwell occupancy for control (unexposed) and exposed Caco-2 cells (n=2).

	% Microwell occupancy				
	Total	**1 cell**	**2 cell**	**> 2 cell**	**> 1 cell**
Control	61.3	79.9	19.5	2.1	21.6
30 nm AuNPs	52.1	71.3	21.6	7.4	29.0
60 nm AuNPs	32.5	83.5	14.0	3.2	17.2

USC UNIVERSIDADE DE SANTIAGO DE COMPOSTELA

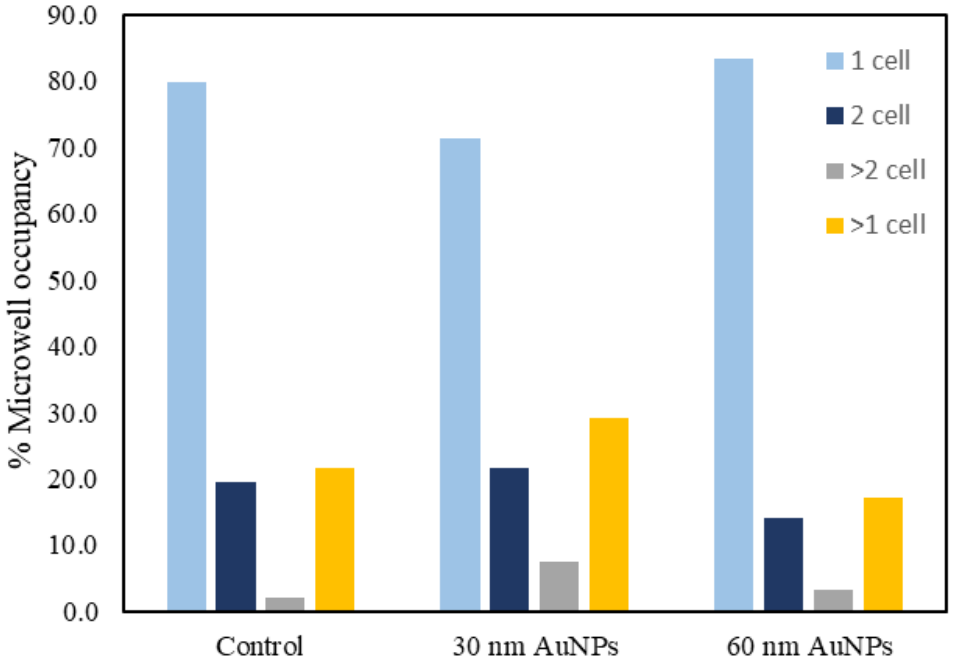

Figure 54. Different behaviour of control (unexposed) Caco-2 cells versus exposed cells to 30 nm AuNPs and 60 nm AuNPs. (Conditions: 24 h exposure, cell:NP ratio 1:50).

From the results it can be seen that control cells achieved the highest overall occupancy (61.3 %). Exposure to 30 nm AuNPs reduced occupancy moderately (52.1 %), whereas 60 nm AuNPs led to a more pronounced reduction (32.5 %). This may suggest that AuNP exposure, particularly with larger particles, decreases the cell trapping efficiency. Although differences in overall occupancy were found, the percentage of microwells containing a single cell was relatively high across conditions: 79.9 % in controls, 71.3 % with 30 nm AuNPs, and 83.5 % with 60 nm AuNPs. Regarding multi-cell occupancy, percentages higher than 20 % were found for both controls and Caco-2 cells exposed to 30 nm AuNPs; while exposure to 60 nm AuNPs showed the lowest > 1 cell occupancy (17.2 %).

In summary, these findings may indicate that NP exposure modulates cell trapping efficiency in a size-dependent manner, with smaller particles promoting cellular aggregation and larger particles reducing overall trapping efficiency.

5.4 Conclusions

This study presents two major contributions to the advancement of LA-ICP-MS: the estbalishment of a gelatine microdroplet-based calibration strategy and the development of a microwell array for controlled single-cell deposition. Together, these innovations address critical methodological limitations in calibration reliability and single-cell handling. Although they are preliminary results, they show promising potential in the applicability of LA-ICP-MS to biological and toxicological research.

The gelatine microdroplet calibration approach demonstrated several advantages over conventional matrix-mathced standards. Complete ablation of mcirodroplets eliminated the representativeness issues common in section- or droplet- bassed approaches. Thereby, showing promising potential as robust standards, facilitating accurate quantification of metals and NPs.

USC
UNIVERSIDADE DE SANTIAGO DE COMPOSTELA

The microwell array provided a platform for high-throughput single-cell trapping. Microwell dimensions need to be carefully studied depending on cell size and exposure conditions.

Future efforts would include validation of these two approaches as well as extend evaluation to additional cell lines ans biological systems.

5.5 REFERENCES

[1] X. Yu, M. He, B. Chen, B. Hu, Recent advances in single-cell analysis by inductively coupled plasma-mass spectrometry: A review, Anal. Chim. Acta. 1137 (2020) 191–207. https://doi.org/10.1016/j.aca.2020.07.041.

[2] M. Nasrollahzadeh, S.M. Sajadi, M. Sajjadi, Z. Issaabadi, Applications of Nanotechnology in Daily Life, 1st ed., Elsevier Ltd., 2019. https://doi.org/10.1016/B978-0-12-813586-0.00004-3.

[3] A. Abend, D. Sperger, D.A. Diaz, R. Guo, R. Reul, S.J. Wu, Industry's perspective on challenges assessing the in vivo impact of removing titanium dioxide (TiO2) from drug products, J. Pharm. Sci. 113 (2024) 3119–3122. https://doi.org/10.1016/j.xphs.2024.08.002.

[4] C.A. Dos Santos, M.M. Seckler, A.P. Ingle, I. Gupta, S. Galdiero, M. Galdiero, A. Gade, M. Rai, Silver nanoparticles: Therapeutical uses, toxicity, and safety issues, J. Pharm. Sci. 103 (2014) 1931–1944. https://doi.org/10.1002/jps.24001.

[5] I.L. Hsiao, F.S. Bierkandt, P. Reichardt, A. Luch, Y.J. Huang, N. Jakubowski, J. Tentschert, A. Haase, Quantification and visualization of cellular uptake of TiO2 and Ag nanoparticles: Comparison of different ICP-MS techniques, J. Nanobiotechnology. 14 (2016) 1–13. https://doi.org/10.1186/s12951-016-0203-z.

[6] S. Becker, S. Becker, Bioimaging of Metals and Proteomic Studies of Clinical Samples by Laser Ablation Inductively Coupled Plasma Mass Spectrometry (LA-ICP-MS), Anal. Tech. Clin. Chem. Methods Appl. (2012) 479–505. https://doi.org/10.1002/9781118271858.ch17.

[7] A. Lores-Padín, B. Fernández, M. García, H. González-Iglesias, R. Pereiro, Real matrix-matched standards for quantitative bioimaging of cytosolic proteins in individual cells using metal nanoclusters as immunoprobes-label: A case study using laser ablation ICP-MS detection, Anal. Chim. Acta. 1221 (2022). https://doi.org/10.1016/j.aca.2022.340128.

[8] A. Lores-Padín, R. Pereiro, B. Fernández, Laser Ablation ICP-MS: New Instrumental Developments, Applications and Trends, in: F. Atta-ur-Rahman, S.A. Ozkan (Eds.), Recent Adv. Anal. Tech., 2020: pp. 1–26.

[9] D. Drescher, C. Giesen, H. Traub, U. Panne, J. Kneipp, N. Jakubowski, Quantitative imaging of gold and silver nanoparticles in single eukaryotic cells by laser ablation ICP-MS, Anal. Chem. 84 (2012) 9684–9688. https://doi.org/10.1021/ac302639c.

[10] A. Arakawa, N. Jakubowski, G. Koellensperger, S. Theiner, A. Schweikert, S. Flemig, D. Iwahata, H. Traub, T. Hirata, Quantitative imaging of silver nanoparticles and essential

elements in thin sections of fibroblast multicellular spheroids by high resolution laser ablation inductively coupled plasma time-of-flight mass spectrometry, Anal. Chem. 91 (2019) 10197–10203. https://doi.org/10.1021/acs.analchem.9b02239.

[11] M. Wang, L.N. Zheng, B. Wang, H.Q. Chen, Y.L. Zhao, Z.F. Chai, H.J. Reid, B.L. Sharp, W.Y. Feng, Quantitative analysis of gold nanoparticles in single cells by laser ablation inductively coupled plasma-mass spectrometry, Anal. Chem. 86 (2014) 10252–10256. https://doi.org/10.1021/ac502438n.

[12] A. Schweikert, S. Theiner, D. Wernitznig, A. Schoeberl, M. Schaier, S. Neumayer, B.K. Keppler, G. Koellensperger, Micro-droplet-based calibration for quantitative elemental bioimaging by LA-ICPMS, Anal. Bioanal. Chem. 414 (2022) 485–495. https://doi.org/10.1007/s00216-021-03357-w.

[13] M. Šala, V.S. Šelih, J.T. Van Elteren, Gelatin gels as multi-element calibration standards in LA-ICP-MS bioimaging: Fabrication of homogeneous standards and microhomogeneity testing, Analyst. 142 (2017) 3356–3359. https://doi.org/10.1039/c7an01361b.

USC UNIVERSIDADE DE SANTIAGO DE COMPOSTELA

SUPPLEMENTARY INFORMATION

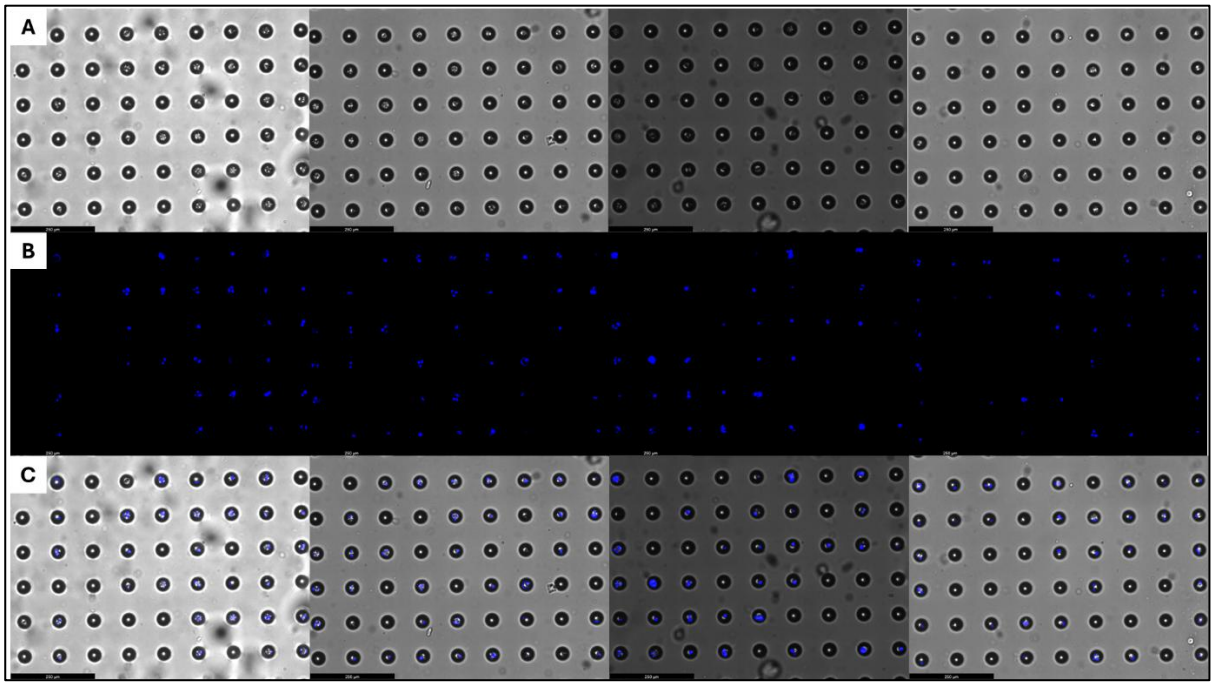

Figure 55. Microscope images under natural lighting (A), using a DAPI filter (B), and the overlay result (C). (Conditions: unexposed Caco-2 cells, 30 min settling time, 100,000 cell mL^{-1}, DMEM resuspension medium, CO_2 atmosphere).

USC
UNIVERSIDADE DE SANTIAGO DE COMPOSTELA

V. INTEGRATIVE DISCUSSION

USC
UNIVERSIDADE
DE SANTIAGO
DE COMPOSTELA

INTEGRATIVE DISCUSSION

This section provides an overview of the development of the doctoral thesis studies. The thesis manuscript is structured as a series of research articles corresponding to different chapters. In general terms, the thesis addresses pressing analytical and toxicological challenges by developing, applying, and refining advanced (ICP-MS)-based techniques. The individual studies collectively contribute to the field of nanometrology by targeting different aspects of NP detection, quantification, and characterization across environmental and biological matrices. The progression across the five chapters could be described as:

- Chapter 1: environmental exposure detection
- Chapter 2 and 3: biological monitoring in fluids
- Chapter 4: cellular uptake dynamics
- Chapter 5: methodological innovative tools for LA-ICP-MS

From the detection of Ag and TiO_2NPs in tap water, through their presence and quantification in human urine and serum, to their uptake at the cellular level, and finally to the development of innovative strategies for LA-ICP-MS, the thesis offers a comprehensive perspective on the fate and measurement of inorganic NPs. While each chapter stands on its own as a contribution to a particular analytical problem, the value of this thesis lies in the way these contributions interlock, providing a bigger picture that links external exposure to internal distribution and cellular interaction. Figure 57 displays a scheme of the thesis development in terms of individual contributions and how they fit together as a whole.

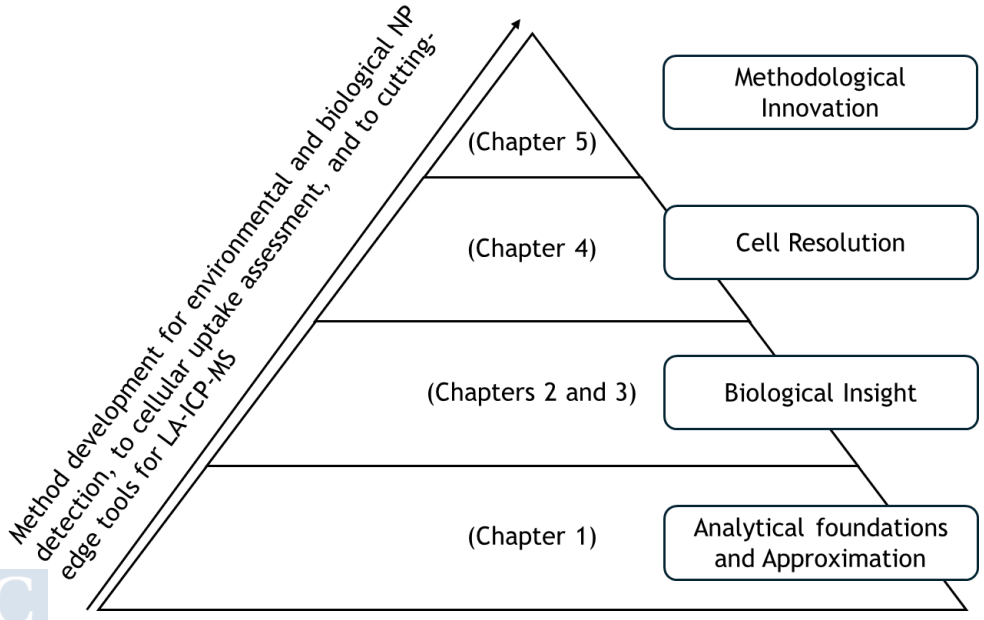

Figure 56. Overview of the connection between chapters.

USC UNIVERSIDADE DE SANTIAGO DE COMPOSTELA

The following discussion integrates the results obtained across the five chapters, hihglighting not only individual findings but also the overall insights from considering them together.

Integrative framework

A central insight that emerges from the five studies is that NP analysis can not be confined to a single domain. The pathways of exposure, distribution, and biological interaction require multiple compartments, from environmental waters that serve as sources of exposure, through human biofluids that reflect distribution and clearance, to the cellular level where toxicological effects are ultimately mediated. Therefore, the integrative framework encompasses both environmental and biological contexts.

- Environmental compartment: tap water as an exposure source

Chapter 1 represents the environmental dimension of NP exposure by investigating the occurrence of Ag and TiO_2NPs in tap water as a representative environmental matrix. Tap water, as a primary route of ingestion, constitutes a critical entry point for NPs into the human body. While measured concentrations are typically low, their presence raises concerns due to the involuntary and constant nature of exposure.

The study highlights two aspects: (i) the optimization of surfactant-assisted dispersive liquid-liquid microextraction (SA-DLLME) to preconcentrate NPs from dilute aqueous matrices, and (ii) the ability of spICP-MS for the detection, quantification, and characterization of NPs in terms of concentration and size distribution.

The findings from this first investigation brought to light the inherent challenges associated with NP detection and quantification. NP integrity emerged as a critical parameter to be considered throughout the analytical process. Since spiked tap water samples were employed, changes in NP pyshico-chemical characteristics were observed due to matrix nature. Specifically, AgNPs exhibited sensitivity to dissolution, whereas TiO_2NPs demonstrated a strong tendency to aggregate and agglomerate. Importantly, these transformations were not induced by the SA-DLLME methodology itself.

- Biofluids as biomonitoring matrices: urine and serum

Once NPs enter the body, they undergo distribution, transformation, and eventual clearance. Biofluids such as urine and serum serve as compartments to obtain information of these processes.

Chapter 2 focuses on urine as a non-invasive source for biomonitoring. Urine provides a unique window into NP fate, representing the clearance route for particles that have circulated systemically and crossed the renal barrier. This study presents a dual pre-treatment approach, comparing centrifugal ultrafiltration (UF) and SA-DLLME as potential extraction techniques. UF, with size-exclusion principle, showed strong performance in terms of recovery and low detection limits, but also highlighted potential risks of NP loss though filter adsorption or pore blockage. On the other hand, SA-DLLME provided rapid and cost-effective extraction; however, it is a multiple procedural steps technique with high degree of manual handling.

Chapter 3 addressed one of the most common analytical biofluids: human serum. Serum is not only a critical compartment for toxicokinetic studies, as it represents the systemic

USC UNIVERSIDADE DE SANTIAGO

circulation of NPs, but it is also a complex matrix due to its high protein content. NPs in serum are known to interact strongly with proteins, forming coronas that can alter size distributions, induce agglomeration, or even mask the NPs entirely. Conventional digestion methods often compromise NP integrity leading to misleading results. This chapter underscores the importance of mild pre-treatments to ensure NP integrity and obtain reliable and representative results. The results obtained from this chapter demonstrated that enzymatic hydrolysis, using a controlled combination of pancreatin and lipase, can effectively degrade serum proteins while preserving NP structure. When combined with UF to remove residual digestion products, the method allowed intact TiO_2NPs recovery and quantification by spICP-MS.

Urine and serum analyses in combination contribute to the development of amore comprehensive biomonitoring toolkit. Urine sampling offers practical advantages through its non-invasive nature, whereas serum sampling provides greater analytical specificity. Methodological innovations adapted to the characteristics of each biological matrix ensure that both approaches can deliver robust and reliable insights.

– Cellular compartment: RBCs as a model of uptake

The culmination of NP tracking lies at the cellular level, where interactions translate into potential biological effects. *Chapter 4* investigates the feasibility of SC-ICP-MS to study the behaviour of human RBCs exposed to AgNPs. The results obtained from this investigation marked a transition from monitoring exposure and distribution to interactions at cellular resolution.

RBCs, although anucleated, are abundant and physiologically relevant in oxygen transport and circulation and represent an important biological model. This study revealed dose- and time-dependence in NP uptake. The findings from this work are of great importance because they demonstrate the great heterogeneous behaviour of a cell population. This heterogeneity observed also highlights the limitations of traditional bulk analyses, which average across cell populations and neglect the cell-to-cell variability. The successful application of SC-ICP-MS in this context demonstrated that NP-cell interactions can be studied quantitatively at single-cell resolution, providing a mechanistic link between external exposure, systemic distribution, and potential toxicological outcomes. These results bridge the gap between biomonitoring data and cellular-level consequences, offering a direct pathway for integrating nanometrology with toxicology.

– Innovative tools for LA-ICP-MS

Finally, *Chapter 5* addressed issues of calibration and cell handling in LA-ICP-MS presenting potential innovations that support and extend its application to biological compartments.

The results showed that gelatine-based microdroplet standards provide homogeneous, reproducible calibrations points that can be completely ablated, overcoming problems associated with heterogeneity and representativeness of previous calibration methods reported in the literature. Furthermore, the development of microwell arrays for single-cell trapping would enable reproducible and systematic ablation of individual cells. While the results from this chapter are primarily methodological and still incomplete, their implications are far-reaching.

USC UNIVERSIDADE DE SANTIAGO DE COMPOSTELA

Taken together, the results of the five chapters construct a coherent and integrative understanding of NP exposure, fate, and measurement. The integration of environmental, biofluid, and cellular studies enabled the thesis to establish a continuous trajectory that traces NP behaviour from entry to impact. In this sense, it effectively closes the loop of NP measurement across a biological organism. Together, these results not only advance the field of nanometrology but also provide meaningful insights for nanotoxicology and risk assessment.

Integrative pre-treatment and extraction techniques

The set of studies in this thesis, while diverse in terms of matrices and objectives, shared one challenge: the critical role of pre-treatment and/or extraction strategies for preserving NP integrity and reliable analysis. Across environmental waters, human urine, serum, and individual cells, the studies demonstrate that NP measurement often requires a (pre) sample treatment step prior to analysis. A close reading of the results shows not only that pre-treatment and extraction are indispensable, but also that innovations in one context were often transferred and adapted to others, producing an integrative methodological evolution trough the five chapters of the thesis.

Chapter 1 provided one of the first demonstrations of the power of SA-DLLME for NP preconcentration. Tap water, although less complex than biological fluids, also posed a challenge for direct detection. As expected environmental concentrations are very low (in the range of ng L^{-1}), direct analysis of tap water samples was not possible. SA-DLLME was introducing in this context as a means of enriching NPs from dilute aqueous solutions. By using surfactants to stabilize NPs during extraction and thoroughly optimization of the extraction method, one of the strengths of SA-DLLME is its demonstrated selectivity, effectively discriminating between the ionic and particulate forms of the analytes. Beyond its immediate application to environmental monitoring, this study laid the groundwork for using SA-DLLME in more complex biological matrices, a trajectory that is visible in subsequent chapters.

Chapter 2, dedicated to the analysis of human urine, is built directly on this methodological foundation. Urine is analytically more challenging than tap water because of its variable salt content, organic molecules, and metabolites, all of which can interfere with ICP-MS detection or destabilize NPs. In this chapter, SA-DLLME was again employed, but now tested against and alternative strategy: centrifugal UF. The comparison provided valuable information into how extraction methods must be adequately matched to the properties of the matrix and the goals of the analysis. UF, through size fractionation of NPs, achieved high recovery rates and very low detection limits, making it particularly suitable for applications requiring maximum sensitivity. However, unlike SA-DLLME, this approach lacks selectivity in terms of distinguishing between ionic and particulate forms of the analyte. Depending on the membrane's MWCO, species bellow the threshold are forced to cross the membrane. This means that while ionic forms of the analyte are effectively separated, smaller NPs may also be lost (depending on the chosen MWCO). The fact that SA-DLLME, first tested on tap water, proved to be transferrable to more complex matrices such as urine, is itself an important integrative point. It highlights that methodological advances are not confined to their original context but can migrate across domains. This study thus shows the evolution of extraction strategies from environmental to biological samples, confirming the versatility of SA-DLLME while also expanding the toolkit through comparison with UF.

Chapter 3 presented another level of complexity working with serum samples. In this chapter the methodological focus shifted from extraction *per se* to pre-treatment. Unlike urine, where the main challenge lies in salts and metabolites, serum is dominated by proteins that can

USC DE COMPOSTELA

bind to NPs, forming coronas. Traditional chemical digestion methods often compromise NPs. Therefore, this study introduced enzymatic hydrolysis as a gentler form of pre-treatment. The application of enzymes such as pancreatin and lipase, degrade the proteins present in serum liberating NPs while preserving their integrity. This strategy was then coupled to UF to remove residual digestion products. Again, a methodological approach presented in a previous chapter was adapted and further developed in the following one, thereby reinforcing the continuity of the works and highlighting the progressive interconnection between chapters. This iterative improvement not only demonstrates methodological consistency but also illustrates how each step builds upon the previous, contributing to a coherent and integrated research.

Considering these three first chapters, studies reveal both continuity and innovation. Continuity, as initially mentioned, arises from the shared principle of NP integrity preservation: whether using surfactants as stabilization agents, or through the use of enzymatic hydrolysis for gentle pre-treatment. On the other hand, innovation arises from the extended applicability of same extraction methods to different matrices, as well as to recognizing that different samples demand different solutions. In this way, the methodological repertoire presented in this thesis for extraction and/or sample pre-treatment includes three approaches: SA-DLLME, UF, and enzymatic hydrolysis.

Chapter 4 further extended the methodological narrative by presenting the analysis of RBCs by SC-ICP-MS. Although this study did not introduce a new extraction method in the narrow sense, it nevertheless incorporates a strong sample preparation component. In order to achieve a sensitive and reliable detection, a careful preparation of cellular suspensions is needed. The research focused on the study of RBCs, a primary component of human blood. The first step involved the isolation of RBCs from human whole blood. Following exposure, cell handling included washing steps to ensure that only NPs associated with individual erythrocytes, rather than free-floating NPs in the media or aggregates were measured. This chapter thus exemplifies the critical role of sample handling and preparation for obtaining reliable results, while also strengthening and extending the trajectory established in previous chapters.

Chapter 5, focusing on innovations in LA-ICP-MS, may at first appear more distant from the pre-treatment and extraction theme, but it in fact reinforces the same principles in a different guise. The development of gelatine microdroplet standards addressed the issue of calibration in ablation-based techniques, ensuring that signal intensities could be interpreted quantitatively. Likewise, the design and manufacture of microwell arrays for controlled cell trapping functions as a form of physical pre-treatment, ensuring that cells could be analysed individually. These strategies in innovation mimic the principles of SA-DLLME, UF, and enzymatic hydrolysis: each is a way of sample preparation so that the analytical technique can provide accurate, reproducible, and representative information. Thereby, the results obtained from this chapter contribute equally to the overarching theme of sample preparation for reliable NP analysis.

The similarities across the five studies are remarkable. In every case, the central challenge was to isolate NPs from their surrounding matrix without altering their fundamental properties. SA-DLLME, first demonstrated in environmental water, became a versatile extraction tool that was later extended to biological matrices. UF, validated in urine, played a complementary role in serum analysis. Enzymatic hydrolysis, introduced to overcome the specific challenge of proteins in serum, expanded the methodological repertoire of extraction/pre-treatment methods. In the case of RBCs, the challenge was the single-entity handling, for which an alternative approach using LA-ICP-MS is proposed in chapter 5. Though the technical details differ, the principle is the same: preparation must be both selective and gentle. Mitigating interferences is of limited value if it compromises NP integrity. The consistency of this principle across all five

USC DE COMPOSTELA

studies highlights the methodological coherence of the thesis and gives integrative meaning to its diverse results.

In conclusion, focusing on extraction and pre-treatment methods, the thesis provides a coherent methodological philosophy: that reliable NP measurement depends on sample preparation strategies that stabilize, preserve, and isolate NPs within complex and interfering matrices.

Analytical innovation as a common thread

A defining characteristic of the five studies presented in this thesis is the shared reliance on methodological innovation to overcome the inherent challenges of NP detection and quantification. The analytical difficulties posed by inorganic NPs demand solutions that extend beyond conventional approaches. ICP-MS in its advanced operational modes–single particle, single cell, or coupled with laser ablation–provides a unifying technological platform. Yet, the success of this technique usually requires adequate sample preparation and calibration strategies. This section explores these methodological innovations followed throughout the thesis.

Chapter 1 introduces the application of SA-DLLME for the extraction of Ag and TiO_2NPs from tap water. Although SA-DLLME was first developed in 2010, its use had been largely focused on the analysis of organic compounds in aqueous samples. At the time of the publication of the article, only two prior works explored the possibilities of SA-DLLME for NP extraction: one in combination with ETV-ICP-MS for AuNPs analysis in environmental waters, and another in combination with ICP-OES for the determination of TiO_2 and ZnONPs in industrial wastewater samples. The innovative contribution of this thesis lies in extending the extraction methodology beyond the initial applications. Furthermore, it integrates SA-DLLME with spICP-MS for the first time for the extraction and quantification of AgNPs and TiO_2NPs from an environmentally relevant matrix. In this sense, this approach offers a novel analytical pathway for broader applicability in NMs research.

Chapter 2 expands the methodological scope by adapting SA-DLLME for the extraction of AgNPs and TiO_2NPs in urine. This extension highlights the versatility of SA-DLLME across contexts: from environmental to human biomonitoring. Proposed methods in the literature for NP extraction in human blood and blood serum usually included treatment with TMAH, Triton X-100, NH_4OH, and EDTA. In *Chapter 3*, a novel evaluation of enzymatic hydrolysis based on pancreatin and lipase mixture is proposed.

Chapter 4 marks a shift from sample preparation innovations to analytical application at the cellular level. Using SC-ICP-MS, the study demonstrates for the first time the feasibility of quantifying AgNPs internalized or surface-adsorbed by exposed human RBCs. The innovation here relies on the application of the analytical platform to a biologically relevant model, generating insights into time- and dose-dependent uptake patterns of AgNPs. Since the pioneering work published in 2005 on SC-ICP-MS, the technique has shown substantial potential and versatility. However, only a limited number of studies have been devoted to the study of AgNPs to date. To the best of the author's knowledge, this includes no more than four published works.

Chapter 5 is possibly the strongest illustration of methodological innovation within the thesis. It presents a calibration and a single-cell handling strategies for LA-ICP-MS. Calibration in laser ablation-based techniques remains a persistent difficulty, typically relying on in-house standard preparations. In this regard, the chapter introduces a novel calibration strategy employing microdroplets, offering a promising alternative to existing practices. In addition, the

USC DE COMPOSTELA

chapter extends the work on single-cell analysis introduced in the previous chapter, presenting the design and fabrication of a microwell array engineered for efficient single-cell trapping. This innovation enables the acquisition of single-cell data *via* LA-ICP-MS, thus broadening the applicability of the technique.

ICP-MS as the backbone of the thesis

The analytical backbone of the thesis is inductively coupled plasma mass spectrometry, not only the reliance on this technology but also the way in which its different operational modes–single-particle, single-cell, and laser ablation ICP-MS–were employed across studies to investigate NPs in different contexts. Each mode offered unique strengths that matched the demands of the sample type, from dilute aqueous environments to complex biofluids and intact cells. Rather than a series of unrelated technical demonstrations, what emerges from the five chapter is a methodological trajectory in which ICP-MS evolves from particle detection in simple matrices to quantitative imaging.

spICP-MS has been the primary mode of application throughout chapters 1, 2, and 3; and carries the most weight in the whole thesis. While ICP-MS technology emerged in the late 1960s, the first theoretical publication of spICP-MS appeared in 2003, only two decades ago, marking the beginning of a technique that has rapidly evolved ever since. By diluting suspensions sufficiently and using high acquisition rates, spICP-MS enables the detection of discrete particle events, which allows for characterization at the single-particle level. In this context, spICP-MS was applied to the determination of AgNPs and TiO_2NPs in tap water extracts in chapter 1. Similarly, spICP-MS was subsequently employed in chapters 2 and 3 for the analysis of more complex biological matrices, human urine and blood serum. Across the diverse case studies, this mode of operation proved indispensable in NP metrology. As stated in *I. Introduction, 5. Assessment of inorganic nanoparticles: advanced analytical techniques*, the challenge in NP determination is that they are size analytes. Thereby, characterization in terms of size and size distribution are as essential as quantification in terms of mass and number concentration. This methodology provides reliable data that covers characterization and quantifications requirements. Moreover, the technique exhibits robustness and versatility through the first three chapters, establishing its significance for advancing the field of NP analysis.

Understanding single-particle fundamentals and principles, mode of operation, and data handling and process, SC-ICP-MS is quite straightforward. Chapter 4 demonstrated the transition to SC-ICP-MS for RBCs analysis. The underlying principle in single-particle and single-cell analysis is conceptually the same: single-event detection. Discrete entities introduced into the plasma produce transient ion clouds, whose frequency relates to entity concentration and intensity to analyte mass. The characteristic of SC-ICP-MS is that the entities considered are whole cells instead of NPs. Therefore, this mode of operation extends the individuality paradigm of spICP-MS to the biological level, allowing to obtain data on cell-to-cell variability, which is increasingly recognized ass critical for understanding toxicological mechanisms.

The final chapter shifted the perspective again, this time to LA-ICP-MS. This change may seem a little bigger. Unlike single-particle and single-cell ICP-MS, which introduce suspensions through nebulizers and spray chambers systems, LA-ICP-MS uses a focused laser to ablate material from solid, semisolid, or immobilized samples, creating aerosol that are then ionized in the plasma. Its advantage lies in spatial resolution: it can provide not only quantitative elemental data, but also distribution maps within tissues or cells. In the context of this thesis,

USC DE COMPOSTELA

the innovations introduced in calibration and cell handling mean to enhance the reliability of LA-ICP-MS for NP analysis. In this sense, LA-ICP-MS complements and reinforces the other ICP-MS modes, providing the infrastructure for spatially resolved analyses.

The integration of spICP-MS, SC-ICP-MS, and LA-ICP-MS across the thesis represents not just a collection of case studies but a demonstration of instrumental evolution. Each mode builds upon the principles of inductively coupled plasma ionization and mass spectrometry, yet each adapts them to the demand of a different analytical context. Single-particle addresses the individuality of particles, single-cell the individuality of cells, and laser-ablation the spatial distribution. From the scientific point of view, this fact is relevant because it shows that a single instrumental family can support research questions from several contexts. The integrative use of ICP-MS provides coherence to the thesis. Rather than treating environmental science and bioanalysis as separate domains, the same technique can transverse both fields. ICP-MS historically evolved from a general-purpose elemental analyser to a pack of specialised techniques capable of addressing the unique challenges of NMs. The unifying factor is that the plasma mass spectrometer is able to transform discrete analysis–particles, cells, or ablated material– into quantifiable ion clouds. In this sense, the thesis illustrates the trajectory from fundamental principles to cutting-edge applications and demonstrates its indispensable role in advancing nanometrology. By linking the different modes of operation, the thesis demonstrates the integrative potential of ICP-MS as the analytical backbone.

General limitations

The integrative evaluation of this thesis reveals not only the methodological advances achieved by the application of ICP-MS in its various modes, but also the limitations that inevitably influenced the development of the work. In some cases, the limitations are not unique to the present investigation but reflect broader challenges within the field of nanometrology. The critical examination of these gaps will help to direct future research and strengthen analytical reliability.

– Calibration and quantification

One of the most persistent challenges across all studies, and in analytical chemistry in general, lies in calibration. In spICP-MS and SC-ICP-MS, quantification relies on transport efficiency calculations based on NPs suspensions of known size and concentration. However, the scarcity of certified reference materials (CRMs) is a major barrier. Unlike dissolved metals, where CRMs exist for multiple matrices, NPs pose additional challenges due to their size-dependent properties and susceptibility to aggregation. Variations in particle coatings, shapes, and dissolution behaviours introduce additional uncertainty. Without widely available reference standards: (i) comparisons between laboratories are challenging, and (ii) transport efficiency calculations remain approximations, particularly for SC-ICP-MS analysis, where NPs are employed to determine bioparticle transport efficiency.

This limitation in calibration is even more acute for LA-ICP-MS. The general tendency in the literature is to develop in-house standards as a calibration strategy. The microdroplet approach presented in chapter 5 requires specialized equipment, thus limiting accessibility. Furthermore, while gelatine mimics some aspects of biological matrices, it does not replicate the full complexity of tissues or cellular environments.

In this respect, quantification accuracy can still be improved, and research in this area is expanding.

– Analytical sensitivity and detection limits

Despite ICP-MS in single-particle and single-cell modes provides high sensitivity, detection limits remain a significant concern. The detection of particles with diameters near or below 10 nm is particularly difficult due to limitations in sensitivity and signal-to-noise ratios. Moreover, distinguishing NPs from dissolved ionic species poses an additional obstacle. For example, dissolution is particularly relevant for AgNPs, which release Ag+ ions that contribute to increased backgrounds levels and complicate the separation of the two distributions obtained. Current ICP-MS instrumentation can not easily distinguish between particle-associated and ionic forms of an analyte without additional separation steps. Consequently, the development and implementation of selective sample pre-treatment and extraction methodologies are of great value, as they enhance the ability to discriminate between particulate and ionic forms, thus improving data accuracy and reliability.

– Scope and endpoints

The studies in this thesis focus on AgNPs and TiO_2NPs, two of the most widely used NPs. While this focus provides depth and relevance, it limits the generalization to the vast array of engineered NMs in use today. NPs vary widely in size, shape, composition, and surface coatings, all of which influence their behaviour in environmental and biological systems. The nanometrological platforms optimized and presented in this thesis may not apply directly to other materials. Expanding the scope of the research to include broader diversity of NPs would be of great interest yet challenging. The unique physicochemical properties of each NP type often determine the appropriate sample pre-treatment strategy, as suitable extraction conditions that are suitable for one material may hinder process of dissolution or aggregation in others. Thus, individual case-specific studies are frequently required for optimal analytical outcomes.

Biological relevance and future directions

The central contribution of this thesis lies on analytically demonstrating the possibility of detecting, quantifying, and characterizing AgNPs and TiO_2NPs in environmental and biological matrices. The significance of the work rests on the methodological breakthroughs that allowed ICP-MS, in its single-particle, single-cell, and laser ablation modes, to generate reliable data under conditions where traditional analytical chemistry has struggled. The importance of NP detection in these matrices resides in establishing sensitive, selective, and reproducible methodologies that enable their monitoring and investigation. In other words, the thesis aims to show that nanometrology is at the point of being able to interrogate real-world samples, not just model systems.

The ability to detect NPs at ultratrace levels in environmental matrices, such as tap water, is a milestone for exposure science. Water is consumed daily and represents one of the most common potential routes of NPs intake. Chapter 1 provides an analytical methodology for the analysis of NPs in real tap water samples. This study provides essential foundations for future surveillance, risk assessment, and quality control assessment. In addition, this chapter represents the start point for the subsequent studies on biological contexts.

Urine is an inherently variable matrix, influenced by diet, hydration, and health status, and it contains a complex mixture of salts and metabolites. The ability to detect NPs in this matrix demonstrates that non-invasive monitoring is feasible, opening possibilities for large-scale studies of human exposure. The biological meaning lies in the capability for reliable NP

measurement allowing: (i) to design population studies, (ii) to compare occupationally exposed versus general population, and (iii) to monitor trends over time.

The work on serum further underscores the biological importance of the thesis. Serum is dominated by proteins that associate to NPs forming coronas, which complicate the analysis and often degrade analytes. The application of enzymatic hydrolysis in Chapter 3 introduces a potential sample pre-treatment for NPs to be freed from protein coronas without significant integrity loss. This advance is biologically meaningful because it allows the study of NP persistence in circulation and demonstrates that analytical barriers to working with protein-rich fluids can be overcome. This ability to detect NPs in serum is critical because it validates blood-based biomonitoring, which offers information about NP distribution and ongoing exposure.

The detection of NPs at the cellular level with SC-ICP-MS represents another transformative step. The biological relevance here is not only that cells can associate with NPs, but that analytical chemistry can now resolve uptake heterogeneity between individual cells. RBCs, used in this thesis as a model, showed marked variability in NP content. The importance is not the fact of uptake, which has been suggested in prior studies, but the demonstration that it can be quantified at the single-cell level with statistical robustness. This capability opens up new avenues for toxicology, as it enables researchers to move beyond average data to distributions, identifying susceptible subpopulations and uncovering variability that could explain differences in toxicological outcomes. It is possible now to detect not only whether NPs associate with cells, but also how differently they do so across individual cells.

The innovations in LA-ICP-MS, while technical in focus, also contribute to the biological relevance of the thesis. Gelatine microdroplets standards and microwell arrays address problems of quantification in NP analysis. These two innovative tools are intended for future biological applications.

Across all chapters, the importance of being able to detect NPs in tap water, urine, serum, and cells have been outlined in terms of methodological and toxicological implications. The biological relevance of this thesis lies in providing an analytical toolkit for NP assessment in different matrices. Without seeming pretentious, these small advances represent a modest contribution to the progress of nanometrology.

USC
UNIVERSIDADE DE SANTIAGO DE COMPOSTELA

VI. CONCLUSIONS

USC
UNIVERSIDADE
DE SANTIAGO
DE COMPOSTELA

CONCLUSIONS

This thesis has explored the detection, characterization, and quantification of ENPs across environmental, biological, and cellular systems by applying advanced modes of ICP-MS together with tailored sample preparation strategies. The work was organized into five independent but interrelated studies, each addressing specific analytical challenges while contributing to a broader understanding of NP fate and assessment. The following section first summarizes the principal conclusions of each chapter individually, and then presents an integrative perspective that highlights the collective meaning and overall significance of the research carried out.

– Chapter 1

Pre-concentration procedures based on SA-DLLME proved reliable for assessing AgNPs and TiO_2NPs in tap water. The technique selectively isolated NP forms without extracting ionic Ag or Ti, providing enrichment factors between 5 and 10. Further spICP-MS analysis confirmed the presence of NPs. AgNPs suffered from partial dissolution while TiO_2NPs had tendency to aggregate/agglomerate. The proposed method may be potentially applied to other water samples such as seawater, river water, wastewater, or bottled water, pending further matrix validation.

– Chapter 2

Two methodologies, SA-DLLME and centrifugal UF, were validated for AgNPs and TiO_2NPs quantification in human urine. While both are time-consuming compared to direct dilution, they enable good sensitivity, selectivity, and reduced matrix interferences. SA-DLLME provided good sensitivity and recoveries but compromised NP integrity, leading to size shifts and possible dissolution/aggregation. UF allowed simultaneous processing of multiple samples and preserved particle integrity, although it required longer handling times. The results highlighted the feasibility of spICP-MS for NP analysis in human urine and underscored the need for improved pre-treatments that preserve NP integrity.

– Chapter 3

Enzymatic hydrolysis using pancreatin/lipase mixture, followed by UF cleaning, provided a gentle and effective pre-treatment for TiO_2NPs assessment in serum. This soft digestion liberated NPs from the protein-rich medium while preserving their size distribution, allowing for a proper spICP-MS characterization.

USC UNIVERSIDADE DE SANTIAGO DE COMPOSTELA

– Chapter 4

The application of SC-ICP-MS enabled the quantification of AgNP uptake by RBCs at the single-cell level after different exposure conditions. Results revealed pronounced cell-to-cell heterogeneity, with some cells accumulating one NP and others up to eight. Uptake depended on both particle size and exposure time, with distinct patterns for 20 nm *versus* 40 nm AgNPs. Only an approximate of 20-25 % of the cell population accumulated 40 nm-AgNPs, whereas the majority accumulated 20 nm-AgNPs. SC-ICP-MS thereby proved a powerful tool for studying NP-cell interactions while capturing inherent cell variability.

– Chapter 5

Two methodological innovations were introduced: gelatine microdroplets as calibration standards and microwell arrays for controlled single-cell deposition. On the one hand, microdroplets allowed complete ablation in short times and overcame representativeness issues of conventional calibration approaches. On the other hand, microwell arrays enabled high-throughput and reproducible cell trapping. Together, these advances address key limitations in LA-ICP-MS applications, and although preliminary they show promising potential.

Taken together, the thesis demonstrates the versatility of ICP-MS for NP detection, characterization, and quantification. Through spICP-MS, SC-ICP-MS, and LA-ICP-MS, the research spans multiple scales of analysis, each linked by common challenges of sensitivity, NP integrity preservation, and reliable calibration. The thesis establishes nanometrological platforms for NP assessment across four different and complex sample types, each requiring matrix-specific pre-treatments. In this sense, the thesis highlights the need for case-by-case evaluation when in NMs studies. Investigating AgNPs and TiO_2NPs, two of the most widely used NPs, the results revealed clear differences in their behaviour, underscoring the difficulty of drawing broad generalizations in nanoscience.

In summary, the thesis introduces promising analytical platforms for NP assessment in tap water, human urine and serum, and erythrocytes. This contribution, though modest, offers valuable tools that may support future nanometrology, toxicology, and biomonitoring studies.

USC
UNIVERSIDADE DE SANTIAGO DE COMPOSTELA

VII. REFERENCES

USC
UNIVERSIDADE
DE SANTIAGO
DE COMPOSTELA

REFERENCES

[1] A. Barhoum, M.L. García-Betancourt, J. Jeevanandam, E.A. Hussien, S.A. Mekkawy, M. Mostafa, M.M. Omran, M.S. Abdalla, M. Bechelany, Review on Natural, Incidental, Bioinspired, and Engineered Nanomaterials: History, Definitions, Classifications, Synthesis, Properties, Market, Toxicities, Risks, and Regulations, Nanomaterials. 12 (2022). https://doi.org/10.3390/nano12020177.

[2] M. Aubert, A. Brumm, M. Ramli, T. Sutikna, E.W. Saptomo, B. Hakim, M.J. Morwood, G.D. Van Den Bergh, L. Kinsley, A. Dosseto, Pleistocene cave art from Sulawesi, Indonesia, Nature. 514 (2014) 223–227. https://doi.org/10.1038/nature13422.

[3] A.K. Yetisen, A.F. Coskun, G. England, S. Cho, H. Butt, J. Hurwitz, M. Kolle, A. Khademhosseini, A.J. Hart, A. Folch, S.H. Yun, Art on the Nanoscale and beyond, Adv. Mater. 28 (2016) 1724–1742. https://doi.org/10.1002/adma.201502382.

[4] H. Berke, The invention of blue and purple pigments in ancient times, Chem. Soc. Rev. 36 (2007) 15–30. https://doi.org/10.1039/b606268g.

[5] D. Johnson-Mcdaniel, C.A. Barrett, A. Sharafi, T.T. Salguero, Nanoscience of an ancient pigment, J. Am. Chem. Soc. 135 (2013) 1677–1679. https://doi.org/10.1021/ja310587c.

[6] G. Verri, The spatially resolved characterisation of Egyptian blue, Han blue and Han purple by photo-induced luminescence digital imaging, Anal. Bioanal. Chem. 394 (2009) 1011–1021. https://doi.org/10.1007/s00216-009-2693-0.

[7] N. Brun, L. Mazerolles, M. Pernot, Microstructure of opaque red glass containing copper, J. Mater. Sci. Lett. 10 (1991) 1418–1420. https://doi.org/10.1007/BF00735696.

[8] G. Artioli, I. Angelini, A. Polla, Crystals and phase transitions in protohistoric glass materials, Phase Transitions. 81 (2008) 233–252. https://doi.org/10.1080/01411590701514409.

[9] D. Schaming, H. Remita, Nanotechnology: from the ancient time to nowadays, Found. Chem. 17 (2015) 187–205. https://doi.org/10.1007/s10698-015-9235-y.

[10] I. Angelini, G. Artioli, P. Bellintani, V. Diella, M. Gemmi, A. Polla, A. Rossi, Chemical analyses of Bronze Age glasses from Frattesina di Rovigo, Northern Italy, J. Archaeol. Sci. 31 (2004) 1175–1184. https://doi.org/10.1016/j.jas.2004.02.015.

[11] P. Colomban, G. March, L. Mazerolles, T. Karmous, N. Ayed, A. Ennabli, H. Slim, Raman identification of materials used for jewellery and mosaics in Ifriqiya, J. Raman Spectrosc. 34 (2003) 205–213. https://doi.org/10.1002/jrs.977.

[12] P. Ricciardi, P. Colomban, A. Tournié, M. Macchiarola, N. Ayed, A non-invasive study of Roman Age mosaic glass tesserae by means of Raman spectroscopy, J. Archaeol. Sci.

USC UNIVERSIDADE DE CANTABRIA

36 (2009) 2551–2559. https://doi.org/10.1016/j.jas.2009.07.008.

[13] I. Freestone, N. Meeks, M. Sax, C. Higgitt, The Lycurgus Cup - A Roman nanotechnology, Gold Bull. 40 (2008) 270–277. https://doi.org/10.1007/BF03215599.

[14] D.J. BARBER, I.C. FREESTONE, an Investigation of the Origin of the Colour of the Lycurgus Cup By Analytical Transmission Electron Microscopy, Archaeometry. 32 (1990) 33–45. https://doi.org/10.1111/j.1475-4754.1990.tb01079.x.

[15] A. Caiger-Smith, Lustre pottery. Technique, tradition and innovation in Islam and the Western World, New Amsterdam Books, New York, USA, 1991.

[16] T. Pradell, A. Climent-Font, J. Molera, A. Zucchiatti, M.D. Ynsa, P. Roura, D. Crespo, Metallic and nonmetallic shine in luster: An elastic ion backscattering study, J. Appl. Phys. 101 (2007) 0–8. https://doi.org/10.1063/1.2734944.

[17] J. Pérez-Arantegui, J. Molera, A. Larrea, T. Pradell, M. Vendrell-Saz, I. Borgia, B.G. Brunetti, F. Cariati, P. Fermo, M. Mellini, A. Sgamellotti, C. Viti, Luster pottery from the thirteenth century to the sixteenth century: A nanostructured thin metallic film, J. Am. Ceram. Soc. 84 (2001) 442–46. https://doi.org/10.1111/j.1151-2916.2001.tb00674.x.

[18] I. Nakai, C. Numako, H. Hosono, K. Yamasaki, Origin of the red color of satsuma copper-ruby glass as determined by EXAFS and optical absorption spectroscopy, J. Am. Ceram. Soc. 82 (1999) 689–695. https://doi.org/10.1111/j.1151-2916.1999.tb01818.x.

[19] J. Bradbury, Nature's nanotechnologists: unveiling the secrets of diatoms, PLoS biology, 2 (10) (2004) https://doi.org/10.1371/journal.pbio.0020306.

[20] M. Faraday, X. The Bakerian Lecture. —Experimental relations of gold (and other metals) to light, Philos. Trans. R. Soc. London. 147 (1857) 145–181. https://doi.org/10.1098/rstl.1857.0011.

[21] F. Haguenau, P.W. Hawkes, J.L. Hutchison, B. Satiat-Jeunemaître, G.T. Simon, D.B. Williams, Key events in the history of electron microscopy, Microsc. Microanal. 9 (2003) 96–138. https://doi.org/10.1017/S1431927603030113.

[22] R.P. Feynman, There's Plenty of Room at the Bottom: An Invitation to Enter a New Field of Physics*, Handb. Nanosci. Eng. Technol. Third Ed. (2012) 3–12. https://doi.org/10.1201/9781315217178-6.

[23] N. Taniguchi, On the basic concept of "nano-technology," Proc. Int. Conf. Prod. Eng. Tokyo, Japan Soc. Precis. Eng. (1974) 18-23 Part II.

[24] P.N. Sudha, K. Sangeetha, K. Vijayalakshmi, A. Barhoum, Chapter 12 - Nanomaterials history, classification, unique properties, production and market, in: Elsevier Inc., 2018: pp. 341–384. https://doi.org/10.1016/B978-0-323-51254-1/00012-9.

[25] The Nobel Prize, (n.d.). https://www.nobelprize.org/ (accessed June 23, 2025).

[26] National Nanotechnology Initiative (NNI), (n.d.). https://www.nano.gov/ (accessed June 23, 2025).

[27] European Union Observatory for Nanomaterials (EUON), (n.d.).

USC UNIVERSIDADE DE SANTIAGO DE COMPOSTELA

https://euon.echa.europa.eu/es/ (accessed May 1, 2023).

[28] Nanotechnology Products Database (NPD), (n.d.). https://product.statnano.com/ (accessed May 1, 2025).

[29] M. Nasrollahzadeh, S.M. Sajadi, M. Sajjadi, Z. Issaabadi, Applications of Nanotechnology in Daily Life, 1st ed., Elsevier Ltd., 2019. https://doi.org/10.1016/B978-0-12-813586-0.00004-3.

[30] R. Kumar, M. Kumar, G. Luthra, Fundamental approaches and applications of nanotechnology: A mini review, Mater. Today Proc. (2023). https://doi.org/10.1016/j.matpr.2022.12.172.

[31] S. Malik, K. Muhammad, Y. Waheed, Nanotechnology: A Revolution in Modern Industry, Molecules. 28 (2023). https://doi.org/10.3390/molecules28020661.

[32] ISO/TS 80004-1:2015. Nanotechnologies - Vocabulary - Part 1: Core Terms, Geneva, 2015. https://www.iso.org/standard/79525.html.

[33] G. Lovestam, H. Rauscher, G. Roebben, B.S. Kluttgen, N. Gibson, J.-P. Putaud, H. Stamm, Considerations on a definition of nanomaterial for regulatory purposes, 2010. https://doi.org/10.2788/98686.

[34] A. Ahlbom, J. Bridges, W. De Jong, T. Jung, J. Hajslova, P. Hartemann, J. Pagés, M.-O. Mattsson, K. Rydzynski, D. Stahl, D. Williams, Opinion on the scientific aspects of the existing and proposed definitions relating to products of nanoscience and nanotechnologies, Eur. Comm. (2008) 1–22. http://ec.europa.eu/health/ph_risk/committees/04_%0Ascenihr/docs/scenihr_o_012.pdf .

[35] Scientific Committee on Consumer Products (SCCP), Opinion on safety of nanomaterials in cosmetics products, 2007. http://ec.europa.eu/health/ph_risk/committees/04_sccp/%0Adocs/sccp_o_123.pdf.

[36] Commission Recommendation 2022/C 229/01 of 10.6.2022 on the definition of nanomaterial, 2022. https://doi.org/10.2788/36237.

[37] J. Labuda, J. Barek, Z. Gajdosechova, H. Goenaga-Infante, L.J. Johnston, Z. Mester, S. Shtykov, Analytical chemistry of engineered nanomaterials: Part 1. Scope, regulation, legislation, and metrology (IUPAC Technical Report), Pure Appl. Chem. 95 (2023) 133–163. https://doi.org/10.1515/pac-2021-1001.

[38] B. Mekuye, B. Abera, Nanomaterials: An overview of synthesis, classification, characterization, and applications, Nano Sel. 4 (2023) 486–501. https://doi.org/10.1002/nano.202300038.

[39] A.B. Asha, R. Narain, Nanomaterials properties, Elsevier Inc., 2020. https://doi.org/10.1016/B978-0-12-816806-6.00015-7.

[40] E. Roduner, Size matters: Why nanomaterials are different, Chem. Soc. Rev. 35 (2006) 583–592. https://doi.org/10.1039/b502142c.

[41] A.K. Clogston, J.D., Patri, Zeta Potential Measurement, in: Charact. Nanoparticles Intend. Drug Deliv., Humana Press, 2010. https://doi.org/10.1007/978-1-60327-198-

1_6.

[42] and N.G. F. Scarpelli, T. F. Mastropietro, T. Poerio, Mesoporous TiO2 thin films: State of the art, in: D. Yang (Ed.), Titan. Dioxide - Mater. a Sustain. Environ., IntechOpen, 2018: p. 518. https://doi.org/10.5772/intechopen.74244.

[43] R. Schlögl, S.B. Abd Hamid, Nanocatalysis: Mature science revisited of something really new?, Angew. Chemie - Int. Ed. 43 (2004) 1628–1637. https://doi.org/10.1002/anie.200301684.

[44] M.V. Uwe Kreibig, Optical Properties of Metal Clusters, 1st Edition, Springer Berlin, Heidelberg, 1995. https://doi.org/10.1007/978-3-662-09109-8.

[45] F. Hubenthal, N. Borg, F. Träger, Optical properties and ultrafast electron dynamics in gold-silver alloy and core-shell nanoparticles, Appl. Phys. B Lasers Opt. 93 (2008) 39–45. https://doi.org/10.1007/s00340-008-3146-8.

[46] O.A. Yeshchenko, I.M. Dmitruk, A.A. Alexeenko, A. V. Kotko, J. Verdal, A.O. Pinchuk, Size and Temperature Effects on the Surface Plasmon Resonance in Silver Nanoparticles, Plasmonics. 7 (2012) 685–694. https://doi.org/10.1007/s11468-012-9359-z.

[47] A. Philip, A.R. Kumar, The performance enhancement of surface plasmon resonance optical sensors using nanomaterials: A review, Coord. Chem. Rev. 458 (2022) 214424. https://doi.org/10.1016/j.ccr.2022.214424.

[48] T.A. Saleh, Nanomaterials: Classification, properties, and environmental toxicities, Environ. Technol. Innov. 20 (2020) 101067. https://doi.org/10.1016/j.eti.2020.101067.

[49] L. An, D. Zhang, L. Zhang, G. Feng, Effect of nanoparticle size on the mechanical properties of nanoparticle assemblies, Nanoscale. 11 (2019) 9563–9573. https://doi.org/10.1039/c9nr01082c.

[50] H. Shi, R. Magaye, V. Castranova, J. Zhao, Titanium dioxide nanoparticles: A review of current toxicological data, Part. Fibre Toxicol. 10 (2013). https://doi.org/10.1186/1743-8977-10-15.

[51] S. Shabbir, M.F. e. A. Kulyar, Z.A. Bhutta, P. Boruah, M. Asif, Toxicological Consequences of Titanium Dioxide Nanoparticles (TiO2NPs) and Their Jeopardy to Human Population, Bionanoscience. 11 (2021) 621–632. https://doi.org/10.1007/s12668-021-00836-3.

[52] F. Xu, Review of analytical studies on TiO2 nanoparticles and particle aggregation, coagulation, flocculation, sedimentation, stabilization, Chemosphere. 212 (2018) 662–677. https://doi.org/10.1016/j.chemosphere.2018.08.108.

[53] H.M.R. Abdel-Latif, M.A.O. Dawood, S. Menanteau-Ledouble, M. El-Matbouli, Environmental transformation of n-TiO2 in the aquatic systems and their ecotoxicity in bivalve mollusks: A systematic review, Ecotoxicol. Environ. Saf. 200 (2020). https://doi.org/10.1016/j.ecoenv.2020.110776.

[54] IARC monographs on the evaluation of carcinogenic risks to humans, IARC Monogr. Eval. Carcinog. Risks to Humans. 93 (2010) 9–38. https://doi.org/10.1136/jcp.48.7.691-a.

USC UNIVERSIDADE DE SANTIAGO DE COMPOSTELA

[55] Court of Justice of the European Union. The General Court annuls the Commission Delegated Regulation of 2019 in so far as it concerns the harmonised classification and labelling of titanium dioxide as a carcinogenic substance by inhalation in certain powd, (2022) 3–5.

[56] M. Younes, G. Aquilina, L. Castle, K.H. Engel, P. Fowler, M.J. Frutos Fernandez, P. Fürst, U. Gundert-Remy, R. Gürtler, T. Husøy, M. Manco, W. Mennes, P. Moldeus, S. Passamonti, R. Shah, I. Waalkens-Berendsen, D. Wölfle, E. Corsini, F. Cubadda, D. De Groot, R. FitzGerald, S. Gunnare, A.C. Gutleb, J. Mast, A. Mortensen, A. Oomen, A. Piersma, V. Plichta, B. Ulbrich, H. Van Loveren, D. Benford, M. Bignami, C. Bolognesi, R. Crebelli, M. Dusinska, F. Marcon, E. Nielsen, J. Schlatter, C. Vleminckx, S. Barmaz, M. Carfí, C. Civitella, A. Giarola, A.M. Rincon, R. Serafimova, C. Smeraldi, J. Tarazona, A. Tard, M. Wright, Safety assessment of titanium dioxide (E171) as a food additive, EFSA J. 19 (2021). https://doi.org/10.2903/j.efsa.2021.6585.

[57] F. Piccinno, F. Gottschalk, S. Seeger, B. Nowack, Industrial production quantities and uses of ten engineered nanomaterials in Europe and the world, J. Nanoparticle Res. 14 (2012). https://doi.org/10.1007/s11051-012-1109-9.

[58] F. Fiordaliso, P. Bigini, M. Salmona, L. Diomede, Toxicological impact of titanium dioxide nanoparticles and food-grade titanium dioxide (E171) on human and environmental health, Environ. Sci. Nano. 9 (2022) 1199–1211. https://doi.org/10.1039/d1en00833a.

[59] A. Abend, D. Sperger, D.A. Diaz, R. Guo, R. Reul, S.J. Wu, Industry's perspective on challenges assessing the in vivo impact of removing titanium dioxide (TiO2) from drug products, J. Pharm. Sci. 113 (2024) 3119–3122. https://doi.org/10.1016/j.xphs.2024.08.002.

[60] N. Thakur, N. Thakur, A. Kumar, V.K. Thakur, S. Kalia, V. Arya, A. Kumar, S. Kumar, G.Z. Kyzas, A critical review on the recent trends of photocatalytic, antibacterial, antioxidant and nanohybrid applications of anatase and rutile TiO2 nanoparticles, Sci. Total Environ. 914 (2024). https://doi.org/10.1016/j.scitotenv.2023.169815.

[61] M. Montazer, S. Seifollahzadeh, Enhanced self-cleaning, antibacterial and UV protection properties of nano TiO2 treated textile through enzymatic pretreatment, Photochem. Photobiol. 87 (2011) 877–883. https://doi.org/10.1111/j.1751-1097.2011.00917.x.

[62] A. Weir, P. Westerhoff, L. Fabricius, K. Hristovski, N. Von Goetz, Titanium dioxide nanoparticles in food and personal care products, Environ. Sci. Technol. 46 (2012) 2242–2250. https://doi.org/10.1021/es204168d.

[63] B. Faure, G. Salazar-Alvarez, A. Ahniyaz, I. Villaluenga, G. Berriozabal, Y.R. De Miguel, L. Bergström, Dispersion and surface functionalization of oxide nanoparticles for transparent photocatalytic and UV-protecting coatings and sunscreens, Sci. Technol. Adv. Mater. 14 (2013). https://doi.org/10.1088/1468-6996/14/2/023001.

[64] E. Baranowska-Wójcik, D. Szwajgier, P. Oleszczuk, A. Winiarska-Mieczan, Effects of Titanium Dioxide Nanoparticles Exposure on Human Health—a Review, Biol. Trace Elem. Res. 193 (2020) 118–129. https://doi.org/10.1007/s12011-019-01706-6.

USC UNIVERSIDADE DE SANTIAGO DE COMPOSTELA

[65] European Union. Regulation (EU) No 2022/63 of the European Commission of 14 January 2022 amending Annexes II and III to Regulation (EC) No 1333/2008 of the European Parliament and of the Council as regards the food additive titanium dioxide (E171), Off. J. Eu. Union. (2022).

[66] Y.T. Sul, Electrochemical growth behavior, surface properties, and enhanced in vivo bone response of Tio2 nanotubes on microstructured surfaces of blasted, screw-shaped titanium implants, Int. J. Nanomedicine. 5 (2010) 87–100. https://doi.org/10.2147/ijn.s8012.

[67] A. Wiesenthal, L. Hunter, S. Wang, J. Wickliffe, M. Wilkerson, Nanoparticles: Small and mighty, Int. J. Dermatol. 50 (2011) 247–254. https://doi.org/10.1111/j.1365-4632.2010.04815.x.

[68] National Center for Biotechnology Information. PubChem Element Summary for Atomic Number 47, Silver., (2025). https://pubchem.ncbi.nlm.nih.gov/element/Silver. (accessed June 24, 2025).

[69] E. McGillicuddy, I. Murray, S. Kavanagh, L. Morrison, A. Fogarty, M. Cormican, P. Dockery, M. Prendergast, N. Rowan, D. Morris, Silver nanoparticles in the environment: Sources, detection and ecotoxicology, Sci. Total Environ. 575 (2017) 231–246. https://doi.org/10.1016/j.scitotenv.2016.10.041.

[70] D.J. Barillo, D.E. Marx, Silver in medicine: A brief history BC 335 to present, Burns. 40 (2014) S3–S8. https://doi.org/10.1016/j.burns.2014.09.009.

[71] I. Iavicoli, V. Leso, M. Piacci, D.L. Cioffi, I.G. Canu, P.A. Schulte, An exploratory assessment of applying risk management practices to engineered nanomaterials, Int. J. Environ. Res. Public Health. 16 (2019). https://doi.org/10.3390/ijerph16183290.

[72] G.R. Tortella, O. Rubilar, N. Durán, M.C. Diez, M. Martínez, J. Parada, A.B. Seabra, Silver nanoparticles: Toxicity in model organisms as an overview of its hazard for human health and the environment, J. Hazard. Mater. 390 (2020). https://doi.org/10.1016/j.jhazmat.2019.121974.

[73] A. Lazareva, A.A. Keller, Estimating potential life cycle releases of engineered nanomaterials from wastewater treatment plants, ACS Sustain. Chem. Eng. 2 (2014) 1656–1665. https://doi.org/10.1021/sc500121w.

[74] S. Foss Hansen, L.R. Heggelund, P. Revilla Besora, A. Mackevica, A. Boldrin, A. Baun, Nanoproducts - What is actually available to European consumers?, Environ. Sci. Nano. 3 (2016) 169–180. https://doi.org/10.1039/c5en00182j.

[75] O. Pryshchepa, P. Pomastowski, B. Buszewski, Silver nanoparticles: Synthesis, investigation techniques, and properties, Adv. Colloid Interface Sci. 284 (2020) 87–100. https://doi.org/10.1016/j.cis.2020.102246.

[76] S.P. Deshmukh, S.M. Patil, S.B. Mullani, S.D. Delekar, Silver nanoparticles as an effective disinfectant: A review, Mater. Sci. Eng. C. 97 (2019) 954–965. https://doi.org/10.1016/j.msec.2018.12.102.

[77] I. Sondi, B. Salopek-Sondi, Silver nanoparticles as antimicrobial agent: A case study on E. coli as a model for Gram-negative bacteria, J. Colloid Interface Sci. 275 (2004) 177–

USC UNIVERSIDADE DE SANTIAGO DE COMPOSTELA

182. https://doi.org/10.1016/j.jcis.2004.02.012.

[78] C.A. Dos Santos, M.M. Seckler, A.P. Ingle, I. Gupta, S. Galdiero, M. Galdiero, A. Gade, M. Rai, Silver nanoparticles: Therapeutical uses, toxicity, and safety issues, J. Pharm. Sci. 103 (2014) 1931–1944. https://doi.org/10.1002/jps.24001.

[79] J.R. Morones, J.L. Elechiguerra, A. Camacho, K. Holt, J.B. Kouri, J.T. Ramírez, M.J. Yacaman, The bactericidal effect of silver nanoparticles, Nanotechnology. 16 (2005) 2346–2353. https://doi.org/10.1088/0957-4484/16/10/059.

[80] J.S. Kim, E. Kuk, K.N. Yu, J.H. Kim, S.J. Park, H.J. Lee, S.H. Kim, Y.K. Park, Y.H. Park, C.Y. Hwang, Y.K. Kim, Y.S. Lee, D.H. Jeong, M.H. Cho, Antimicrobial effects of silver nanoparticles, Nanomedicine Nanotechnology, Biol. Med. 3 (2007) 95–101. https://doi.org/10.1016/j.nano.2006.12.001.

[81] M. Banerjee, S. Mallick, A. Paul, A. Chattopadhyay, S.S. Ghosh, Heightened reactive oxygen species generation in the antimicrobial activity of a three component iodinated chitosan?silver nanoparticle composite, Langmuir. 26 (2010) 5901–5908. https://doi.org/10.1021/la9038528.

[82] L. Rizzello, P.P. Pompa, Nanosilver-based antibacterial drugs and devices: Mechanisms, methodological drawbacks, and guidelines, Chem. Soc. Rev. 43 (2014) 1501–1518. https://doi.org/10.1039/c3cs60218d.

[83] S.S.D. Kumar, N.K. Rajendran, N.N. Houreld, H. Abrahamse, Recent advances on silver nanoparticle and biopolymer-based biomaterials for wound healing applications, Int. J. Biol. Macromol. 115 (2018) 165–175. https://doi.org/10.1016/j.ijbiomac.2018.04.003.

[84] E. Marsich, A. Travan, I. Donati, G. Turco, J. Kulkova, N. Moritz, H.T. Aro, M. Crosera, S. Paoletti, Biological responses of silver-coated thermosets: An in vitro and in vivo study, Acta Biomater. 9 (2013) 5088–5099. https://doi.org/10.1016/j.actbio.2012.10.002.

[85] R.A. Bapat, T. V. Chaubal, C.P. Joshi, P.R. Bapat, H. Choudhury, M. Pandey, B. Gorain, P. Kesharwani, An overview of application of silver nanoparticles for biomaterials in dentistry, Mater. Sci. Eng. C. 91 (2018) 881–898. https://doi.org/10.1016/j.msec.2018.05.069.

[86] M. Rai, K. Kon, A. Ingle, N. Duran, S. Galdiero, M. Galdiero, Broad-spectrum bioactivities of silver nanoparticles: The emerging trends and future prospects, Appl. Microbiol. Biotechnol. 98 (2014) 1951–1961. https://doi.org/10.1007/s00253-013-5473-x.

[87] J.F. Borzelleca, Paracelsus: Herald of modern toxicology, Toxicol. Sci. 53 (2000) 2–4. https://doi.org/10.1093/toxsci/53.1.2.

[88] W. Yang, L. Wang, E.M. Mettenbrink, P.L. Deangelis, S. Wilhelm, Nanoparticle Toxicology, Annu. Rev. Pharmacol. Toxicol. 61 (2021) 269–289. https://doi.org/10.1146/annurev-pharmtox-032320-110338.

[89] S. Sabella, R.P. Carney, V. Brunetti, M.A. Malvindi, N. Al-Juffali, G. Vecchio, S.M. Janes, O.M. Bakr, R. Cingolani, F. Stellacci, P.P. Pompa, A general mechanism for intracellular toxicity of metal-containing nanoparticles, Nanoscale. 6 (2014) 7052–7061.

USC UNIVERSIDADE DE SANTIAGO DE COMPOSTELA

https://doi.org/10.1039/c4nr01234h.

[90] J. R. Lead, S. H. Doak, M. J. D. Clift (Eds.), Nanotoxicology in Humans and the Environment, Springer Cham, 2021. https://doi.org/10.1007/978-3-030-79808-6.

[91] Z. Magdolenova, A. Collins, A. Kumar, A. Dhawan, V. Stone, M. Dusinska, Mechanisms of genotoxicity. A review of in vitro and in vivo studies with engineered nanoparticles, Nanotoxicology. 8 (2014) 233–278. https://doi.org/10.3109/17435390.2013.773464.

[92] M. Khatri, D. Bello, P. Gaines, J. Martin, A.K. Pal, R. Gore, S. Woskie, Nanoparticles from photocopiers induce oxidative stress and upper respiratory tract inflammation in healthy volunteers, Nanotoxicology. 7 (2013) 1014–1027. https://doi.org/10.3109/17435390.2012.691998.

[93] N.L. Mills, M.R. Miller, A.J. Lucking, J. Beveridge, L. Flint, A.J.F. Boere, P.H. Fokkens, N.A. Boon, T. Sandstrom, A. Blomberg, R. Duffin, K. Donaldson, P.W.F. Hadoke, F.R. Cassee, D.E. Newby, Combustion-derived nanoparticulate induces the adverse vascular effects of diesel exhaust inhalation, Eur. Heart J. 32 (2011) 2660–2671. https://doi.org/10.1093/eurheartj/ehr195.

[94] A.K. Srivastava, D.M. Snapper, J. Zheng, B.S. Yildrim, S. Srivastava, S.C. Wood, Examining the role of nickel and NiTi nanoparticles promoting inflammation and angiogenesis, J. Immunotoxicol. 19 (2022) 61–73. https://doi.org/10.1080/1547691X.2022.2080307.

[95] M. You, Y. Huang, Y. Chen, D. Li, Y. Tang, Y. kuan Du, H. Yang, A. Liang, G. Hu, Y. Chen, ZnO nanoparticles induce melanoma-like lesions via recruiting dermal dendritic cells in barrier-damaged skin in mice, Food Chem. Toxicol. 193 (2024) 114948. https://doi.org/10.1016/j.fct.2024.114948.

[96] J. Rawat, V. Kumar, P. Ahlawat, L.K. Tripathi, R. Tomar, R. Kumar, S. Dholpuria, P.K. Gupta, Current Trends on the Effects of Metal-Based Nanoparticles on Microbial Ecology, Appl. Biochem. Biotechnol. 195 (2023) 6168–6182. https://doi.org/10.1007/s12010-023-04386-0.

[97] H. Tian, M. Kah, K. Kariman, Are Nanoparticles a Threat to Mycorrhizal and Rhizobial Symbioses? A Critical Review, Front. Microbiol. 10 (2019) 1–15. https://doi.org/10.3389/fmicb.2019.01660.

[98] A.R. Vandevoort, Y. Arai, Macroscopic observation of soil nitrification kinetics impacted by copper nanoparticles: Implications for micronutrient nanofertilizer, Nanomaterials. 8 (2018). https://doi.org/10.3390/nano8110927.

[99] C. Chaves-Lopez, H.N. Nguyen, R.C. Oliveira, E.T. Nadres, A. Paparella, D.F. Rodrigues, A morphological, enzymatic and metabolic approach to elucidate apoptotic-like cell death in fungi exposed to h- and α-molybdenum trioxide nanoparticles, Nanoscale. 10 (2018) 20702–20716. https://doi.org/10.1039/c8nr06470a.

[100] Q. Ma, Q. Zhang, S. Yang, A. Yilihamu, M. Shi, B. Ouyang, X. Guan, S.T. Yang, Toxicity of nanodiamonds to white rot fungi Phanerochaete chrysosporium through oxidative stress, Colloids Surfaces B Biointerfaces. 187 (2020) 110658. https://doi.org/10.1016/j.colsurfb.2019.110658.

USC UNIVERSIDADE DE SANTIAGO DE COMPOSTELA

[101] A. Cacciamali, L. Pascucci, R. Villa, S. Dotti, Engineered nanoparticles toxicity on adipose tissue derived mesenchymal stem cells: A preliminary investigation, Res. Vet. Sci. 152 (2022) 134–149. https://doi.org/10.1016/j.rvsc.2022.08.002.

[102] M.F. Gutierrez, A. Ale, V. Andrade, C. Bacchetta, A. Rossi, J. Cazenave, Metallic, metal oxide, and metalloid nanoparticles toxic effects on freshwater microcrustaceans: An update and basis for the use of new test species, Water Environ. Res. 93 (2021) 2505–2526. https://doi.org/10.1002/wer.1637.

[103] D. Batir-Marin, M. Boev, O. Cioanca, I.I. Lungu, G.A. Marin, A.F. Burlec, A.M. Mitran, C. Mircea, M. Hancianu, Exploring Oxidative Stress Mechanisms of Nanoparticles Using Zebrafish (Danio rerio): Toxicological and Pharmaceutical Insights, Antioxidants. 14 (2025) 1–22. https://doi.org/10.3390/antiox14040489.

[104] S. El Kholy, Y. Al Naggar, Insights into the mechanism of histamine synthesis and recycling disruption induced by exposure to CdO NPs in the fruit fly (Drosophila melanogaster), Environ. Sci. Pollut. Res. (2023) 27936–27947. https://doi.org/10.1007/s11356-023-28211-7.

[105] M. Awashra, P. Młynarz, The toxicity of nanoparticles and their interaction with cells: an in vitro metabolomic perspective, Nanoscale Adv. 5 (2023) 2674–2723. https://doi.org/10.1039/d2na00534d.

[106] S. Tenzer, D. Docter, J. Kuharev, A. Musyanovych, V. Fetz, R. Hecht, F. Schlenk, D. Fischer, K. Kiouptsi, C. Reinhardt, K. Landfester, H. Schild, M. Maskos, S.K. Knauer, R.H. Stauber, Rapid formation of plasma protein corona critically affects nanoparticle pathophysiology, Nat. Nanotechnol. 8 (2013) 772–781. https://doi.org/10.1038/nnano.2013.181.

[107] D. Westmeier, S.K. Knauer, R.H. Stauber, D. Docter, Bio – Nano Interactions, Second Edition, Elsevier Inc., 2017. https://doi.org/10.1016/B978-0-12-809199-9/00001-X.

[108] T. Sun, Y. Kang, J. Liu, Y. Zhang, L. Ou, X. Liu, R. Lai, L. Shao, Nanomaterials and hepatic disease: toxicokinetics, disease types, intrinsic mechanisms, liver susceptibility, and influencing factors, J. Nanobiotechnology. 19 (2021) 1–23. https://doi.org/10.1186/s12951-021-00843-2.

[109] W. Thongkam, K. Gerloff, D. van Berlo, C. Albrecht, R.P.F. Schins, Oxidant generation, DNA damage and cytotoxicity by a panel of engineered nanomaterials in three different human epithelial cell lines, Mutagenesis. 32 (2017) 105–115. https://doi.org/10.1093/MUTAGE/GEW056.

[110] A. Ivask, M. Visnapuu, P. Vallotton, E.R. Marzouk, E. Lombi, N.H. Voelcker, Quantitative multimodal analyses of silver nanoparticle-cell interactions: Implications for cytotoxicity, NanoImpact. 1 (2016) 29–38. https://doi.org/10.1016/j.impact.2016.02.003.

[111] S. Salazar-García, A.S. Silva-Ramírez, M.A. Ramirez-Lee, H. Rosas-Hernandez, E. Rangel-López, C.G. Castillo, A. Santamaría, G.A. Martinez-Castañon, C. Gonzalez, Comparative effects on rat primary astrocytes and C6 rat glioma cells cultures after 24-h exposure to silver nanoparticles (AgNPs), J. Nanoparticle Res. 17 (2015) 1–13. https://doi.org/10.1007/s11051-015-3257-1.

USC UNIVERSIDADE DE COMPOSTELA

[112] Z. Wang, S. Liu, J. Ma, G. Qu, X. Wang, S. Yu, J. He, J. Liu, T. Xia, G. Bin Jiang, Silver nanoparticles induced RNA polymerase-silver binding and RNA transcription inhibition in erythroid progenitor cells, ACS Nano. 7 (2013) 4171–4186. https://doi.org/10.1021/nn400594s.

[113] M.J. Piao, K.A. Kang, I.K. Lee, H.S. Kim, S. Kim, J.Y. Choi, J. Choi, J.W. Hyun, Silver nanoparticles induce oxidative cell damage in human liver cells through inhibition of reduced glutathione and induction of mitochondria-involved apoptosis, Toxicol. Lett. 201 (2011) 92–100. https://doi.org/10.1016/j.toxlet.2010.12.010.

[114] N. El Yamani, A.R. Collins, E. Rundén-Pran, L.M. Fjellsbø, S. Shaposhnikov, S. Zienolddiny, M. Dusinska, In vitro genotoxicity testing of four reference metal nanomaterials, titanium dioxide, zinc oxide, cerium oxide and silver: Towards reliable hazard assessment, Mutagenesis. 32 (2017) 117–126. https://doi.org/10.1093/mutage/gew060.

[115] A.R. Gliga, S. Skoglund, I. Odnevall Wallinder, B. Fadeel, H.L. Karlsson, Size-dependent cytotoxicity of silver nanoparticles in human lung cells: The role of cellular uptake, agglomeration and Ag release, Part. Fibre Toxicol. 11 (2014) 1–17. https://doi.org/10.1186/1743-8977-11-11.

[116] E.J. Park, J. Yi, Y. Kim, K. Choi, K. Park, Silver nanoparticles induce cytotoxicity by a Trojan-horse type mechanism, Toxicol. Vitr. 24 (2010) 872–878. https://doi.org/10.1016/j.tiv.2009.12.001.

[117] C. Andreoli, V. Prota, I. De Angelis, E. Facchini, A. Zijno, E. Meccia, B. Barletta, C. Butteroni, S. Corinti, C. Chatgilialoglu, M.G. Krokidis, A. Masi, M. Condello, S. Meschini, G. Di Felice, F. Barone, A harmonized and standardized in vitro approach produces reliable results on silver nanoparticles toxicity in different cell lines, J. Appl. Toxicol. 41 (2021) 1980–1997. https://doi.org/10.1002/jat.4178.

[118] M. Milić, G. Leitinger, I. Pavičić, M. Zebić Avdičević, S. Dobrović, W. Goessler, I. Vinković Vrček, Cellular uptake and toxicity effects of silver nanoparticles in mammalian kidney cells, J. Appl. Toxicol. 35 (2015) 581–592. https://doi.org/10.1002/jat.3081.

[119] N. Von Moos, V.I. Slaveykova, Oxidative stress induced by inorganic nanoparticles in bacteria and aquatic microalgae - State of the art and knowledge gaps, Nanotoxicology. 8 (2014) 605–630. https://doi.org/10.3109/17435390.2013.809810.

[120] A. Oukarroum, S. Bras, F. Perreault, R. Popovic, Inhibitory effects of silver nanoparticles in two green algae, Chlorella vulgaris and Dunaliella tertiolecta, Ecotoxicol. Environ. Saf. 78 (2012) 80–85. https://doi.org/10.1016/j.ecoenv.2011.11.012.

[121] O. Choi, Z. Hu, Size dependent and reactive oxygen species related nanosilver toxicity to nitrifying bacteria, Environ. Sci. Technol. 42 (2008) 4583–4588. https://doi.org/10.1021/es703238h.

[122] T.P. Dasari, H.M. Hwang, The effect of humic acids on the cytotoxicity of silver nanoparticles to a natural aquatic bacterial assemblage, Sci. Total Environ. 408 (2010) 5817–5823. https://doi.org/10.1016/j.scitotenv.2010.08.030.

USC UNIVERSIDADE DE SANTIAGO DE COMPOSTELA

[123] S. Asghari, S.A. Johari, J.H. Lee, Y.S. Kim, Y.B. Jeon, H.J. Choi, M.C. Moon, I.J. Yu, Toxicity of various silver nanoparticles compared to silver ions in Daphnia magna, J. Nanobiotechnology. 10 (2012) 1–11. https://doi.org/10.1186/1477-3155-10-14.

[124] F. Ribeiro, J.A. Gallego-Urrea, K. Jurkschat, A. Crossley, M. Hassellöv, C. Taylor, A.M.V.M. Soares, S. Loureiro, Silver nanoparticles and silver nitrate induce high toxicity to Pseudokirchneriella subcapitata, Daphnia magna and Danio rerio, Sci. Total Environ. 466–467 (2014) 232–241. https://doi.org/10.1016/j.scitotenv.2013.06.101.

[125] S.-Y. Park, J.-H. Choi, Geno- and Ecotoxicity Evaluation of Silver Nanoparticles in Freshwater Crustacean Daphnia magna, Environ. Eng. Res. 15 (2010) 23–27. https://doi.org/10.4491/eer.2010.15.1.428.

[126] H.C. Poynton, J.M. Lazorchak, C.A. Impellitteri, B.J. Blalock, K. Rogers, H.J. Allen, A. Loguinov, J.L. Heckman, S. Govindasmawy, Toxicogenomic responses of nanotoxicity in Daphnia magna exposed to silver nitrate and coated silver nanoparticles, Environ. Sci. Technol. 46 (2012) 6288–6296. https://doi.org/10.1021/es3001618.

[127] M. Sakamoto, J.Y. Ha, S. Yoneshima, C. Kataoka, H. Tatsuta, S. Kashiwada, Free Silver Ion as the Main Cause of Acute and Chronic Toxicity of Silver Nanoparticles to Cladocerans, Arch. Environ. Contam. Toxicol. 68 (2015) 500–509. https://doi.org/10.1007/s00244-014-0091-x.

[128] C. Völker, C. Boedicker, J. Daubenthaler, M. Oetken, J. Oehlmann, Comparative Toxicity Assessment of Nanosilver on Three Daphnia Species in Acute, Chronic and Multi-Generation Experiments, PLoS One. 8 (2013). https://doi.org/10.1371/journal.pone.0075026.

[129] H.S. Park, M. Behzadi Tayemeh, I.J. Yu, S.A. Johari, Evaluation of silver nanowires (AgNWs) toxicity on reproductive success of Daphnia magna over two generations and their teratogenic effect on embryonic development, J. Hazard. Mater. 412 (2021). https://doi.org/10.1016/j.jhazmat.2021.125339.

[130] V. Galhano, S. Hartmann, M.S. Monteiro, R. Zeumer, D. Mozhayeva, B. Steinhoff, K. Müller, K. Prenzel, J. Kunze, K.D. Kuhnert, H. Schönherr, C. Engelhard, C. Schlechtriem, S. Loureiro, A.M.V.M. Soares, K. Witte, I. Lopes, Impact of wastewater-borne nanoparticles of silver and titanium dioxide on the swimming behaviour and biochemical markers of Daphnia magna: An integrated approach, Aquat. Toxicol. 220 (2020). https://doi.org/10.1016/j.aquatox.2020.105404.

[131] P. Bonfanti, A. Colombo, R. Bengalli, M. Gualtieri, I. Zanoni, M. Blosi, A. Costa, P. Mantecca, Functional silver-based nanomaterials affecting zebrafish development: the adverse outcomes in relation to the nanoparticle physical and chemical structure, Environ. Sci. Nano. 11 (2024) 2521–2540. https://doi.org/10.1039/d3en00813d.

[132] N.B. Abramenko, T.B. Demidova, E. V. Abkhalimov, B.G. Ershov, E.Y. Krysanov, L.M. Kustov, Ecotoxicity of different-shaped silver nanoparticles: Case of zebrafish embryos, J. Hazard. Mater. 347 (2018) 89–94. https://doi.org/10.1016/j.jhazmat.2017.12.060.

[133] L. Qiang, Z.H. Arabeyyat, Q. Xin, V.N. Paunov, I.J.F. Dale, R.I.L. Mills, J.M. Rotchell, J. Cheng, Silver nanoparticles in Zebrafish (Danio rerio) embryos: Uptake, growth and

USC UNIVERSIDADE DE COMPOSTELA

molecular responses, Int. J. Mol. Sci. 21 (2020) 1–14. https://doi.org/10.3390/ijms21051876.

[134] R. Bautista-Pérez, A. Cano-Martínez, M.A. Herrera-Rodríguez, M.D.P. Ramos-Godinez, O.L. Pérez Reyes, Y.I. Chirino, Z.J. Rodríguez Serrano, R. López-Marure, Oral Exposure to Titanium Dioxide E171 and Zinc Oxide Nanoparticles Induces Multi-Organ Damage in Rats: Role of Ceramide, Int. J. Mol. Sci. 25 (2024). https://doi.org/10.3390/ijms25115881.

[135] K.P. Priyanka, V.S. Harikumar, K.M. Balakrishna, T. Varghese, Inhibitory effect of TiO2 NPs on symbiotic arbuscular mycorrhizal fungi in plant roots, IET Nanobiotechnology. 11 (2017) 66–70. https://doi.org/10.1049/iet-nbt.2016.0032.

[136] A. Dabrunz, L. Duester, C. Prasse, F. Seitz, R. Rosenfeldt, C. Schilde, G.E. Schaumann, R. Schulz, Biological surface coating and molting inhibition as mechanisms of TiO2 nanoparticle toxicity in daphnia magna, PLoS One. 6 (2011) 1–7. https://doi.org/10.1371/journal.pone.0020112.

[137] M. Renzi, A. Blašković, Ecotoxicity of nano-metal oxides: A case study on daphnia magna, Ecotoxicology. 28 (2019) 878–889. https://doi.org/10.1007/s10646-019-02085-3.

[138] F. Seitz, M. Bundschuh, R.R. Rosenfeldt, R. Schulz, Nanoparticle toxicity in Daphnia magna reproduction studies: The importance of test design, Aquat. Toxicol. 126 (2013) 163–168. https://doi.org/10.1016/j.aquatox.2012.10.015.

[139] X. Zhu, Y. Chang, Y. Chen, Toxicity and bioaccumulation of TiO2 nanoparticle aggregates in Daphnia magna, Chemosphere. 78 (2010) 209–215. https://doi.org/10.1016/j.chemosphere.2009.11.013.

[140] S.B. Lovern, J.R. Strickler, R. Klaper, Behavioral and physiological changes in Daphnia magna when exposed to nanoparticle suspensions (titanium dioxide, nano-C60, and C 60HxC70Hx), Environ. Sci. Technol. 41 (2007) 4465–4470. https://doi.org/10.1021/es062146p.

[141] C. Noss, A. Dabrunz, R.R. Rosenfeldt, A. Lorke, R. Schulz, Three-dimensional analysis of the swimming behavior of daphnia magna exposed to nanosized titanium dioxide, PLoS One. 8 (2013). https://doi.org/10.1371/journal.pone.0080960.

[142] G. Caruso, E.M. Scalisi, R. Pecoraro, V. Cardaci, A. Privitera, E. Truglio, F. Capparucci, R. Jarosova, A. Salvaggio, F. Caraci, M.V. Brundo, Effects of carnosine on the embryonic development and TiO2 nanoparticles-induced oxidative stress on Zebrafish, Front. Vet. Sci. 10 (2023). https://doi.org/10.3389/fvets.2023.1148766.

[143] S. Halappanavar, L. Rahman, J. Nikota, S.S. Poulsen, Y. Ding, P. Jackson, H. Wallin, O. Schmid, U. Vogel, A. Williams, Ranking of nanomaterial potency to induce pathway perturbations associated with lung responses, NanoImpact. 14 (2019) 100158. https://doi.org/10.1016/j.impact.2019.100158.

[144] C.W. Chen, J.H. Huang, T.C. Lai, Y.H. Jan, M. Hsiao, C.H. Chen, Y.K. Hwu, R.S. Liu, Evaluation of the intracellular uptake and cytotoxicity effect of TiO2 nanostructures for various human oral and lung cells under dark conditions, Toxicol. Res. (Camb). 5 (2015) 303–311. https://doi.org/10.1039/c5tx00312a.

USC UNIVERSIDADE DE SANTIAGO DE COMPOSTELA

[145] L. Chen, L. Zhou, Y. Liu, S. Deng, H. Wu, G. Wang, Toxicological effects of nanometer titanium dioxide (nano-TiO2) on Chlamydomonas reinhardtii, Ecotoxicol. Environ. Saf. 84 (2012) 155–162. https://doi.org/10.1016/j.ecoenv.2012.07.019.

[146] D. Lin, J. Ji, Z. Long, K. Yang, F. Wu, The influence of dissolved and surface-bound humic acid on the toxicity of TiO2 nanoparticles to Chlorella sp., Water Res. 46 (2012) 4477–4487. https://doi.org/10.1016/j.watres.2012.05.035.

[147] L.K. Adams, D.Y. Lyon, A. McIntosh, P.J.J. Alvarez, Comparative toxicity of nano-scale TiO2, SiO2 and ZnO water suspensions, Water Sci. Technol. 54 (2006) 327–334. https://doi.org/10.2166/wst.2006.891.

[148] C. Cherchi, T. Chernenko, M. Diem, A.Z. Gu, Impact of nano titanium dioxide exposure on cellular structure of Anabaena variabilis and evidence of internalization, Environ. Toxicol. Chem. 30 (2011) 861–869. https://doi.org/10.1002/etc.445.

[149] G. Gogniat, S. Dukan, TiO2 photocatalysis causes DNA damage via fenton reaction-generated hydroxyl radicals during the recovery period, Appl. Environ. Microbiol. 73 (2007) 7740–7743. https://doi.org/10.1128/AEM.01079-07.

[150] C.M. Hessler, M.Y. Wu, Z. Xue, H. Choi, Y. Seo, The influence of capsular extracellular polymeric substances on the interaction between TiO2 nanoparticles and planktonic bacteria, Water Res. 46 (2012) 4687–4696. https://doi.org/10.1016/j.watres.2012.06.009.

[151] European Union. Commission Regulation (EC) No 450/2009 of 29 May 2009 on active and intelligent materials and articles intended to come into contact with food, Off. J. Eur. Union. (2009).

[152] European Union. Regulation (EC) No 1223/2009 of the European Parliament and of the Council of 30 November 2009 on cosmetic products, Off. J. Eur. Union. (2009).

[153] European Union. Regulation (EC) No 1169/2011 of the European Parliament and of the Council of 25 October 2011 on the provision of food information to consumers, amending Regulations (EC) No 1924/2006 and (EC) No 1925/2006 of the European Parliament and of, Off. J. Eur. Union. (2011).

[154] European Union. Regulation (EU) No 528/2012 of the European Parliament and of the Council of 22 May 2012 concerning the making available on the market and use of biocidal products, Off. J. Eur. Union. (2012).

[155] European Union. Regulation (EU) No 2015/2283 of the European Parliament and of the Council of 25 November 2015 on novel foods, amending Regulation (EU) No 1169/2011 of the European Parliament and of the Council and repealing Regulation (EC) No 258/97 of t, Off. J. Eur. Union. (2015).

[156] European Union. Regulation (EU) 2017/745 of the European Parliament and of the Council of 5 April 2017 on medical devices, amending Directive 2001/83/EC, Regulation (EC) No 178/2002 and Regulation (EC) No 1223/2009 and repealing Council Directives 90/385/, Off. J. Eur. Union. (2017).

[157] European Chemicals Agency (ECHA), Appendix for nanoforms applicable to the Guidance on Registration and Substance Identification - Version 2.0, 2020.

USC DE COMPOSTELA

https://data.europa.eu/doi/10.2823/40.

[158] V. Silano, C. Bolognesi, K. Chipman, J.P. Cravedi, K.H. Engel, P. Fowler, R. Franz, K. Grob, R. Gürtler, T. Husøy, S. Kärenlampi, W. Mennes, M.R. Milana, K. Pfaff, G. Riviere, J. Srinivasan, M. de F. Tavares Poças, C. Tlustos, D. Wölfle, H. Zorn, M. Kolf-Clauw, E. Lampi, K. Svensson, A. Lioupis, L. Castle, Safety assessment of the active substance selenium nanoparticles, for use in active food contact materials, EFSA J. 16 (2018) 1–7. https://doi.org/10.2903/j.efsa.2018.5115.

[159] European Commission, Scientific Committee on Consumer Safety. SCCS Opinion on Colloidal Silver (nano), SCCS/1596/18, Off. J. Eur. Union. (2018).

[160] SCCS (Scientific Committee on Consumer Safety), Opinion on the safety of Silver (CAS/EC No. 7440-22-4/231-131-3) used in cosmetic products, preliminary version of 27 March 2024, final version of 20 June, SCCS/1665/24, (n.d.).

[161] SCCS (Scientific Committee on Consumer Safety), Opinion on Platinum (nano), Colloidal Platinum (nano) and Acetyl tetrapeptide-17 Colloidal Platinum (nano), final version of 24-25 June 2021, SCCS/1630/21, (n.d.).

[162] SCCS (Scientific Committee on Consumer Safety), Opinion on Gold (nano), Colloidal Gold (nano), Gold Thioethylamino Hyaluronic Acid (nano) and Acetyl heptapeptide-9 Colloidal Gold (nano), final version of 24-25 June 2021, SCCS/1629/2021, (n.d.).

[163] I. Corsi, A. Bellingeri, M.C. Eliso, G. Grassi, G. Liberatori, C. Murano, L. Sturba, M.L. Vannuccini, E. Bergami, Eco-interactions of engineered nanomaterials in the marine environment: Towards an eco-design framework, Nanomaterials. 11 (2021). https://doi.org/10.3390/nano11081903.

[164] T. Devasena, B. Iffath, R. Renjith Kumar, N. Muninathan, K. Baskaran, T. Srinivasan, S.T. John, Insights on the Dynamics and Toxicity of Nanoparticles in Environmental Matrices, Bioinorg. Chem. Appl. 2022 (2022). https://doi.org/10.1155/2022/4348149.

[165] P.A. Holden, J.L. Gardea-Torresdey, F. Klaessig, R.F. Turco, M. Mortimer, K. Hund-Rinke, E.A. Cohen Hubal, D. Avery, D. Barceló, R. Behra, Y. Cohen, L. Deydier-Stephan, P.L. Ferguson, T.F. Fernandes, B. Herr Harthorn, W.M. Henderson, R.A. Hoke, D. Hristozov, J.M. Johnston, A.B. Kane, L. Kapustka, A.A. Keller, H.S. Lenihan, W. Lovell, C.J. Murphy, R.M. Nisbet, E.J. Petersen, E.R. Salinas, M. Scheringer, M. Sharma, D.E. Speed, Y. Sultan, P. Westerhoff, J.C. White, M.R. Wiesner, E.M. Wong, B. Xing, M. Steele Horan, H.A. Godwin, A.E. Nel, Considerations of Environmentally Relevant Test Conditions for Improved Evaluation of Ecological Hazards of Engineered Nanomaterials, Environ. Sci. Technol. 50 (2016) 6124–6145. https://doi.org/10.1021/acs.est.6b00608.

[166] T.K. Tran, M.K. Nguyen, C. Lin, T.D. Hoang, T.C. Nguyen, A.M. Lone, A.P. Khedulkar, M.S. Gaballah, J. Singh, W.J. Chung, D.D. Nguyen, Review on fate, transport, toxicity and health risk of nanoparticles in natural ecosystems: Emerging challenges in the modern age and solutions toward a sustainable environment, Sci. Total Environ. 912 (2024) 169331. https://doi.org/10.1016/j.scitotenv.2023.169331.

[167] J. Geng, W. Fang, M. Liu, J. Yang, Z. Ma, J. Bi, Advances and future directions of environmental risk research: A bibliometric review, Sci. Total Environ. 954 (2024)

USC UNIVERSIDADE DE SANTIAGO DE COMPOSTELA

176246. https://doi.org/10.1016/j.scitotenv.2024.176246.

[168] World Economic forum, The Global Risk Report 2024, 19th Edition, https://www.weforum.org/publications/ global-risks-report-2024/.

[169] G. Vale, K. Mehennaoui, S. Cambier, G. Libralato, S. Jomini, R.F. Domingos, Manufactured nanoparticles in the aquatic environment-biochemical responses on freshwater organisms: A critical overview, Aquat. Toxicol. 170 (2016) 162–174. https://doi.org/10.1016/j.aquatox.2015.11.019.

[170] M. Heinlaan, A. Ivask, I. Blinova, H.C. Dubourguier, A. Kahru, Toxicity of nanosized and bulk ZnO, CuO and TiO2 to bacteria Vibrio fischeri and crustaceans Daphnia magna and Thamnocephalus platyurus, Chemosphere. 71 (2008) 1308–1316. https://doi.org/10.1016/j.chemosphere.2007.11.047.

[171] C.N. Lok, C.M. Ho, R. Chen, Q.Y. He, W.Y. Yu, H. Sun, P.K.H. Tam, J.F. Chiu, C.M. Che, Silver nanoparticles: Partial oxidation and antibacterial activities, J. Biol. Inorg. Chem. 12 (2007) 527–534. https://doi.org/10.1007/s00775-007-0208-z.

[172] R. Ma, J. Stegemeier, C. Levard, J.G. Dale, C.W. Noack, T. Yang, G.E. Brown, G. V. Lowry, Sulfidation of copper oxide nanoparticles and properties of resulting copper sulfide, Environ. Sci. Nano. 1 (2014) 347–357. https://doi.org/10.1039/c4en00018h.

[173] R.F. Domingos, C. Franco, J.P. Pinheiro, The role of charged polymer coatings of nanoparticles on the speciation and fate of metal ions in the environment, Environ. Sci. Pollut. Res. 22 (2015) 2900–2906. https://doi.org/10.1007/s11356-014-3546-8.

[174] B. Thalmann, A. Voegelin, B. Sinnet, E. Morgenroth, R. Kaegi, Sulfidation kinetics of silver nanoparticles reacted with metal sulfides, Environ. Sci. Technol. 48 (2014) 4885–4892. https://doi.org/10.1021/es5003378.

[175] K. Hund-Rinke, M. Simon, Ecotoxic effect of photocatalytic active nanoparticles (TiO2) on algae and daphnids, Environ. Sci. Pollut. Res. 13 (2006) 225–232. https://doi.org/10.1065/espr2006.06.311.

[176] A.S. El-Kalliny, M.S. Abdel-Wahed, A.A. El-Zahhar, I.A. Hamza, T.A. Gad-Allah, Nanomaterials: a review of emerging contaminants with potential health or environmental impact, Discov. Nano. 18 (2023). https://doi.org/10.1186/s11671-023-03787-8.

[177] B. Avant, D. Bouchard, X. Chang, H.S. Hsieh, B. Acrey, Y. Han, J. Spear, R. Zepp, C.D. Knightes, Environmental fate of multiwalled carbon nanotubes and graphene oxide across different aquatic ecosystems, NanoImpact. 13 (2019) 1–12. https://doi.org/10.1016/j.impact.2018.11.001.

[178] S.D. Richardson, T.A. Ternes, Water Analysis: Emerging Contaminants and Current Issues, Anal. Chem. 90 (2018) 398–428. https://doi.org/10.1021/acs.analchem.7b04577.

[179] F. Gottschalk, T. Sun, B. Nowack, Environmental concentrations of engineered nanomaterials: Review of modeling and analytical studies, Environ. Pollut. 181 (2013) 287–300. https://doi.org/10.1016/j.envpol.2013.06.003.

[180] C. Neal, H. Jarvie, P. Rowland, A. Lawler, D. Sleep, P. Scholefield, Titanium in UK rural, agricultural and urban/industrial rivers: Geogenic and anthropogenic colloidal/sub-

colloidal sources and the significance of within-river retention, Sci. Total Environ. 409 (2011) 1843–1853. https://doi.org/10.1016/j.scitotenv.2010.12.021.

[181] N. Sani-Kast, M. Scheringer, D. Slomberg, J. Labille, A. Praetorius, P. Ollivier, K. Hungerbühler, Addressing the complexity of water chemistry in environmental fate modeling for engineered nanoparticles, Sci. Total Environ. 535 (2015) 150–159. https://doi.org/10.1016/j.scitotenv.2014.12.025.

[182] P.S. Tourinho, C.A.M. van Gestel, S. Lofts, C. Svendsen, A.M.V.M. Soares, S. Loureiro, Metal-based nanoparticles in soil: Fate, behavior, and effects on soil invertebrates, Environ. Toxicol. Chem. 31 (2012) 1679–1692. https://doi.org/10.1002/etc.1880.

[183] T.Y. Sun, N.A. Bornhöft, K. Hungerbühler, B. Nowack, Dynamic Probabilistic Modeling of Environmental Emissions of Engineered Nanomaterials, Environ. Sci. Technol. 50 (2016) 4701–4711. https://doi.org/10.1021/acs.est.5b05828.

[184] B. Giese, F. Klaessig, B. Park, R. Kaegi, M. Steinfeldt, H. Wigger, A. Von Gleich, F. Gottschalk, Risks, Release and Concentrations of Engineered Nanomaterial in the Environment, Sci. Rep. 8 (2018) 1–18. https://doi.org/10.1038/s41598-018-19275-4.

[185] C.D. Metcalfe, T. Sultana, J. Martin, K. Newman, P. Helm, Silver near municipal wastewater discharges into western Lake Ontario, Canada, Environ Monit Assess 190, 555 (2018) https://doi.org/10.1007/s10661-018-6922-x.

[186] Y. Cong, G.T. Banta, H. Selck, D. Berhanu, E. Valsami-Jones, V.E. Forbes, Toxicity and bioaccumulation of sediment-associated silver nanoparticles in the estuarine polychaete, Nereis (Hediste) diversicolor, Aquat. Toxicol. 156 (2014) 106–115. https://doi.org/10.1016/j.aquatox.2014.08.001.

[187] Z. Luo, Z. Wang, Q. Li, Q. Pan, C. Yan, F. Liu, Spatial distribution, electron microscopy analysis of titanium and its correlation to heavy metals: Occurrence and sources of titanium nanomaterials in surface sediments from Xiamen Bay, China, J. Environ. Monit. 13 (2011) 1046–1052. https://doi.org/10.1039/c0em00199f.

[188] M.A. Kiser, P. Westerhoff, T. Benn, Y. Wang, J. Pérez-Rivera, K. Hristovski, Titanium nanomaterial removal and release from wastewater treatment plants, Environ. Sci. Technol. 43 (2009) 6757–6763. https://doi.org/10.1021/es901102n.

[189] A.C. Johnson, M.J. Bowes, A. Crossley, H.P. Jarvie, K. Jurkschat, M.D. Jürgens, A.J. Lawlor, B. Park, P. Rowland, D. Spurgeon, C. Svendsen, I.P. Thompson, R.J. Barnes, R.J. Williams, N. Xu, An assessment of the fate, behaviour and environmental risk associated with sunscreen TiO2 nanoparticles in UK field scenarios, Sci. Total Environ. 409 (2011) 2503–2510. https://doi.org/10.1016/j.scitotenv.2011.03.040.

[190] K. Khosravi, M.E. Hoque, B. Dimock, H. Hintelmann, C.D. Metcalfe, A novel approach for determining total titanium from titanium dioxide nanoparticles suspended in water and biosolids by digestion with ammonium persulfate, Anal. Chim. Acta. 713 (2012) 86–91. https://doi.org/10.1016/j.aca.2011.11.048.

[191] P. Luo, I. Morrison, A. Dudkiewicz, K. Tiede, E. Boyes, P. O'Toole, S. Park, A.B. Boxall, Visualization and characterization of engineered nanoparticles in complex environmental and food matrices using atmospheric scanning electron microscopy, J. Microsc. 250 (2013) 32–41. https://doi.org/10.1111/jmi.12014.

USC UNIVERSIDADE DE SANTIAGO DE COMPOSTELA

[192] V. Adam, A. Caballero-Guzman, B. Nowack, Considering the forms of released engineered nanomaterials in probabilistic material flow analysis, Environ. Pollut. 243 (2018) 17–27. https://doi.org/10.1016/j.envpol.2018.07.108.

[193] J. Zhao, X. Wang, S.A. Hoang, N.S. Bolan, M.B. Kirkham, J. Liu, X. Xia, Y. Li, Silver nanoparticles in aquatic sediments: Occurrence, chemical transformations, toxicity, and analytical methods, J. Hazard. Mater. 418 (2021) 126368. https://doi.org/10.1016/j.jhazmat.2021.126368.

[194] C. Meier, A. Voegelin, A. Pradas Del Real, G. Sarret, C.R. Mueller, R. Kaegi, Transformation of Silver Nanoparticles in Sewage Sludge during Incineration, Environ. Sci. Technol. 50 (2016) 3503–3510. https://doi.org/10.1021/acs.est.5b04804.

[195] A.S. El-Kalliny, M.S. Abdel-Wahed, A.A. El-Zahhar, I.A. Hamza, T.A. Gad-Allah, Nanomaterials: a review of emerging contaminants with potential health or environmental impact, Discov. Nano. 18 (2023). https://doi.org/10.1186/s11671-023-03787-8.

[196] World Health Organization (WHO), The top 10 causes of death, 7 August 2024. (n.d.). https://www.who.int/news-room/fact-sheets/detail/the-top-10-causes-of-death (accessed July 14, 2025).

[197] World Health Organization (WHO), Ambient air pollution: A global assessment of exposure and burden of disease, 2016, https://www.who.int/publications/i/item/9789241511353 (accessed July 14, 2025).

[198] C. Li, A. van Donkelaar, M.S. Hammer, E.E. McDuffie, R.T. Burnett, J. V. Spadaro, D. Chatterjee, A.J. Cohen, J.S. Apte, V.A. Southerland, S.C. Anenberg, M. Brauer, R. V. Martin, Reversal of trends in global fine particulate matter air pollution, Nat. Commun. 14 (2023) 1–12. https://doi.org/10.1038/s41467-023-41086-z.

[199] United States Environmental Protection Agency (US EPA), Emerging Contaminants – Nanomaterials At a Glance. (2010). https://archive.epa.gov/region9/mediacenter/web/pdf/emerging_contaminant_nanomaterials.pdf.

[200] B. Nowack, N.C. Mueller, Exposure modeling of engineered nanoparticles in the environment, EMPA Act. 41 (2008) 63.

[201] F. Gottschalk, T. Sonderer, R.W. Scholz, B. Nowack, Modeled environmental concentrations of engineered nanomaterials (TiO2, ZnO, Ag, CNT, fullerenes) for different regions, Environ. Sci. Technol. 43 (2009) 9216–9222. https://doi.org/10.1021/es9015553.

[202] S. Aredes, B. Klein, M. Pawlik, The removal of arsenic from water using natural iron oxide minerals, J. Clean. Prod. 29–30 (2012) 208–213. https://doi.org/10.1016/j.jclepro.2012.01.029.

[203] S. Sarkar, L.M. Blaney, A. Gupta, D. Ghosh, A.K. SenGupta, Use of ArsenXnp, a hybrid anion exchanger, for arsenic removal in remote villages in the Indian subcontinent, React. Funct. Polym. 67 (2007) 1599–1611. https://doi.org/10.1016/j.reactfunctpolym.2007.07.047.

USC UNIVERSIDADE DE SANTIAGO DE COMPOSTELA

[204] A.K. Gupta, D. Deva, A. Sharma, N. Verma, Fe-grown carbon nanofibers for removal of arsenic(V) in wastewater, Ind. Eng. Chem. Res. 49 (2010) 7074–7084. https://doi.org/10.1021/ie100392q.

[205] K. Stojak Repa, Perspectives on the use of magnetic materials for environmental remediation: A mini review, Phys. Lett. Sect. A Gen. At. Solid State Phys. 539 (2025) 130341. https://doi.org/10.1016/j.physleta.2025.130341.

[206] A. K, Y. Devarajan, Nanomaterials-Based Wastewater Treatment: Addressing Challenges and Advancing Sustainable Solutions, Bionanoscience. 15 (2025). https://doi.org/10.1007/s12668-024-01780-8.

[207] I. Gehrke, A. Geiser, A. Somborn-Schulz, Innovations in nanotechnology for water treatment, Nanotechnol. Sci. Appl. 8 (2015) 1–17. https://doi.org/10.2147/NSA.S43773.

[208] R. Nawaz, M.M. Hanafiah, Z. Sakawi, Z.A. Baki, S.B.Z. Abidin, M. Anjum, A. Fazli Ismail, U. Arshad, A review of the defective TiO2 materials-based photocatalysis for environmental remediation: exploring the nexus between light wavelength and energy consumption, Appl. Energy. 393 (2025) 126143. https://doi.org/10.1016/j.apenergy.2025.126143.

[209] A.A. Shvedova, N. Yanamala, E.R. Kisin, T.O. Khailulli, M.E. Birch, L.M. Fatkhutdinova, Integrated analysis of dysregulated ncRNA and mRNA expression profiles in humans exposed to carbon nanotubes, PLoS One. 11 (2016) 1–32. https://doi.org/10.1371/journal.pone.0150628.

[210] S.H. Liou, C.S.J. Tsai, D. Pelclova, M.K. Schubauer-Berigan, P.A. Schulte, Assessing the first wave of epidemiological studies of nanomaterial workers, J. Nanoparticle Res. 17 (2015) 1–19. https://doi.org/10.1007/s11051-015-3219-7.

[211] W. Te Wu, H.Y. Liao, Y.T. Chung, W.F. Li, T.C. Tsou, L.A. Li, M.H. Lin, J.J. Ho, T.N. Wu, S.H. Liou, Effect of nanoparticles exposure on fractional exhaled nitric Oxide(FENO) in workers exposed to nanomaterials, Int. J. Mol. Sci. 15 (2014) 878–894. https://doi.org/10.3390/ijms15010878.

[212] E. Asmatulu, M.N. Andalib, B. Subeshan, F. Abedin, Impact of nanomaterials on human health: a review, Environ. Chem. Lett. 20 (2022) 2509–2529. https://doi.org/10.1007/s10311-022-01430-z.

[213] E. Mostovenko, C.G. Canal, M.J. Cho, K. Sharma, A. Erdely, M.J. Campen, A.K. Ottens, Indirect mediators of systemic health outcomes following nanoparticle inhalation exposure, Pharmacol. Ther. 235 (2022) 108120. https://doi.org/10.1016/j.pharmthera.2022.108120.

[214] A. Pietroiusti, H. Stockmann-Juvala, F. Lucaroni, K. Savolainen, Nanomaterial exposure, toxicity, and impact on human health, Wiley Interdiscip. Rev. Nanomedicine Nanobiotechnology. 10 (2018) 1–21. https://doi.org/10.1002/wnan.1513.

[215] M.G. Soliman, A. Martinez-Serra, G. Antonello, M. Dobricic, T. Wilkins, T. Serchi, I. Fenoglio, M.P. Monopoli, Understanding the role of biomolecular coronas in human exposure to nanomaterials, Environ. Sci. Nano. 11 (2024) 4421–4448. https://doi.org/10.1039/d4en00488d.

USC UNIVERSIDADE DE SANTIAGO DE COMPOSTELA

[216] O. Creutzenberg, G. Pohlmann, D. Schaudien, H. Kock, Toxicokinetics of Nanoparticles Deposited in Lungs Using Occupational Exposure Scenarios, Front. Public Heal. 10 (2022) 909247. https://doi.org/10.3389/fpubh.2022.909247.

[217] A.T. Hak Soo Choi, Yoshitomo Ashitate, Jeong Heon Lee, Soon Hee Kim, Aya Matsui, Numpon Insin, Moungi G Bawendi, Manuela Semmler-Behnke, John V Frangioni, Rapid translocation of nanoparticles from the lung airspaces to the body, Nat. Biotechnol. 28 (2010) 1300–1303. https://doi.org/10.1038/nbt.1696.

[218] A. Elder, R. Gelein, V. Silva, T. Feikert, L. Opanashuk, J. Carter, R. Potter, A. Maynard, Y. Ito, J. Finkelstein, G. Oberdörster, Translocation of inhaled ultrafine manganese oxide particles to the central nervous system, Environ. Health Perspect. 114 (2006) 1172–1178. https://doi.org/10.1289/ehp.9030.

[219] H.M. Braakhuis, I. Gosens, P. Krystek, J.A.F. Boere, F.R. Cassee, P.H.B. Fokkens, J.A. Post, H. van Loveren, M.V.D.Z. Park, Particle size dependent deposition and pulmonary inflammation after short-term inhalation of silver nanoparticles, Part. Fibre Toxicol. 11 (2014) 1–16. https://doi.org/10.1186/s12989-014-0049-1.

[220] G. Oberdörster, J. Ferin, B.E. Lehnert, Correlation between particle size, in vivo particle persistence, and lung injury, Environ. Health Perspect. 102 (1994) 173–179. https://doi.org/10.1289/ehp.102-1567252.

[221] V. Sharma, A. Kumar, A. Dhawan, Nanomaterials: Exposure, Effects and Toxicity Assessment, Proc. Natl. Acad. Sci. India Sect. B Biol. Sci. 82 (2012) 3–11. https://doi.org/10.1007/s40011-012-0072-7.

[222] A. Pietroiusti, A. Magrini, L. Campagnolo, New frontiers in nanotoxicology: Gut microbiota/microbiome-mediated effects of engineered nanomaterials, Toxicol. Appl. Pharmacol. 299 (2016) 90–95. https://doi.org/10.1016/j.taap.2015.12.017.

[223] Y. Bi, A.K. Marcus, H. Robert, R. Krajmalnik-Brown, B.E. Rittmann, P. Westerhoff, M.H. Ropers, M. Mercier-Bonin, The complex puzzle of dietary silver nanoparticles, mucus and microbiota in the gut, J. Toxicol. Environ. Heal. - Part B Crit. Rev. 23 (2020) 69–89. https://doi.org/10.1080/10937404.2019.1710914.

[224] J. Li, M. Tang, Y. Xue, Review of the effects of silver nanoparticle exposure on gut bacteria, J. Appl. Toxicol. 39 (2019) 27–37. https://doi.org/10.1002/jat.3729.

[225] P. Ganguly, A. Breen, S.C. Pillai, Toxicity of Nanomaterials: Exposure, Pathways, Assessment, and Recent Advances, ACS Biomater. Sci. Eng. 4 (2018) 2237–2275. https://doi.org/10.1021/acsbiomaterials.8b00068.

[226] F.A.W. Ingrid L. Bergin, Nanoparticle toxicity by the gastrointestinal route: eviddence and knowledge gaps, Int. J. Biomed. Nanosci. Nanotechnol. 3 (2013) 1–44. https://doi.org/10.1504/IJBNN.2013.054515.

[227] A.A.M. Kämpfer, M. Busch, R.P.F. Schins, Advanced in vitro testing strategies and models of the intestine for nanosafety research, Chem. Res. Toxicol. 33 (2020) 1163–1178. https://doi.org/10.1021/acs.chemrestox.0c00079.

[228] E.I. Medina-Reyes, C. Rodríguez-Ibarra, A. Déciga-Alcaraz, D. Díaz-Urbina, Y.I. Chirino, J. Pedraza-Chaverri, Food additives containing nanoparticles induce

USC DE COMPOSTELA

gastrotoxicity, hepatotoxicity and alterations in animal behavior: The unknown role of oxidative stress, Food Chem. Toxicol. 146 (2020). https://doi.org/10.1016/j.fct.2020.111814.

[229] M.-H. Ropers, H. Terrisse, M. Mercier-Bonin, B. Humbert, Titanium Dioxide as Food Additive, Appl. Titan. Dioxide. (2017) 3–22. https://doi.org/10.5772/intechopen.68883.

[230] W. Xie, Z. Xiong, H. Wang, X. Liu, H. Cui, Q. Huang, Y. Tang, The nanosafety assessment of ENMs under a dermal exposure scenario: from key molecular events to in silico modeling tools, Environ. Sci. Nano. 11 (2023) 708–738. https://doi.org/10.1039/d3en00585b.

[231] T. Zaiter, R. Cornu, W. El Basset, H. Martin, M. Diab, A. Béduneau, Toxicity assessment of nanoparticles in contact with the skin, J. Nanoparticle Res. 24 (2022). https://doi.org/10.1007/s11051-022-05523-2.

[232] B. Baroli, M.G. Ennas, F. Loffredo, M. Isola, R. Pinna, M.A. López-Quintela, Penetration of metallic nanoparticles in human full-thickness skin, J. Invest. Dermatol. 127 (2007) 1701–1712. https://doi.org/10.1038/sj.jid.5700733.

[233] M. Crosera, M. Bovenzi, G. Maina, G. Adami, C. Zanette, C. Florio, F. Filon Larese, Nanoparticle dermal absorption and toxicity: A review of the literature, Int. Arch. Occup. Environ. Health. 82 (2009) 1043–1055. https://doi.org/10.1007/s00420-009-0458-x.

[234] F.F. Larese, F. D'Agostin, M. Crosera, G. Adami, N. Renzi, M. Bovenzi, G. Maina, Human skin penetration of silver nanoparticles through intact and damaged skin, Toxicology. 255 (2009) 33–37. https://doi.org/10.1016/j.tox.2008.09.025.

[235] T.G.M. Smijs, J.A. Bouwstra, Focus on skin as a possible port of entry for solid nanoparticles and the toxicological impact, J. Biomed. Nanotechnol. 6 (2010) 469–484. https://doi.org/10.1166/jbn.2010.1146.

[236] J. Wu, W. Liu, C. Xue, S. Zhou, F. Lan, L. Bi, H. Xu, X. Yang, F.D. Zeng, Toxicity and penetration of TiO2 nanoparticles in hairless mice and porcine skin after subchronic dermal exposure, Toxicol. Lett. 191 (2009) 1–8. https://doi.org/10.1016/j.toxlet.2009.05.020.

[237] A.K. Kohli, H.O. Alpar, Potential use of nanoparticles for transcutaneous vaccine delivery: Effect of particle size and charge, Int. J. Pharm. 275 (2004) 13–17. https://doi.org/10.1016/j.ijpharm.2003.10.038.

[238] Y.K. Tak, S. Pal, P.K. Naoghare, S. Rangasamy, J.M. Song, Shape-Dependent Skin Penetration of Silver Nanoparticles: Does It Really Matter?, Sci. Rep. 5 (2015) 1–11. https://doi.org/10.1038/srep16908.

[239] S. Zhu, L. Gong, Y. Li, H. Xu, Z. Gu, Y. Zhao, Safety Assessment of Nanomaterials to Eyes: An Important but Neglected Issue, Adv. Sci. 6 (2019). https://doi.org/10.1002/advs.201802289.

[240] M.I. Sriram, K. Kalishwaralal, S. Barathmanikanth, S. Gurunathani, Size-based cytotoxicity of silver nanoparticles in bovine retinal endothelial cells, Nanosci. Methods. 1 (2012) 56–77. https://doi.org/10.1080/17458080.2010.547878.

[241] E. Söderstjerna, P. Bauer, T. Cedervall, H. Abdshill, F. Johansson, U.E. Johansson,

Silver and gold nanoparticles exposure to in Vitro cultured retina - Studies on nanoparticle internalization, apoptosis, oxidative stress, glial- and microglial activity, PLoS One. 9 (2014). https://doi.org/10.1371/journal.pone.0105359.

[242] A. Malakar, S.R. Kanel, C. Ray, D.D. Snow, M.N. Nadagouda, Nanomaterials in the environment, human exposure pathway, and health effects: A review, Sci. Total Environ. 759 (2021) 143470. https://doi.org/10.1016/j.scitotenv.2020.143470.

[243] J.A. Chávez-Hernández, A.J. Velarde-Salcedo, G. Navarro-Tovar, C. Gonzalez, Safe nanomaterials: from their use, application, and disposal to regulations, Nanoscale Adv. 6 (2024) 1583–1610. https://doi.org/10.1039/d3na01097j.

[244] Z. Piperigkou, K. Karamanou, A.B. Engin, C. Gialeli, A.O. Docea, D.H. Vynios, M.S.G. Pavão, K.S. Golokhvast, M.I. Shtilman, A. Argiris, E. Shishatskaya, A.M. Tsatsakis, Emerging aspects of nanotoxicology in health and disease: From agriculture and food sector to cancer therapeutics, Food Chem. Toxicol. 91 (2016) 42–57. https://doi.org/10.1016/j.fct.2016.03.003.

[245] and J.R. Mingguang Li, Khuloud T. Al-Jamal, Kostas Kostarelos, Physiologically Based Pharmacokinetic Modeling of Nanoparticles, Am. Chem. Soc. Nano. 4 (2010) 6303–6317. https://doi.org/10.1021/nn1018818.

[246] J.H. Byun, D.G. Han, H.J. Cho, I.S. Yoon, I.H. Jung, Recent advances in physiologically based pharmacokinetic and pharmacodynamic models for anticancer nanomedicines, Arch. Pharm. Res. 43 (2020) 80–99. https://doi.org/10.1007/s12272-020-01209-2.

[247] H. Soo Choi, W. Liu, P. Misra, E. Tanaka, J.P. Zimmer, B. Itty Ipe, M.G. Bawendi, J. V. Frangioni, Renal clearance of quantum dots, Nat. Biotechnol. 25 (2007) 1165–1170. https://doi.org/10.1038/nbt1340.

[248] L. Yuan, Q. Chen, J.E. Riviere, Z. Lin, Pharmacokinetics and tumor delivery of nanoparticles, J. Drug Deliv. Sci. Technol. 83 (2023) 104404. https://doi.org/10.1016/j.jddst.2023.104404.

[249] P. Ravindran S, Suthar JK, Rokade R, Deshpande P, Singh P, U.S. A, Khambadkhar R, Pharmacokinetics, metabolism, distribution and permeability of nanomedicine, Curr. Drug Metab. 19 (2018) 327–334 https://doi.org/10.2174/1389200219666180305154119.

[250] A.H. Faraji, P. Wipf, Nanoparticles in cellular drug delivery, Bioorganic Med. Chem. 17 (2009) 2950–2962. https://doi.org/10.1016/j.bmc.2009.02.043.

[251] J. Bourquin, A. Milosevic, D. Hauser, R. Lehner, F. Blank, A. Petri-Fink, B. Rothen-Rutishauser, Biodistribution, Clearance, and Long-Term Fate of Clinically Relevant Nanomaterials, Adv. Mater. 30 (2018) 1–31. https://doi.org/10.1002/adma.201704307.

[252] A. Zhang, K. Meng, Y. Liu, Y. Pan, W. Qu, D. Chen, S. Xie, Absorption, distribution, metabolism, and excretion of nanocarriers in vivo and their influences, Adv. Colloid Interface Sci. 284 (2020) 102261. https://doi.org/10.1016/j.cis.2020.102261.

[253] Z. Lin, N.A. Monteiro-Riviere, J.E. Riviere, Pharmacokinetics of metallic nanoparticles, Wiley Interdiscip. Rev. Nanomedicine Nanobiotechnology. 7 (2015) 189–217. https://doi.org/10.1002/wnan.1304.

[254] S.H. W. G. Kreyling, U. Holzwarth, N. Haberl, J. Kozempel, M.S.-B. A. Wenk, C. Schleh, M. Schäffler, J. Lipka, N. Gibson, Quantitative biokinetics of titanium dioxide nanoparticles after intravenous injection in rats: Part 1, Nanotoxicology. 11 (2017) 434–442. https://doi.org/10.1080/17435390.2017.1306892.

[255] A.W. W. G. Kreyling, U. Holzwarth, C. Schleh, J. Kozempel, M.S.-B. N. Haberl, S. Hirn, M. Schäffler, J. Lipka, N. Gibson, Quantitative biokinetics of titanium dioxide nanoparticles after oral application in rats: Part 2, Nanotoxicology. 11 (2017) 443–453. https://doi.org/10.1080/17435390.2017.1306893.

[256] N. Kreyling, W. G., Holzwarth, U., Haberl, N., Kozempel, J., Wenk, A., Hirn, S., … Gibson, Quantitative biokinetics of titanium dioxide nanoparticles after intratracheal instillation in rats: Part 3, Nanotoxicology. 11 (2017) 454–464. https://doi.org/10.1080/17435390.2017.1306894.

[257] W.S. Cho, B.C. Kang, J.K. Lee, J. Jeong, J.H. Che, S.H. Seok, Comparative absorption, distribution, and excretion of titanium dioxide and zinc oxide nanoparticles after repeated oral administration, Part. Fibre Toxicol. 10 (2013) 1–9. https://doi.org/10.1186/1743-8977-10-9.

[258] American Society of Hematology, Blood Basics, (n.d.). https://www.hematology.org/ (accessed July 28, 2025).

[259] J. Bartel, J. Krumsiek, K. Schramm, J. Adamski, C. Gieger, C. Herder, M. Carstensen, A. Peters, W. Rathmann, M. Roden, K. Strauch, K. Suhre, G. Kastenmüller, H. Prokisch, F.J. Theis, The Human Blood Metabolome-Transcriptome Interface, PLoS Genet. 11 (2015) 1–32. https://doi.org/10.1371/journal.pgen.1005274.

[260] M. Lundqvist, C. Augustsson, M. Lilja, K. Lundkvist, B. Dahlbäck, S. Linse, T. Cedervall, The nanoparticle protein corona formed in human blood or human blood fractions, PLoS One. 12 (2017) 1–15. https://doi.org/10.1371/journal.pone.0175871.

[261] O. Kiseleva, I. Kurbatov, E. Ilgisonis, E. Poverennaya, Defining blood plasma and serum metabolome by gc-ms, Metabolites. 12 (2022). https://doi.org/10.3390/metabo12010015.

[262] R. Dejonghe, E. Bolea-Fernandez, A. Lores-Padin, T. Van Acker, A. Rua-Ibarz, O. De Wever, F. Vanhaecke, An evaluation of the analytical and biological robustness of a method for quantifying iron in individual red blood cells via single-cell tandem ICP-mass spectrometry, Microchem. J. 207 (2024). https://doi.org/10.1016/j.microc.2024.112013.

[263] N. Mohandas, P.G. Gallagher, Red cell membrane: Past, present, and future, Blood. 112 (2008) 3939–3948. https://doi.org/10.1182/blood-2008-07-161166.

[264] V. Pretini, M.H. Koenen, L. Kaestner, M.H.A.M. Fens, R.M. Schiffelers, M. Bartels, R. Van Wijk, Red blood cells: Chasing interactions, Front. Physiol. 10 (2019) 1–17. https://doi.org/10.3389/fphys.2019.00945.

[265] M.R. Farag, M. Alagawany, Erythrocytes as a biological model for screening of xenobiotics toxicity, Chem. Biol. Interact. 279 (2018) 73–83. https://doi.org/10.1016/j.cbi.2017.11.007.

USC UNIVERSIDADE DE SANTIAGO DE COMPOSTELA

[266] B.J. Bain, Structure and function of red and white blood cells and platelets, Med. (United Kingdom). 49 (2021) 183–188. https://doi.org/10.1016/j.mpmed.2021.01.001.

[267] M. Culenova, A. Nicodemou, Z.V. Novakova, M. Debreova, V. Smolinská, S. Bernatova, D. Ivanisova, O. Novotna, J. Vasicek, I. Varga, S. Ziaran, L. Danisovic, Isolation, culture and comprehensive characterization of biological properties of human urine-derived stem cells, Int. J. Mol. Sci. 22 (2021) 1–15. https://doi.org/10.3390/ijms222212503.

[268] S. Bouatra, F. Aziat, R. Mandal, A.C. Guo, M.R. Wilson, C. Knox, T.C. Bjorndahl, R. Krishnamurthy, F. Saleem, P. Liu, Z.T. Dame, J. Poelzer, J. Huynh, F.S. Yallou, N. Psychogios, E. Dong, R. Bogumil, C. Roehring, D.S. Wishart, The Human Urine Metabolome, PLoS One. 8 (2013). https://doi.org/10.1371/journal.pone.0073076.

[269] S. Pan, J. Tang, Clinical Molecular Diagnostics, 2021. https://doi.org/10.1007/978-981-16-1037-0.

[270] A. Marimuthu, R.N. O'Meally, R. Chaerkady, Y. Subbannayya, V. Nanjappa, P. Kumar, D.S. Kelkar, S.M. Pinto, R. Sharma, S. Renuse, R. Goel, R. Christopher, B. Delanghe, R.N. Cole, H.C. Harsha, A. Pandey, A comprehensive map of the human urinary proteome, J. Proteome Res. 10 (2011) 2734–2743. https://doi.org/10.1021/pr2003038.

[271] E.A. Thévenot, A. Roux, Y. Xu, E. Ezan, C. Junot, Analysis of the Human Adult Urinary Metabolome Variations with Age, Body Mass Index, and Gender by Implementing a Comprehensive Workflow for Univariate and OPLS Statistical Analyses, J. Proteome Res. 14 (2015) 3322–3335. https://doi.org/10.1021/acs.jproteome.5b00354.

[272] J. Wu, Y. Gao, Physiological conditions can be reflected in human urine proteome and metabolome, Expert Rev. Proteomics. 12 (2015) 623–636. https://doi.org/10.1586/14789450.2015.1094380.

[273] SCENIHR/002/05 Scientific Committee On Emerging and Newly Identified Health Riks (SCENIHR) modified Opinion (after public consultation) on The appropriateness of existing methodologies to assess the potential risks associated with engineered and adventit, 2006.

[274] C.F. Poole, Milestones in the development of liquid-phase extraction techniques, in: Liq. Extr., Elsevier Inc., 2020: pp. 1–44. https://doi.org/10.1016/B978-0-12-816911-7.00001-3.

[275] M.A.L. N. M. Rice, H. M. N. H. Irving, International Union of Pure and Applied Chemistry, Nomenclature for liquid-liquid distribution (solvent extraction) (IUPAC Recommendations 1993), Pure Appl. Chem. 65 (1993) 2373–2396.

[276] J.C.W. Paul T Anastas, Green Chemistry: Theory and Practice, Oxford University Press, 2000. https://doi.org/10.1093/oso/9780198506980.001.0001.

[277] M. Rutkowska, J. Płotka-Wasylka, M. Sajid, V. Andruch, Liquid–phase microextraction: A review of reviews, Microchem. J. 149 (2019). https://doi.org/10.1016/j.microc.2019.103989.

[278] A. Spietelun, Ł. Marcinkowski, M. De La Guardia, J. Namieśnik, Green aspects, developments and perspectives of liquid phase microextraction techniques, Talanta. 119

USC UNIVERSIDADE DE COMPOSTELA

(2014) 34–45. https://doi.org/10.1016/j.talanta.2013.10.050.

[279] M. Rezaee, Y. Assadi, M.R. Milani Hosseini, E. Aghaee, F. Ahmadi, S. Berijani, Determination of organic compounds in water using dispersive liquid-liquid microextraction, J. Chromatogr. A. 1116 (2006) 1–9. https://doi.org/10.1016/j.chroma.2006.03.007.

[280] J.M. Kokosa, Dispersive liquid-liquid microextraction, in: Liq. Extr., Elsevier Inc., 2019: pp. 473–497. https://doi.org/10.1016/B978-0-12-816911-7.00016-5.

[281] I. Notardonato, P. Avino, Dispersive Liquid–Liquid Micro Extraction: An Analytical Technique Undergoing Continuous Evolution and Development—A Review of the Last 5 Years, Separations. 11 (2024). https://doi.org/10.3390/separations11070203.

[282] J. Grau, C. Azorín, J.L. Benedé, A. Chisvert, A. Salvador, Use of green alternative solvents in dispersive liquid-liquid microextraction: A review, J. Sep. Sci. 45 (2022) 210–222. https://doi.org/10.1002/jssc.202100609.

[283] D. Linke, Chapter 34 Detergents. An Overview, 1st ed., Elsevier Inc., 2009. https://doi.org/10.1016/S0076-6879(09)63034-2.

[284] Y. Yamini, N. Feizi, M. Moradi, Surfactant-based extraction systems, Elsevier Inc., 2019. https://doi.org/10.1016/B978-0-12-816911-7.00007-4.

[285] R.W. Egan, M.A. Jones, A.L. Lehninger, Hydrophile lipophile balance and critical micelle concentration as key factors influencing surfactant disruption of mitochondrial membranes, J. Biol. Chem. 251 (1976) 4442–4447. https://doi.org/10.1016/s0021-9258(17)33316-1.

[286] M. Saraji, A.A.H. Bidgoli, Dispersive liquid-liquid microextraction using a surfactant as disperser agent, Anal. Bioanal. Chem. 397 (2010) 3107–3115. https://doi.org/10.1007/s00216-010-3894-2.

[287] M. Moradi, Y. Yamini, A. Esrafili, S. Seidi, Application of surfactant assisted dispersive liquid-liquid microextraction for sample preparation of chlorophenols in water samples, Talanta. 82 (2010) 1864–1869. https://doi.org/10.1016/j.talanta.2010.08.002.

[288] Q. Wu, Q. Chang, C. Wu, H. Rao, X. Zeng, C. Wang, Z. Wang, Ultrasound-assisted surfactant-enhanced emulsification microextraction for the determination of carbamate pesticides in water samples by high performance liquid chromatography, J. Chromatogr. A. 1217 (2010) 1773–1778. https://doi.org/10.1016/j.chroma.2010.01.060.

[289] M. Behbahani, F. Najafi, S. Bagheri, M.K. Bojdi, M. Salarian, A. Bagheri, Application of surfactant assisted dispersive liquid-liquid microextraction as an efficient sample treatment technique for preconcentration and trace detection of zonisamide and carbamazepine in urine and plasma samples, J. Chromatogr. A. 1308 (2013) 25–31. https://doi.org/10.1016/j.chroma.2013.07.088.

[290] M. Sadeghi, F. Shiri, D. Kordestani, P. Mohammadi, A. Alizadeh, SBA-15/Metformin as a novel sorbent combined with surfactant-assisted dispersive liquid–liquid microextraction (SA-DLLME) for highly sensitive determination of Pb, Cd and Ni in food and environmental samples, J. Iran. Chem. Soc. 15 (2018) 753–768. https://doi.org/10.1007/s13738-017-1272-0.

USC UNIVERSIDADE DE SANTIAGO DE COMPOSTELA

[291] M. Moradi, Y. Yamini, T. Baheri, Analysis of abuse drugs in urine using surfactant-assisted dispersive liquid-liquid microextraction, J. Sep. Sci. 34 (2011) 1722–1729. https://doi.org/10.1002/jssc.201100132.

[292] R. Gharanjik, M. Nassiri, S.H. Hashemi, Spectrophotometric determination of copper and nickel in marine brown algae after perconcentration with surfactant assisted dispersive liquid-liquid microextraction, Iran. J. Chem. Chem. Eng. 39 (2020) 117–126 https://doi.org/10.30492/ijcce.2020.34832.

[293] N. Dokpikul, W.C. Chaiyasith, R. Sananmuang, R.J. Ampiah-Bonney, Surfactant-assisted emulsification dispersive liquid-liquid microextraction using 2-thenoyltrifluoroacetone as a chelating agent coupled with electrothermal atomic absorption spectrometry for the speciation of chromium in water and rice samples, Food Chem. 246 (2018) 379–385. https://doi.org/10.1016/j.foodchem.2017.11.050.

[294] H.R. Sobhi, E. Azadikhah, M. Behbahani, A. Esrafili, M. Ghambarian, Application of a surfactant-assisted dispersive liquid-liquid microextraction method along with central composite design for micro-volume based spectrophotometric determination of low level of Cr(VI) ions in aquatic samples, Spectrochim. Acta - Part A Mol. Biomol. Spectrosc. 202 (2018) 36–40. https://doi.org/10.1016/j.saa.2018.05.031.

[295] I. Timofeeva, K. Stepanova, A. Bulatov, In-a-syringe surfactant-assisted dispersive liquid-liquid microextraction of polycyclic aromatic hydrocarbons in supramolecular solvent from tea infusion, Talanta. 224 (2021) 121888. https://doi.org/10.1016/j.talanta.2020.121888.

[296] C. Liu, Z. Liu, M. Wang, Y. Yang, Surfactant-assisted dispersive liquid–liquid micro-extraction combined with magnetic solid-phase extraction for analysis of polyphenols in tobacco samples, J. Iran. Chem. Soc. 15 (2018) 1561–1568. https://doi.org/10.1007/s13738-018-1354-7.

[297] S.B. Mammana, E. del C. Abraham, A.B. Camargo, Á. Vázquez, J.C. Altamirano, Enzymatic Digestion Coupled to Surfactant-Assisted Dispersive Liquid-Liquid Microextraction: A Mild Approach for Determining Polybrominated Diphenyl Ethers in Human Hair Sample, ChemistrySelect. 5 (2020) 2179–2184. https://doi.org/10.1002/slct.201904795.

[298] Y. Liu, M. He, B. Chen, B. Hu, Ultra-trace determination of gold nanoparticles in environmental water by surfactant assisted dispersive liquid liquid microextraction coupled with electrothermal vaporization-inductively coupled plasma-mass spectrometry, Spectrochim. Acta - Part B At. Spectrosc. 122 (2016) 94–102. https://doi.org/10.1016/j.sab.2016.04.009.

[299] S.K. Selahle, P.N. Nomngongo, Quantification of TiO2 and ZnO nanoparticles in wastewater using inductively coupled plasma optical emission spectrometry, Toxicol. Environ. Chem. 101 (2019) 204–214. https://doi.org/10.1080/02772248.2019.1686151.

[300] K. Loeschner, M.E. Johnson, A.R. Montoro Bustos, Application of Single Particle ICP-MS for the Determination of Inorganic Nanoparticles in Food Additives and Food: A Short Review, Nanomaterials. 13 (2023). https://doi.org/10.3390/nano13182547.

[301] A. Moreda-Piñeiro, J. Moreda-Piñeiro, P. Bermejo-Barrera, Sample Pre-treatment

USC UNIVERSIDADE DE SANTIAGO DE COMPOSTELA

Methods for Organometallic Species Determination, in: Speciat. Stud. Soil, Sediment Environ. Samples, 2013: pp. 9–26. https://doi.org/10.1201/b15501-3.

[302] M.V. Taboada-López, S. Iglesias-López, P. Herbello-Hermelo, P. Bermejo-Barrera, A. Moreda-Piñeiro, Ultrasound assisted enzymatic hydrolysis for isolating titanium dioxide nanoparticles from bivalve mollusk before sp-ICP-MS, Anal. Chim. Acta. 1018 (2018) 16–25. https://doi.org/10.1016/j.aca.2018.02.075.

[303] M.V. Taboada-López, P. Herbello-Hermelo, R. Domínguez-González, P. Bermejo-Barrera, A. Moreda-Piñeiro, Enzymatic hydrolysis as a sample pre-treatment for titanium dioxide nanoparticles assessment in surimi (crab sticks) by single particle ICP-MS, Talanta. 195 (2019) 23–32. https://doi.org/10.1016/j.talanta.2018.11.023.

[304] M.V. Taboada-López, N. Alonso-Seijo, P. Herbello-Hermelo, P. Bermejo-Barrera, A. Moreda-Piñeiro, Determination and characterization of silver nanoparticles in bivalve molluscs by ultrasound assisted enzymatic hydrolysis and sp-ICP-MS, Microchem. J. 148 (2019) 652–660. https://doi.org/10.1016/j.microc.2019.05.023.

[305] M.V. Taboada-López, D. Bartczak, S. Cuello-Núñez, H. Goenaga-Infante, P. Bermejo-Barrera, A. Moreda-Piñeiro, F4-UV-ICP-MS for detection and quantification of silver nanoparticles in seafood after enzymatic hydrolysis, Talanta. 232 (2021). https://doi.org/10.1016/j.talanta.2021.122504.

[306] A. Chalifoux, M. Hadioui, N. Amiri, K.J. Wilkinson, Analysis of Silver Nanoparticles in Ground Beef by Single Particle Inductively Coupled Plasma Mass Spectrometry (SP-ICP-MS), Molecules. 28 (2023). https://doi.org/10.3390/molecules28114442.

[307] Y. Suzuki, M. Harimoto, M. Takahashi, H. Akiyama, A. Hirose, T. Tsutsumi, Analysis of Silver-containing Nanoparticles in Oysters Using Single-particle ICP-MS, J. Environ. Chem. 34 (2024) 9–20. https://doi.org/10.5985/jec.34.9.

[308] F. Laborda, E. Bolea, G. Cepriá, M.T. Gómez, M.S. Jiménez, J. Pérez-Arantegui, J.R. Castillo, Detection, characterization and quantification of inorganic engineered nanomaterials: A review of techniques and methodological approaches for the analysis of complex samples, Anal. Chim. Acta. 904 (2016) 10–32. https://doi.org/10.1016/j.aca.2015.11.008.

[309] J.B. Whitlam, K.F. Brown, Ultrafiltration in serum protein binding determinations, J. Pharm. Sci. 70 (1981) 146–150. https://doi.org/10.1002/jps.2600700208.

[310] M. Loginov, F. Samper, G. Gésan-Guiziou, T. Sobisch, D. Lerche, E. Vorobiev, Centrifugal ultrafiltration for determination of filter cake properties of colloids, J. Memb. Sci. 536 (2017) 59–75. https://doi.org/10.1016/j.memsci.2017.04.064.

[311] N. Alele, R. Streubel, L. Gamrad, S. Barcikowski, M. Ulbricht, Ultrafiltration membrane-based purification of bioconjugated gold nanoparticle dispersions, Sep. Purif. Technol. 157 (2016) 120–130. https://doi.org/10.1016/j.seppur.2015.11.033.

[312] V.J. Pansare, D. Tien, P. Thoniyot, R.K. Prud'homme, Ultrafiltration of nanoparticle colloids, J. Memb. Sci. 538 (2017) 41–49. https://doi.org/10.1016/j.memsci.2017.03.041.

[313] D.A. Ladner, M. Steele, A. Weir, K. Hristovski, P. Westerhoff, Functionalized

USC DE COMPOSTELA

nanoparticle interactions with polymeric membranes, J. Hazard. Mater. 211–212 (2012) 288–295. https://doi.org/10.1016/j.jhazmat.2011.11.051.

[314] A.L. Fabricius, L. Duester, B. Meermann, T.A. Ternes, ICP-MS-based characterization of inorganic nanoparticles-sample preparation and off-line fractionation strategies, Anal. Bioanal. Chem. 406 (2014) 467–479. https://doi.org/10.1007/s00216-013-7480-2.

[315] G. Cornelis, J.K. Kirby, D. Beak, D. Chittleborough, M.J. McLaughlin, A method for determination of retention of silver and cerium oxide manufactured nanoparticles in soils, Environ. Chem. 7 (2010) 298–308. https://doi.org/10.1071/EN10013.

[316] Y. Sivry, A. Gelabert, L. Cordier, R. Ferrari, H. Lazar, F. Juillot, N. Menguy, M.F. Benedetti, Behavior and fate of industrial zinc oxide nanoparticles in a carbonate-rich river water, Chemosphere. 95 (2014) 519–526. https://doi.org/10.1016/j.chemosphere.2013.09.110.

[317] Z. Wang, N. Li, J. Zhao, J.C. White, P. Qu, B. Xing, CuO nanoparticle interaction with human epithelial cells: Cellular uptake, location, export, and genotoxicity, Chem. Res. Toxicol. 25 (2012) 1512–1521. https://doi.org/10.1021/tx3002093.

[318] T.B. Reed, Induction-Coupled Plasma Torch, J. Appl. Phys. 32 (1961) 821–824. https://doi.org/10.1063/1.1736112.

[319] T.B. Reed, Growth of refractory crystals using the inductively coupled plasma, J. Appl. Phys. 32 (1961) 2534–2535. https://doi.org/10.1063/1.1728345.

[320] T.B. Reed, Plasma torches, Int. J. Sci. Technol. 6 (1962) 42–48.

[321] C.T. Greenfield, S., Jones, I.Ll. and Berry, High-pressure plasmas as spectroscopic emission sources, Analyst. 89 (1964) 713–720.

[322] V.A. Wendt, R.H. and Fassel, Induction coupled plasma spectrometric excitation source, Anal. Chem. 37 (1965) 920–922.

[323] W. Hittorf, Ueber die Electricitätsleitung der Gase, Ann. Phys. 257 (1884) 90–139.

[324] J.M. Mermet, Fundamental Principles of Inductively Coupled Plasmas, Inductively Coupled Plasma Spectrom. Its Appl. 1040 (2007) 27–60. https://doi.org/10.1002/9780470988794.ch2.

[325] A. Montaser, Inductively coupled plasma mass spectromety, Willey-VCH, 1998.

[326] R.S. Houk, V.A. Fassel, G.D. Flesch, H.J. Svec, A.L. Gray, C.E. Taylor, Inductively coupled argon plasma as an ion source for mass spectrometric determination of trace elements, Anal. Chem. 52 (1980) 2283–2289. https://doi.org/10.1021/ac50064a012.

[327] S.M. Nelms, Inductively Coupled Plasma Mass Spectrometry Handbook, Wiley-Blackwell, 2009.

[328] R. Thomas, Practical guide to ICP-MS: A tutorial for beginners, CRC Press, Taylor and Francis Group, 2008. https://doi.org/10.1201/9781420067873.

[329] J.L. Todoli, F. Vanhaecke, Liquid Sample Introduction and Electrothermal Vaporisation for ICP-MS: Fundamentals and Applications, in: 2005: pp. 182–227. https://doi.org/10.1002/9781444305463.ch5.

[330] B.L. Sharp, C. O'Connor, Aerosol Generation and Sample Transport, 2007. https://doi.org/10.1002/9780470988794.ch4.

[331] K.E. Jarvis, A.L. Gray, R.S. Houk, Handbook of Inductively Coupled Plasma Mass Spectrometry, 1992.

[332] R. Campargue, Progress in overexpanded supersonic jets and skimmed molecular-beams in free-jet zones of silence., Phys. Chem. 88 (1984) 4466–4474. https://doi.org/10.1021/j150664a004.

[333] G. O'Connor, E. Hywel Evans, Fundamental Aspects of Inductively Coupled Plasma-Mass Spectrometry (ICP-MS), Inductively Coupled Plasma Spectrom. Its Appl. (2007) 134–159. https://doi.org/10.1002/9780470988794.ch5.

[334] J. Labuda, J. Barek, Z. Gajdosechova, S. Jacob, L. Johnston, P. Krystek, Z. Mester, J. Moreira, V. Svitkova, K.J. Wilkinson, Analytical chemistry of engineered nanomaterials: Part 2. analysis in complex samples (IUPAC Technical Report), Pure Appl. Chem. 95 (2023) 1159–1196. https://doi.org/10.1515/pac-2022-0401.

[335] J.M. Costa-Fernández, M. Menéndez-Miranda, D. Bouzas-Ramos, J.R. Encinar, A. Sanz-Medel, Mass spectrometry for the characterization and quantification of engineered inorganic nanoparticles, TrAC - Trends Anal. Chem. 84 (2016) 139–148. https://doi.org/10.1016/j.trac.2016.06.001.

[336] F. Laborda, A.C. Gimenez-Ingalaturre, E. Bolea, J.R. Castillo, Single particle inductively coupled plasma mass spectrometry as screening tool for detection of particles, Spectrochim. Acta - Part B At. Spectrosc. 159 (2019) 105654. https://doi.org/10.1016/j.sab.2019.105654.

[337] F. Laborda, E. Bolea, J. Jimenez-Lamana, Single Particle Inductively Coupled Plasma Mass Spectrometry: A Powerful Tool for Nanoanalysis, Anal. Chem. 86 (2014) 2270–2278. https://doi.org/10.1021/ac402980q.

[338] F. Laborda, E. Bolea, J. Jiménez-Lamana, Single particle inductively coupled plasma mass spectrometry for the analysis of inorganic engineered nanoparticles in environmental samples, Trends Environ. Anal. Chem. 9 (2016) 15–23. https://doi.org/10.1016/j.teac.2016.02.001.

[339] F. Laborda, J. Jiménez-Lamana, E. Bolea, J.R. Castillo, Critical considerations for the determination of nanoparticle number concentrations, size and number size distributions by single particle ICP-MS, J. Anal. At. Spectrom. 28 (2013) 1220–1232. https://doi.org/10.1039/c3ja50100k.

[340] I. Abad-Álvaro, E. Peña-Vázquez, E. Bolea, P. Bermejo-Barrera, J.R. Castillo, F. Laborda, Evaluation of number concentration quantification by single-particle inductively coupled plasma mass spectrometry: microsecond vs. millisecond dwell times, Anal. Bioanal. Chem. 408 (2016) 5089–5097. https://doi.org/10.1007/s00216-016-9515-y.

[341] F. Laborda, A.C. Gimenez-Ingalaturre, E. Bolea, J.R. Castillo, About detectability and limits of detection in single particle inductively coupled plasma mass spectrometry, Spectrochim. Acta - Part B At. Spectrosc. 169 (2020) 105883. https://doi.org/10.1016/j.sab.2020.105883.

USC UNIVERSIDADE DE SANTIAGO DE COMPOSTELA

[342] A.C. Gimenez-Ingalaturre, I. Abad-Álvaro, P. Goñi, K. Billimoria, H. Goenaga-Infante, F. Laborda, Performance of single-cell ICP-MS for quantitative biodistribution studies of silver interactions with bacteria, J. Anal. At. Spectrom. 39 (2024) 743–753. https://doi.org/10.1039/d3ja00378g.

[343] J. Jiménez-Lamana, J. Szpunar, R. Łobinski, New Frontiers of Metallomics: Elemental and Species-Specific Analysis and Imaging of Single Cells, Adv. Exp. Med. Biol. 1055 (2018) 245–270. https://doi.org/10.1007/978-3-319-90143-5_10.

[344] M. Resano, M. Aramendía, E. García-Ruiz, A. Bazo, E. Bolea-Fernandez, F. Vanhaecke, Living in a transient world: ICP-MS reinvented via time-resolved analysis for monitoring single events, Chem. Sci. 13 (2022) 4436–4473. https://doi.org/10.1039/d1sc05452j.

[345] X. Yu, M. He, B. Chen, B. Hu, Recent advances in single-cell analysis by inductively coupled plasma-mass spectrometry: A review, Anal. Chim. Acta. 1137 (2020) 191–207. https://doi.org/10.1016/j.aca.2020.07.041.

[346] A.L. Gray, Solid sample introduction by laser ablation for inductively coupled plasma source mass spectrometry, Analyst. 110 (1985) 551–556.

[347] P. Arrowsmith, Laser ablation of solids for elemental analysis by indutively coupled plasma mass spectrometry, Anal. Chem. 59 (1987) 1437–1444.

[348] P. Arrowsmith, Analysis of solids by laser ablation plasma source mass spectrometry, ICP Inform. Newsl. 12 (1987) 579–608.

[349] C. Tye, J. Gordon, P. Webb, Analysis of uranium using laser ablation ICP-MS, Int. Lab. December (1987) 3–41.

[350] J.W. Hager, Relative elemental responses for laser ablation-inductively coupled plasma mass spectrometry, Anal. Chem. 61 (1989) 1243–1248.

[351] T. Mochizuki, A. Sakashita, H. Iwata, T. Kagaya, T. Shimamura, P. Blair, Laser ablation for direct elemental analysis of solid samples by inductively coupled plasma mass spectrometry, Anal. Sci. 4 (1988) 403–409.

[352] T. Mochizuki, A. Sakashita, H. Iwata, Laser ablation for direct elemental analysis of solid samples by ICP-atomic emission spectrometry and ICP-mass spectrometry, N K K Tech. Rev. 58 (1990) 19–27.

[353] J. Koch, D. Günther, Review of the State-of-the- Art of Laser Ablation Inductively Coupled Plasma Mass Spectrometry, Appl. Spectrosc. (2011) 155–162. https://doi.org/10.1366/11-06255.

[354] M.V. Galiová, V. Kanický, Chapter 9. Laser Ablation Inductively Coupled Plasma Mass Spectrometry as a Tool in Biological Sciences, in: V. Havlíček, J. Spížek (Eds.), Nat. Prod. Anal. Instrumentation, Methods, Appl., 2014: pp. 313–348.

[355] A. Lores-Padín, R. Pereiro, B. Fernández, Laser Ablation ICP-MS: New Instrumental Developments, Applications and Trends, in: F. Atta-ur-Rahman, S.A. Ozkan (Eds.), Recent Adv. Anal. Tech., 2020: pp. 1–26.

USC UNIVERSIDADE DE SANTIAGO DE COMPOSTELA

ANNEX I. PERMISSIONS

USC
UNIVERSIDADE
DE SANTIAGO
DE COMPOSTELA

ANNEX I. PERMISSIONS

All figures included in this thesis are the original work of Ana Justo Vega. In addition, reproduction permissions for the published articles have been obtained and are included herein.

CHAPTER 1

CCC Marketplace

This is a License Agreement between Ana Justo Vega ("User") and Copyright Clearance Center, Inc. ("CCC") on behalf of the Rightsholder identified in the order details below. The license consists of the order details, the Marketplace Permissions General Terms and Conditions below, and any Rightsholder Terms and Conditions which are included below.

All payments must be made in full to CCC in accordance with the Marketplace Permissions General Terms and Conditions below.

Order Date	01-Oct-2025	Type of Use	Republish in a thesis/dissertation
Order License ID	1657281-1	Publisher	ROYAL SOCIETY OF CHEMISTRY,
ISSN	1364-5544	Portion	Chapter/article

LICENSED CONTENT

Publication Title	Journal of analytical atomic spectrometry	Publication Type	e-Journal
Article Title	Prospects of surfactant assisted dispersive liquid liquid microextraction for the selective extraction of silver and titanium dioxide nanoparticles from waters and determination by sp-ICP-MS	Start Page	573
		End Page	581
		Issue	2
		Volume	39
Author / Editor	Royal Society of Chemistry (Great Britain)	URL	http://firstsearch.oclc.org
Date	01/01/1986		
Language	English		
Country	United Kingdom of Great Britain and Northern Ireland		
Rightsholder	Royal Society of Chemistry		

CHAPTER 2

Surfactant-assisted dispersive liquid–liquid microextraction and centrifugal ultrafiltration as potential extraction procedures for silver and titanium dioxide nanoparticles from human urine

Author:
Ana Justo-Vega,Claudia Torrente-Seco,Lidia Janza-Candal,Manuel Aboal-Somoza,Raquel Domínguez-González,Pilar Bermejo-Barrera,Antonio Moreda-Piñeiro

Publication: Microchemical Journal

Publisher: Elsevier

Date: April 2025

© 2025 The Authors. Published by Elsevier B.V.

Quick Price Estimate

This service provides permission for reuse only. If you do not have a copy of the content, you may be able to purchase a copy using RightsLink as an additional transaction. Simply select 'I would like to..... 'Purchase this content'.

Unclear about who you are?

Please note that, as the author of this Elsevier article, you retain the right to include it in a thesis or dissertation, provided it is not published commercially. Permission is not required, but please ensure that you reference the journal as the original source. For more information on this and on your other retained rights, please visit: https://www.elsevier.com/about/our-business/policies/copyright#Author-rights

USC UNIVERSIDADE DE SANTIAGO DE COMPOSTELA

CHAPTER 3

Enzymatic hydrolysis for pre-treating human serum before titanium dioxide nanoparticles assessment by spICP-MS

Author: Ana Justo-Vega,Sara Vázquez-Pérez,Raquel Domínguez-González,Pilar Bermejo-Barrera,Antonio Moreda-Piñeiro
Publication: Talanta
Publisher: Elsevier
Date: 15 August 2025

© 2025 The Authors. Published by Elsevier B.V.

Quick Price Estimate

This service provides permission for reuse only. If you do not have a copy of the content, you may be able to purchase a copy using RightsLink as an additional transaction. Simply select 'I would like to..... 'Purchase this content'.

Unclear about who you are?

Please note that, as the author of this Elsevier article, you retain the right to include it in a thesis or dissertation, provided it is not published commercially. Permission is not required, but please ensure that you reference the journal as the original source. For more information on this and on your other retained rights, please visit: https://www.elsevier.com/about/our-business/policies/copyright#Author-rights

CHAPTER 4

Silver nanoparticles behaviour in exposed human red blood cells by single cell–inductively coupled plasma–mass spectrometry

Author: Ana Justo-Vega,Raquel Domínguez-González,Pilar Bermejo-Barrera,Antonio Moreda-Piñeiro,Javier Jiménez-Lamana
Publication: Talanta
Publisher: Elsevier
Date: 1 February 2026

© 2025 The Authors. Published by Elsevier B.V.

Quick Price Estimate

This service provides permission for reuse only. If you do not have a copy of the content, you may be able to purchase a copy using RightsLink as an additional transaction. Simply select 'I would like to..... 'Purchase this content'.

Unclear about who you are?

Please note that, as the author of this Elsevier article, you retain the right to include it in a thesis or dissertation, provided it is not published commercially. Permission is not required, but please ensure that you reference the journal as the original source. For more information on this and on your other retained rights, please visit: https://www.elsevier.com/about/our-business/policies/copyright#Author-rights

Engineered nanoparticles (ENPs) have become ubiquitous in modern society, yet their detection in environmental and biological systems remains analytically challenging. This thesis advances the field of nanometrology by developing and applying innovative strategies based on inductively coupled plasma mass spectrometry (ICP-MS) in its most advanced operational modes: single-particle, single-cell, and laser ablation ICP-MS. The development of matrix-specific pre-treatments strategies enable reliable NP characterization and quantification in tap water, human serum and urine, and red blood cells (RBCs). The present thesis targets different aspects of NP assessment: environmental exposure detection, biological monitoring in fluids, and cellular uptake dynamics.